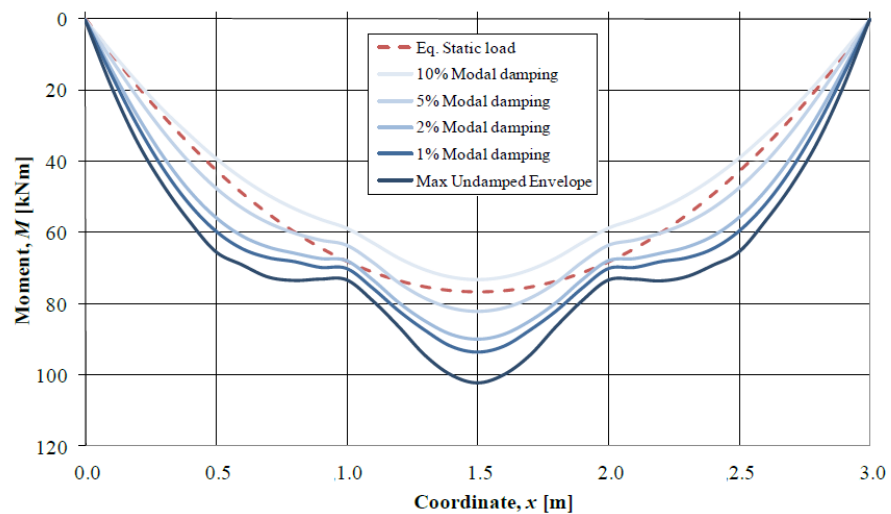# STRUCTURAL RESPONSE WITH REGARD TO EXPLOSIONS - Mode Superposition, Damping and Curtailment

## MATTIAS CARLSSON and ROBIN KRISTENSSON

Structural Mechanics

*Master's Dissertation*

# STRUCTURAL RESPONSE WITH REGARD TO EXPLOSIONS - Mode Superposition, Damping and Curtailment

Master's Dissertation by

MATTIAS CARLSSON and ROBIN KRISTENSSON

Supervisors:

Per-Erik Austrell, *Senior Lecturer,*
*Div. of Structural Mechanics, LTH, Lund*

Morgan Johansson,
*Reinertsen Sverige AB*

Examiner:

Kent Persson, *PhD,*
*Dept. of Construction Sciences, LTH, Lund*

ABSTRACT

When a structure is subjected to an explosion, it will have a response that differs from the one that arises from a static load. Engineers are used to design for static loads but the common knowledge of how to design for explosions is weak. There are guidelines for how to design for explosions with simplified methods but they are partly outdated and the explanation of how they are derived is vague. This Master thesis compiles some of the most important guidelines and explains the underlying theory. In order to understand the structural response one must first study basic theory of explosions, different material behaviours and basic dynamics, which are also presented in the thesis.

A structure can be simplified by transformation into a single degree of freedom-system (SDOF-system), and the reliability of such an SDOF-system is evaluated within this thesis. The SDOF-system is created by using a system point where the maximum displacement will occur, and it is compared to hand calculations for the maximum values and to non-linear finite element analyses. The SDOF-model assumes a specific deflection shape which is taken into account by using certain transformation factors. The simplified methods of calculating the structural response are presented in general, but the examples are made for reinforced concrete beams as these, due to their high mass and ductile behaviour, often are used as protection from explosions. Since no actual tests could be performed to collect empirical data about the response, FE-analyses are performed with the finite element software ADINA and even for a complex material such as concrete these analyses are assumed to represent the actual response of a structure.

In order to speed up the analyses, adequate simplifications of the motion can be described with mode superposition, and the effectiveness of these simplifications is shown in the thesis. When the mode superposition-analysis is made with only one mode, the results can verify the accuracy of the SDOF-model.

When designing structures it is important that the calculations are on the safe side to minimize the risk of damage and above all, failure, and therefore damping is often neglected as it is both easier to calculate without it and the results will be on the safe side. However, in order to get more accurate results the damping should also be included and therefore different approaches for this are described.

For impulse loads the moments near the supports are initially larger than for a static load which could pose a problem when the reinforcement is shortened in these areas. In this Master thesis the response for curtailed concrete beams is studied.


Key words: Explosion, impulse load, SDOF, FE-analysis, dynamic response, reinforced concrete, equivalent static load, damping, mode superposition, curtailment.

SAMMANFATTNING

När en struktur utsätts för en explosion kommer den ha en respons som skiljer sig från den som uppstår från en statisk last. Ingenjörer är vana vid att dimensionera för statiska laster, men den allmänna kunskapen om hur man dimensionerar vid explosioner är dålig. Det finns riktlinjer för hur man dimensionerar för explosioner med förenklade metoder, men de är delvis utdaterade och förklaringen till hur de är härledda är oklar. Det här examensarbetet sammanställer några av de viktigaste riktlinjerna och förklarar den underliggande teorin. För att kunna förstå den strukturella responsen måste man först studera grundläggande teori om explosioner, olika materialuppförande och grundläggande dynamik, som också presenteras i rapporten.

En struktur kan förenklas genom att transformeras till ett enfrihetsgradssystem (SDOF-system), och SDOF-systemets tillförlitlighet utvärderas i denna rapport. SDOF-systemet skapas genom att använda en systempunkt där den maximala förskjutningen kommer att uppstå, och jämförs med handberäkningar för maximala värden och med olinjära finita element-analyser. SDOF-modellen antar en specifik utböjningsform som anpassas med hjälp av specifika transformationsfaktorer. De förenklade metoderna för att beräkna strukturell respons presenteras generellt, men exemplen är gjorda för armerade betongbalkar eftersom dessa ofta, på grund av deras höga massa och duktila beteende, används som skydd för explosioner. Eftersom inga riktiga test kunde utföras för att samla empirisk data om responsen är FE-analyserna utförda med det finita element-programmet ADINA och även för ett komplext material såsom betong antas dessa analyser representera den verkliga responsen för en struktur.

För att snabba upp analyserna kan tillräckliga förenklingar beskrivas med modsuperposition, och effektiviteten av dessa förenklingar visas i rapporten. När sedan modsuperpositionsanalysen utförs med endast en mod kan precisionen av SDOF-modellen bekräftas.

När man dimensionerar strukturer är det viktigt att beräkningarna är på säkra sidan för att minimera risk för skada och framförallt brott, och därför brukar dämpningen ofta bortses ifrån eftersom det är både enklare att räkna utan den och värdena kommer bli på den säkra sidan. För att kunna få mer noggranna resultat borde dämpningen också vara inkluderad och därför beskrivs olika tillvägagångssätt för detta.

För impulslaster är momenten nära stöd inledningsvis större än för en statisk last vilket skulle kunna innebära ett problem när armeringen är avkortad i dessa områden. I det här examensarbetet studeras responsen för avkortade betongbalkar.


Nyckelord:  Explosion, impulslast, SDOF, FE-analys, dynamisk respons, armerad betong, ekvivalent statisk last, dämpning, modsuperposition, avkortning

# Contents

IV

# Preface

This Master thesis is regarding the structural response for structures with different material responses when subjected to an explosion. The work has been carried out at the office of Reinertsen Sverige AB in Gothenburg during the period from June to October 2012. The Master thesis is a collaboration between Reinertsen Sverige AB and the Department of Structural Mechanics at Lund Institute of Technology, Lund University, Sweden.

We would like to express our gratitude toward Morgan Johansson, Reinertsen Sverige AB. He has helped us immensely throughout this Master thesis and has always been available for guidance. Special thanks also go to Sebastian Andersson and Hampus Karlsson at Reinertsen for their help with this Master thesis.

We would also like to thank the staff at Reinertsen Sverige AB in Gothenburg for making the time spent at the office a memorable experience.

Our supervisor at the Department of Structural Mechanics, Per-Erik Austrell has given us helpful comments and helped us with the layout and thanks go to him.

Furthermore, we thank our families for their support throughout our education.

Finally, we want to thank each other for having great discipline throughout the project and having worked hard during these very intense but educational months.

Gothenburg, October 2012

Mattias Carlsson and Robin Kristensson

# Notations

**Roman upper case letters**

| | |
|---|---|
| $A$ | Area |
| $A_s$ | Area of reinforcement |
| $C$ | Damping matrix |
| $E$ | Young's modulus |
| $E_c$ | Young's modulus for concrete |
| $E_s$ | Young's modulus for steel |
| $E_I$ | Young's modulus for reinforced concrete in stadium I |
| $E_{II}$ | Young's modulus for reinforced concrete in stadium II |
| $E_k$ | Kinetic energy |
| $E_{pl}$ | Initial Young's modulus for cracked reinforced concrete |
| $F$ | External force |
| $F_c$ | Force in concrete |
| $F_e$ | Equivalent force |
| $F_k$ | Characteristic pressure load |
| $F_s$ | Force in steel |
| $G$ | Shear modulus |
| $I$ | Moment of inertia |
| $I$ | Impulse |
| $I_I$ | Moment of inertia state I |
| $I_{II}$ | Moment of inertia state II |
| $I_k$ | Characteristic impulse |
| $I_z$ | Moment of inertia around z-axis |
| $K$ | Stiffness matrix |
| $L$ | Length |
| $M$ | Mass matrix |
| $M$ | Moment |
| $M_{el}$ | Maximum moment in elastic range |
| $M_{pl}$ | Ultimate moment |
| $M_{max}$ | Maximum moment |
| $M_{Rd}$ | Ultimate moment capacity |
| $P$ | Pressure |
| $P_0$ | Ambient air pressure |
| $P_{peak}$ | Peak pressure load |

| | |
|---|---|
| $Q$ | Equivalent static load |
| $Q_{el}$ | Elastic equivalent static load |
| $Q_{pl}$ | Plastic equivalent static load |
| $R$ | Internal resisting force |
| $R_{dyn}$ | Dynamic internal resisting force |
| $R_m$ | Maximum internal resisting force |
| $R_{sta}$ | Static internal resisting force |
| $T$ | Natural period |
| $W$ | Amount of energy |
| $W_e$ | External energy |
| $W_{el}$ | Elastic section modulus |
| $W_i$ | Internal energy |
| $W_{i,el}$ | Elastic internal energy |
| $W_{i,pl}$ | Plastic internal energy |
| $W_{i,ep}$ | Elasto-plastic internal energy |
| $W_k$ | Kinetic energy |
| $W_{pl}$ | Plastic section modulus |
| $W_{tot}$ | Total energy |
| $Z$ | Scaled distance |

**Roman lower case letters**

| | |
|---|---|
| $a$ | Acceleration |
| $\bar{a}$ | Mean acceleration |
| $c$ | Concrete cover |
| $c$ | Damping |
| $c_e$ | Equivalent damping |
| $c_p$ | Pressure wave velocity |
| $c_s$ | Shear wave velocity |
| $d$ | Effective depth of cross-section |
| $f_{cc}$ | Concrete compressive strength |
| $f_{cd}$ | Design value of concrete compressive strength |
| $f_{sy}$ | Yield stress for steel |
| $f_y$ | Yield stress |

| | |
|---|---|
| $f_{yd}$ | Design value of yield stress |
| $h$ | Height of cross-section |
| $i$ | Impulse intensity |
| $k$ | Stiffness |
| $k_e$ | Equivalent stiffness |
| $k_I$ | Stiffness state I |
| $k_{II}$ | Stiffness state II |
| $k_\lambda$ | Multiplying factor for allowed rotation capacity |
| $l_0$ | Distance from plastic hinge to zero moment |
| $m$ | Mass |
| $m_e$ | Equivalent mass |
| $p$ | Momentum |
| $q$ | Distributed load |
| $q$ | Modal coordinate |
| $r$ | Radius of reinforcement bar |
| $r$ | Real distance |
| $s$ | Reinforcement bar spacing |
| $t$ | Time |
| $t_a$ | Arrival time |
| $u$ | Direction |
| $u$ | Displacement |
| $\dot{u}$ | First derivative of $u$ with respect to time $t$, velocity |
| $\ddot{u}$ | Second derivative of $u$ with respect to time $t$, acceleration |
| $u_{el}$ | Elastic displacement |
| $u_{el,I}$ | Elastic displacement in stadium I |
| $u_{el,II}$ | Elastic displacement in stadium II |
| $u_{ep}$ | Elasto-plastic displacement |
| $u_{ep,el}$ | Elastic part of elasto-plastic displacement |
| $u_{ep,pl}$ | Plastic part of elasto-plastic displacement |
| $u_{max}$ | Maximum displacement |

X

| | |
|---|---|
| $u_{pl}$ | Plastic displacement |
| $u_s$ | Displacement of system point |
| $u_{tot}$ | Total displacement |
| $u_x$ | Displacement of wave in horizontal direction |
| $u_y$ | Displacement of wave in vertical direction |
| $v$ | Direction |
| $v$ | Velocity |
| $\bar{v}$ | Mean velocity |
| $v_s$ | Velocity in system point |
| $w$ | Direction |
| $w$ | Amount of explosive |
| $w$ | Width |
| $x$ | Coordinate |
| $x$ | Depth of compression zone |
| $x_{cg}$ | Distance to centre of gravity |
| $y$ | Coordinate |
| $z$ | Coordinate |
| $z$ | Internal lever arm for reinforcement |

**Greek upper case letters**

| | |
|---|---|
| $\Delta$ | Incremental |

**Greek lower case letters**

| | |
|---|---|
| $\alpha$ | Damping constant Rayleigh damping |
| $\alpha$ | Ratio between Young's modulus for steel and concrete |
| $\beta$ | Damping constant Rayleigh damping |
| $\varepsilon$ | Strain |
| $\varepsilon_{cu}$ | Ultimate concrete strain |
| $\varepsilon_{el}$ | Elastic strain |
| $\varepsilon_{pl}$ | Plastic strain |
| $\varepsilon_s$ | Steel strain |

| | |
|---|---|
| $\varepsilon_x$ | Horizontal strain |
| $\phi$ | Bar diameter |
| $\phi$ | Modal vector |
| $\gamma_c$ | Partial factor for concrete |
| $\gamma_s$ | Partial factor for steel |
| $\kappa$ | Curvature |
| $\kappa_c$ | Transformation factor for the damping |
| $\kappa_{cF}$ | Transformation factor with regard to the damping and the external load |
| $\kappa_k$ | Transformation factor for the internal force |
| $\kappa_F$ | Transformation factor for the external load |
| $\kappa_m$ | Transformation factor for the mass |
| $\kappa_{mF}$ | Transformation factor with regard to the mass and the external load |
| $\lambda$ | Shear slenderness |
| $\lambda$ | Wave length |
| $\theta$ | Support rotation |
| $\theta_{pl}$ | Plastic rotation |
| $\theta_{rd}$ | Design value of allowed plastic rotation |
| $\rho$ | Density |
| $\rho$ | Radius of curvature |
| $\sigma$ | Stress |
| $\sigma_s$ | Stress in reinforcement |
| $\sigma_x$ | Horizontal stress |
| $\sigma_y$ | Yield stress |
| $\upsilon$ | Poisson's ratio |
| $\omega$ | Angular frequency |
| $\xi$ | Damping ratio |
| $\xi$ | Factor |
| $\xi$ | Relative error |

# 1 Introduction

## 1.1 Background

Explosions are extreme loads that need to be considered in the design of structures for various applications. Except from apparent cases, such as military installations and civil defence shelters, design with regard to explosions is required for instance in the processing industry and for tunnels. In a world where the common knowledge of how to develop bombs and the level of threat from terrorist attacks grow bigger, it is also of interest to make sure that potential targets of terrorist attacks can withstand an explosion. Stockholm, December 2010, and Oslo, July 2011, are just two examples of recent events where terrorist attacks have involved explosions in city environment.

It is also necessary to be able to analyse a structure subjected to an accidental explosion. A structure subjected to such an accident may very well be thinner than and not at all as strong as a structure designed to withstand an explosion. Whatever the cause might be and the strength of a structure the devastation can be considerable.

Today, the knowledge of how to design buildings to withstand the effect of explosions and other impact loads is limited. The Swedish Fortification Agency (in Swedish; Fortifikationsverket) used to be the ones in Sweden with the most experience with regard to explosions, and they produced handbooks that are to be used when designing but they are difficult to follow and understand if one is not well-read in the subject. The standards of how to design with regard to explosions are far from perfect and therefore MSB (Myndigheten för Samhällsskydd och Beredskap) has for many years been working to increase the knowledge within the field of physical protection. Their goal is also to inform and enlighten today's engineers and increase their understanding of explosions. The engineers of this decade need to become more familiar with dynamic and especially impulse loaded structures.

This project is a continuation of four previous Master theses carried out by Nyström (2006), Ek and Mattsson (2009), Augustsson and Härenstam (2010) and Andersson and Karlsson (2012), in which the behaviour of concrete beams and slabs due to impulse loads were studied.

## 1.2 Aim

The aim of this Master thesis is to put together information about available design approaches for impact loading on concrete structures. It will be a complement to previous Master theses in this field.

Since the response for a structure subjected to a dynamic load differs from that of a static load, one objective is to investigate if the moment is, at any time, too high during the dynamic loading.

The damping of the structure will also be an important aspect of this Master thesis. Will the damping have a great impact on the results? When neglecting the damping one will obtain results on the safe side but when a more detailed analysis is conducted the damping could very well be important.

An objective is to improve the SDOF-model so it can be more reliable. Often the damping has been neglected but when it is included in the SDOF-analysis the transformation factor for the damping needs to be determined.

Curtailment of the reinforcement (shortened reinforcement) will also be investigated. Structures intended to withstand explosions should be carried out with no reinforcement curtailment. However, this is not necessarily the case for a civil building. Hence, what will happen when the explosion hits a civil building? Will the moment capacity be sufficient to carry this kind of load?

## 1.3    Method

A literature study was made mainly from reports and previous Master theses in the subject to be able to compile existing knowledge and to explain the underlying theory of explosions, material responses, dynamics and transformation of a structure to an SDOF-system.

An SDOF-model was made in Matlab for calculating the displacements, moments, energies and internal resistance for an arbitrary beam. The results for a certain studied beam were compared to the maximum values from hand calculations based on a characteristic impulse and a static equivalent load. This was done for a linear elastic, ideal plastic and elasto-plastic material response.

Because there were no possibilities in actually testing the studied beam and comparing the theoretical results to collected empirical data, non-linear FE-analyses were made with the FEM software ADINA (2011), which were assumed to represent the true behaviour.

The beam was modelled with 30 two-dimensional beam elements, which means that there were limitations to the accuracy of the results, so therefore they have been critically evaluated.

## 1.4    Limitations

No other material than reinforced concrete was analysed in this Master thesis. However, the methods can very well be used for different materials with certain changes. The material response is approximated with a linear elastic response, a plastic response and an elasto-plastic response. These material responses have previously been shown to be good approximations for this kind of analysis.

When the energy is calculated in the SDOF-model the transformation factors used does not vary in time which.

This Master thesis does not cover any effects of shear as the time was limited and there were other subjects of more interest. The shear force has also been studied thoroughly in previous Master thesis by Andersson and Karlsson (2012). The analyses are limited to simply supported beams without initial strain/stress and no torsion is regarded.

The loading is chosen as an impulse load that can be interpreted as an explosion, where the explosion is limited to a detonation, which means that explosions of gas clouds are left out. Only the primary effects (shock waves) of explosions will be studied, which means no regard is taken to shrapnel or nearby buildings falling.

## 1.5    Outline of the report

The report is divided into Background theory (Chapter 2), Structural response of a concrete beam (Chapter 3), Initial analyses and verification of the modelling (Chapter 4), Mode superposition and damping (Chapter 5),

Curtailment (Chapter 0) and Final remarks (Chapter 7).

Chapter 2 provides an introduction to explosions, material responses and basic dynamics needed to explain the results in upcoming sections. The method for transforming a real structure into a single degree of freedom-system is also presented.

Chapter 3 is the introduction to the reinforced concrete beam mainly studied in this Master thesis. The properties and cross-section for the beam is shown along with different load cases, and simple hand calculations for displacements, moments and energies are made. It is also covered how the beam is modelled using the finite element method, which is used for further analysis of the beam.

Chapter 4 shows the results of the finite element analysis for different material responses in terms of displacement, moment and energy compared to the single degree of freedom analysis and hand calculations made in the previous section. This section is important for the understanding of the structural response due to an explosion.

Chapter 5 describes how to simplify the dynamic analysis of a structure by only using the necessary modes of vibration. The effect of damping is regarded to present the importance of such.

Chapter 0 studies the possibilities of curtailment of concrete beams when subjected to impact loading. This is investigated to determine whether problems will arise due to the early moment development near the supports.

Chapter 7 concludes the Master thesis and gives recommendations for further studies within this field.

# 2    Background theory

In order to understand as much as possible of this Master thesis, basic background theory is provided. The background theory will not cover everything and is often merely an introduction of different subjects. The reader is referred to other given literature for more information on the subjects. Since this Master thesis will deal with structures exposed to explosions the reader needs to be familiar with the effects of an explosion. It is also necessary that the reader understands how different materials behave when loaded. The statics and dynamics are also important subjects needed to be familiar with. In addition to this, an introduction of the SDOF-system is made.

## 2.1    Explosions

Explosions give rise to completely different loads compared to the more often used static loads. Today's engineers are more used to work with static loads but it is necessary to study the dynamic response from explosions. Some basic theories in the field of explosions will be presented and the reader is referred to Johansson and Laine (2007) for more comprehensive information.

### 2.1.1    What is an explosion?

An explosion is a sudden release of energy with a related volume expansion. The explosion will lead to an increase of light and temperature but above all a high increase of pressure. For an explosion in midair the pressure will create a pressure wave which will advance in a spherical motion originating from the point of source, see Figure 2.1. The pressure will decrease with increasing distance from the source, and hence, the distance is of utmost importance when regarding explosions. The time it takes for the pressure wave to reach the object is referred to as arrival time, $t_a$, and is a way to relate the distance from the explosion to a certain object.



Explosion centre

Pressure decreases further
away from the centre
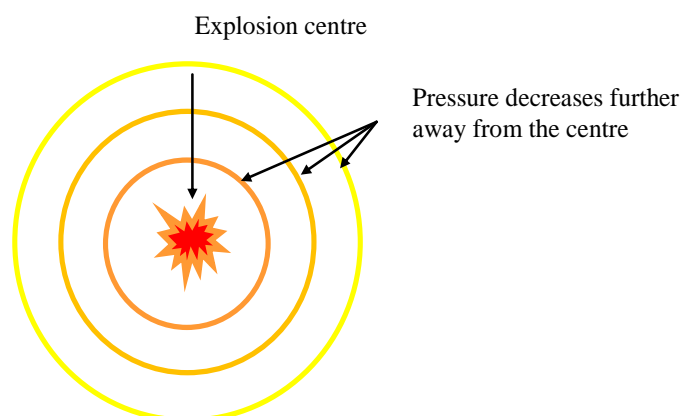
*Figure 2.1.    An illustration of how the energy propagates outwards from the source of the explosion.*

An explosion can be idealized with two phases, one positive and one negative phase. The ordinary atmospheric pressure, which is referred to as ambient air pressure $P_0$, is at a temperature of 15°C approximately 101,3 kPa. The positive phase is when the

pressure is increased to a pressure higher than $P_0$. Due to the pressure wave the air will move outwards creating a partial vacuum behind it, lack of air, which is referred to as the negative phase. The pressure is here lower than the ambient air, and thus perceived as a negative pressure. This development can be described with a pressure-time relationship, as schematically shown in Figure 2.2. The overpressure in the positive phase is considerably higher than in the negative phase. Further, the duration in the former is shorter than in the latter, resulting in an impulse of the negative phase that is somewhat larger than in the positive phase, approximately ten percent. According to Johansson and Laine (2007) the pressure-time relationship is often simplified with a linear decreasing pressure and the negative phase neglected due to its minor influence, see Figure 2.3.
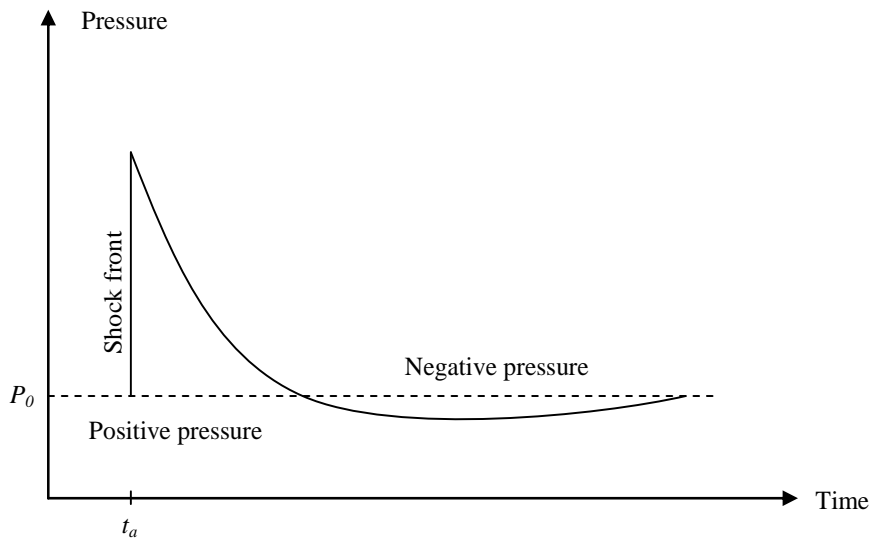
*Figure 2.2.    An idealised shock wave from an explosion. The high amplitude positive phase is followed by a longer negative phase with lower amplitude.*
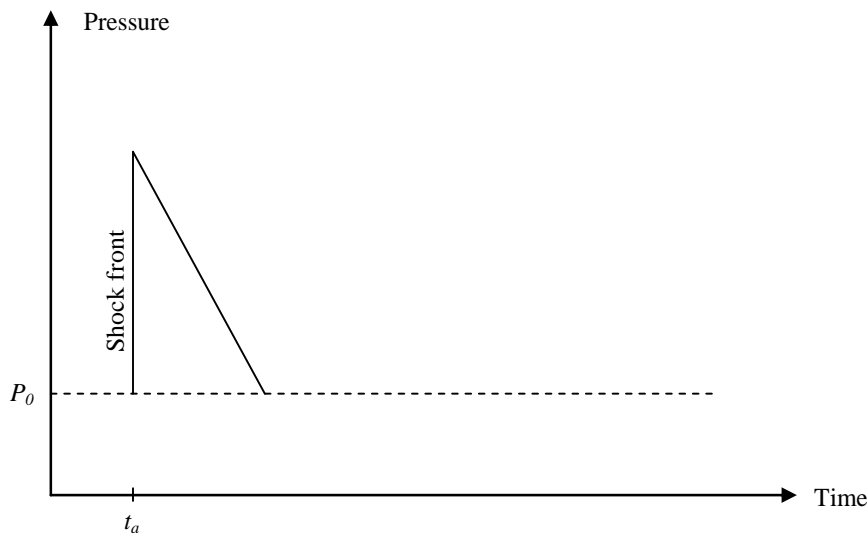
*Figure 2.3    A simplified shockwave assumes linearly decreasing pressure and neglects the negative phase.*

When looking at blast loads it is of interest to compare the load velocity for different kinds of loading. In Figure 2.4 a comparison has been made between different types of load cases. The reader can see that the blast load is $10^7$-$10^8$ faster than a static load.



| Creep | Static | Earthquake | Impact | Blast load |

| 0.001 | 0.01 | 0.1 | 1 | 10 | 100 | 1000 | $10^4$ | $10^5$ | $10^6$ | $10^7$ | $10^8$ |
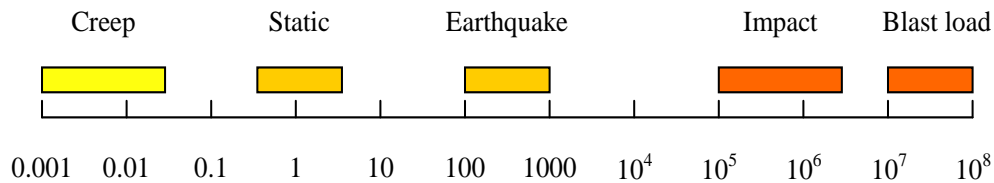
*Figure 2.4    Difference in load velocity between different types of loading, the values are obtained in relation to static load.*

The ignition of an explosive is usually divided into high and low degree of explosion. The higher degree of explosion is referred to as detonation and is the type of explosion used in this Master thesis. A detonation will occur when the ignition of the source of explosion occurs in supersonic speed, i.e. velocity above speed of sound, which results in a high degree of explosion due to the very fast development. This is the case for e.g. TNT and ANFO, where TNT is the commonly known explosive, Trinitrotoluene, which is used as a standard measure of strength of bombs and other explosives. ANFO is a worldwide industrial bulk explosive which consist of mainly ammonium nitrate and less than 10 percent fuel oil. Since ANFO is both low in cost and easy to mix it is widely used in civil explosions, such as mining and demolition, even though it lacks in water resistance and performance in small spaces and is less explosive. Because the ingredients to ANFO are easy to acquire it has also been used in several terrorist attacks. However, the term is often used loosely in media in describing IEDs, improvised explosive devices, in cases of fertilizer bombs. For instance, the bomb used in the Oslo bombing on July 22, 2011 was a 950 kg fertilizer bomb of type ANNM, ammonium nitrate and nitro methane, which increases demolition power 10-30 percent over plain ANFO, according to Bloomberg (2011).

The other alternative for an explosion is referred to as deflagration. This is a low degree of explosion because the ignition is of subsonic nature, velocity below speed of sound. An example of deflagration is the ignition of a gas cloud.

### 2.1.2    Effects of explosions

There are certain concepts that the reader needs to be familiar with to understand the variation in magnitude and duration for a single explosion. A simplified case can be referred to with four basic concepts which are reflection, mirroring, confinement and diffraction. Reflection occurs when the pressure wave hits a stiffer medium such as a wall. According to Johansson and Laine (2007) the pressure of the wave can be increased by up to 20 times due to reflection. This phenomenon is important to keep in mind when dealing with explosions close to a building, and especially in city environment.

Mirroring is a kind of reflection. It occurs when the explosion detonates close to a reflecting surface, see Figure 2.5. In theory the magnitude can double but due to some energy loss to the ground or surface, the mirroring factor will decrease. According to Johansson (2000) a mirror factor of 1.8 is often used.
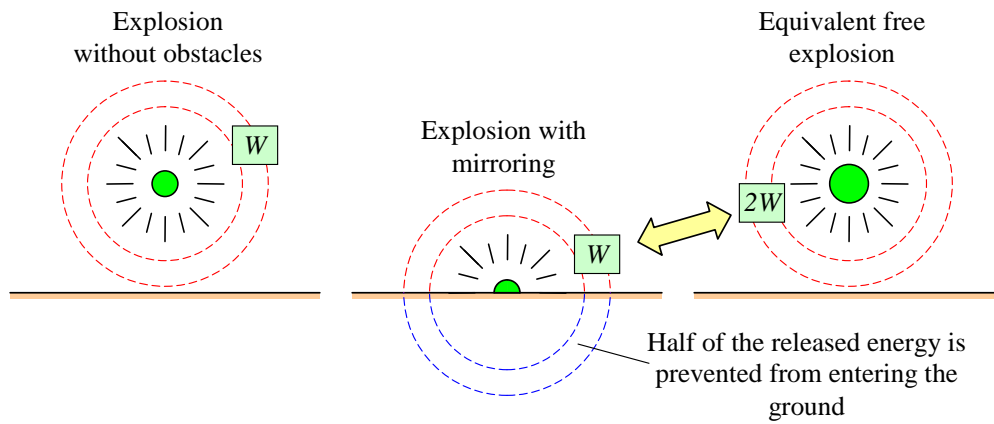
*Figure 2.5    Schematic figure illustrating the ideal mirroring.*

The explosion is often sought to act with high energy in only one direction, which can be achieved by confining the explosive. The reflections of the explosive within the confinement delay the energy dispersal, and thereby increase the impact.

Diffraction is another important phenomenon. This occurrence will give rise to change of direction for the wave front. In that way a wave front can reach behind and past buildings and objects, see Figure 2.6. This is a complex phenomenon but important to regard when designing structures.
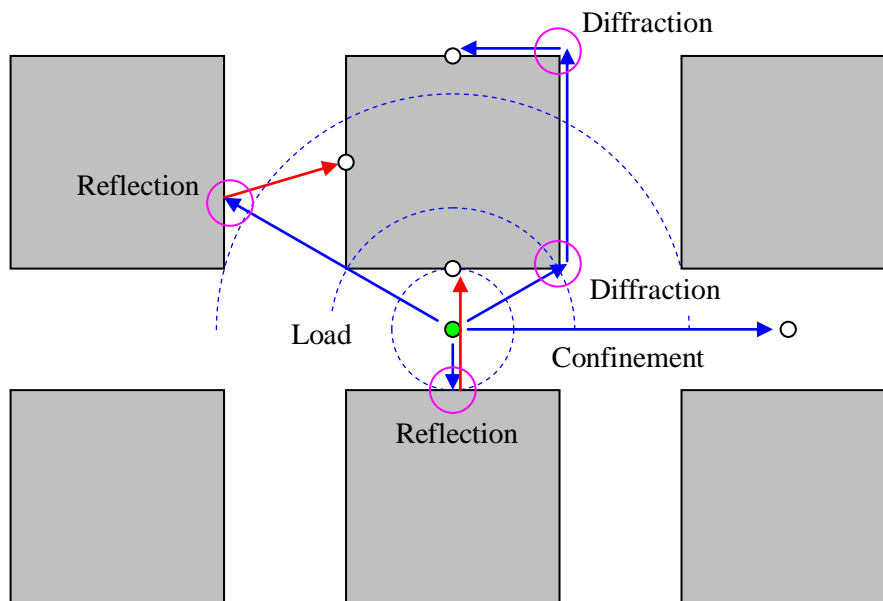


*Figure 2.6    Clarification of the shock wave phenomena that occurs in urban environment. Johansson and Laine (2007)*

The distance from the point of source is a very important factor to consider when dealing with explosions. There are scale laws that are used to compare different loads and distances. For the case when the detonation occurs with free expansion on all sides, thus allowing a spherically expanding wave front, the scaled distance can be expressed as

$$Z = \frac{r}{W^{1/3}} \qquad\qquad (2.1)$$

10

where *r* is the real distance and *W* is the energy amount (generally referred to the equivalent amount of kg TNT). For other cases than explosions in mid air the reader is referred to Johansson and Laine (2007).

Experiments have been made to determine the equivalent amount of a specified explosive to the amount of TNT. Usage of Table 2.1 is a fast way to do this comparison and it can be beneficial to combine with Equation (2.1). The amount of energy released, *W*, will then be referred to as

$$W = w \cdot equivalent\ weight \tag{2.2}$$

where *w* is the amount of explosive.

*Table 2.1 Equivalent weight of various types of explosive where TNT is used as reference. Note that different equivalent weights are obtained for the pressure and impulse. From ConWep (1992).*

| Explosive | Equivalent weight | |
|---|---|---|
| | Pressure | Impulse |
| ANFO [1] | 0.82 | 0.82 |
| Composite A-3 | 1.09 | 1.07 |
| Composite B | 1.11 | 0.98 |
| Composite C-4 | 1.37 | 1.19 |
| H-6 | 1.38 | 1.15 |
| HBX-1 | 1.17 | 1.16 |
| Pentolite | 1.42 | 1.00 |
| RDX | 1.14 | 1.09 |
| *TNT* | *1.00* | *1.00* |
| Tritonal | 1.07 | 0.96 |

[1] A mixture of diesel and fertilizer.

The so called Archive bomb is an example of an explosion used by MSB to describe a weapon effect in the design of civil defence shelters in Sweden, Johansson and Laine (2007). This bomb contains 125 kg of TNT and detonates 5 m away from the studied target, affecting it with a uniform pressure that decreases with time. The blast is assumed to have a spherical spreading, with a peak pressure of 5000 kPa and an impulse intensity of 2800 Ns/m². When assuming a triangular load the corresponding load duration will for this detonation be 1.12 ms. This is a relatively strong explosion and ordinary buildings will not be able to withstand such an explosion.

There are guidelines for how much TNT that can be contained in different explosion sources, see Table 2.2. These guidelines have been compiled in order to quickly be able to draw conclusions of an explosion.

*Table 2.2    Definition of the explosive amount for different types of containers where the quantity is indicated by the equivalent amount of TNT. Johansson and Laine (2007).*

| Explosion source | | Amount TNT [kg] | Limit for damage to the eardrum [1] | Slight damage to residental houses [2] | Limit for window damage [3] |
|---|---|---|---|---|---|
| Pipe bomb | | 2.3 kg | - | 21 m (8 kPa, 26 Pas) | 259 m (0.3 kPa, 2 Pas) |
| Suitcase bomb | | 23 kg | - | 46 m (8 kPa, 56 Pas) | 564 m (0.2 kPa, 4 Pas) |
| Small passenger car | | 227 kg | 30 m (44 kPa, 370 Pas) | 98 (8 kPa, 120 Pas) | 457 m (1 kPa, 25 Pas) |
| Big passenger car | | 455 kg | 38 m (44 kPa, 460 Pas) | 122 (8 kPa, 150 Pas) | 534 m (1 kPa, 34 Pas) |
| Van/ Minivan | | 1 818 kg | 61 m (43 kPa, 720 Pas) | 195 (8 kPa, 240 Pas) | 838 m (1 kPa, 54 Pas) |
| Small truck | | 4 545 kg | 91 m (37 kPa, 900 Pas) | 263 (8 kPa, 330 Pas) | 1143 m (1 kPa, 73 Pas) |
| Truck without trailer | | 13 636 kg | 137 m (34 kPa, 1250 Pas) | 375 (8 kPa, 480 Pas) | 1982 m (1 kPa, 87 Pas) |
| Truck with trailer | | 27 273 kg | 183 m (31 kPa, 1490 Pas) | 475 (8 kPa, 600 Pas) | 2134 m (1 kPa, 130 Pas) |

[1] Lethal air blast range
[2] Building evacuation distance
[3] Outdoor evacuation distance

## 2.2 Materials

When studying the response of loaded structures, the behaviour of the material is often complex but can be simplified with help of linear elastic, ideal plastic and elasto-plastic response. These simplifications usually give close approximations to the actual material response. Often these approximations are seen as potential sources of error but since comparisons between different methods are made, all using these approximations, it is disregarded in this Master thesis. In this section an introduction to the different responses are presented.

### 2.2.1 Linear elastic

For linear elastic behaviour there is a linear relation between stress and strain, as can be seen in Figure 2.7. The strain increases with increased stress and after unloading the strains will go back to zero. This means that the strain is proportional to the stress for materials with linear elastic behaviour and the stress, $\sigma$, can be expressed with Hooke's Law:

$$\sigma = E \cdot \varepsilon \tag{2.3}$$

where $E$ is the Young's modulus and $\varepsilon$ is the strain.
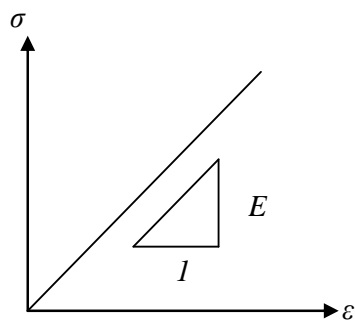


*Figure 2.7    Stress, σ, as function of strain, ε, for linear elastic materials.*

When a structure of linear elastic material is deformed it will gain an internal resisting force, *R*, proportional to the displacement, *u,* as can be seen in Figure 2.8. This relation is described by

$$R = k \cdot u \tag{2.4}$$

where $k$ is the structural stiffness.
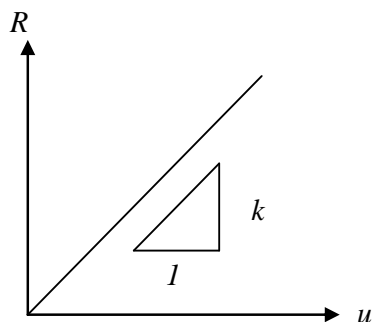


*Figure 2.8.    Structural response, R, as function of displacement, u.*

13

A simply supported beam with linear elastic material response will deform, when subjected to a uniformly distributed load, with the shape shown in Figure 2.9.
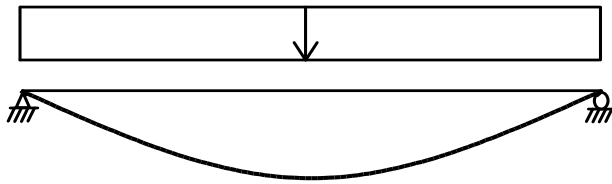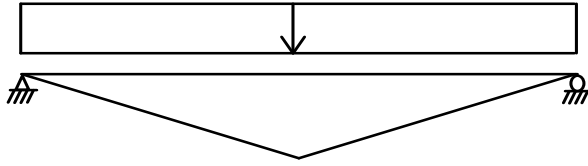


*Figure 2.9.    Deformation shape for simply supported beam when using linear elastic material and subjected to a uniformly distributed load.*

## 2.2.2    Ideal plastic

For materials with ideal plastic behaviour the deformations are zero until the stress reaches the material yield stress. When this happens the deformations will occur, as seen in Figure 2.10. In theory these deformations are infinite but in reality there are limits such as the plastic rotation capacity for beams subjected to a bending moment and the ultimate strain limit for tensioned reinforcement bars. With the external static load, $F$, on the structure, the internal force, $R$, can be expressed as

$$R = \begin{cases} F \text{ for } F < R_m \text{ and } u = 0 \\ R_m \text{ for } F \geq R_m \text{ for all } u > 0 \end{cases} \tag{2.5}$$

where $R_m$ is the maximum internal force.
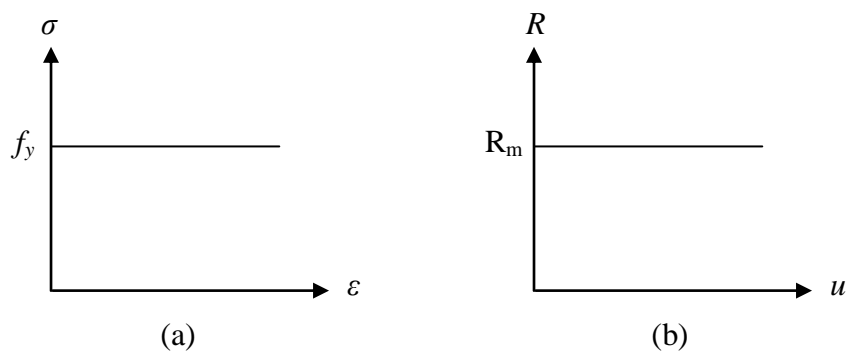


*Figure 2.10    Ideal plastic material response, where (a) is the material response; (b) is the structural response.*

A beam with ideal plastic material response will deform with the shape shown in Figure 2.11, when subjected to a uniformly distributed load.

*Figure 2.11. Deformation shape for a simply supported beam when using ideal plastic material subjected to a uniformly distributed load.*

## 2.2.3 Elasto-plastic

The elasto-plastic material behaviour is a combination between linear elastic behaviour and ideal plastic behaviour, see Figure 2.12. The material is fully reversible while in its elastic phase but when the load reaches the yield limit it will initiate permanent deformations. When unloaded, the deformations will decrease, following a curve parallel to the linear elastic curve. If the body is loaded again, the deformations will follow the elastic behaviour until the yield limit is reached and the plastic deformations will continue where it last ended. With the external load, $F$, on the structure, the internal force, $R$, can be expressed as

$$R = \begin{cases} ku_{el} & \text{for } F < R_m \\ R_m & \text{for } F \geq R_m \end{cases} \tag{2.6}$$

where $u_{el}$ is the elastic displacement.
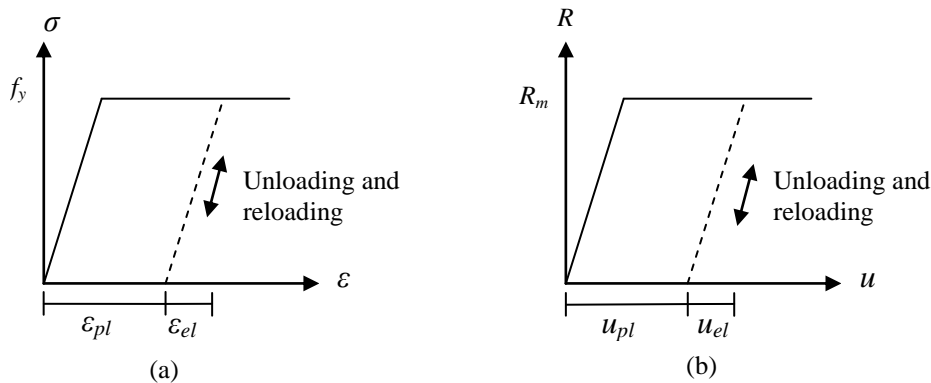


*Figure 2.12. Elasto-plastic case (a) material response; (b) structural response.*

## 2.2.4 Theory of plasticity and plastic hinges

When looking at a beam with rectangular cross-section subjected to pure bending, it is assumed for both theory of elasticity and theory of plasticity that the stress and strain is symmetric and linearly distributed over the height of the cross-section, see Figure 2.13. While the stresses in the beam are below the yield stress the cross-section will have an elastic response according to Hooke's Law, and the elastic moment can be described as

$$M_{el} = \frac{\sigma \cdot I}{h/2} \qquad\qquad (2.7)$$

where $\sigma$ is the stress in the outer fibre and $I$ is the moment of inertia for the cross-section. For a rectangular cross-section this is calculated as

$$I = \frac{wh^3}{12} \qquad\qquad (2.8)$$

where $w$ is the width and $h$ is the height of the cross-section. Combining Equation (2.7) and (2.8) the elastic moment can be written as

$$M_{el} = \sigma \cdot W_{el} \qquad\qquad (2.9)$$

where

$$W_{el} = \frac{wh^2}{6} \qquad\qquad (2.10)$$

When the stress reaches the yield stress $f_y$ the cross-section will start to yield. If the load is further increased the beam enters an elasto-plastic behaviour until the whole cross-section has yielded, see Figure 2.13. When the elasto-plastic state is reached only the inner elastic part will follow Hooke's Law. For the plastic part the strain response stays linear but the stresses are modified to not exceed the yield limit.

Just before the whole cross-section yields the maximum moment capacity, $M_{pl,}$ is reached and according to Isaksson *et al*. (2010) for rectangular cross-sections it can be described as

$$M_{pl} = f_y \cdot W_{pl} \qquad\qquad (2.11)$$

where

$$W_{pl} = \frac{wh^2}{4} \qquad\qquad (2.12)$$
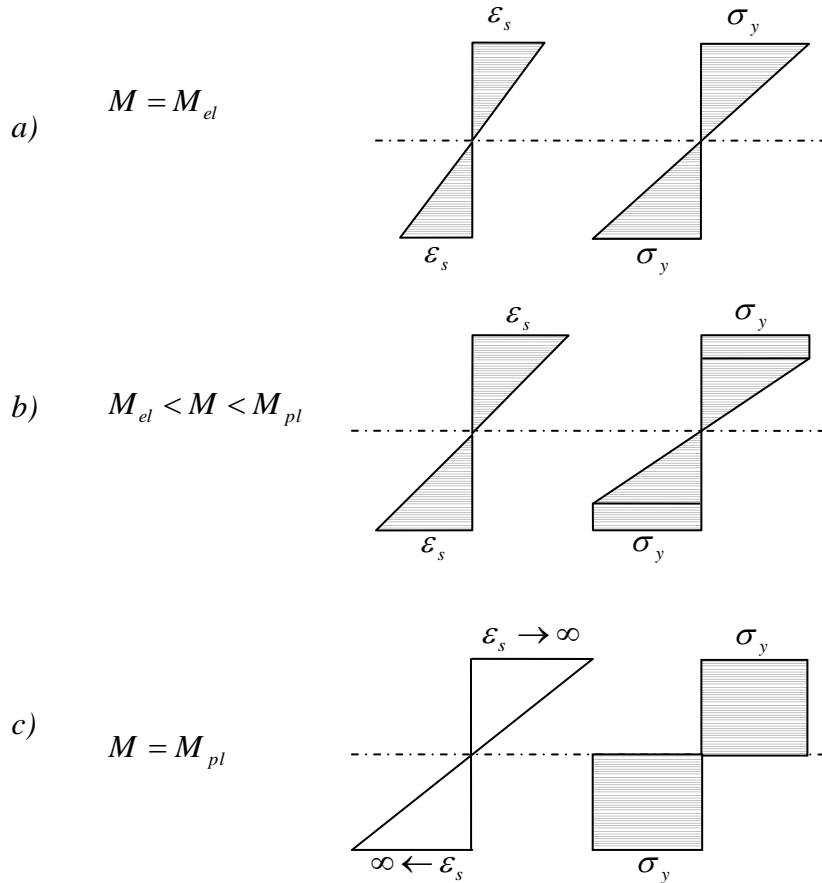
*Figure 2.13. Stress- and strain distribution for (a) before yielding starts; (b) part of the cross-section is yielding; (c) the whole cross-section is yielding (ultimate moment capacity).*

When the beam reaches its full plastic capacity the majority of deformations will occur in the most strained area of the beam. The moments and curvature of this small area will be large in comparison to the rest of the beam and this will cause a local plastic rotation in the area. The small deformable area where this large curvature is developed is called a plastic hinge, and the moments in the plastic hinge are assumed to be $M_{pl}$. For statically determined systems only one plastic hinge will develop, and a mechanism is formed. For statically undetermined systems of order $n$ there will be $n+1$ plastic hinges before the mechanism is formed. This is illustrated in Figure 2.14. If the beam is subjected to a dynamic load more plastic hinges can be formed.
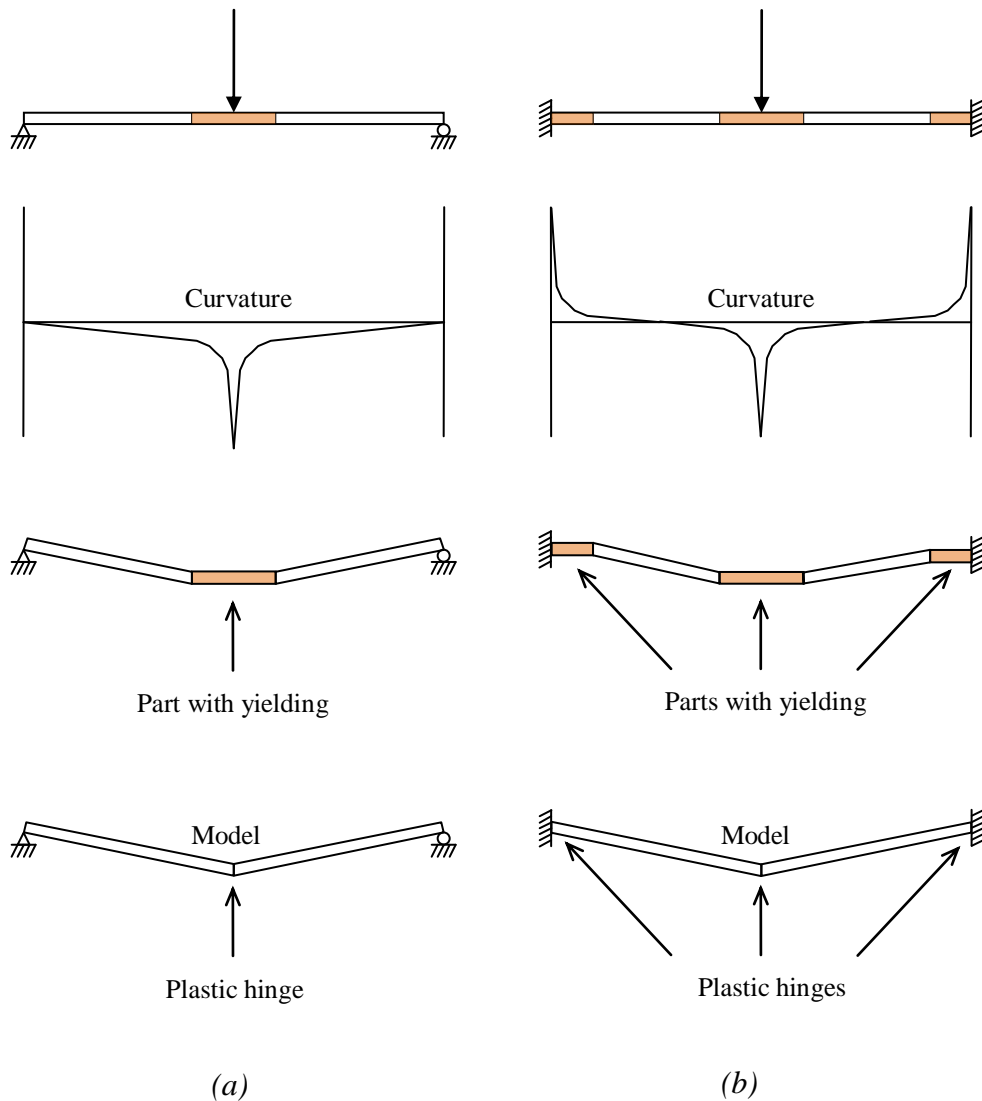
*Figure 2.14.  Schematics of plastic hinges for a (a) simply supported beam; (b) fixed beam, Nyström (2006).*

After the plastic hinge has been developed the beam can still be deformed. How much, though, is determined by the plastic rotation capacity.

## 2.2.5  Plastic rotation capacity

Rotation capacity refers to the yield capacity during bending and is measured in the maximum angular change that a plastic hinge can go through while keeping the maximum moment capacity. This means that when a plastic or elasto-plastic material reaches its yield stress it can deform further until the maximum rotation capacity is reached and failure occurs.

For concrete members there are several methods of determining the rotational capacity, but they may provide different results. According to Johansson (1997) one of the reasons may be because of the significant difference in steel properties used in reinforcement bars over the last decades.

From Eurocode 2, CEN (2004), the method of estimating the maximum allowed rotation capacity is acquired from a diagram with regard to the quality of concrete, reinforcement class and the ratio between the compressed zone $x$ and the effective depth $d$, as seen in Figure 2.15.
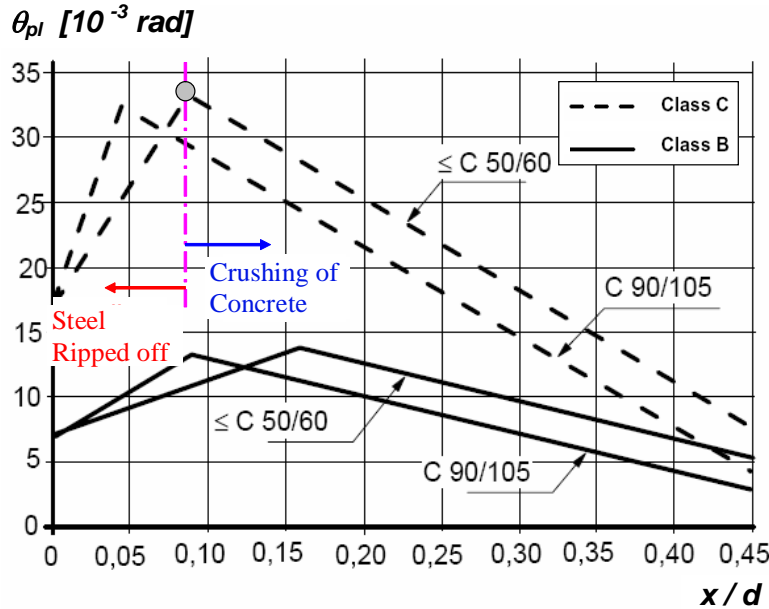


*Figure 2.15. Diagram based on Eurocode 2 CEN (2004) describing maximum allowed plastic rotation.*

The lines in the Figure 2.15 are based on a shear slenderness $\lambda=3.0$, where $\lambda$ is given by

$$\lambda = \frac{l_0}{d} \tag{2.13}$$

where $l_0$ is the length between the point of zero moment and the plastic hinge and $d$ is the effective depth to the reinforcement.

If $\lambda$ has values other than 3, the rotation capacity should be multiplied with a factor

$$k_\lambda = \sqrt{\frac{\lambda}{3}} \tag{2.14}$$

in the following manner:

$$\theta_{rd} = k_\lambda \cdot \theta_{pl} \tag{2.15}$$

## 2.3 Dynamics

To fully understand how an explosive load affects a structure it is important to look at the dynamic conditions. While structures are usually designed to withstand static loads for infinite load time, an explosion will affect the structure with high pressure during a short duration of time. This means that even though the pressure from the explosion is much higher than the pressure of the static load the structure is designed for, the structure might still withstand. When designing structures from a dynamic perspective it is therefore important to compare the energy from the explosion to the energy required for the structure to collapse. The basics of dynamics are given in this section so that the reader may understand this concept of designing.

### 2.3.1 Kinematics

#### 2.3.1.1 Velocity

The definition of velocity is change of displacement over time, i.e. if an object moves from $u_0$ to $u_1$ during time $t_0$ to $t_1$ the mean velocity of that object is expressed as

$$\bar{v} = \frac{u_1 - u_0}{t_1 - t_0} \tag{2.16}$$

By letting the time step be infinitesimal the change in motion will also be infinitesimal and the velocity at time $t$ can be determined as

$$v(t) = \frac{u_1 - u_0}{t_1 - t_0} = \frac{du}{dt} = \dot{u} \tag{2.17}$$

#### 2.3.1.2 Acceleration

The definition of acceleration is the change of velocity over time, which means the mean acceleration is defined as

$$\bar{a} = \frac{v_1 - v_0}{t_1 - t_0} \tag{2.18}$$

In the same way as for velocity, if the time step is infinitesimal the change of velocity will also be infinitesimal and the acceleration at time $t$ can be determined as

$$a(t) = \frac{v_1 - v_0}{t_1 - t_0} = \frac{dv}{dt} = \ddot{u} \tag{2.19}$$

### 2.3.2 Kinetics

#### 2.3.2.1 Force and Pressure

According to Newton's second law a force $F$ is defined as the acceleration of a mass:

$$F = m \cdot a \tag{2.20}$$

where $m$ is mass and $a$ is acceleration.

The pressure $P$ is defined as the force $F$ over an area $A$:

$$P = \frac{F}{A} \tag{2.21}$$

### 2.3.2.2 Momentum, impulse and impulse intensity

The momentum, $p$, of an object is defined as the objects mass $m$ times its velocity $v$:

$$p = mv \tag{2.22}$$

If the object is subjected to a force $F$ from time $t_0$ to $t_1$ the difference in momentum can be written as

$$\Delta p = \int_{t_0}^{t_1} F(t)dt \tag{2.23}$$

If an object is already moving with velocity $v_0$ and momentum $p_0$ when it is subjected to the force the new momentum $p_1$ can be written as

$$p_1 = p_0 + \Delta p \tag{2.24}$$

where $\Delta p$ is the so called impulse $I$. By insertion of Equation (2.19) and (2.20) in (2.23) the impulse can be rewritten as

$$I = \int_{t_0}^{t_1} F(t)dt = \int_{t_0}^{t_1} ma(t)dt = m\int_{t_0}^{t_1} a(t)dt = mv \tag{2.25}$$

Since shockwaves are measured in pressure the impulse from an explosion can also be written as

$$I = A\int_{t_0}^{t_1} P(t)dt \tag{2.26}$$

The intensity $i$ of the impulse can be described as an impulse acting on an area, or the pressure over time, as

$$i = \frac{I}{A} = \int_{t_0}^{t_1} P(t)dt \tag{2.27}$$

For the idealized shockwave in Figure 2.16 the impulse intensity is illustrated as the area under the pressure-time graph.
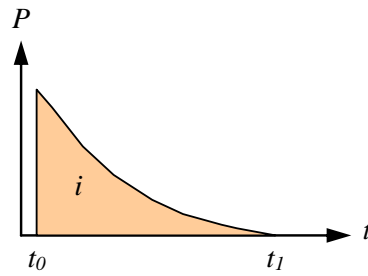
*Figure 2.16   The impulse intensity i is the area under the pressure-time curve.*

Since the impulse is defined as the area times the force over time there are two extreme cases for the impulse intensity. Either the pressure is infinitely high for an infinitesimal time or the force is constant for an infinitely long time, see Figure 2.17. The first case with the infinitely high pressure is called the characteristic impulse $I_k$ and the latter is called the pressure load, $F_k$.
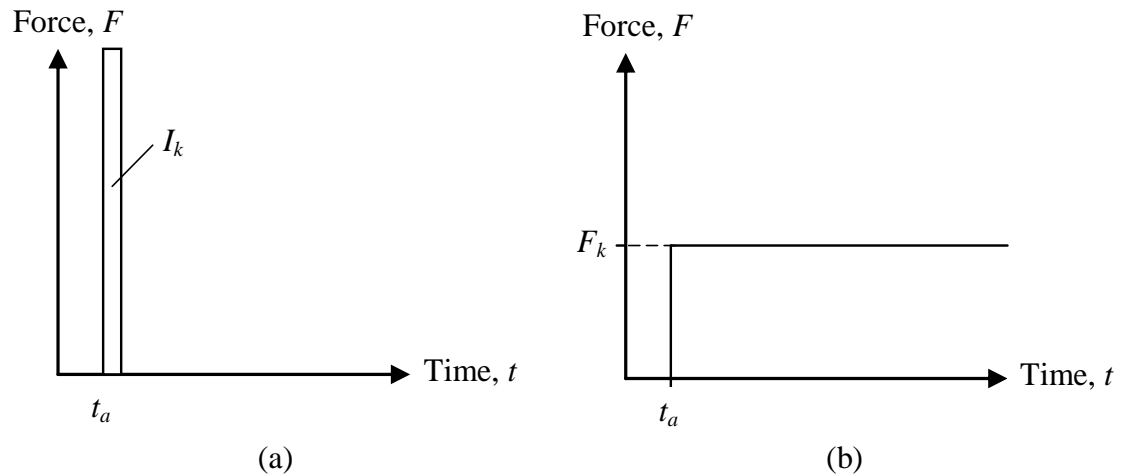


*Figure 2.17   Illustration of extreme dynamic cases starting at time $t_a$:*
            *(a) characteristic impulse, $I_k$ and (b) characteristic pressure load, $F_k$.*

### 2.3.3   Work

The term work refers to the amount of energy required to move a body subjected to a force. Work can be expressed either in potential or kinetic energy, $W_k$, and is usually divided into internal work, $W_i$, and external work, $W_e$, which is a useful tool for studying the response of a structure subjected to a load. In a closed system all energies are said to be conserved, which means no energy will be added or lost from the system but only transformed. This means, according to work equilibrium:

$$W_e = W_i + W_k \tag{2.28}$$

In reality, though, there will always be energy losses due to friction and heat development, i.e. the damping of the system.

22

### 2.3.3.1 External work

External work refers to either the external forces that move the body through space or as the impact transferring kinetic energy into potential energy in the body. The kinetic energy $E_k$ of a body with mass is given by the equation

$$E_k = \frac{mv^2}{2} \tag{2.29}$$

where $m$ is the mass and $v$ is the velocity.

By inserting Equation (2.25) in (2.29) the kinetic energy and external work for a body subjected to an impulse can be expressed as

$$W_e = E_k = \frac{I^2}{2m} \tag{2.30}$$

When transferring kinetic energy into potential energy in a structure the stiffness will induce a resistance that increases with time, but internal work induced during the duration of the load is negligible compared to the external work. Therefore Equation (2.30) is only correct when the load duration and resistance is infinitesimal, i.e. when the impulse $I$ corresponds to the characteristic impulse $I_k$:

$$W_e = E_k = \frac{I_k^2}{2m} \tag{2.31}$$

Since the resistance increases with time, the structure will have time to absorb more energy from a long impulse, and hence, the external work will decrease for a longer impulse load than for the characteristic impulse. This is illustrated in Figure 2.18.
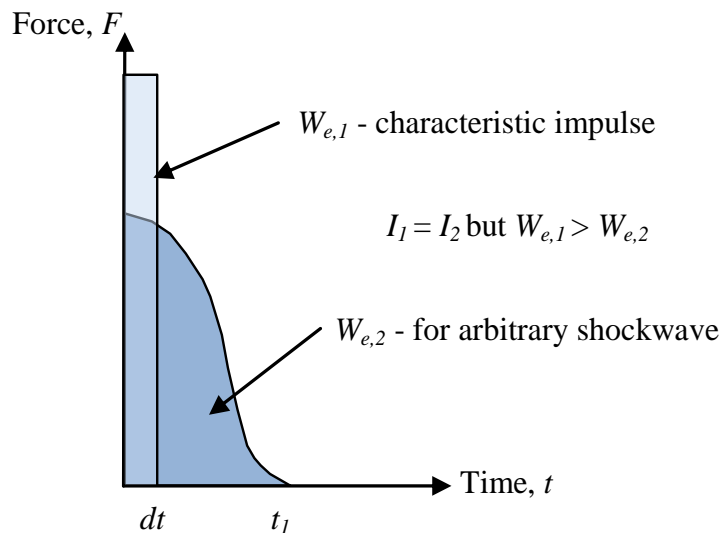


*Figure 2.18   Different external work on the structure for the same total impulse but with different durations.*

### 2.3.3.2 Internal work

The internal work arises as a response to the load and is dependent of the structure's geometry and material behaviour. Although depending on which type of material the structure has the properties for the internal work will differ but the final value will always be the same, see Figure 2.19.
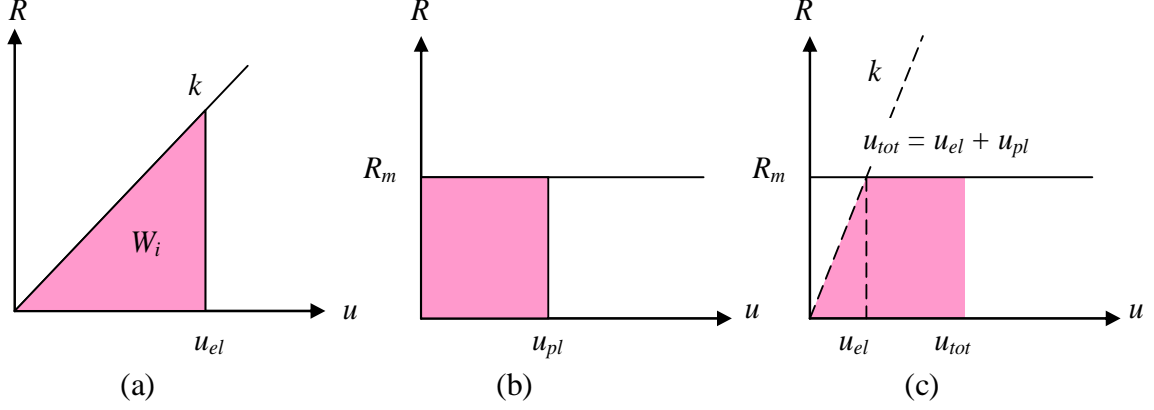


*Figure 2.19   Structural response when assuming (a) linear elastic response, (b) plastic response, (c) elasto-plastic response.*

The definition for internal work is the absorbed energy in the structure over the deformation and is expressed by

$$W_i = \int_{u_0}^{u_1} R(u)du \tag{2.32}$$

where $R(u)$ is the resisting force of the structure. From Section 2.2 the different types of idealized material behaviour are linear elastic, ideal plastic and elasto-plastic behaviour. By combining Equations (2.6) and (2.32) the three equations can be given as

$$W_{i,el} = \int_{0}^{u_{el}} R(u_{el})du = \int_{0}^{u_{el}} ku_{el}du = \frac{ku_{el}^2}{2} \tag{2.33}$$

$$W_{i,pl} = \int_{0}^{u_{pl}} R(u_{pl})du = \int_{0}^{0} Pdu + \int_{0}^{u_{p1}} R_m du = 0 + R_m u_{pl} = R_m u_{pl} \tag{2.34}$$

$$W_{i,ep} = \int_{0}^{u_{tot}} R(u_{ep})du = \int_{0}^{u_{el,1}} ku_{el}du + \int_{u_{el,1}}^{u_{p1,1}} R_m du = \frac{ku_{el}^2}{2} + R_m u_{pl} \tag{2.35}$$

From the work equilibrium, Equation (2.28), the deformations for elastic and plastic behaviour can be given respectively as

$$u_{el} = \frac{I_k}{\sqrt{km}} = \frac{I_k}{m\omega} \tag{2.36}$$

where

$$\omega = \sqrt{\frac{k}{m}} \tag{2.37}$$

is the angular frequency and

$$u_{pl} = \frac{I_k{}^2}{2mR_m} \tag{2.38}$$

For elasto-plastic behaviour the structure is first deformed from $u = 0$ with elastic behaviour until the load reaches the limit $R_m$. This happens at $u_{el,1}$ and if the load $F \geq R_m$ the deformations will be plastic until $u_{tot}$, see Figure 2.20.
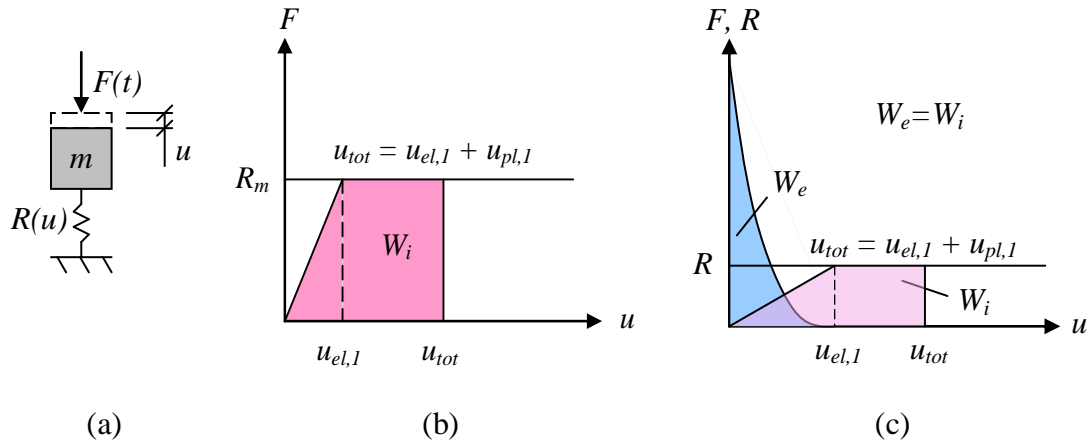


*Figure 2.20   System with elasto-plastic response: (a) single degree of freedom-system, (b) force-displacement relation, (c) energy equilibrium between external , $W_e$, and internal energy, $W_i$.*

If the pressure load, $F_k$, is applied to a structure with elasto-plastic behaviour, the plastic deformations can be reached even though the magnitude of the load is lower than the response limit, $R_m$. This is due to the need of fulfilling the work equilibrium in Equation (2.28) and the fact that the external work from pressure load has a rectangular shape whilst the internal work has a triangular shape during elastic deformations, see Figure 2.21. If the pressure load, $F_k$, is half the size of the response limit, $R_m$, or larger, plastic deformations will be formed; the size of the plastic deformations depend on the stiffness, $k$.
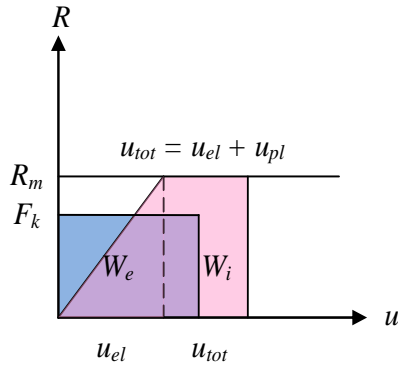
*Figure 2.21   System with elasto-plastic response. Plastic deformations are formed even though the load is lower than the response limit, $R_m$, due to the energy equilibrium between external, $W_e$, and internal energy, $W_i$.*

As seen from Figure 2.20 the internal work for elasto-plastic behaviour can be written as

$$W_i = \frac{R_m}{2}(u_{el,1} + 2u_{pl,1}) \tag{2.39}$$

where $u_{el,1}$ is the limit where the material behaviour goes from elastic to plastic response is defined as

$$u_{el,1} = \frac{R_m}{k} \tag{2.40}$$

By combining Equation (2.31) and (2.39) in the work equilibrium Equation (2.28) the plastic deformations for elasto-plastic behaviour can be expressed as

$$u_{pl,1} = \frac{I_k^{\,2}}{2mR_m} - \frac{u_{el,1}}{2} = u_{pl} - \frac{u_{el,1}}{2} \tag{2.41}$$

where $u_{pl}$ is the response for an ideally plastic material behaviour, also seen in Equation (2.38). The total deformation is given by

$$u_{tot} = u_{el,1} + u_{pl,1} = u_{pl} + \frac{u_{el,1}}{2} \tag{2.42}$$

### 2.3.3.3   Work with regard to recoil

For doubly reinforced concrete beams with different amount of top and bottom reinforcement the material response differs depending on which direction the beam is deflecting. As an example, in Figure 2.13 the material response is shown for a doubly reinforced concrete beam with (a) equal bottom and top reinforcement and maximum internal resistance; (b) equal bottom and top reinforcement but lower maximum internal resistance for the recoil, and (c) more bottom than top reinforcement, resulting in both lower stiffness, $k_2$, and maximum internal resistance, $R_{m,2}$, when the beam is deflecting upward compared to when it is deflecting downward with stiffness, $k_1$, and maximum internal resistance, $R_{m,1}$.

26
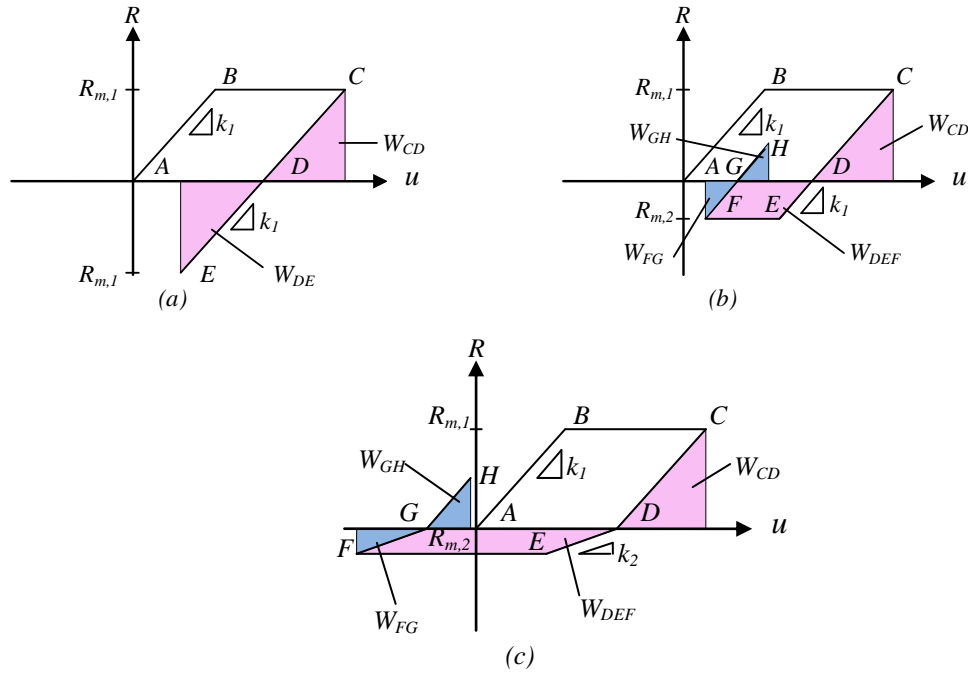
*Figure 2.22. Internal resistance as function of displacement for a beam with (a) $k_1=k_2$ and $R_{m,1}=R_{m,2}$; (b) $k_1=k_2$ and $R_{m,1}>R_{m,2}$ and (c) $k_1>k_2$ and $R_{m,1}>R_{m,2}$.*

The internal resistance varies linearly between A and B where the maximum internal resistance is reached. The beam then yields until all kinetic energy has been transformed into potential energy in C. The beam then has a surplus of energy and wants to return to its new equilibrium D, where all potential energy is transformed into kinetic energy. The beam in (a) here continues to deflect until all kinetic energy has been transformed to potential energy and the beam oscillates between C and E. The integral over CD describes the work $W_{CD}$ and the integral over DE describes the work $W_{DE}$. If no additional loads and no energy losses are assumed, $W_{CD} = W_{DE}$.

For a beam with properties according to (b), where the second maximum internal resistance $R_{m,2}$ is smaller than $R_{m,1}$, the beam will yield before all kinetic energy has been absorbed. The yield limit F is determined by the energy equilibrium where $W_{CD}=W_{DEF}$. Here, the beam will oscillate between F and H as $W_{FG}=W_{GH}$.

For a beam with properties according to (c), where both the secondary stiffness $k_2$ and maximum internal resistance $R_{m,2}$ is smaller than for the beam in (b), the beam can yield further in the second direction if the load is large enough. When the beam starts to deflect downward the internal resistance varies linearly from A to B, where the yielding starts. The beam yields from B to C until all kinetic energy has been translated into potential energy, and the beam begins to return to its new equilibrium D. As the resistance passes D, due to the kinetic energy, the stiffness properties change and the resistance varies linearly with the lower stiffness $k_2$ until the maximum resistance $R_{m,2}$ is reached in E. Here the beam yields until all kinetic energy has been transformed into potential energy in F. The beam then begins to return to the new equilibrium G. The resistance varies with the same stiffness between F and G as between E and D. When G has been passed, the beam is deflecting downward again and so the resistance varies between G and H with the same stiffness as between A and B and between C and D. As the beam reaches H, all kinetic energy has been consumed and transformed into potential energy, so the beam starts to return to

equilibrium G. The beam will now oscillate between H, G and F without any further plastic deformations.

This material response was from the beginning intended to be studied in this thesis with regard to the recoil of the beam. However, due to lack of time this has not been done.

### 2.3.4 Equivalent static load

Instead of using the dynamic impulse, it is possible to translate it into an equivalent static load which is more intuitive for most structural engineers. The equivalent static load is derived, mainly from the equations in Section 2.3.3.2, so that its maximum deflection will be the same as the impulse load. For this statement to be true, the maximum potential energy from the static load should be equal to the maximum potential energy from the dynamic load. Since the total energy of an undamped closed system is constant over time it is fair to assume that the maximum kinetic energy is reached when the potential energy is zero. Therefore

$$\text{Potential energy, static case} = \text{Maximum kinetic energy, dynamic case} \qquad (2.43)$$

#### 2.3.4.1 Elastic response

For an elastic system the static load, $Q$, can be expressed as

$$Q = ku_{el} \qquad (2.44)$$

and the external energy, $W_e$, as

$$W_e = \frac{ku_{el}^2}{2} = \frac{Q^2}{2k} \qquad (2.45)$$

Insertion of Equation (2.31) and (2.45) in (2.43) gives

$$\frac{ku_{el}^2}{2} = \frac{Q^2}{2k} = \frac{I_k^2}{2m} \qquad (2.46)$$

thus

$$Q = I_k \sqrt{\frac{k}{m}} = I_k \omega \qquad (2.47)$$

#### 2.3.4.2 Plastic response

For the plastic case the maximum static load $Q$ is determined by the maximum resistance $R_m$

$$Q = R_m \qquad (2.48)$$

and so the external energy can be expressed as

$$W_e = R_m u_{pl} = Q u_{pl} \tag{2.49}$$

Insertion of Equation (2.49), (2.31) and (2.45) in (2.43) gives

$$Q u_{pl} = \frac{I_k^2}{2m} \tag{2.50}$$

thus $Q$ can also be expressed as

$$Q = \frac{I_k^2}{2m u_{pl}} \tag{2.51}$$

### 2.3.4.3   Elasto-plastic response

The elasto-plastic response is a combination of elastic and plastic response which means that the equivalent static load is, as in the plastic response determined by

$$Q = R \tag{2.52}$$

but where $R$ is determined by elastic stiffness $k$, through the elastic deformation $u_{el,1}$ from Equation (2.40), and the plastic deformation $u_{pl,1}$ from Equation (2.41):

$$R = k u_{pl} \tag{2.53}$$

## 2.3.5   Wave propagation

When a body is subjected to an impulse load, the energy will propagate through the body as mechanical waves. Depending on the speed of these waves, different parts of the body will be affected by the impulse at different times, which is of great importance in structures subjected to explosions. In order to explain what happens, the wave propagation is discussed. This is illustrated in Figure 2.23 where a 3 m high and 5 m deep concrete structure is subjected to an explosion from the left side. The speed of which information travels in concrete is about 3500 m/s, which means that it will take about 1.4 ms before the rear wall "knows" about the explosion. This can be seen, as the rear wall after 1 ms is still unaffected by the load, but after 2 ms it has started to deform. The dark colour indicates that cracks have developed fully in the front wall after 2 ms while the floor and roof is still unaffected. After 3 ms, though, the cracking has begun in floor, roof and rear wall. It is not until after 5 ms that the largest deformations in the front wall occur.
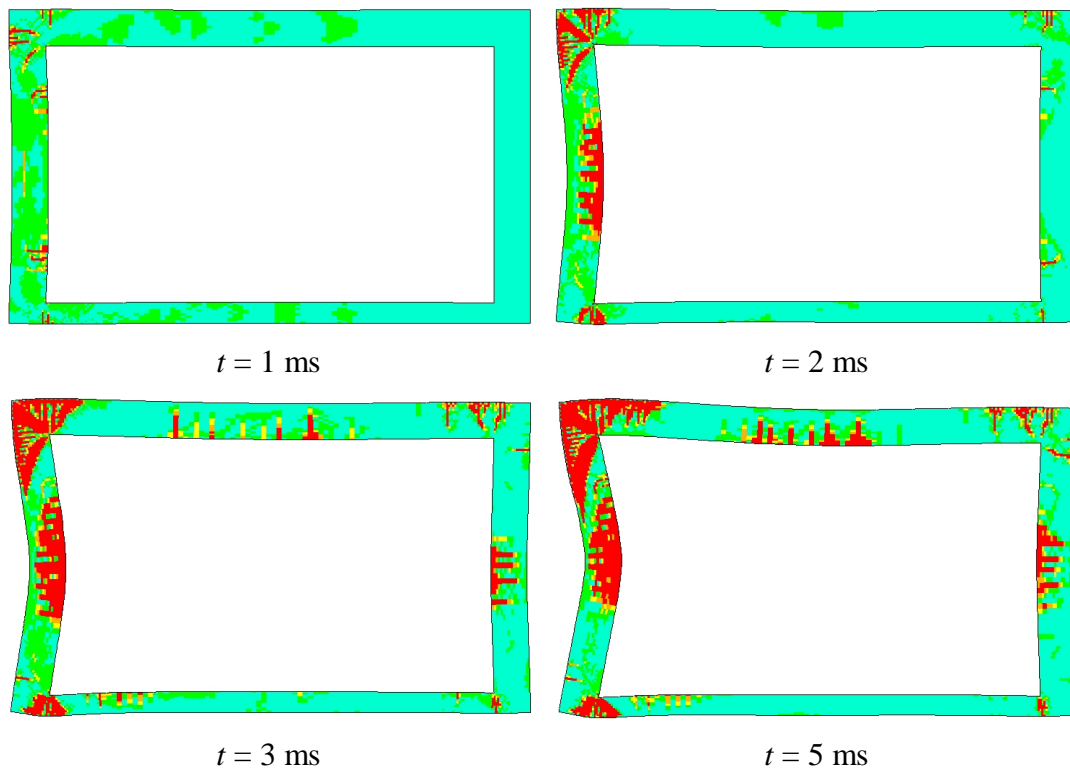
*Figure 2.23    Response of a shelter subjected to an explosion from the left. The deformations are enhanced 20 times and the dark colour marks fully developed cracks. From Johansson (1999)*

In order for mechanical waves to be able to propagate they require a medium (gas, fluid or solid) which means they cannot propagate through vacuum, as electromagnetic waves can. Mechanical waves can further be categorized as longitudinal waves, transverse waves and surface waves.

Longitudinal waves, often called pressure waves or compressional waves, travel parallel to the direction of energy while transverse waves, commonly called shear waves, travel perpendicular to the direction of energy, see Figure 2.24. Surface waves travel in elliptical patterns and can be seen for example as ripples on a water surface.
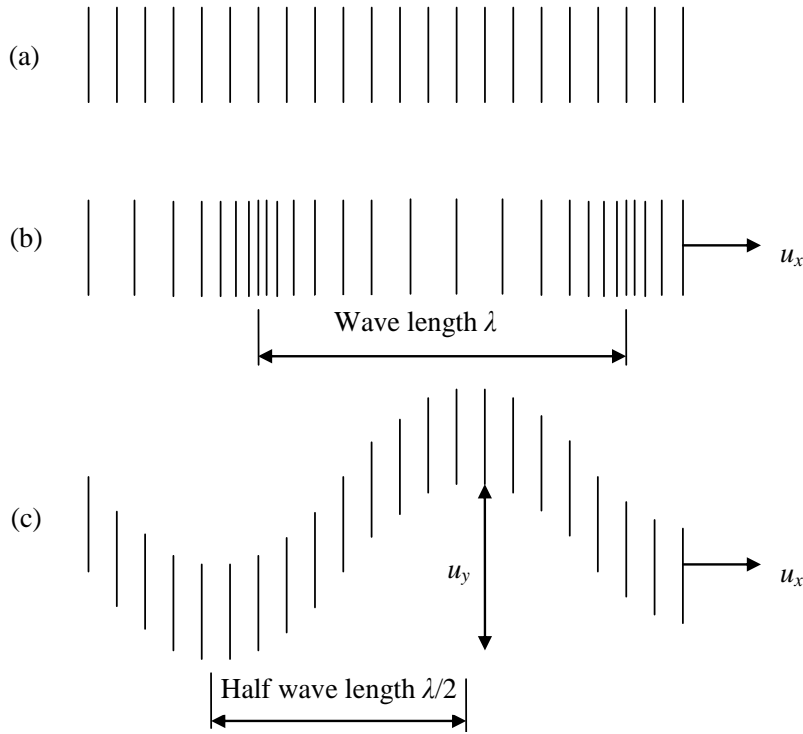
*Figure 2.24   Waves propagating through a body for (a) material at rest; (b) pressure wave; (c) shear wave.*

Mechanical waves are caused by the oscillation of particles in the body and are therefore highly dependent on the elastic and internal properties of the material, NDT (2009). Pressure waves are both stronger and faster than shear waves and can travel through all mediums, while shear waves can only travel through solids. According to Laine (2012) the celerity of a pressure wave, $c_p$, is

$$c_p = \sqrt{\frac{(1-v) \cdot E}{3 \cdot (1+v) \cdot (1-2v) \cdot \rho}}$$
(2.54)

where $E$ is the Young's modulus of elasticity, $\rho$ is the density and $v$ is the Poisson's ratio. Usually the energy propagates through the body as a combination of all the waves, but the type and direction of the load will affect the type of wave that will be dominant in the body. For example, the majority of information in a beam loaded by an axial force will propagate as a pressure wave while in the case of a load perpendicular to the longitudinal axis the shear wave will be much more prominent. The velocity of the shear wave, $c_s$, is greatly affected by the shear modulus of the material and can be written as

$$c_s = \sqrt{\frac{G}{\rho}}$$
(2.55)

with the shear modulus given by

$$G = \frac{E}{2(1+v)}$$
(2.56)

31

Pressure waves are also commonly referred to as sound. The speed of sound for different mediums is seen in Table 2.3. These values are estimated velocities that varies with change in density, e.g. from change in temperature or pressure.

*Table 2.3.    Estimated velocity of sound for different mediums. Based on The engineering toolbox (2012).*

| Medium | Velocity (m/s) |
| --- | --- |
| Air | 343 |
| Aluminium | 6420 |
| Concrete | 3200-3600 |
| Iron | 5130 |
| Lead | 1158 |
| Rubber | 40-150 |
| Steel | 6100 |
| Water | 1433 |

## 2.3.6   Vibrations

A beam subjected to a dynamic load can be described by a mass-spring system as seen in Figure 2.25. The deformation resistance of the spring is generally referred to as stiffness, $k$. The stiffness depends on the Young's modulus $E$, moment of inertia $I$ and length $L$ of the beam. The response of a beam depends on the type of loading, for example a point source or a distributed load, and also the boundary conditions, for example simply supported or a clamped beam. When dealing with arbitrary dynamic loads the damping, $c$, is often included.
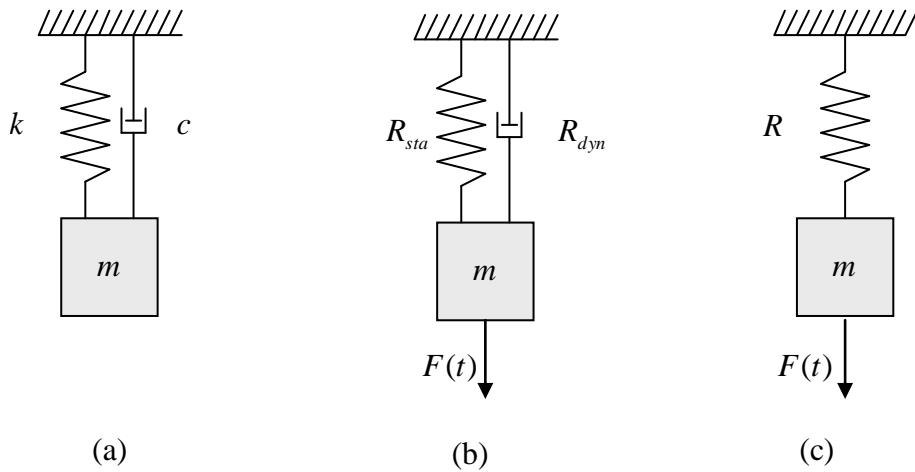
*Figure 2.25   Mass spring system with (a) properties; (b) damped mechanical forced vibration; (c) undamped mechanical forced vibration.*

When the mass-spring system is externally loaded by the dynamic load *F(t)* the internal forces $R_{sta}$ and $R_{dyn}$ act in opposite direction in an attempt to bring the displaced beam back to its equilibrium position. The internal forces $R_{sta}$ and $R_{dyn}$ refer to the static and dynamic resistance in a structure and for a linear elastic response and they are given by

$$R_{sta} = ku \tag{2.57}$$

$$R_{dyn} = c\dot{u} \tag{2.58}$$

where $k$ is the stiffness, $c$ is the damping, $u$ is the displacement and $\dot{u}$ is the velocity of the body.

According to Newton's second law of motion, seen in Equation (2.20), there is equilibrium when

$$F(t) - R_{dyn} - R_{sta} = m\ddot{u} \tag{2.59}$$

or

$$m\ddot{u} + R_{dyn} + R_{sta} = F(t) \tag{2.60}$$

By insertion of Equations (2.57) and (2.58) in (2.60) the dynamic equation of motion can be written as

$$m\ddot{u} + c\dot{u} + ku = F(t) \tag{2.61}$$

In an idealized closed system with no friction, no energy losses and the driving force *F(t)=0*, this motion is called an undamped free vibration and will continue to oscillate with the same frequency to infinity if not disturbed. In case of explosions there will be a driving force in form of a short impulse to the structure and during this time the motion will be a so called forced vibration until the load wears off and the motion becomes a free vibration. In reality, though, all structures have a damping effect that

will reduce the displacements in the oscillation so the simplification of an idealized undamped structure will always be on the safe side. Because of this, it is not always necessary to regard the damping, which makes the equation more complex, and the equation can thus be simplified further by neglecting the effect of damping.

The simplified method is initially presented and used during this Master thesis, but in Section 5.2 the effects of damping are included and compared to the undamped case.

## 2.4    Transformation to SDOF-system

When working with dynamic loads it is common to transform the affected structure into a single degree of freedom-system. This is done to simplify the calculations and can often be sufficiently accurate. When transforming an impulse loaded beam into an SDOF-system, so called transformation factors are used.

### 2.4.1    SDOF-system

A beam is often referred to as a simple structure, Chopra (2011). This is because a beam's deflection approximately can be simplified as the movement of only one point in one direction. This point is called the system point and is usually placed where the beam's deflection is largest, which for a simply supported beam that is subjected to a uniformly distributed load is in the mid span. By idealizing a beam in this order one will simplify the calculations, making it easy to determine the deflection for a specific load. When only using one point to describe the displacement for a certain system it is called a single degree of freedom-system, referred to as an SDOF-system, see Figure 2.26. In order to perform the calculations for a beam it is necessary to concentrate the equivalent mass, $m_e$, to the system point, also called lumped mass.
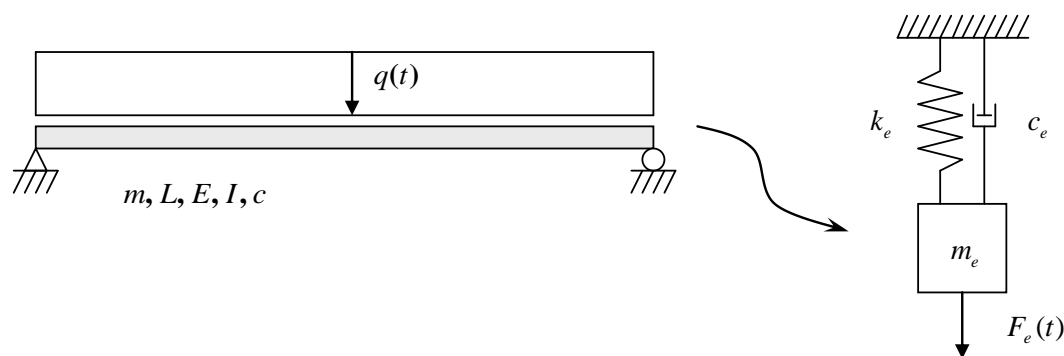


*Figure 2.26. Transformation of the beam into a single degree of freedom-system.*

When transforming the beam into an SDOF-system the properties of the beam, such as length $L$, Young's modulus $E$ and the moment of inertia $I$, will be included in the stiffness $k$. For a simply supported beam and a uniformly distributed load the stiffness can be derived from the maximum displacement in the mid span:

$$u_{max} = \frac{5qL^4}{384EI} \qquad \text{or} \qquad \frac{384EI}{5L^3}u_{max} = qL \qquad (2.62)$$

It is also known that the force is equal to the stiffness times the displacement:

$$F = ku \qquad (2.63)$$

$$F = qL \qquad (2.64)$$

and thus

$$k = \frac{384EI}{5L^3} \qquad (2.65)$$

A beam deflects differently depending on the loading. In cases with dynamic loading the beam is affected by the frequency of the load. Different mode shapes can be used to describe the deflection, see Figure 2.27. The lower the frequency, the lower the degree of mode shapes. An SDOF-system, however, is only able to describe the first mode shape. In theory, if an impulse that consists of every frequency, a so called Dirac-impulse, affects a beam it will excite every mode of vibration with equal energy. However, if the Dirac-impulse is evenly distributed over a perfectly symmetrical beam it will only excite every other mode, the symmetrical modes, since the non-symmetrical modes has a net deflection of zero. Since the first mode shape only has one deflection it will be the most prominent; hence the SDOF-system is a good way to describe the deflection.

To be able to describe higher order of mode shapes it is necessary to use multi degree of freedom, MDOF, systems. The number of degrees of freedom corresponds with the number of mode shapes it can describe. For example, a three degree of freedom system can describe the first three mode shapes, also seen in Figure 2.27. The number of mode shapes excited mainly depends on the time interval of the impulse. Higher mode shapes oscillate with higher frequencies, which is reversely proportional to time. For longer time intervals mainly lower frequencies will be excited, but as the time interval approaches zero the frequencies become infinite.

First bending mode

Second bending mode

Third bending mode
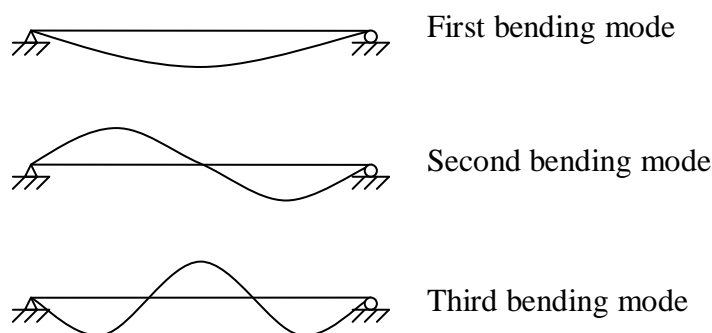
*Figure 2.27. The three first mode shapes for a simply supported beam.*

## 2.4.2 Transformation into an equivalent SDOF-model

When transforming a beam, subjected to an impulse, into an SDOF-model it is not sufficient to calculate the stiffness for the beam and use the same mass for example. It is necessary to transform the SDOF-model into an equivalent SDOF-model. This transformation is done with help of transformation factors $\kappa$, Johansson and Laine (2009). The transformation factors have indexes indicating which parameter they are affecting and $m$, $c$, $k$ and $F$ are the beam's real mass, damping, stiffness and external force respectively:

$$m_e = \kappa_m m \tag{2.66}$$

$$c_e = \kappa_c c \tag{2.67}$$

$$k_e = \kappa_k k \tag{2.68}$$

$$F_e = \kappa_F F \tag{2.69}$$

where the index $e$ denotes that it is an equivalent parameter. The initial equation of motion, Equation (2.61), can now be re-written:

$$\kappa_m m \ddot{u} + \kappa_c c \dot{u} + \kappa_k k u = \kappa_F F(t) \tag{2.70}$$

When deriving the transformation factors an assumption of conservation of energy is made. This is the foundation for the transformation factors. For $\kappa_m$, $\kappa_k$, and $\kappa_F$, there is an assumption of conservation of kinetic-, internal- and external energy respectively. According to Biggs (1964) the transformation factors for internal energy $\kappa_k$ is equal to the factor for external energy $\kappa_F$:

$$\kappa_k = \kappa_F \tag{2.71}$$

The derivation of the transformation factors is regarded to the support conditions, stiffness distribution, load profile and material model, i.e. the deformation of the beam is of utmost importance. The expression of the mass factor $\kappa_m$ and the external force factor $\kappa_F$ will be as follows:

$$\kappa_m = \frac{1}{L} \int_{x=0}^{x=L} \frac{u(x)^2}{u_s^2} dx \tag{2.72}$$

$$\kappa_F = \frac{1}{L} \int_{x=0}^{x=L} \frac{u(x)}{u_s} dx \tag{2.73}$$

where $u_s$ is the maximum displacement and $u(x)$ is the deflection of the beam. For the full derivation of the transformation factors the reader is referred to Johansson and Laine (2009).

In order to simplify the equations, Equation (2.70) is divided by $\kappa_F$:

$$\frac{\kappa_m}{\kappa_F} m\ddot{u} + \frac{\kappa_c}{\kappa_F} c\dot{u} + \frac{\kappa_k}{\kappa_F} ku = F(t) \tag{2.74}$$

which leads to

$$\kappa_{mF} m\ddot{u} + \kappa_{cF} c\dot{u} + ku = F(t) \tag{2.75}$$

when implementing (2.71) and where

$$\kappa_{mF} = \frac{\kappa_m}{\kappa_F} \tag{2.76}$$

and

$$\kappa_{cF} = \frac{\kappa_c}{\kappa_F} \tag{2.77}$$

The values for some transformation factors for different load cases, material models and supports for beams are gathered in Table 2.4 and Table 2.5.

*Table 2.4.    Transformation factors for a beam subjected to a point load. From Johansson and Laine (2009).*
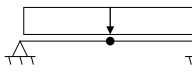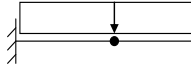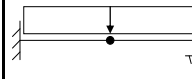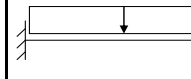
| | Point load on beam element | | | |
|---|---|---|---|---|
| |  | | | |
| | Elastic deformation curve | | | |
| $\kappa_m$ | 0.486 | 0.371 | 0.445 | 0.236 |
| $\kappa_F$ | 1.000 | 1.000 | 1.000 | 1.000 |
| $\kappa_{mF}$ | 0.486 | 0.371 | 0.446 | 0.236 |
| | Plastic deformation curve | | | |
| $\kappa_m$ | 0.333 | 0.333 | 0.333 | 0.333 |
| $\kappa_F$ | 1.000 | 1.000 | 1.000 | 1.000 |
| $\kappa_{mF}$ | 0.333 | 0.333 | 0.333 | 0.333 |

*Table 2.5.* *Transformation factors for a beam subjected to uniform load. From Johansson and Laine (2009).*

| | Uniformly distributed load on beam element | | | |
|---|---|---|---|---|
| |  | | | |
| | Elastic deformation curve | | | |
| $\kappa_m$ | 0.504 | 0.406 | 0.483 | 0.257 |
| $\kappa_F$ | 0.640 | 0.533 | 0.600 | 0.400 |
| $\kappa_{mF}$ | 0.788 | 0.762 | 0.805 | 0.642 |
| | Plastic deformation curve | | | |
| $\kappa_m$ | 0.333 | 0.333 | 0.333 | 0.333 |
| $\kappa_F$ | 0.500 | 0.500 | 0.500 | 0.500 |
| $\kappa_{mF}$ | 0.667 | 0.667 | 0.667 | 0.667 |

The $\kappa_c$ factor has not been derived in the same manner as the other transformation factors, the damping in general is difficult to determine. It is believed that $\kappa_c=\kappa_k$ but has not fully been studied. Since an impulse has a very short duration the impact of the damping is very small and has often been neglected. It is also on the safe side to neglect the damping which is why Equation (2.75) often is simplified to

$$\kappa_{mF}m\ddot{u} + ku = F(t) \tag{2.78}$$

In this Master thesis it will be investigated whether the assumption

$$\kappa_{cF} = \frac{\kappa_c}{\kappa_F} \approx 1 \tag{2.79}$$

is correct or not.

There are no special elasto-plastic transformation factors so when dealing with elasto-plastic materials one is referred to either use elastic, plastic or both transformation factors. In previous Master theses it has been shown that using these transformation factors, shown in Table 2.5, for an elasto-plastic material is not fully satisfying. Andersson and Karlsson (2012) have studied the possibility of having time dependent transformation factors. They show that this type of modelling can be very satisfying. The factors are then derived using a FE-analysis and the beams deformation at multiple times. However, usage of time dependent transformation factors are not desirable because the simplicity of the SDOF-model loses its benefits when a FE-analysis need to be performed simultaneously. This Master thesis will use the ordinary transformation factors and discuss the agreement.

## 2.4.3 Equivalent work

With the knowledge of the transformation factors it is now possible to derive the equivalent work an SDOF-model performs. In alignment with Section 2.3.3 the external, internal and kinetic energy can be re-written to include the transformation factors:

$$W_e = \kappa_F F u_s \tag{2.80}$$

$$W_i = \kappa_F R(u) u_s \tag{2.81}$$

$$W_k = \frac{\kappa_m m v_s^2}{2} \tag{2.82}$$

As mentioned before, there has to be equilibrium between the different energy levels. For a characteristic impulse the external energy is equal to the kinetic energy, according to Equation (2.31). The goal is to derive the equivalent work achieved by a characteristic impulse. In order to do so it is necessary to consider the equivalent equation of motion in its basic form from Section 2.4.2:

$$m_e \ddot{u} + k_e u = F_e(t) \tag{2.83}$$

where

$$m_e = \kappa_m m \tag{2.84}$$

$$k_e = \kappa_k k \tag{2.85}$$

$$F_e = \kappa_F F \tag{2.86}$$

The definition of an impulse in Equation (2.25) can be expressed for an equivalent SDOF-model in the following manner:

$$I_{SDOF} = \kappa_F \int_{t_0}^{t_1} F(t)dt = \kappa_m m v_s \tag{2.87}$$

Since the equivalent impulse should be equal to the characteristic impulse times the force transformation factor

$$I_{SDOF} = \kappa_F I_k \tag{2.88}$$

the following expression can be derived:

$$\kappa_m m v_s = \kappa_F I_k \tag{2.89}$$

Since the goal is to derive the equivalent work achieved by a characteristic impulse the expression for the velocity is squared and then inserted in the equation for kinetic energy, Equation (2.82):

$$v_s^2 = \left( \frac{\kappa_F I_k}{\kappa_m m} \right)^2 \tag{2.90}$$

$$E_k = \frac{I_k^2}{2\kappa_m m} \kappa_F^2 = \frac{I_k^2}{2\kappa_{mF} m} \kappa_F \tag{2.91}$$

40

$$v_s^2 = \left( \frac{\kappa_F I_k}{\kappa_m m} \right)^2$$

$$E_k = \frac{I_k^2}{2\kappa_m m} \kappa_F^2 = \frac{I_k^2}{2\kappa_{mF} m} \kappa_F$$

# 3 Structural response of a concrete beam

A wall with the purpose of withstanding an impact load is normally designed with a symmetric cross-section, with equal amount of reinforcement on both sides and no curtailment. Impact loads from explosions are usually anticipated for buildings such as nuclear power plants, petro-chemical industries and protective facilities, but generally not in other civil structures. In civil structures there is therefore a risk that even if the wall does not fail from the first hit it might fail from either the negative phase of the explosion, the recoil from internal stiffness or a combination of them.

When designing with regard to an explosion the engineer needs to understand how the structure can absorb energy without getting a brittle failure. A reinforced concrete beam is good in this aspect since the mass is high and the structure can be designed to have a ductile behaviour. There is a big difference between a statically loaded structure and a dynamically loaded. When subjected to an explosion it is good if the structure can yield since the energy absorption then increases. Hence, it is better to have a structure with the ability to absorb energy than one with high stiffness that is reluctant to deform since this might lead to a brittle failure. However, a structure with high stiffness and good yielding ability is also good with regard to an explosion.

When performing analyses of a wall it is sometimes beneficial to simplify it as a beam because the calculations become simpler and the results are on the safe side; a beam can only carry the load in one direction while a wall carries it in two. To better explain the behaviour of an impulse loaded beam, an example is made for a reinforced concrete beam subjected to an explosion. With no possibility of actually testing the beam, it is modelled and analysed with the finite element software ADINA (2011) which is considered to represent the true behaviour good enough. An equivalent SDOF-system and simplified hand calculations are also made for the beam and these are compared to the results from ADINA. The beam is further simplified by limiting it to the three material behaviours explained in Section 2.2, i.e. linear elastic, ideal plastic and elasto-plastic, where the linear elastic is divided into stadium I (uncracked concrete) and stadium II (cracked concrete).

## 3.1 Geometry and loading

The analysed beam is a simplification of a 1 m wide strip from a 3 m high and 200 mm deep concrete wall with no openings, see Figure 3.1. The wall is situated in a civil building meaning the reinforcements in both sides does not have to be equal, in contrary to for example civil defence shelters and military facilities. However, the reinforcement in this wall is steel B500B Φ10 s150, with a concrete cover of 45 mm on both sides. The reinforcement in compression is mainly included to be the reinforcement in tension when the wall recoils and it could be neglected as reinforcement in compression. In this example it is included to better show the calculation method.

The wall is mainly analysed for an impulse with the intensity $i$ of 1000 Pas; the peak pressure will be 500 kPa and the load duration 4 ms. If the bomb is assumed to have a hemispherical spreading this load characteristics would, according to ConWep (1992), approximately correspond to two, so called, suitcase bombs, see Table 2.2, placed on the ground 10 m away from the wall. Each suitcase bomb contains approximately 25 kg TNT, i.e. a total of 50 kg TNT. This is shown in Figure 3.2. Since the distance

to the wall would correspond to 10 m the load will affect the wall with a near uniformly distributed pressure that decreases with time.
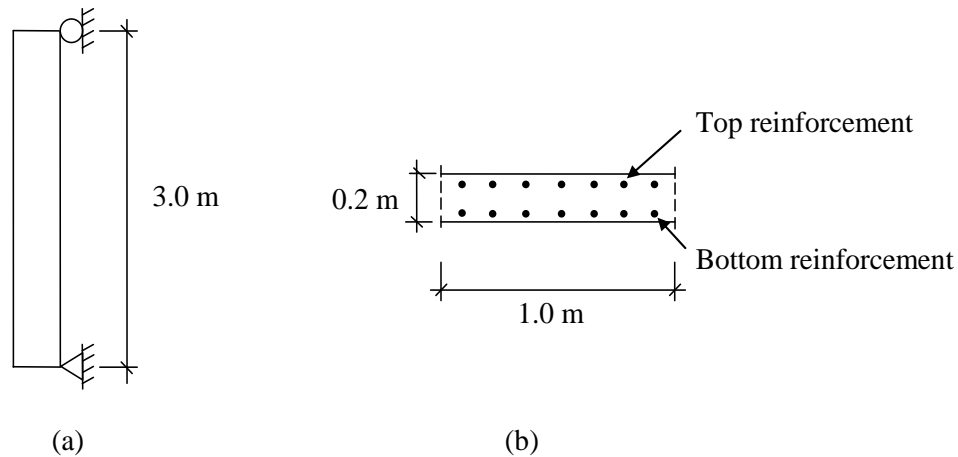


*Figure 3.1. (a) Impact loaded wall with boundary conditions; (b) Cross-section.*
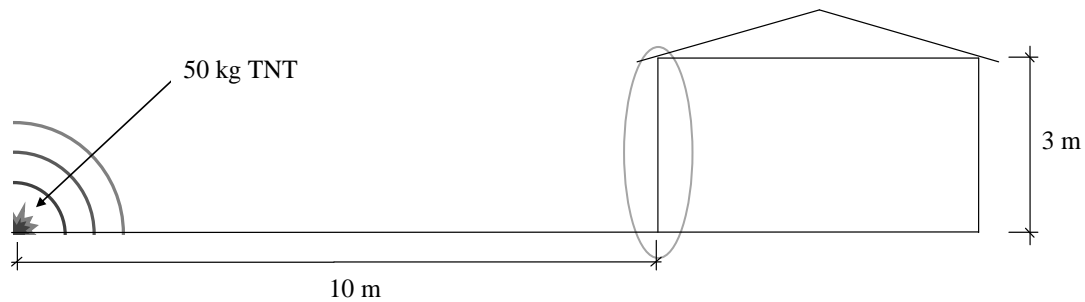


*Figure 3.2. Schematic figure of the explosion and the impact loaded wall.*

In order to give the reader better understanding in the importance of load time, the wall is also analysed for other load cases with different peak pressures, but with the same impulse intensity as the first load case. It is in Section 5.1 shown that the different load cases will influence the result a lot. It is then interesting to have both more and less intense impulses to compare with the default load case. The load case denoted as load case 1 will be the default load case in this Master thesis unless anything else is mentioned. All load cases are shown in Figure 3.3.

| Load case | $P_{peak}$ [kPa] | $t$ [ms] |
|-----------|-----------|--------|
| LC0 | 250 | 8 |
| **LC1** | **500** | **4** |
| LC2 | 1,000 | 2 |
| LC3 | 4,000 | 0.5 |
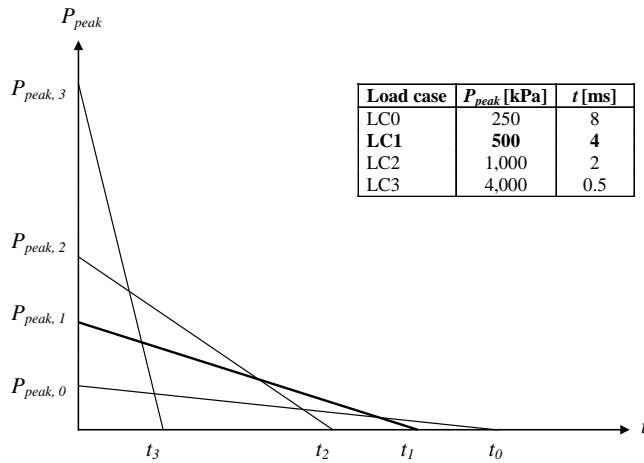
*Figure 3.3. The different load cases with the same impulse intensity i=1000 Pas. LC1 is the default load case used in this Thesis.*

The support condition for the wall is in reality somewhere between clamped and simply supported, but in the analyses it is assumed to be simply supported along its top and bottom, which also gives values on the safe side. The wall can then be simplified to a 1.0 m wide, simply supported beam with properties according to Table 3.1. When structures are subjected to accidental loads the partial factors, $\gamma_c$ and $\gamma_s$, are set to 1.2 and 1.0 for concrete and steel, respectively.

*Table 3.1. Properties for the beam*

| | |
|---|---|
| Concrete | C30/37 |
| Reinforcement | Φ10 s150 B500B |
| $E_c$ | 33 GPa |
| $E_s$ | 200 GPa |
| $f_{cc}$ | 30 MPa |
| $\gamma_c$ | 1.2 |
| $f_{sy}$ | 500 MPa |
| $\gamma_s$ | 1.0 |
| Concrete cover, $c$ | 45 mm |
| Height, $h$ | 0.2 m |
| Length, $L$ | 3.0 m |
| Width, $w$ | 1.0 m |
| Effective height, $d$ | 150 mm |

## 3.2 Hand calculations

While the SDOF- and FE-solutions display results for displacements, forces and energies over time, it is often of interest to perform a quick check of the maximum values. This is easily done by hand, and uses only parts of the input for the SDOF-analysis.

To determine the displacements by hand, Equation (2.36), (2.38) and (2.42) from Section 2.3.3.2 are used:

$$u_{el} = \frac{I_k}{\sqrt{k_e m_e}} = \frac{I_k}{m_e \omega} \tag{3.1}$$

$$u_{pl} = \frac{I_k^2}{2 m_e R_m} \tag{3.2}$$

$$u_{ep} = u_{ep,el} + u_{ep,pl} = \frac{R}{2 k_e} + \frac{I_k^2}{2 m_e R} \tag{3.3}$$

In order to calculate these, the equivalent mass, stiffness and maximum internal resistance must first be determined.

### 3.2.1 Mass and stiffness

With a density of 2400 kg/m³ the mass for the beam can be calculated to

$$m = \rho \cdot w \cdot h \cdot L = 2400 \cdot 1.0 \cdot 0.2 \cdot 3.0 = 1440 \, \text{kg} \tag{3.4}$$

In order to obtain the right deformation shape, the mass is transformed to equivalent mass for the elastic and the plastic case by multiplying it with the transformation factor $k_{mF}$ from Table 2.5:

$$m_{el} = \kappa_{mF} m = 0.788 \cdot 1440 = 1135 \, \text{kg} \tag{3.5}$$

$$m_{pl} = \kappa_{mF} m = 0.667 \cdot 1440 = 960 \, \text{kg} \tag{3.6}$$

For the case of a simply supported beam, the stiffness of the beam is calculated as

$$k = \frac{384 EI}{5 L^3} \tag{3.7}$$

where $E$ is Young's modulus of elasticity, $I$ is the moment of inertia and $L$ is the length of the beam. Depending on whether the cross-section is cracked or not, the moment of inertia can, for the elastic material response, further be divided into $I_I$ and $I_{II}$ for stadium I and II, respectively.

Because the amount of reinforcement is low it is likely that the top reinforcement in stadium II will be in tension and not in compression, and the lever will be very small in comparison to the bottom reinforcement. When designing, the forces in the top

reinforcement can be assumed to be negligible, but for this analysis they are regarded to keep down the potential sources of error. The moment of inertia for stadium I is then given by

$$I_I = \frac{wh^3}{12} + wh \cdot (\frac{h}{2} - x_{cg})^2 + (\alpha - 1) \cdot A_s' \cdot (d' - x_{cg})^2 + (\alpha - 1) \cdot A_s \cdot (d - x_{cg})^2 \qquad (3.8)$$

where $x_{cg}$ is the centre of gravity for the cross-section, $\alpha$ is the ratio between the Young´s modulus for steel and concrete, $d$ and $d'$ is the distance from the top to the bottom and top reinforcement, respectively, and $A_s$ and $A_s'$ is the area of the bottom and top reinforcement bars:

$$\alpha = \frac{E_s}{E_c} = \frac{200}{33} = 6.06 \qquad (3.9)$$

$$A_s = A_s' = \frac{\pi \cdot \phi^2}{4} \cdot \frac{b}{s} = \pi \cdot 5^2 \cdot \frac{1000}{150} = 523 \, mm^2 \qquad (3.10)$$

Since the cross-section is symmetric

$$x_{cg} = \frac{h}{2} = 100 \, mm \qquad (3.11)$$

inserting Equation (3.9), (3.10) and (3.11) in (3.8), the moment of inertia can be calculated as

$$I_I = \frac{1000 \cdot 200^3}{12} + 1000 \cdot 200 \cdot (\frac{200}{2} - 100)^2 + (6.06 - 1) \cdot 523 \cdot (50 - 100)^2 +$$
$$(6.06 - 1) \cdot 523 \cdot (150 - 100)^2 = 6.80 \cdot 10^8 \, mm^4 \qquad (3.12)$$

In the case of elastic stadium II where the cross-section has cracked the moment of inertia is

$$I_{II} = \frac{wx^3}{3} + \alpha A_s \cdot (d - x)^2 + \alpha A_s' \cdot (x - d')^2 \qquad (3.13)$$

where $x$ is the height of the compressed zone. Since, there are no normal forces acting on the cross-section, i.e. pure bending, the compression zone can be determined using area equilibrium:

$$\frac{wx^2}{2} + (\alpha - 1) \cdot A_s' \cdot (x - d') - \alpha A_s \cdot (d - x) = 0 \qquad (3.14)$$

Solving for $x$ gives the height of the compressed zone:

$$x = 30 \, mm \qquad (3.15)$$

By inserting (3.15) in (3.13) the moment of inertia for the cracked case is given as

$$I_{II} = \frac{1000 \cdot 30^3}{3} + 6.06 \cdot 523 \cdot (150 - 30)^2 + 6.06 \cdot 523 \cdot (30 - 50)^2 =$$
$$= 5.60 \cdot 10^7 \text{ mm}^4$$

(3.16)

The stiffness for elastic stadium I and II, respectively, can now be calculated using Equation (3.7):

$$k_I = \frac{384 \cdot 33 \cdot 10^9 \cdot 6.80 \cdot 10^{-4}}{5 \cdot 3^3} = 6.38 \cdot 10^7 \text{ N/m}$$

(3.17)

$$k_{II} = \frac{384 \cdot 33 \cdot 10^9 \cdot 5.60 \cdot 10^{-5}}{5 \cdot 3^3} = 5.26 \cdot 10^6 \text{ N/m}$$

(3.18)

### 3.2.2 Maximum internal resistance

For a simply supported beam when loaded with a distributed load the maximum internal resistance is defined as

$$R_m = \frac{8M_{Rd}}{L} \cdot w$$

(3.19)

where $w$ is the width and $L$ is the length, which means in order to acquire the maximum resistance $R_m$ the moment capacity $M_{Rd}$ must first be determined. For a doubly reinforced concrete beam the moment capacity can be derived from the model of the cross-section seen in Figure 3.4.
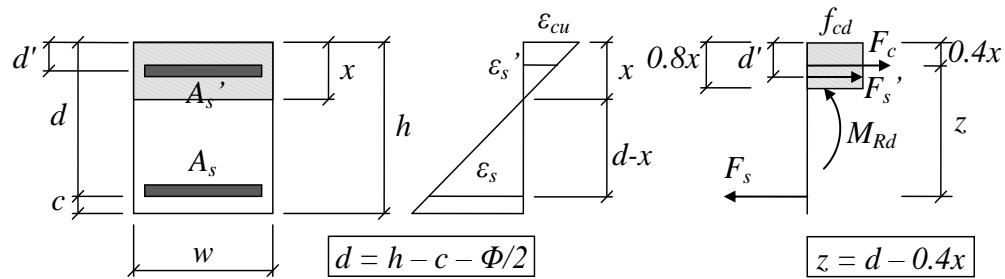


*Figure 3.4. Model for moment capacity for a doubly reinforced concrete beam.*

As seen in Figure 3.4 the height of the compressed zone $x$ can be determined by force equilibrium:

$$f_{cd} \cdot 0.8 \cdot x \cdot w + A_s' \cdot \sigma_s' - A_s \sigma_s = 0$$

(3.20)

where the top reinforcement is still assumed to be in tension so the term $A_s' \cdot \sigma_s'$ becomes negative for this beam, see Figure 3.5.
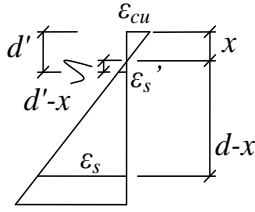
*Figure 3.5. Actual strain for the beam.*

It is also assumed that the steel in both top and bottom reinforcement yields while the outmost fibres in the upper part of the concrete reach its ultimate compressive strain. This means that $\sigma_s$ and $\sigma_s'$ is set to the designing yield strength $f_{yd}$.

Solving Equation (3.20) for $x$ gives the height of the compressed zone:

$$x = 26 \, \text{mm} \tag{3.21}$$

A control of the assumption is done:

$$\varepsilon_s' = \varepsilon_{cu} \cdot \frac{d'-x}{x} = 3.5 \cdot 10^{-3} \cdot \frac{50-26}{26} = 3.23 \cdot 10^{-3} \tag{3.22}$$

$$3.23 \cdot 10^{-3} \geq \frac{f_{sd}}{E_s} = 2.5 \cdot 10^{-3} \rightarrow OK \tag{3.23}$$

When solving the moment equilibrium around the bottom reinforcement the moment capacity is given as

$$\begin{aligned} M_{Rd} &= f_{cd} \cdot 0.8 \cdot x \cdot w \cdot (d - 0.4 \cdot x) - A_s' \cdot \sigma_s' \cdot (d - d') = \\ &= \frac{30}{1.2} \cdot 0.8 \cdot 26 \cdot 1000 \cdot (150 - 0.4 \cdot 26) - 523 \cdot 500 \cdot (150 - 50) = 46.9 \, \text{kNm} \end{aligned} \tag{3.24}$$

Finally the maximum internal resistance can be calculated as

$$R_m = \frac{8 \cdot M_{Rd}}{L} \cdot w = \frac{8 \cdot 46.9}{3.0} \cdot 1.0 = 125 \, \text{kN} \tag{3.25}$$

### 3.2.3   Deformation

With the equivalent mass, stiffness and internal resistance calculated, the maximum deformations can now be calculated. Using Equation (3.1), the maximum deformation for elastic stadium I and II are calculated, respectively, as

$$u_{el,I} = \frac{1.0 \cdot 3.0 \cdot 1000}{\sqrt{1135 \cdot 6.38 \cdot 10^7}} = 11.2 \, \text{mm} \tag{3.26}$$

$$u_{el,II} = \frac{1.0 \cdot 3.0 \cdot 1000}{\sqrt{1135 \cdot 5.26 \cdot 10^6}} = 38.8 \, \text{mm} \tag{3.27}$$

From Equation (3.2) the maximum plastic deformation is calculated:

$$u_{pl} = \frac{(1.0 \cdot 3.0 \cdot 1000)^2}{2 \cdot 960 \cdot 125 \cdot 10^3} = 37.5 \text{ mm} \tag{3.28}$$

For elasto-plastic behaviour the deformation is subdivided in elastic and plastic deformation as seen in Equation (3.3). By inserting known values in this equation the maximum elasto-plastic deformation can be determined as

$$u_{ep} = \frac{125 \cdot 10^3}{2 \cdot 5.26 \cdot 10^6} + \frac{(1.0 \cdot 3.0 \cdot 1000)^2}{2 \cdot 960 \cdot 125 \cdot 10^3} = 49.4 \text{ mm} \tag{3.29}$$

where the elastic part of the deformation is

$$u_{ep,el} = \frac{R}{k} = \frac{125 \cdot 10^3}{5.26 \cdot 10^6} = 23.8 \text{ mm} \tag{3.30}$$

and therefore the plastic part is given by

$$u_{ep,pl} = u_{ep} - u_{ep,el} = 49.4 - 23.8 = 25.6 \text{ mm} \tag{3.31}$$

### 3.2.4 Equivalent static loads

In Section 2.3.4 it was shown how dynamic loads can be translated into equivalent static loads, and thus, the dynamic reactions can be calculated when maximum deflection occurs. From Equation (2.47) the equivalent load for the uncracked case is

$$Q_{el,I} = I_k \omega = 1.0 \cdot 3.0 \cdot 1000 \cdot \sqrt{\frac{6.38 \cdot 10^7}{1135}} = 711 \text{ kN} \tag{3.32}$$

and for the cracked case

$$Q_{el,II} = 1.0 \cdot 3.0 \cdot 1000 \cdot \sqrt{\frac{5.26 \cdot 10^6}{1135}} = 204 \text{ kN} \tag{3.33}$$

From Equation (2.51) the equivalent load for the plastic case is calculated as

$$Q_{pl} = R_m = 125 \text{ kN} \tag{3.34}$$

## 3.3   ADINA – Methods and modelling

In this Master thesis the commercial finite element program ADINA (2011) is used when performing FE-analyses. In order to help the reader understand the procedures when discussing the beam and the results, descriptions about how ADINA works and how the beam is modelled in ADINA have been included. This will also help the interested to make the calculations with a different finite element program if desired.

### 3.3.1 Methods in ADINA

To model a simply supported beam for dynamic analyses where the strain is small it is beneficial to use beam elements. The beam elements are 2-noded beams with constant cross-sections, and comes in two sub-types, namely two-dimensional (2D) and three-dimensional (3D) beam elements. 3D beam elements use seven integration points when calculating the stress distribution over the height of the cross-section, as seen in Figure 3.6, and it is in ADINA not possible to choose any other combination. This is one of the reasons why it is beneficial to use 2D beam elements in ADINA since it is then possible to make a choice of the number of integration points.
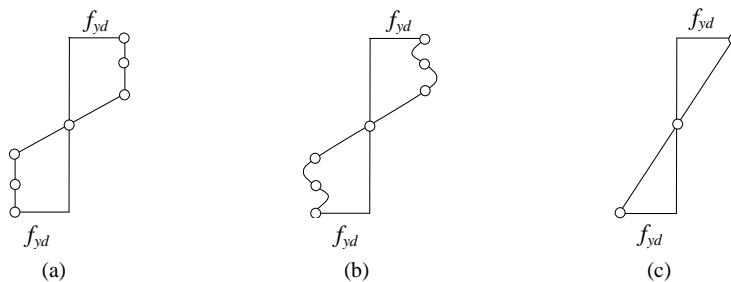


*Figure 3.6. (a) Expected stress using 7 integration points; actual stress distribution using (b) 7 integration points, (c) 3 integration points.*

If one for a 2D beam element chooses three integration points the stress varies linearly over the height of the cross-section whilst for the 3D beam elements it varies with a $6^{th}$ degree polynomial, resulting in a divergence between the expected stress distribution shown in Figure 3.6a and the one used in ADINA, Augustsson and Härenstam (2010). However, when only using three integration points one can have more control over the calculations. The stress distribution is then known and hence, 2D beam elements with three integration points are chosen as the elements used in this Master thesis.

There is a second option available but this can only be used when using a linear elastic material response. The moments are extracted as nodal forces in ADINA. A third option for extracting the moments from ADINA is to extract the stresses. This has not been done in this Master thesis but it is discussed in Andersson and Karlsson (2012) that it may be beneficial to do so. This is because when studying the moment envelope one can see that the yield moment is actually exceeded somewhat, even though this should not be possible. However, when extracting the results as stresses, this does not occur; the yield moment is never exceeded using this method. Why ADINA lets the nodal moment exceed the yield moment is not known but it is believed to be the result from numerical errors in the post processing of the results. This is not further investigated as the yield moment is not exceeded by much. However, because of this the figures of moment envelopes with plastic and elasto-plastic material response will be modified so that the yield moment is never exceeded.

When solving dynamic problems in ADINA with the direct integration method one can choose between two different integration schemes. One can either solve the system using an implicit or an explicit integration scheme. In the implicit solution method ADINA uses Newmark's constant-average-acceleration method (commonly known as the trapezoidal rule), where the parameters $\delta$ and $\alpha$ from the Newmark

method are set to 0.5 and 0.25, respectively. For the explicit solution method the central difference method, described in Appendix A, is used. This is a special case of the Newmark method with the parameters $\delta$ and $\alpha$ set to 0.5 and 0, respectively. The central difference method is a fast and efficient solving method but it is only conditionally stable, meaning it requires a time step $\Delta t$ smaller than a critical time step $\Delta t_{cr}$ to give accurate results, Bathe (1996). If the time steps are too large, though, the method will be unstable, meaning that the result will become incorrect. When solving problems regarding explosions the time steps will be very small in order to describe the motion accurately, since the duration of the pressure increase is so short, and therefore the central difference method can be effectively used even in complex analyses. According to Bathe (1996), the central difference method is mainly used when a lumped matrix can be assumed and when the velocity-dependent damping is neglectable. The solutions for a linearly elastic beam using both the implicit and explicit solution methods as well as a hand calculation are compared in Figure 3.7.
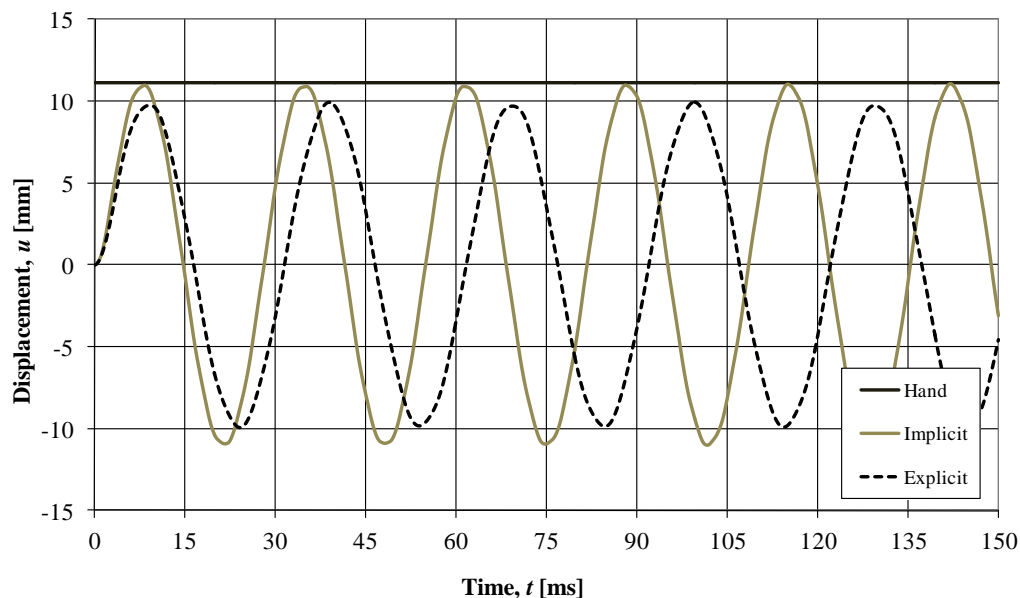


*Figure 3.7*     *Comparison between implicit and explicit analysis in ADINA and the hand calculation.*

As can be seen from the figure, the implicit solution agrees well with the hand calculation while the explicit solution differs from the implicit in both amplitude and frequency. This is probably because the explicit solution uses a lumped mass matrix while in the implicit method a consistent mass matrix is used, ADINA (2011). The phase difference may depend on the fact that the angular frequency will change with a modification of the mass, see Equation (2.37).

Since the central difference method is a very good method when using lumped mass, the method is preferable for the SDOF-model. This means that even though the beam will be modelled with an explicit method for the SDOF-model, the FE-analysis will be performed with the implicit method. The FE-analysis will also be performed with a mode superposition-analysis which will be dealt with in Section 5.1.

50

### 3.3.2 Modelling in ADINA

Due to the fact that ADINA gives an incorrect stress distribution when using 3D-elements, see Section 3.3.1, the beam has been modelled with 30 rectangular 2D beam-elements and meshed with two nodes per element. To capture the different material behaviours described in Section 2.2 the elements are modelled either with elastic isotropic or plastic bi-linear materials. Since ADINA cannot easily handle the cracks in the elastic stadium II response an equivalent Young's modulus is acquired by multiplying the Young's modulus with the ratio between the moments of inertia from Equation (3.12) and (3.16):

$$E_{II} = \frac{I_{II}}{I_I} E_I = \frac{5.6 \cdot 10^7}{6.8 \cdot 10^8} \cdot 33 = 2.72 \, \text{GPa} \tag{3.35}$$

Further, ADINA cannot handle an ideal plastic material; therefore these elements are modelled with a bi-linear material with very high initial stiffness:

$$E_{pl} = 100 \cdot E_I = 3300 \, \text{GPa} \tag{3.36}$$

and yield limit as follows:

$$f_{yd} = \frac{M_{Rd}}{W_{el}} = \frac{46.9 \cdot 10^3 \cdot 6}{1.0 \cdot 0.2^2} = 7.0 \, \text{MPa} \tag{3.37}$$

When modelling the plastic material in this way the wave speed will be changed, due to the high Young's modulus, and problems will occur. These problems will however not be of great impact for this Master thesis and is therefore neglected. This has been investigated in a previous Master thesis and the interested reader is referred to Andersson and Karlsson (2012). In the elasto-plastic analysis the equivalent Young´s modulus $E_{II}$, Equation (3.35), is used together with the yield limit $f_{yd}$, Equation (3.37). Thus, using equivalent values on $E_{II}$ and $f_{yd}$ it is possible to simulate the correct mechanical properties of the reinforced concrete beam.

The modelled force acting on the beam is a distributed line load that goes from zero to $P_{peak,n}$ in 0.01 ms, and then subsides linearly until the time $t_n$ where the pressure becomes zero, see Figure 3.3. The modelled force is an attempt to imitate load case 1. The reason for the linearly increasing pressure with one time step of 0.01 ms is because ADINA cannot deal with an increase from zero to $P_{peak}$ in no time without cutting the top values.

It is very important that the right time increments are chosen so that the characteristics of the load are implemented properly, as this is easily missed. If the time increments are too large or not adjusted to synchronise with $P_{peak}$, ADINA will assume a lower load, i.e. it is important that the time step is adjusted to $P_{peak}$ or vice versa. This is shown in Figure 3.8 where Load 1 is the sought load and Load 2 is the, by ADINA, wrongfully assumed load due to too large time increments.
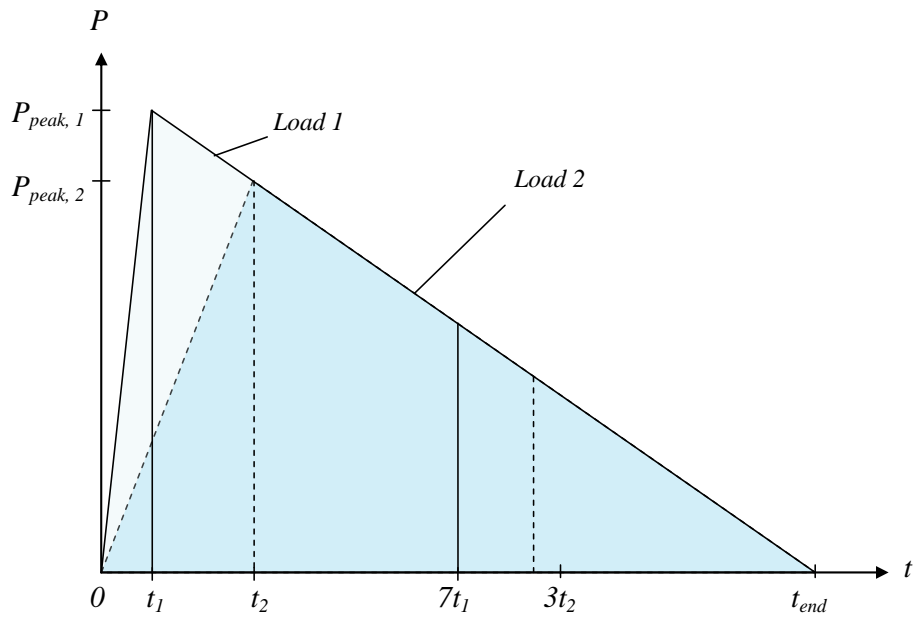
*Figure 3.8.    Assumed loads in ADINA depending on size of time increments.*

The beam is modelled as a simply supported beam and is restricted to move in the x-direction at one of the supports. Remember that even though the beam often is referred to as a horizontal beam it may as well be part of a wall and thus vertically situated and horizontally loaded.
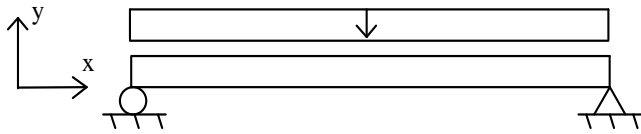


*Figure 3.9.    Boundary conditions for the studied beam.*

# 4 Initial analyses and verification of the modelling

To present an overall picture of the structural response due to a dynamic load, analyses of the beam from the previous section is made in this section. This is done with regard to the three material responses: elastic, plastic and elasto-plastic material response. The analyses are also made in order to verify the material responses described in Chapter 2, and they are made in three steps: Displacement, moment and energy balance.

## 4.1 Displacement

By comparing the displacements to the maximum deformation capacity it is possible to determine which material response the beam will take on for a specific load case, and ultimately if it will be able to resist an explosion. The displacements are calculated and compared for the beam described in Chapter 3.

The deformations from different solution methods are compared for the four different material behaviours so that the accuracy of the SDOF-method can be evaluated. It is important to find how well the SDOF-solution correlates with the corresponding FE-solution.

Firstly, the midpoint displacement is plotted. The system point in the SDOF-model is situated in the middle of the beam, thus will the SDOF-analysis also refer to the midpoint. Secondly, the deformation shapes from the FE-analysis are plotted to see if the transformation factors used in the SDOF-analysis are obtained from a correct assumption of the actual deformation shape.

### 4.1.1 Elastic response

In the analysis for linear elastic stadium I it can be seen that the SDOF-analysis correlates very well with both the FE-analysis from ADINA and the hand calculations made in Section 3.2.3, see Figure 4.1. The hand calculations, which are theoretical maximum values of the displacement, will generally give higher results compared to the more exact solution because they are derived using the simplification that the impulse load is equivalent to a characteristic impulse load.
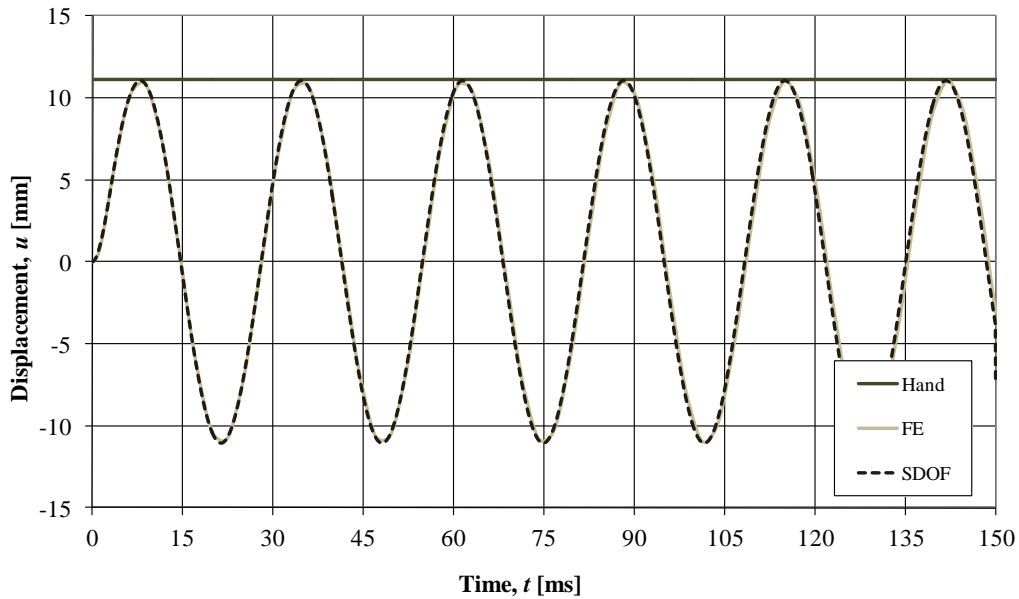
*Figure 4.1    Midpoint displacement for elastic stadium I material response.*

Similar to stadium I the maximum displacement in elastic stadium II correlates well between the FE- and SDOF-solution and the hand calculations, but there is a noticable difference in the two numerical solutions, see Figure 4.2. While the SDOF-solution has a smoothe curve the FE-solution shows a somewhat irregular pattern. This is because the FE-model considers several bending modes while the simplified SDOF-model only uses the fundamental, first, bending mode.
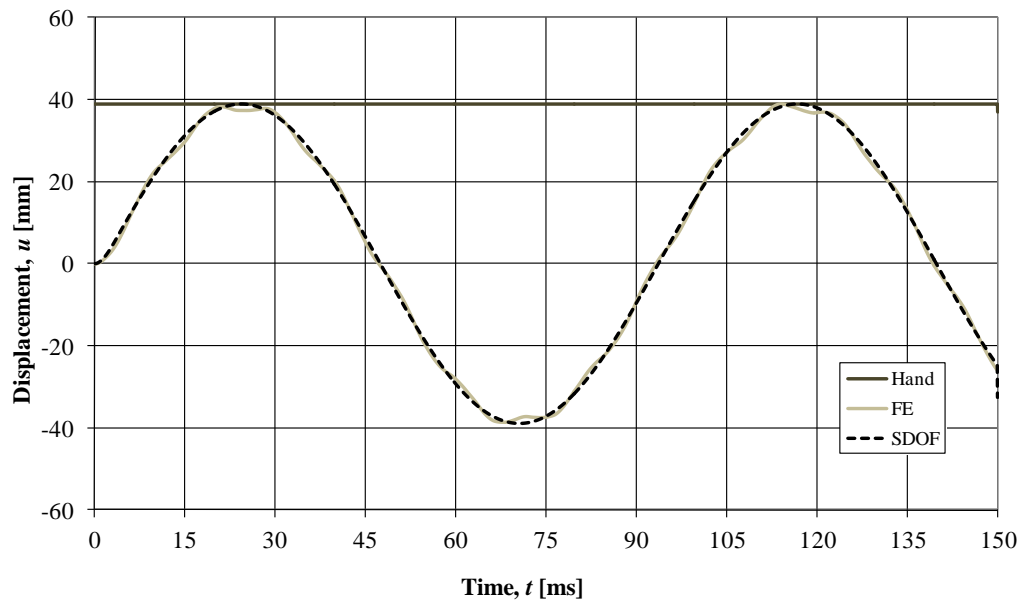


*Figure 4.2    Midpoint displacement for elastic stadium II material response.*

It can also be seen that the amplitude of the oscillations in stadium II are higher but the frequency is lower than in stadium I, which is due to the decreased stiffness in the cracked concrete. This once again depends on the important relation in Equation (2.37).

By looking at the elastic deformation shapes for different time steps plotted in Figure 4.3 and Figure 4.4 it is clear that several different transformation factors are

54

required to accurately describe the deformation shape of the beam. In the beginning it appears like the beam has a rigid body motion. It is not until after about two ms that the deformation shape resembles the assumed shape for stadium I, and more than five ms for stadium II. The interesting thing is to look at the deformation shape for the first five ms where it differs in time; after this the shape will look the same but with larger deflection. This development of deformation shapes in time is seen for all types of cross-sections, different stiffness for the beam and for larger or smaller loads. It is only the deformation magnitude and the occurence in time that is different.
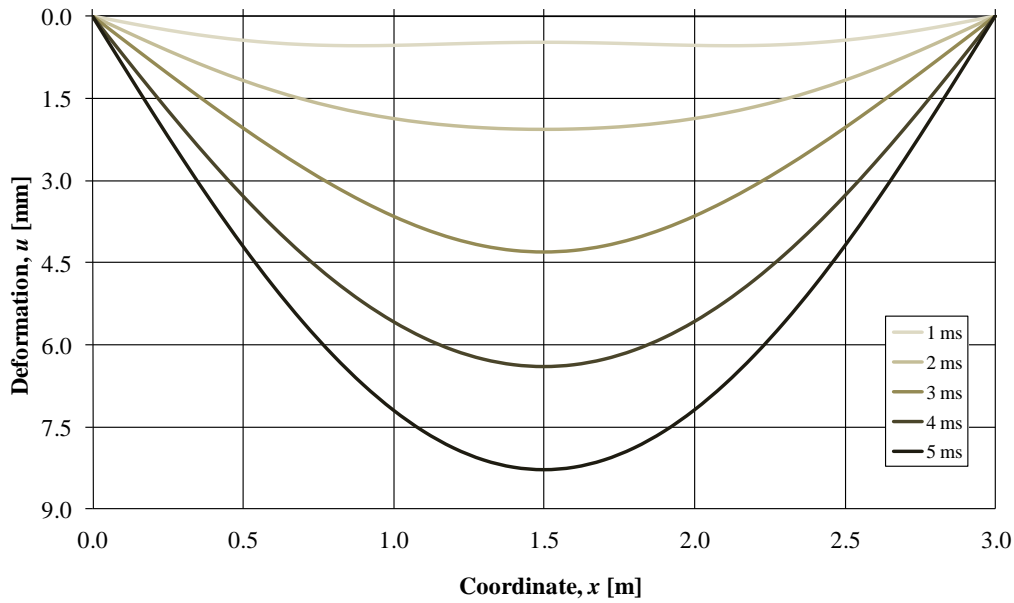


*Figure 4.3    Deformation shapes at different time steps for elastic stadium I material response.*
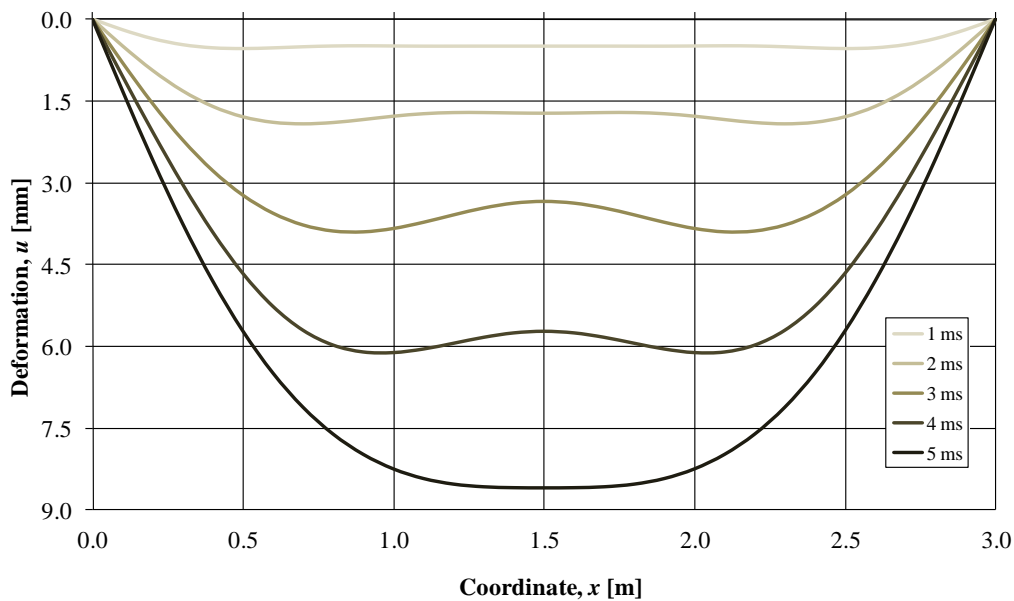


*Figure 4.4    Deformation shapes at different time steps for elastic stadium II material response.*

To give a better picture of how the deformation shape differs with time from that of a rigid body motion, the deformation shapes at different time steps are plotted against the corresponding rigid body motion in Figure 4.5. Initially the beam moves like a rigid body, but it appears as if vertical waves propagate from the ends of the beam, causing parts of the beam to deflect faster than with the rigid body motion. While the wave propagation becomes clearer with time, the midpoint displacements follow the rigid body motion, but after about 3 and 4 ms the two waves meet and the midpoint starts to deflect faster. Why this phenomenon occurs is not fully understood but a connection between the wave propagation in the beam and the duration of the effect can be seen.
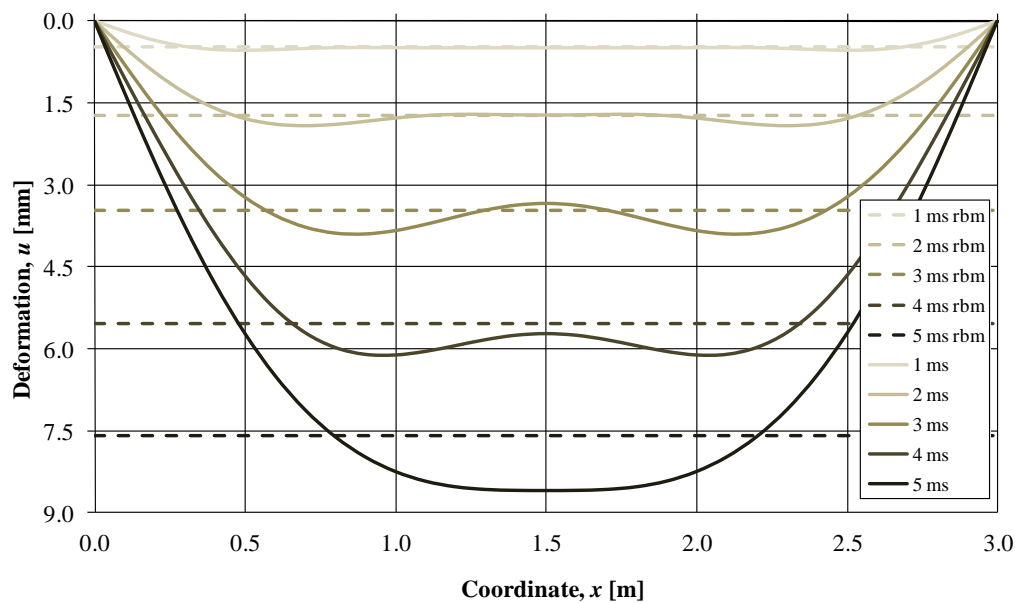


*Figure 4.5    Deformation shapes at different time steps for elastic stadium II material response compared to the corresponding rigid body motion.*

## 4.1.2   Plastic response

In the plastic analysis there is a significant difference between the three solution methods, see Figure 4.6. As for the elastic case, the hand calculations are derived from the assumption of the characteristic impulse load which explains the gap between the hand calculation and the SDOF-results. The reason why the plastic SDOF-solution differs from that of the FE-solution is believed to be because the assumed deformation shape in the SDOF-model differs from the one obtained in the FE-analysis. In the SDOF-model the transformation factor is set constant and will always be underestimated, which leads to overestimated displacements. Also, because the beam is first modelled with an elastic material response with very high stiffness, the celerity of the waves will be 10 times higher which will affect the FE-solution but not the SDOF-solution.
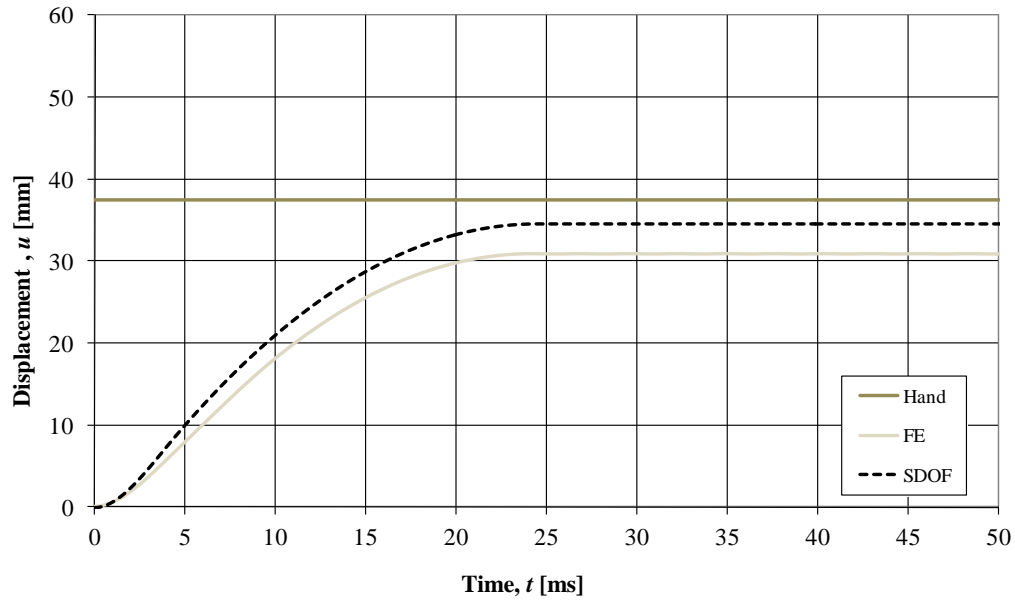
*Figure 4.6    Midpoint displacement for plastic material response.*

In Figure 4.7 the plastic deformation shape is plotted from 3 to 11 ms to show when the plastic hinge develops. It can be seen that the deformation shape starts out as a rigid body motion for the middle of the beam while the beam ends are prohibited to move. This shape is seen for different load cases but the length of the part that moves like a rigid body is shorter for less impulsive loads. As the beam proceeds to deflect further, the strained ends become longer while the almost uncurved part in the middle becomes shorter. As the middle part is decreasing, a concentrated plastic hinge becomes more prominent. It is not until after 11 ms that the deformation shape is similar to the assumed shape shown in Figure 2.11.
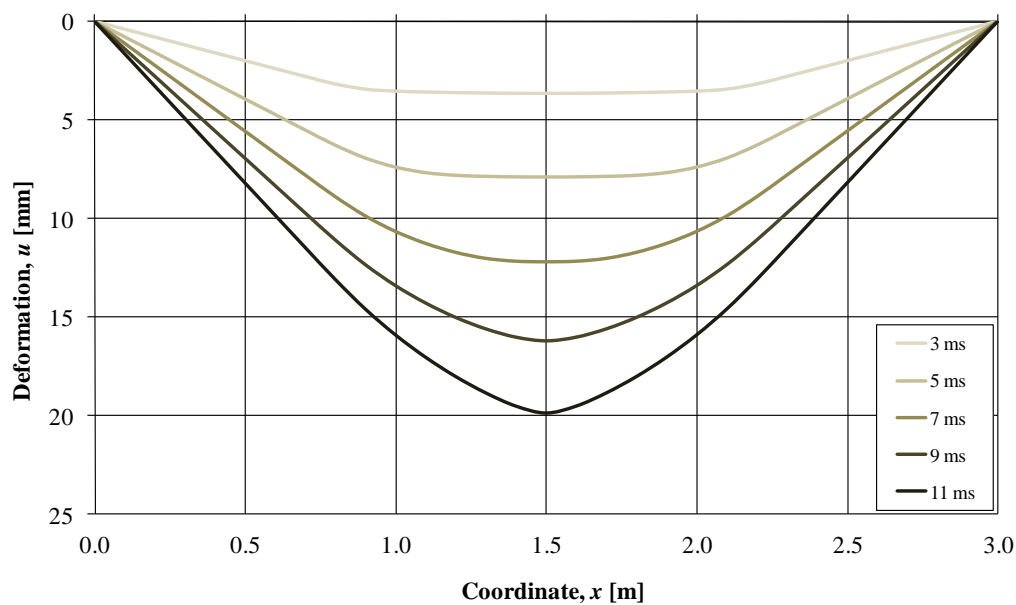


*Figure 4.7    Deformation shapes at different time steps for plastic material response.*

### 4.1.3 Elasto-plastic response

The elasto-plastic material behaviour is the one that best describes the true response of the concrete beam. Both the SDOF- and FE-model are modelled so that the beam acts as an elastic material until the yield limit is reached and the yielding starts. However, the beam will revert to elastic oscillations, and because the beam has yielded some it will oscillate about a position different from the initial position.

Since the SDOF-model is based on assumptions of the deformation shape, it is important to find one that corresponds well to the actual shape. To find the best corresponding deformation shape of the elasto-plastic behaviour in the SDOF-model it is modelled for three different cases. In the first and second case it is assumed to have elastic and plastic deformation respectively by setting the transformation factors to the ones used for linear elastic or ideal plastic behaviour. In the third case the elasto-plastic deformations are modelled by using transformation factors for linear elastic behaviour until the beam starts to yield, then switches to transformation factors for ideal plastic behaviour. Even for the best estimation of the deformation shape in the SDOF-model its solution still significantly differs from the FE-solution, see Figure 4.8.
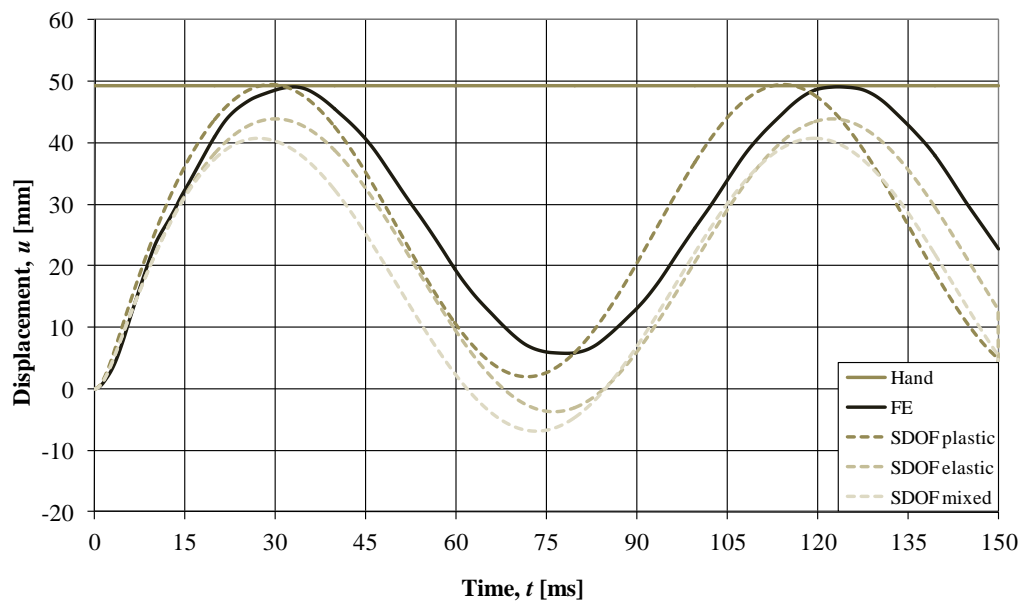


*Figure 4.8    Midpoint displacement for elasto-plastic material response.*

The difference between the FE- and SDOF-solution arises mainly when the assumption of the deformation shape is not good enough. It can also be mentioned that the agreement between the FE-solution and the hand calculation is a coincidence. In previous Master theses, though, a divergence has been seen.

It can be seen in Figure 4.8 that when using only plastic transformation factors the SDOF-analysis initially resembles the FE-analysis best and the top values are just slightly higher. However, since the frequency is higher for the SDOF-solution it will eventually get out of phase. If modelled with only elastic transformation factors, the SDOF-analysis has almost the same frequency as the FE-analysis but the top values differ about ten percent. For the third case where the transformation factors are mixed the worst correlation is achieved, even though this in theory should give the best correlation. This was also shown by Andersson and Karlsson (2012) where the

58

differences are believed to come from the synergy of different errors. However, it was shown by Andersson and Karlsson (2012) that when varying the transformation factors in time with transformation factors retrieved from the FE-analysis at several time steps the SDOF- and FE-solutions correlate very well. This method has not been further used here.

The deformation shape for the elasto-plastic material behaviour will initially be the same as for an elastic beam, see Figure 4.4. The deformation shape is plotted up to 60 ms when the yielding has begun, see Figure 4.9. The displacements of the beam are plotted as solid lines while it is still moving downward, but after 21 ms when it turns back up the displacements are plotted with dashed lines until the beam eventually stops at about 60 ms. It can also be seen for the different time steps how the plastic hinge is formed in the middle and after about 60 ms the deformation shape resembles the assumed plastic deformation shape.
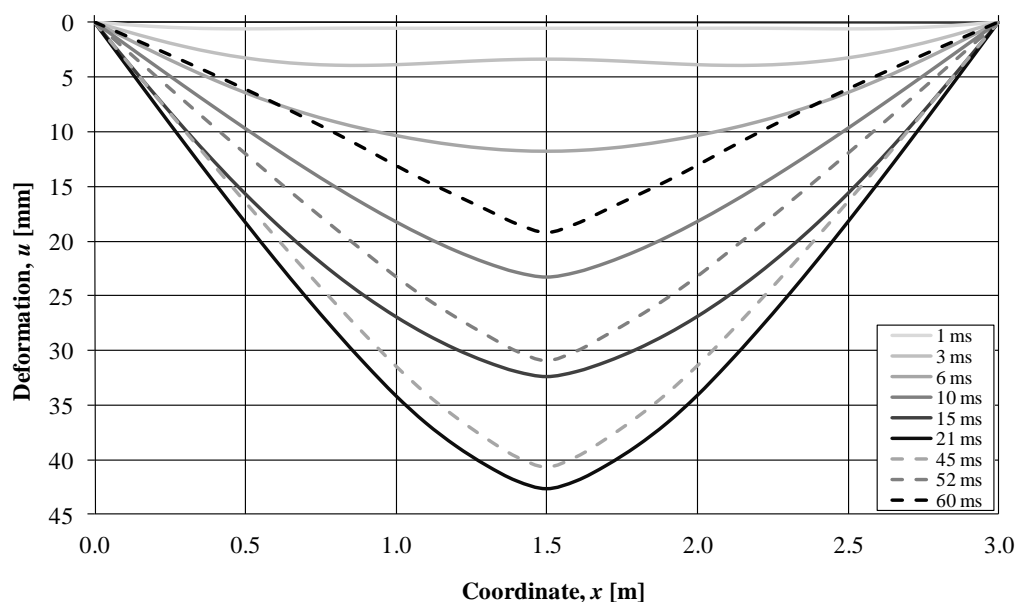


*Figure 4.9    Deformation shapes at different time steps for elasto-plastic material response.*

## 4.2    Moment

The moment is often crucial when designing beams, and therefore it is important to study how it varies over the beam with time for dynamic loads. For an elastic material response the moment is often the designing factor. In theory, the moment can be infinitely high but in reality the response will be limited. When studying the plastic and elasto-plastic material response the moment is limited by the yield moment. When the yield moment is reached the beam will start to yield and it is necessary to design such beams with regard to plastic deformation capacity. To show this, the beam from Chapter 3 has been analysed. The elastic response will from hereon be represented only by stadium II, since this better correspond to the possible response of a reinforced concrete beam.

To find the location on the beam where the time dependent moments are critical, a moment envelope will be made and compared to the equivalent static load. A moment

envelope is a moment distribution where the maximum value in the time history is saved for each node in the beam. The equivalent static load is calculated from the dynamic response from the explosion.

The moment distribution for the equivalent static load is expressed by

$$M(x) = \frac{Q}{2}(x - \frac{x^2}{L})$$
(4.1)

where $x$ is the location on the beam and $Q$ is the equivalent static load.

## 4.2.1 Elastic response

The moment distribution for a simply supported beam subjected to an impulse load initially differs a lot from that of a static load for elastic materials. As was seen for the deformation shapes in Section 4.1.1 the moment distribution also varies significantly with time. This is no coincidence, as the moment is directly related to the deformation, or rather to the curvature of the beam. The moment distribution over the beam is plotted for different time steps in Figure 4.10, and it can be seen that the moments appear to progress from the beam edges like waves through the beam. Between 1 and 5 ms the moments are about 10 to 30 kNm close to the edges and either 0 kNm or slightly negative in the middle. After 5 ms the moments near the supports are decreasing and the moment in the middle is increasing.
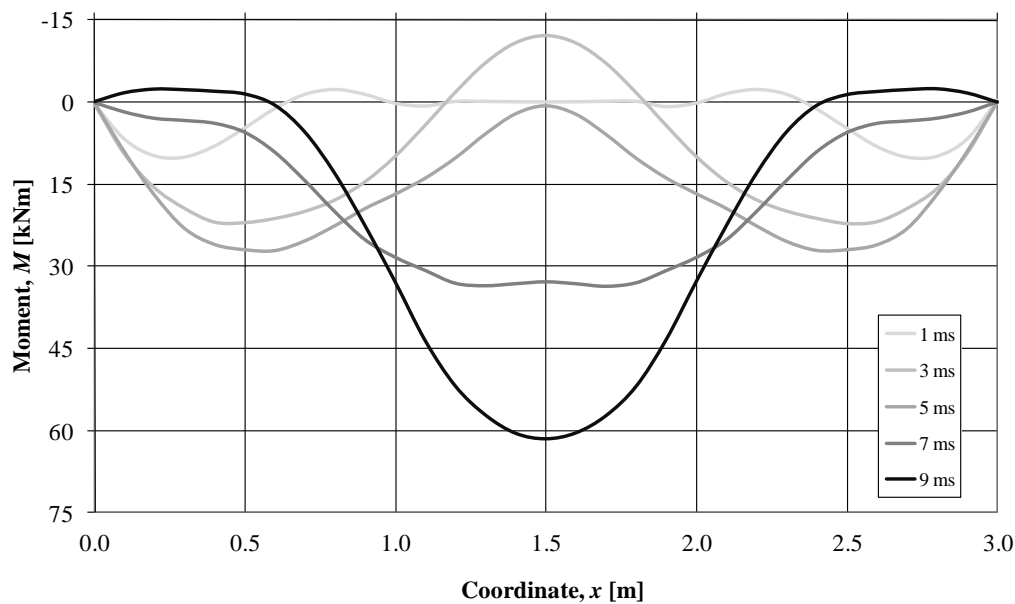


*Figure 4.10   Moment distribution at different time steps for elastic stadium II material response.*

Using Equation (2.47) from Section 2.3.4.1 the equivalent static load for elastic stadium II is calculated as

$$Q = 3 \cdot 1000 \cdot \sqrt{\frac{5.26 \cdot 10^6}{1135}} = 204.23 \, \text{kN}$$
(4.2)

60

When inserting Equation (4.2) in (4.1), the maximum equivalent moment is given as

$$M_{max} = 76.6 \, \text{kNm} \tag{4.3}$$

The moment envelope from the FE-analysis has been calculated and plotted against the moment distribution for the equivalent static load, see Figure 4.11. It is seen that the equivalent static load underestimates the maximum moment in every node along the beam, especially in the middle where the difference is about 30 percent. The simple hand calculation for an equivalent static load is a fast way to get an indication of the maximum load but it misses crucial information about the moment distribution that can be important in design. It is also worth noticing that the moment envelope in Figure 4.11 resembles the shape from the maximum moment for all times from Figure 4.10, but consists of moment distributions from more times.
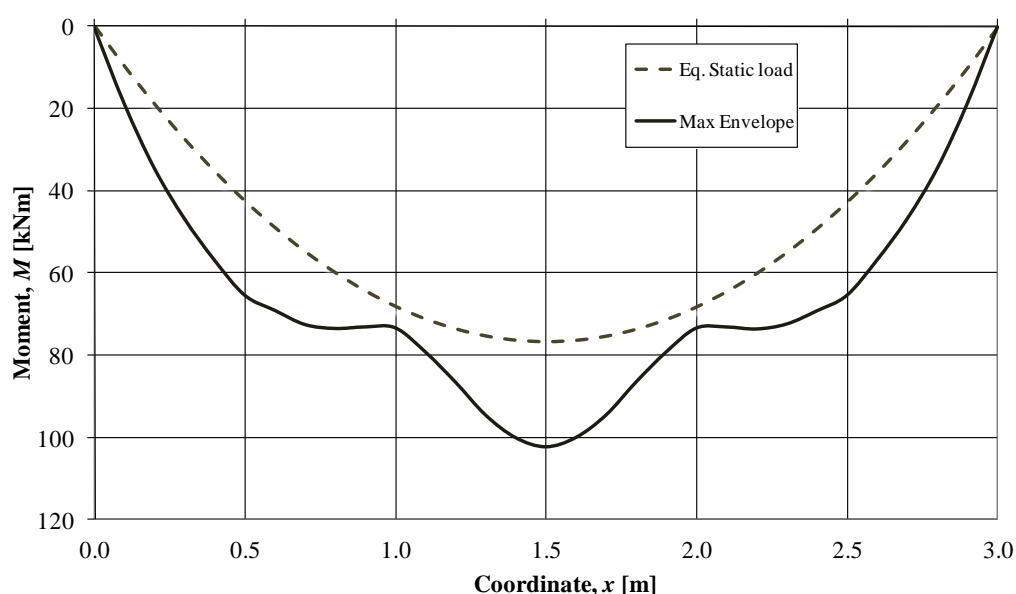


*Figure 4.11   Moment envelope and moment from the equivalent static load for the elastic stadium II material response.*

To investigate why the difference in maximum moments is of this magnitude, the midpoint moment is plotted over time, together with the maximum positive and negative moments from the equivalent static load, as seen in Figure 4.12. It appears as if the moment varies with minor oscillations about a major oscillation with a period of about 90 ms. The midpoint moment is influenced by more modes than the midpoint displacement. This can be seen when comparing Figure 4.2 with Figure 4.12. The displacement is basically only one sinusoidal function while the moment has more irregularities. It can also be seen that the maximum and minimum moments, are about the same but with different signs, and they are repeated for the next oscillations. If there would have been no minor oscillations but only the major oscillation the midpoint moment would probably not exceed that of the equivalent static load. The reader is also reminded that these results are from a model without damping and for a realistic case the oscillations would decrease with time and the minor oscillations could be much smaller even in an early stage. This is further studied in Section 5.2.
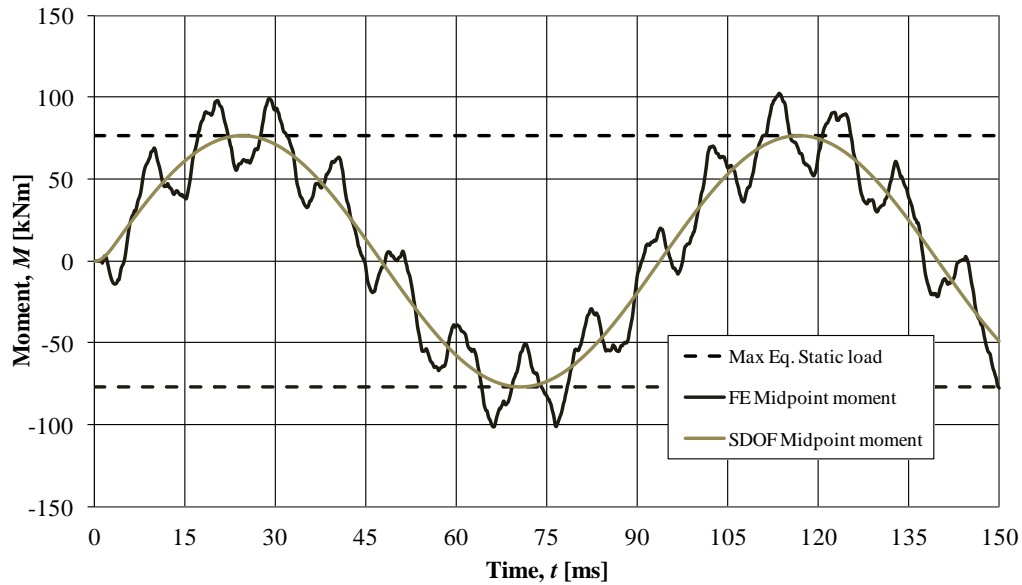
*Figure 4.12   Midpoint moment for the elastic stadium II material response.*

## 4.2.2   Plastic response

When considering the plastic response, the beam behaves in a different way in comparison to the elastic analysis. In the plastic analysis the beam has a much more predictable moment distribution over time. For an ideal plastic beam, the maximum moment will be reached instantly across the whole beam, then gradually decrease inward. A plastic hinge will develop in the middle of the beam with time, as the outer parts get strained. In the FE-analysis, though, the material is modelled as partially elastic and will therefore strain earlier. The yield moment is in Section 3.2.2 calculated to 46.9 kNm and in Figure 4.13 it is seen that the moment never exceeds this value. At 1 ms the region with maximum moment is about 60 percent of the beam length, at 5 ms it is about 25 percent of the length and at 9 ms it is less than 10 percent of the length.
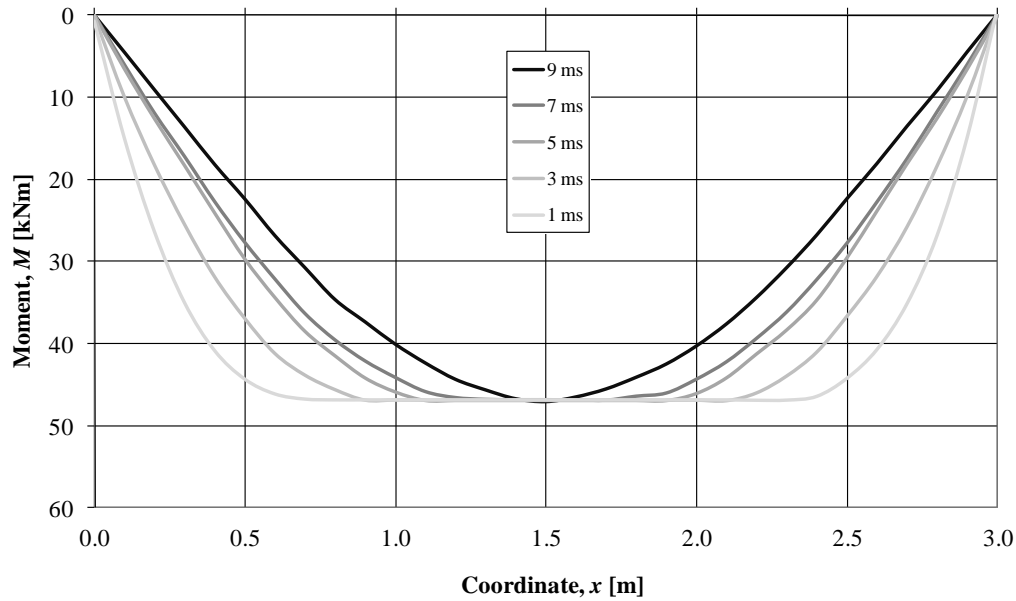
*Figure 4.13   Moment distribution at different time steps for the plastic material response.*

The moment envelope is plotted against the moment from the equivalent static load, see Figure 4.14. It is seen that the static load will underestimate the moment for large parts of the beam. The yield moment will be reached for almost the entire beam at some point, even close to the supports. Nevertheless, the maximum absolute moment in the midpoint is well described by the equivalent static load since it is easy to determine the yield moment.
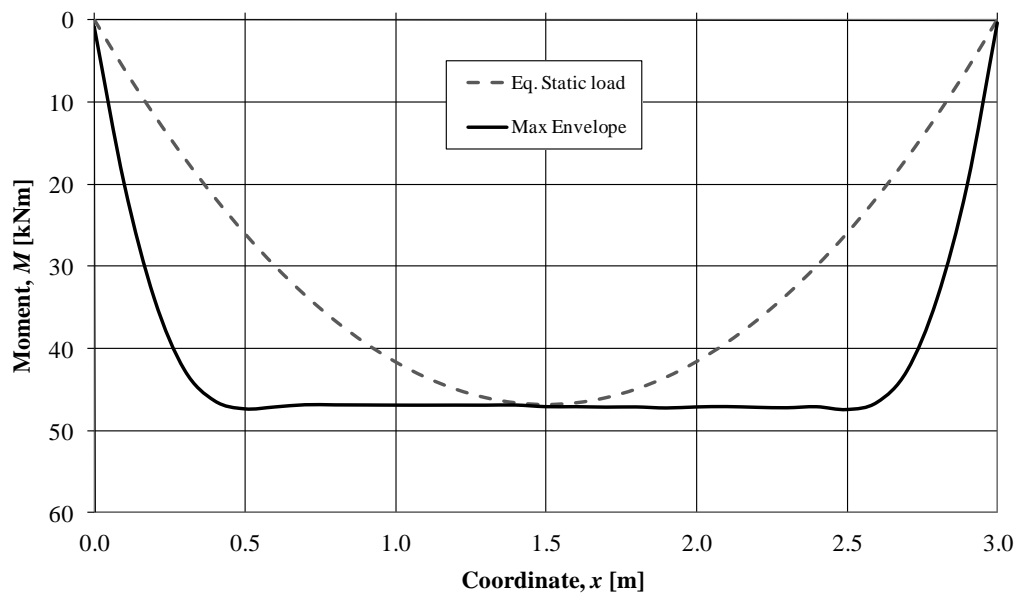


*Figure 4.14   Moment envelope and moment from the equivalent static load for the plastic material response.*

Now when the moment envelope has been studied it can be a good idea to study the plastic strain. Since almost the entire beam has reached the yield moment at one time or another the zone where the plastic strain has formed will be very wide. The beam will start to develop plastic strain closer to the supports and after approximately 5 ms

63

the beam will start to develop its strain in the middle of the beam. After approximately 30 ms the strain will be fully developed.
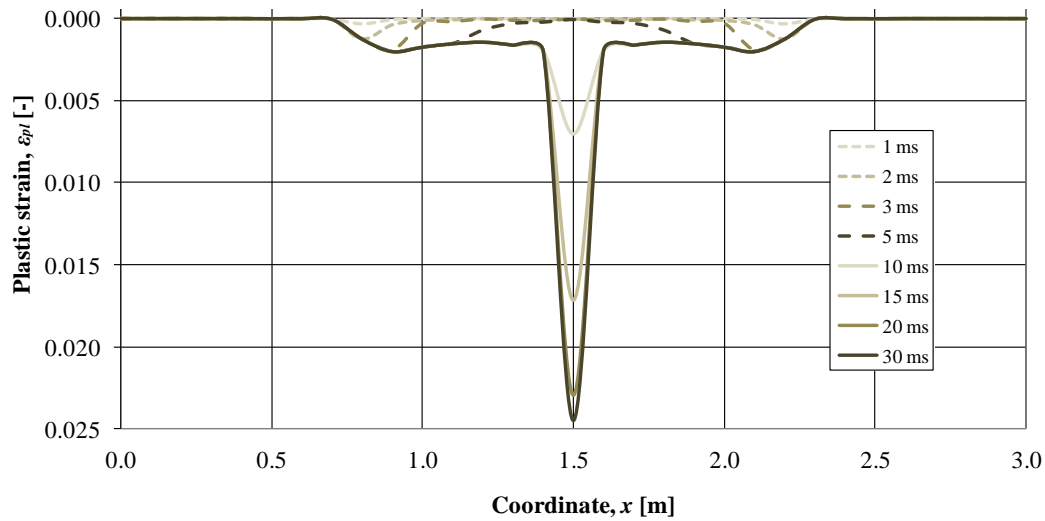


*Figure 4.15   Plastic strain for the plastic material response.*

When the midpoint moment is plotted for the plastic response, see Figure 4.16, peculiar oscillations start to occur after about 23 ms, i.e. same time as the maximum deformation is reached, see Figure 4.6. The anticipated response is what the first 23 ms shows. The oscillations after that are believed to be a result of elastic oscillations which will not occur in an ideal plastic material. ADINA does not model the plastic response in a correct way, but when only considering the first 23 ms the response is well defined.
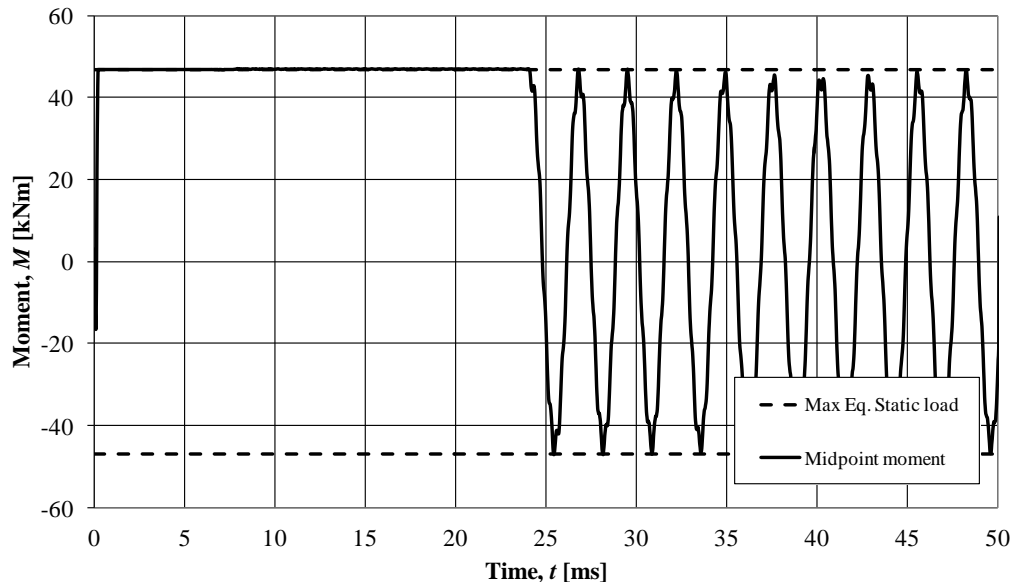


*Figure 4.16   Midpoint moment for the plastic material response.*

### 4.2.3 Elasto-plastic response

When studying the results from the elasto-plastic analysis one can see that this response is very similar to the elastic response, compare Figure 4.10 and Figure 4.17. During the first 7 ms the two responses are almost identical and it is not until after 9 ms a noticeable deviation occurs. With an elastic response there is no yield moment, and hence, the beam will be able to withstand an infinitely large moment while a beam with an elasto-plastic response will yield in the same manner as for the plastic response when the yield moment of 46.9 kNm is reached. The yield moment is 46.9 kNm, as shown in Section 3.2.2. This simplified response is the one closest to the real response for a concrete beam.
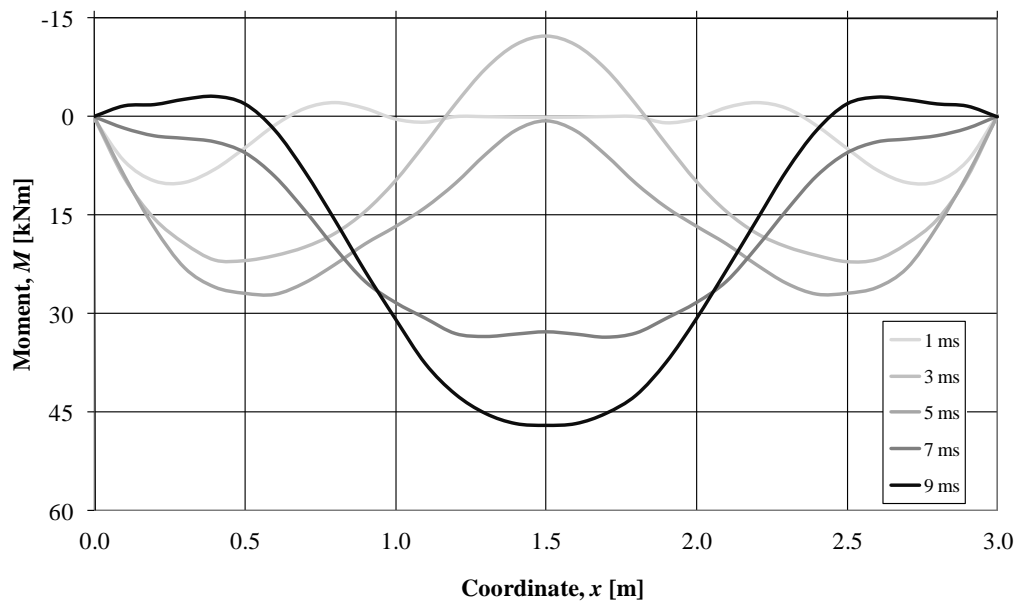


*Figure 4.17   Moment distribution at different time steps for the elasto-plastic material response.*

When the yield moment is reached a plastic hinge is created in the mid span. This can be seen very clearly when plotting the plastic strain, see Figure 4.18. At 40 ms the plastic strain is fully developed for the elasto-plastic material response. The strain has approximately the same vale as for the plastic response. A significant difference, though, is that the area of plastic strain is much wider for the plastic response compared to the elasto-plastic.
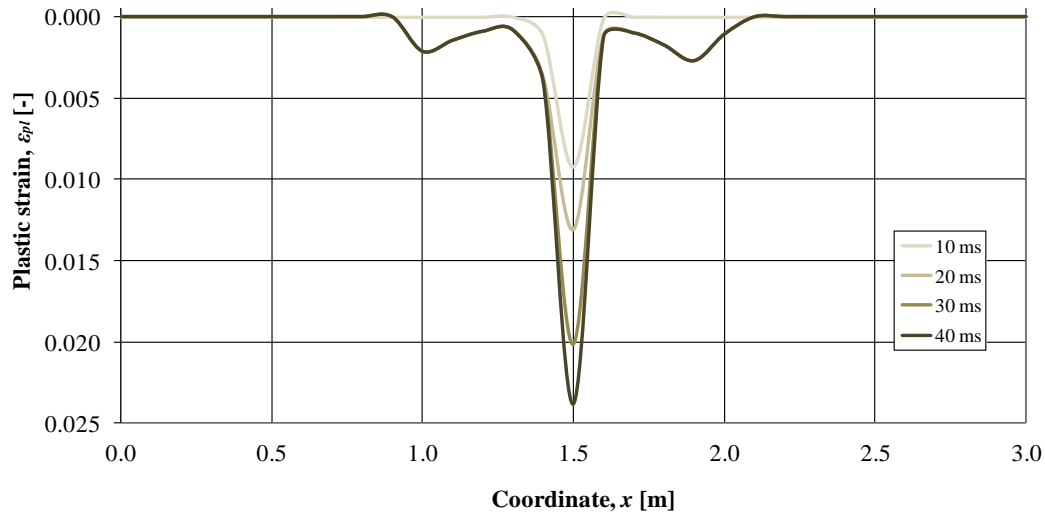
*Figure 4.18   Plastic strain for the elasto-plastic material response.*

When plotting the moment envelope for the elasto-plastic response together with the equivalent static response, Figure 4.19, one can see that the moment response is similar to that from the plastic response. This is also due to the fact that the moment cannot increase when the yield moment is reached. However, there is a deviation between the plastic and the elasto-plastic response and it is the length of the region where the yield moment has been reached. Since the elasto-plastic response has an elastic part which can absorb energy, the length of the area where the yield moment is reached is smaller than for the plastic case. However, this can still be a problem for occasions with curtailment (shortening of reinforcement) of the beam. If the moment capacity is exceeded the reinforcement will yield and can eventually brake. This is a topic in structural response with regard to explosions that have not been studied thoroughly, but in Section 0 a study has been made for this problem.

Once again the equivalent static load response is insufficient for large parts but is well defined in the mid span. Same as for the plastic envelope, the results from ADINA sometimes presented moments that slightly exceeded the yield moment which is not possible, and were therefore not accounted for.
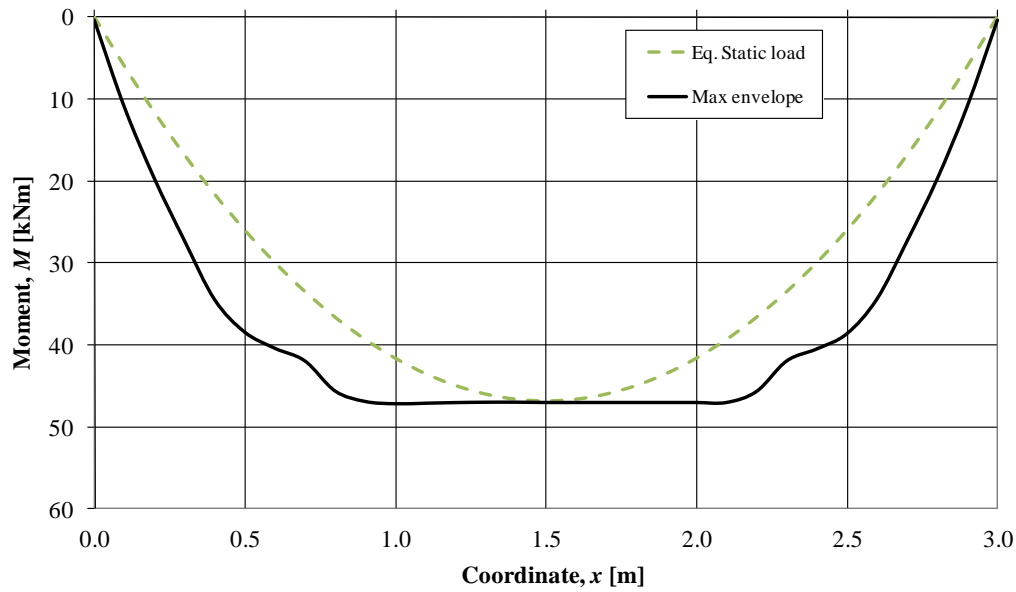
*Figure 4.19   Moment envelope and moment from the equivalent static load for the elasto-plastic material response.*

Figure 4.20 clearly shows the elasto-plastic response for the midpoint moment. This is a typical behaviour for an elasto-plastic material. When the beam is struck by the shock wave from an explosion the moment in the midpoint will increase until the yield moment is reached and a part of the beam will yield. When the beam swings back, enough energy has been absorbed for the beam to only just reach the yield moment. Due to some minor oscillations there are two peaks which almost reach the yield moment 46.9 kNm.
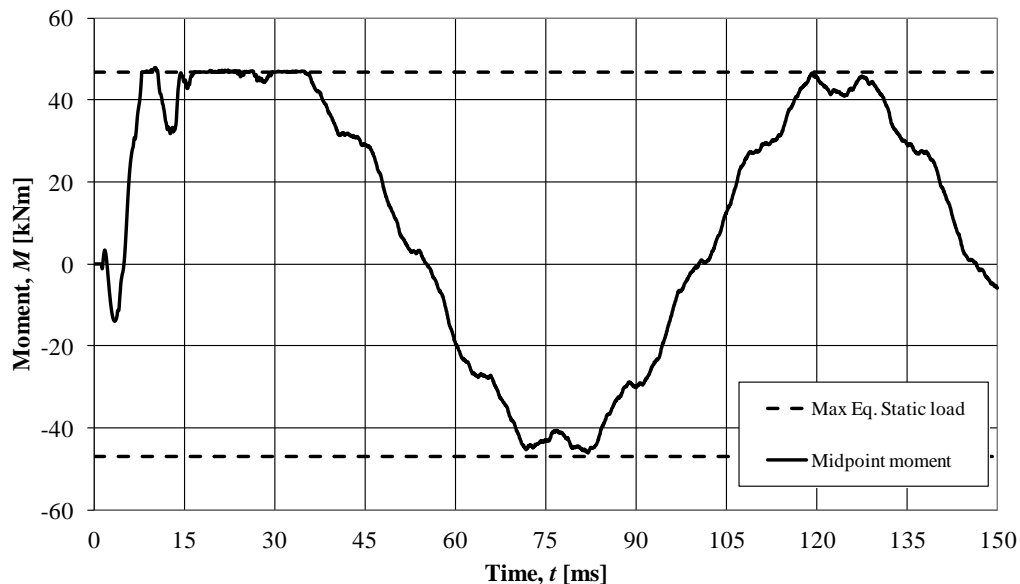


*Figure 4.20   Midpoint moment for the elasto-plastic material response.*

## 4.3    Energy balance

It is often beneficial, and sometimes necessary, to think in terms of energy balance when dealing with the structural response from an explosion. This is also another approach in checking the correspondence between the SDOF- and the FE-solution. The structural response has a direct relationship with the energy put into the system, the external energy $W_e$. Thus, the response can often be determined from simple calculations. As seen in Section 2.3.3 the external energy applied should be equal to the sum of internal energy, $W_i$, and kinetic energy, $W_k$, in order to have energy equilibrium:

$$W_e = W_i + W_k \tag{4.4}$$

When this state of equilibrium is reached the maximum deformation is obtained. The external energy is determined from the force times the displacement caused. For the FE-analysis this is done by integrating the force in every node and multiplying it with the corresponding displacement for every time step, sees Equation (4.5) in Table 4.1. Since the forces are extracted from nodes in the FE-analysis, the classic integration cannot be made, but it is accomplished by taking the sum of the force times the displacement in every node for every time step. For the SDOF-model the same procedure is used but then only for the system point.

It is somewhat more difficult to comprehend the calculations for the internal energy in the FE-analysis, but it can be explained as the energy needed to bend the beam. The internal energy is calculated by taking half of the integral of the moment times the change in rotation, the curvature, according to Equation (4.6). According to Appendix A, the curvature is the second derivative of the displacement. For the SDOF-model the internal energy is simpler to determine as the inner resistance times the corresponding displacement for all time steps.

Finally the kinetic energy is calculated by taking half of the integral of the mass times the square of the velocity for the elements in the FE-analysis, see Equation (4.7). For the SDOF-model the same equation is used. Equations (4.5) to (4.7) are gathered in Table 4.1.

*Table 4.1.* *Definition of work for the FE-analysis and the SDOF-model respectively.*

|  | FE-analysis | SDOF-model |  |
|---|---|---|---|
| External energy | $W_e = \int\limits_{x=0}^{x=L} q(x)u(x)dx$ | $W_e = \kappa_F F u_s$ | (4.5) |
| Internal energy | $W_i = \dfrac{1}{2}\int\limits_{x=0}^{x=L} M(x)u''(x)dx$ | $W_i = \kappa_F R u_s$ | (4.6) |
| Kinetic energy | $W_k = \int\limits_{x=0}^{x=L} \dfrac{m(x)v(x)^2}{2}dx$ | $W_k = \dfrac{\kappa_m m v_s^2}{2}$ | (4.7) |

When deriving the energy from the SDOF-system it is important to keep in mind that the energy is proportional to

$$W \propto \frac{\kappa_F^2}{\kappa_m} \tag{4.8}$$

whilst the displacement is proportional to

$$u \propto \frac{\kappa_F}{\kappa_m} \tag{4.9}$$

This is of matter when scaling the transformation factors with a factor $\xi$. In that case the energy level can become higher whilst the deformation stays the same:

$$\left(\frac{\kappa_F}{\kappa_m}\right)_{new} = \frac{\xi\kappa_F}{\xi\kappa_m} = \frac{\kappa_F}{\kappa_m} \tag{4.10}$$

$$\left(\frac{\kappa_F^2}{\kappa_m}\right)_{new} = \frac{\left(\xi\kappa_F\right)^2}{\xi\kappa_m} = \xi \cdot \frac{\kappa_F^2}{\kappa_m} \tag{4.11}$$

It is now of interest to compare the energy balance for the FE-analysis with the SDOF-model and the hand calculations. This is once again done for the three different ideal materials, the elastic, plastic and elasto-plastic material response. The elastic response will be represented by stadium II. With the comparison between material responses the reader can get an indication of the accuracy of the SDOF-model and the hand calculations and if the energy balance is achieved for the two analyses. It is also of interest to see how the structure absorbs the external energy throughout the time span.

### 4.3.1 Elastic response

The hand calculation for the energy, which is the theoretical maximum energy, is made according to Section 2.4.3. When the force from the pressure hits the beam its kinetic energy will increase rapidly. When calculating the theoretical maximum energy it is assumed that all of the external energy is transferred into kinetic energy, hence will the energy level for the elastic stadium II analysis be calculated as

$$W_e = W_k = \frac{I_k^2}{2\kappa_{mF} m}\kappa_F = \frac{3000^2}{2 \cdot 0.788 \cdot 1440} \cdot 0.64 = 2538 \, \text{J} \tag{4.12}$$

As can be seen in Figure 4.21 the energy balance for the FE-analysis is satisfyingly met. The energy put into the system is in equilibrium with the energy used, as anticipated. The hand calculation, though, is not fully corresponding with the FE-analysis. This can be explained by the transformation factors. In a previous Master thesis by Andersson and Karlsson (2012) it is shown that the hand calculation better corresponds to the FE-analysis when the impulse load is less intense, i.e. behaves more like a static load. The agreement between the FE-analysis and the hand calculation decreases for a very impulsive load. The transformation factors are derived from the deflection of a beam when loaded statically; the closer the deflection of the actual beam is to a statically loaded beam, the better the correspondence.
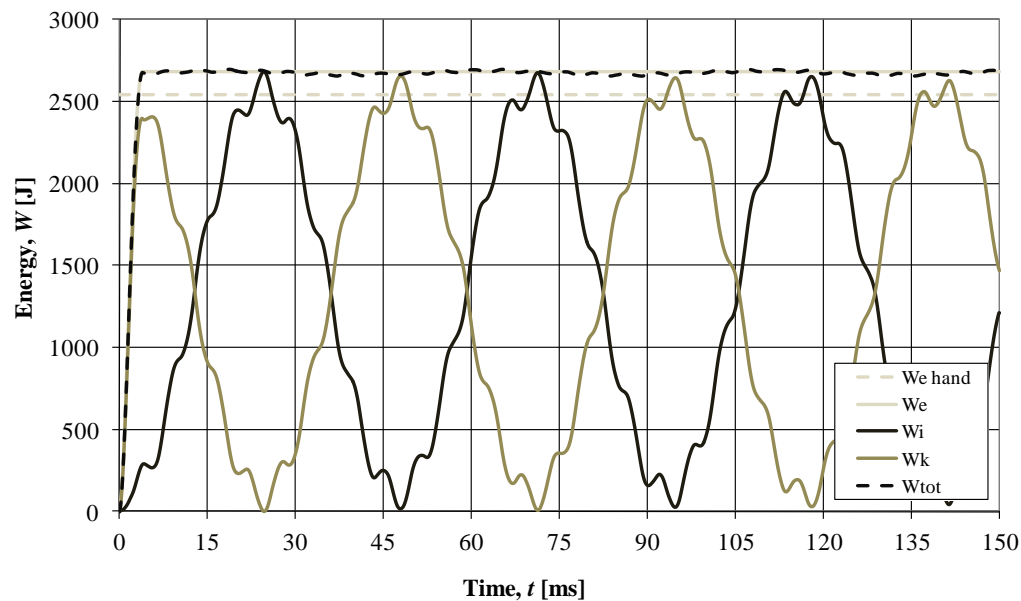


*Figure 4.21. The energy balance for the FE-analysis and the hand calculation for the elastic stadium II material response.*

The agreement between the SDOF-model and hand calculation is very good, but most important is to have good correspondence between the SDOF-model and the FE-analysis. In this case the SDOF-model gives energy levels on the unsafe side, which is unwanted, see Figure 4.22. The same source of error applies here, the divergence is due to the transformation factors and the errors are incorporated when using a static deformation shape. The discrepancy in energy levels are however relatively close and can be acceptable.
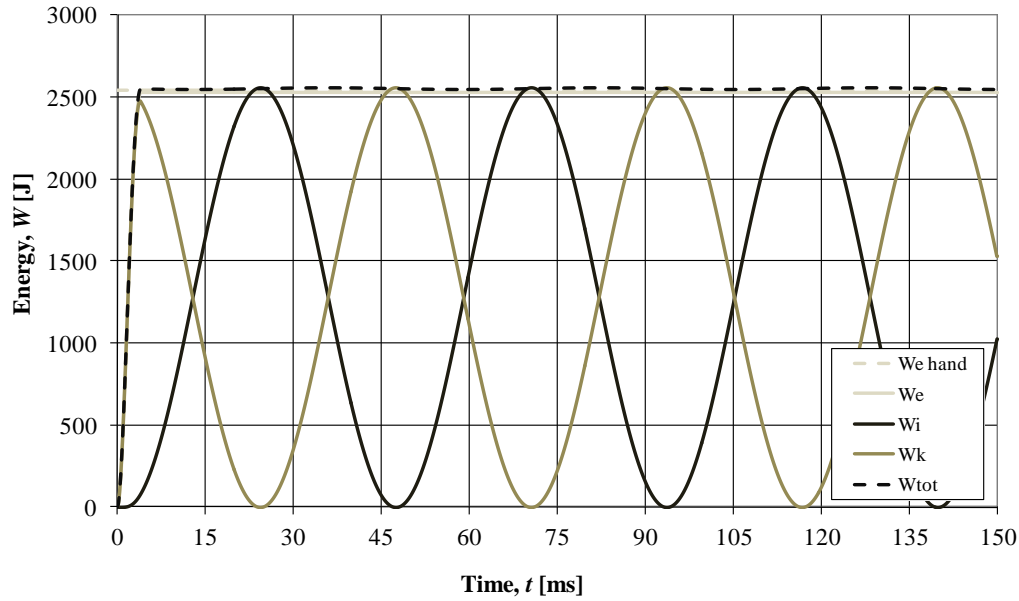
*Figure 4.22. The energy balance for the SDOF-model and the hand calculation with the elastic stadium II material response.*

Both for the FE-analysis and the SDOF-model the response of the beam will alternate between fully developed kinetic energy and then fully developed internal resistance. This is a typical response for an ideal elastic material when the beam sways back and forth. Furthermore, the energies in the SDOF-model are smoother than the energies from the FE-analysis. As was mentioned in Section 4.1.1, this is due to the fact that the SDOF-model only takes the first bending mode for the beam into account whilst the FE-analysis takes more modes into account.

### 4.3.2  Plastic response

In plastic analysis the transformation factors are determined based on an appearance according to Figure 2.11. A hand calculation of the energy for the plastic response is made with the new transformation factors:

$$W_e = W_k = \frac{3000^2}{2 \cdot 0.667 \cdot 1440} 0.5 = 2343 \, \text{J} \tag{4.13}$$

When comparing the FE-analysis, Figure 4.23, with the SDOF-model for the plastic response, Figure 4.24, the agreement is very good. The SDOF-model gives an energy level just below the FE-analysis. The relative error, $\xi$, is calculated as

$$W_{tot}^{FE} = 2235 \, \text{J} \tag{4.14}$$

$$W_{tot}^{SDOF} = 2157 \, \text{J} \tag{4.15}$$

$$\xi = \frac{W_{tot}^{SDOF} - W_{tot}^{FE}}{W_{tot}^{FE}} = -3.5\% \tag{4.16}$$

71

The main reason for the deviation between FE-analysis and the theoretical maximum energy calculated by hand is believed to be because there are differences in the transformation factors. As can be seen in Figure 4.23, the kinetic energy $W_k$ is not fully developed within the first 4 ms because the external energy $W_e$ is still increasing.
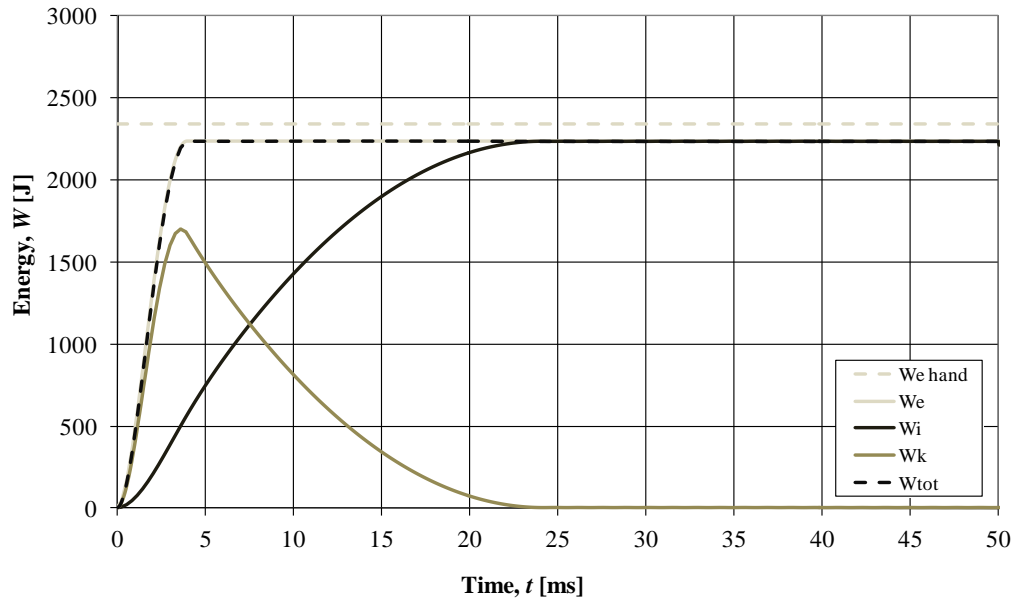


*Figure 4.23. The energy balance for the FE-analysis and the hand calculation with plastic material response.*
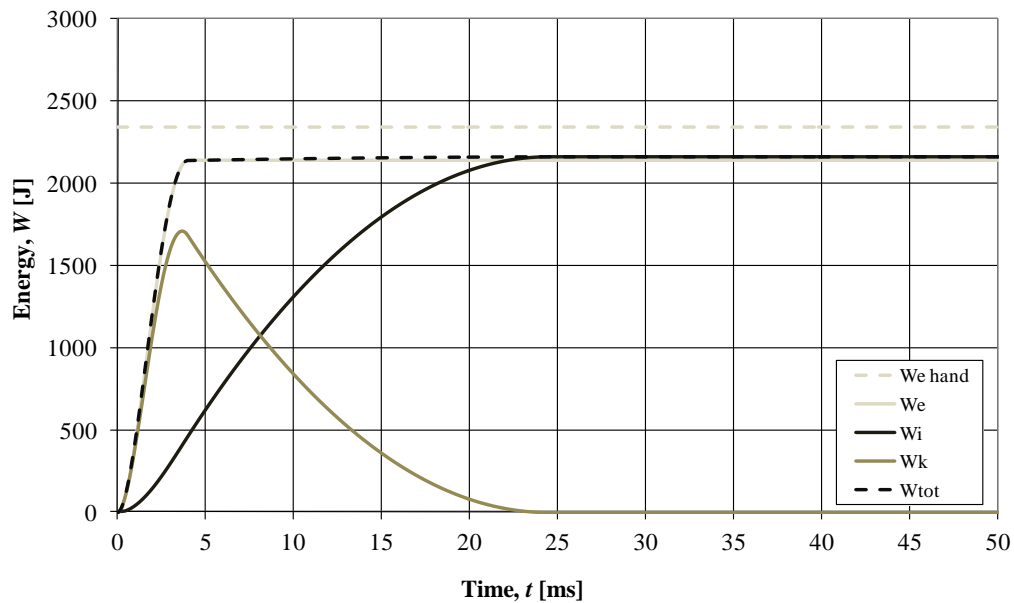


*Figure 4.24. The energy balance for the SDOF-model and the hand calculation with plastic material response.*

Because the stiffness is high for the plastic material response, the internal energy will increase early, thus, in order to maintain energy equilibrium, the kinetic energy must be low. The beam does not sway back and forth as for an elastic response. The beam

yields and the beam's way to absorb the external energy is through internal resistance, hence the low kinetic energy and high internal energy.

An interesting observation is that although the energy level is lower for the SDOF-model compared to the FE-analysis it is in reversed order for the displacement, see Figure 4.6. This occurs because of the relationships between the transformation factor and the energy and the displacement respectively, as mentioned earlier, Equation (4.8) to (4.11).

### 4.3.3 Elasto-plastic response

As mentioned in Section 2.4.2, there are no special elasto-plastic transformation factors. Instead, usage of either the elastic, plastic or both transformation factors are made. The theoretical maximum value of energy is calculated with either Equation (4.12) or Equation (4.13) as can be seen in Figure 4.25 for the FE-analysis. Here it is clear that the elastic transformation factors give better correspondence with the FE-analysis.
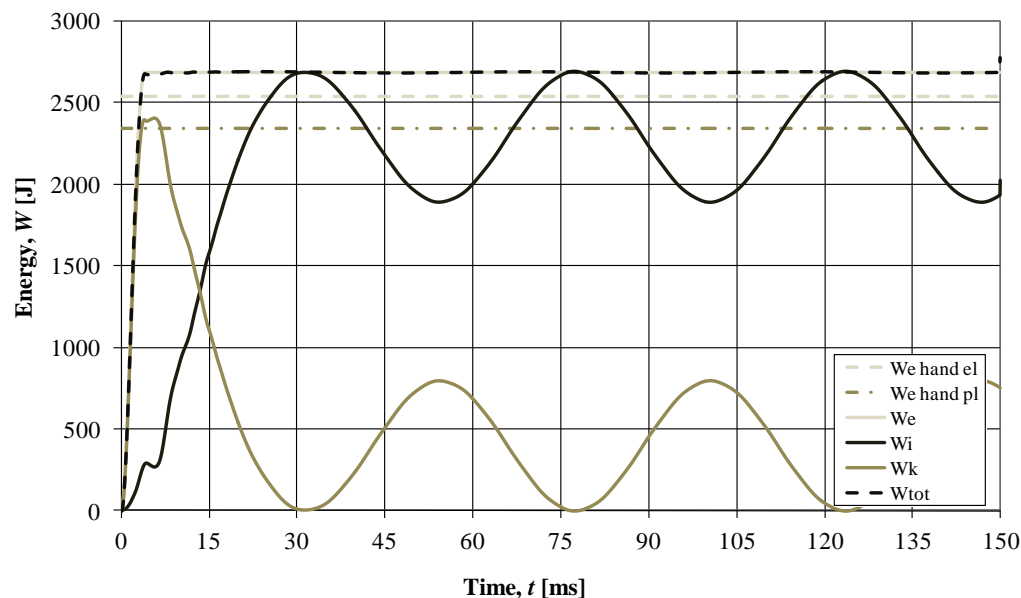


*Figure 4.25. The energy balance for the FE-analysis and the hand calculation with elasto-plastic material response.*

When studying the SDOF-model and using constant transformation factors, there are three different cases that are of interest. The SDOF-model is either modelled with only elastic transformation factors, only plastic transformation factors or a combination of them both. All three cases will present lower energies than the FE-analysis. In Figure 4.26 the SDOF-model has been modelled with the elastic transformation factors. This gives a fairly good agreement between the FE-analysis and the SDOF-model.
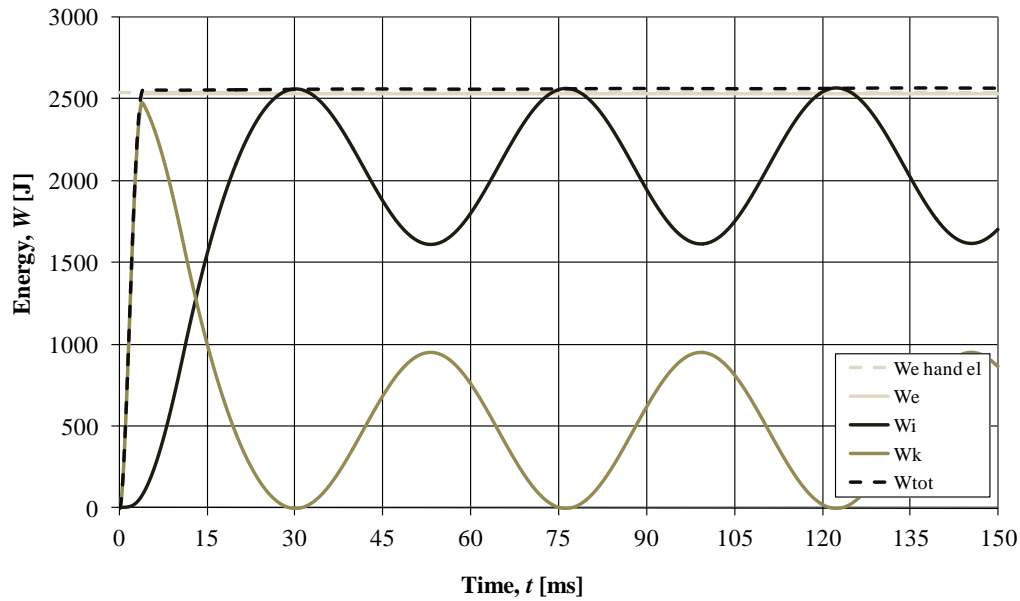
*Figure 4.26. The energy balance for the SDOF-model and the hand calculation with elasto-plastic material response and elastic transformation factors.*

In Figure 4.27 the plastic transformation factors have been used. This results in less agreement with the FE-analysis than from the case with elastic transformation factors, the energy level is decreased.
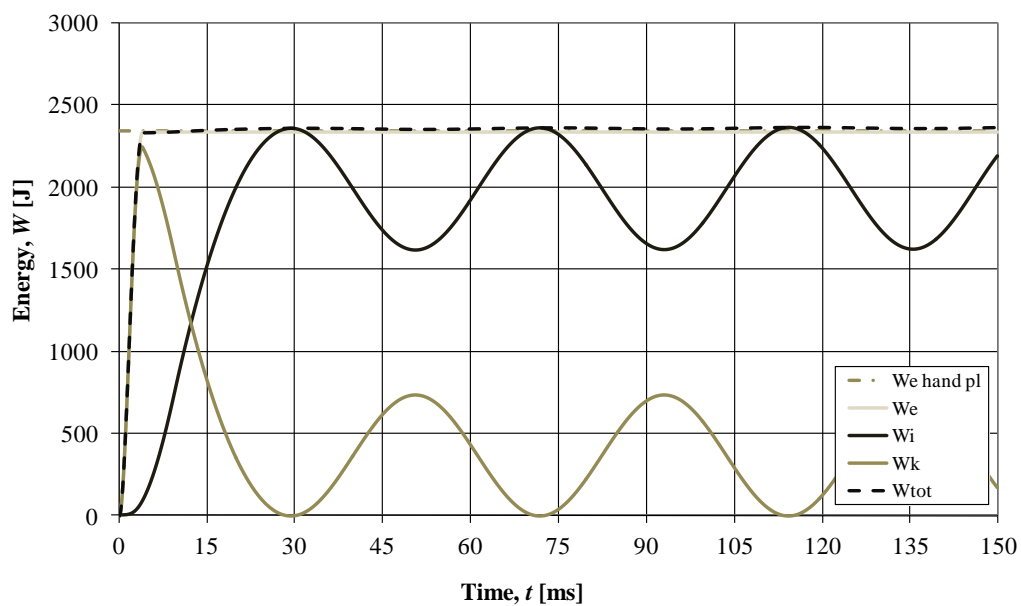


*Figure 4.27. The energy balance for the SDOF-model and the hand calculation with elasto-plastic material response and plastic transformation factors.*

The third option is shown in Figure 4.28 where the transformation factors change when the yield limit is reached. First the elastic factor is used when the beam is in its elastic stadium. When the force has increased enough the beam will start to yield and the plastic factor is used. In contrary to the first two cases, this will result in an unbalanced energy and the agreement with the FE-analysis is less than with only plastic transformation factors. In order to achieve good correspondence between the SDOF- and the FE-analysis it is necessary to use transformation factors that vary in

74

time to give a better assumption of the deformation shape. This is not studied in this Master thesis but it has been shown successfully in Andersson and Karlsson (2012).
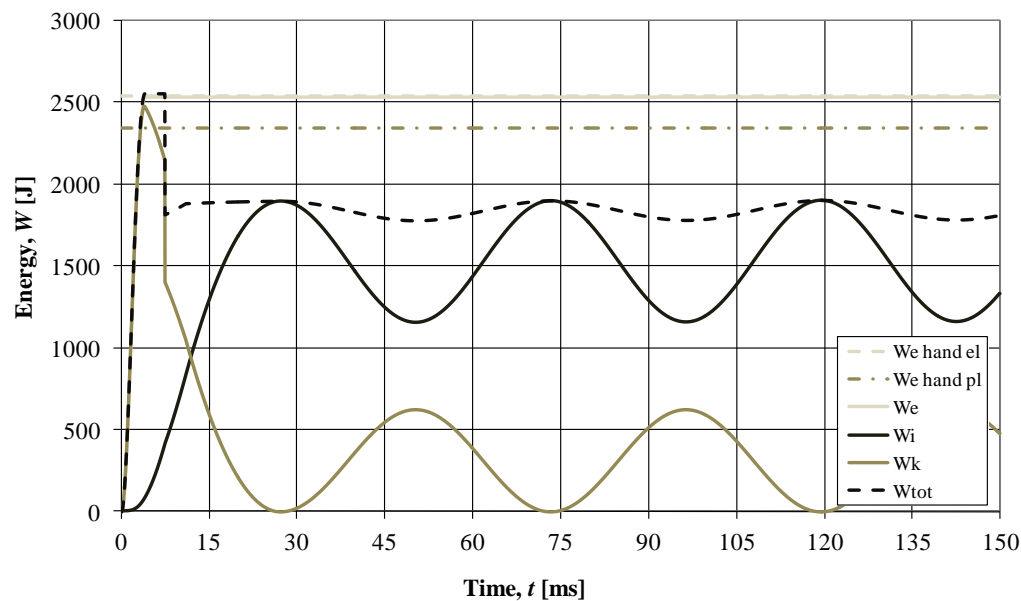


*Figure 4.28. The energy balance for the SDOF-model and the hand calculation with elasto-plastic material response and both elastic and plastic transformation factors.*

## 4.4    Discussion

The results from the displacement analysis indicate that the SDOF-model very well describes the midpoint displacement when an elastic material response is applicable. The hand calculation is a good method to quickly determine the maximum displacements which also correspond well to the FE-analysis. With an elastic response the deformation shape will be easier to approximate with the transformation factors. However, when the plastic- and elasto-plastic material response applies the agreement will be worse between the SDOF-model and the FE-model. This is believed to depend on the fact that the deformation shapes are difficult to describe with constant transformation factors. In the beginning the beam appears to have a rigid body motion, which does not fulfil the assumed deformation shape. It is concluded that several transformation factors are needed to describe the deformation of the beam if an almost exact approximation is wanted, when a plastic- or elasto-plastic material response is used. If one can tolerate some divergence, the SDOF-model can be used when the plastic transformation factor is used for the elasto-plastic case. The reason why the SDOF-model with plastic transformation factors gives such a good result, though, is unknown.

The most important aspect with regard to the moment is that the moment calculated from the equivalent static load underestimates the moments from the FE-analysis in all nodes. This can be of concern when other materials than reinforced concrete is used. A reinforced concrete beam is able to redistribute the forces in a beneficial way but for e.g. a timber structure the arising moments may very well lead to failure. Another interesting aspect with regard to the moment is that the moment is relatively

large close to the supports the first few ms. This raises the question about curtailment. The Swedish "Fortifikationsverket" have determined that when designing bomb shelters no curtailment is allowed, and when studying the moment development this is easy to understand, but what happens when a structure with curtailment is subjected to an explosion? This will be investigated in Section 5.3. When it comes to the agreement between the SDOF- and the FE-analysis it is easy to see that the moment is more influenced by more bending modes than the displacements. This indicates that an SDOF-solution is inadequate when regarding the moment and that a more detailed approximation could be relevant. This is studied in Section 5.2.

When studying the response of a structure subjected to an explosion it is beneficial to study the energy acting in the structural system. This will help in order to understand the behaviour as the energy put into the system will be in equilibrium with the energy consumed. The SDOF-analysis presents reasonable agreement with the FE-analysis for all material responses, especially when the elastic transformation factors are used for the elasto-plastic behaviour.

The reader is reminded of that these analyses have been carried out without taking regard to the damping of the structure. This means that the real structure will behave differently. However, it is important to understand the response without damping before analyses are performed with regard to damping. In Section 5.2 the damping will be included to the analyses which will make it more realistic.

76

# 5 Mode superposition and damping

As mentioned in Section 2.4.1, the deformation shapes of impact loaded structures consists of a combination of several bending modes. By using the method of mode superposition, which is described in Appendix D, for linear elastic analyses any requested number of modes can be conjoined to describe the response of the structure. If the structure is complex and/or consists of many parts, an analysis of the structure might take a long time, especially if many modes are to be regarded. Because of this, it is important to know how to make relevant simplifications that still provide accurate results. By investigating which modes have the most influence on the deformation shape, a good approximation can be made by modelling the motion with only these modes. In that way time can be saved when analysing the structure. However, since the structure in this Master thesis is a simply supported beam with relatively few nodes, the time saved will be negligible.

Another important aspect is to try once again to verify the usefulness of the SDOF-model. Hence, it is investigated whether a single degree of freedom is sufficient to describe the motion for an impulse loaded beam or if it is necessary to introduce more degrees of freedom to the simplified calculation method. Will it be sufficient in order to determine both displacement and moment, with and without damping? In order to determine this some guidelines of how big the error can be is used. If the error lies within one percent is it a very good approximation and if it lies within five percent is it acceptable.

Since all structures in reality have damping that differs with mode shape it is natural to regard the damping while making a mode superposition-analysis. The damping is often analysed as Rayleigh damping, described in Appendix E, or modal damping. If there is a lot of information about the damping of the structure the modal damping is the best choice as it has the possibility to choose specific damping for every mode. However, if there is lack of information about the structure, the Rayleigh damping might be a better choice as it is more general and usually can be regarded to be on the safe side.

The main reason for analysing the damping is that one can be concerned for the high values of the midpoint moment within the first few ms. The FE-analysis, see Figure 4.12, has previously shown that the maximum midpoint moment within 15 to 35 ms is much larger than the equivalent static load, which is more commonly used when designing structures. A question needed to be answered is if the damping will decrease the midpoint moment enough for the first 35 ms so that the equivalent static load will be a satisfactory simplification.

As an example the beam in Chapter 3 is further analysed with focus on the midpoint moment with mode superposition-analysis for an elastic stadium II material response and later the damping is analysed. The direct integration analysis will for simplicity still be referred to as "FE-analysis" and the mode superposition-analysis, which also is a type of FE-analysis, will be referred to as "modal-analysis".

## 5.1 Modal-analysis

When performing a modal-analysis to study the response in the midpoint of a simply supported beam subjected to a distributed load one can exclude the modes that have a stationary node in the middle. In this case the aforementioned property exist for every even number of modes, see Figure F.1 in Appendix F. Hence, for this analysis only the odd numbers of modes will be regarded. The subject of interest is in this analysis the agreement between the SDOF-analysis and the modal-analyses with different amount of modes compared to the FE-analysis for all time steps. It is not sufficient to just have the same maximum value but it is the general agreement with the FE-analysis that is important. When choosing number of modes to use in ADINA it is important to remember that not all modes give a contribution to the midpoint moments and displacements, and also that longitudinal modes can be contributed in the analysis.

As can be seen from Figure 5.1, when analysing the midpoint displacement by only using the first mode in the modal-analysis, the result will, as expected, be in good agreement with the SDOF-solution. The result from using the first three modes is improved significantly from the modal-analysis with only one mode, but it will later be shown that it is not until the fifth mode that the results are almost identical to the FE-analysis. However, the first three included modes in the modal-analysis give a very satisfactory approximation to the FE-analysis, even though the second mode does not give any contribution.
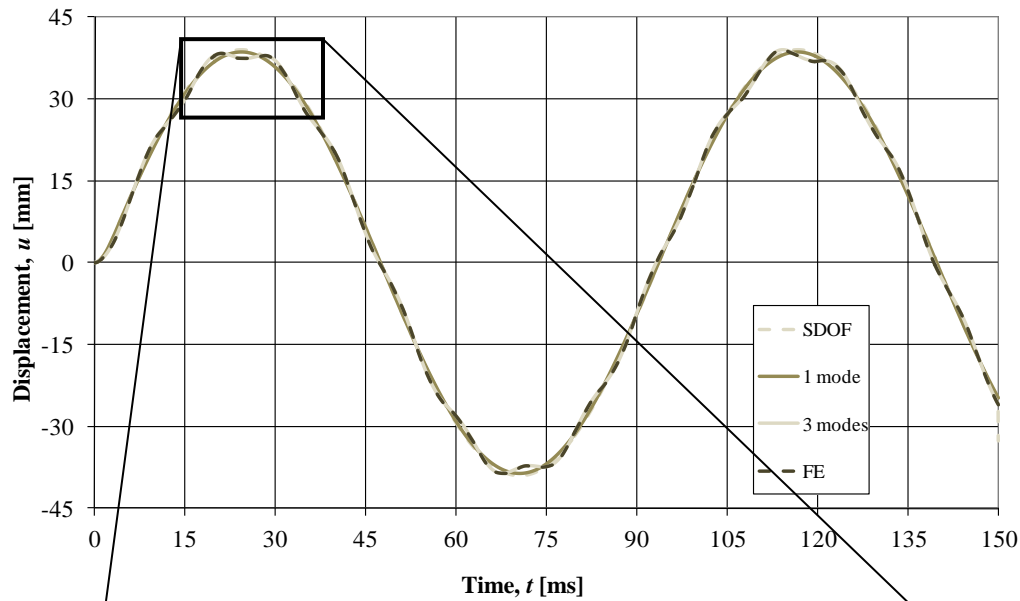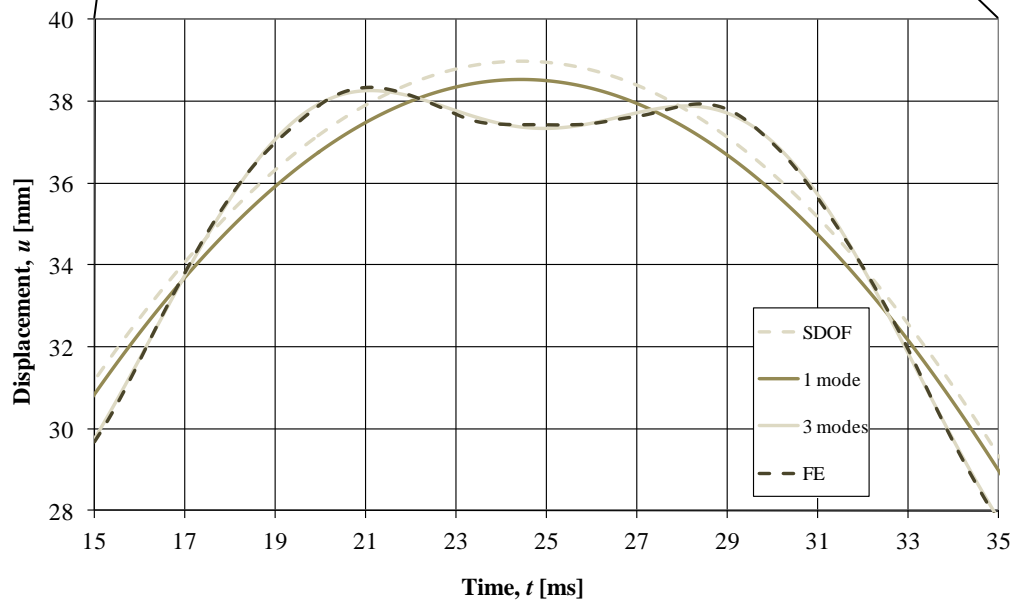
*Figure 5.1.* *(a) Modal-analysis for midpoint displacement using one and three modes, compared to results from SDOF- and FE-analysis, (b) zoomed in. Maximum displacement is about 38 mm.*

The difference between the FE-analysis and the modal-analysis for three, five and seven modes is shown in Figure 5.2 and it can be seen that five and seven modes does not contribute to a significantly better approximation of the displacement compared to an analysis using three modes. The difference is shown between 15 and 35 ms, which mean that maybe the largest difference is not shown, but the most relevant are, as the difference is shown at and directly about the maximum displacement. The error in comparison to the maximum displacement for the FE-analysis, which is approximately 38 mm, will be very small for the displacement. Hence, it is for the studied beam sufficient to include three modes, and even one mode give a very satisfactory result, in a modal-analysis. This is true for the response from load case 1.
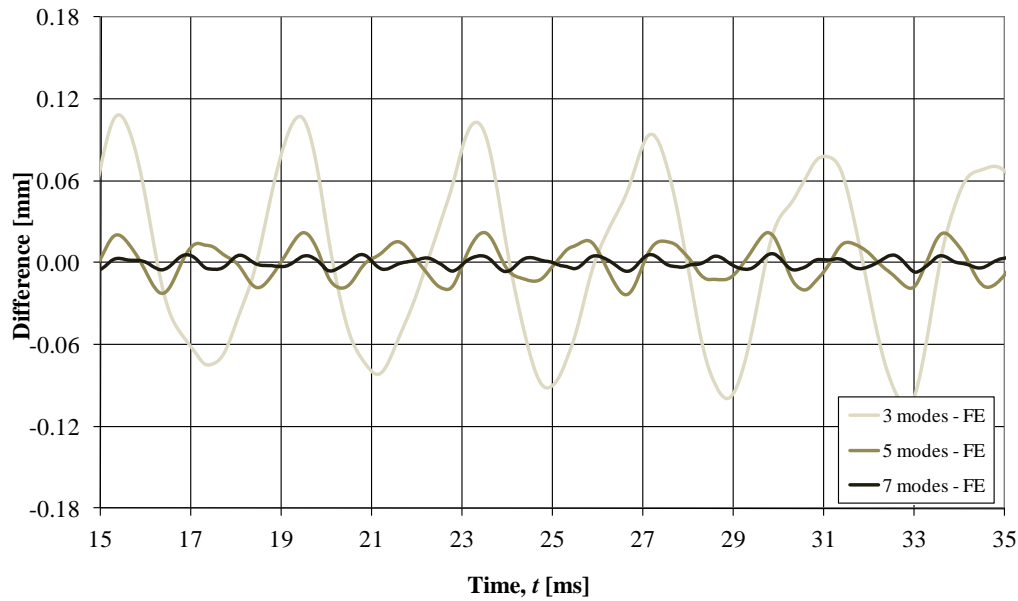
*Figure 5.2.* *Difference between midpoint displacements for modal-analysis with three, five and seven modes and the FE-analysis. Maximum displacement is about 38 mm, see Figure 5.1.*

A modal-analysis is made for the midpoint moment, in the same way as for the midpoint displacement, and is shown in Figure 5.3. It can be seen that the result from only using the first mode is far from satisfying. When including mode three the correspondence improves significantly. However, when taking a closer look at the zoomed in part of Figure 5.3 one can see that not even three modes are completely satisfying. Unlike the midpoint displacement the midpoint moment is not thoroughly described until the fifth mode is introduced to the modal-analysis when studying the figure. From this, it is obvious that the moment is more difficult to describe with fewer modes compared to the displacement. This is also to be expected since the moment is proportional to the second derivative of the displacement.

Another interesting point is that the two peaks in Figure 5.3 (b) are centred on the highest value for the first mode. If the eigenmodes are excited differently there will be a phase shift and it is highly possible that one of the peaks will coincide with the peak from the first mode. Because of this it is possible to get a higher maximum moment. This is seen in Figure 5.3 (a) at 25 ms and 115 ms.
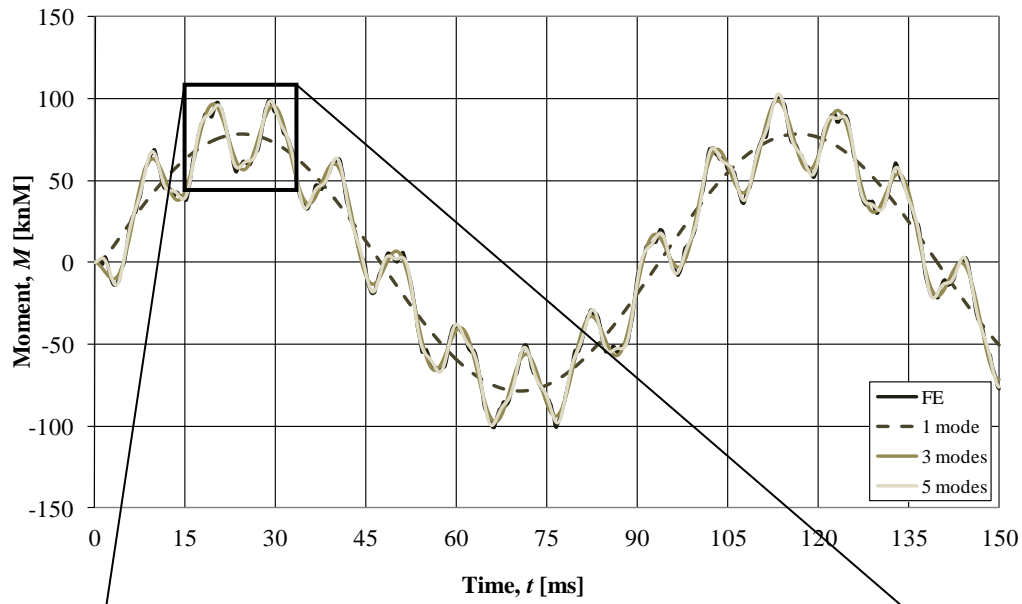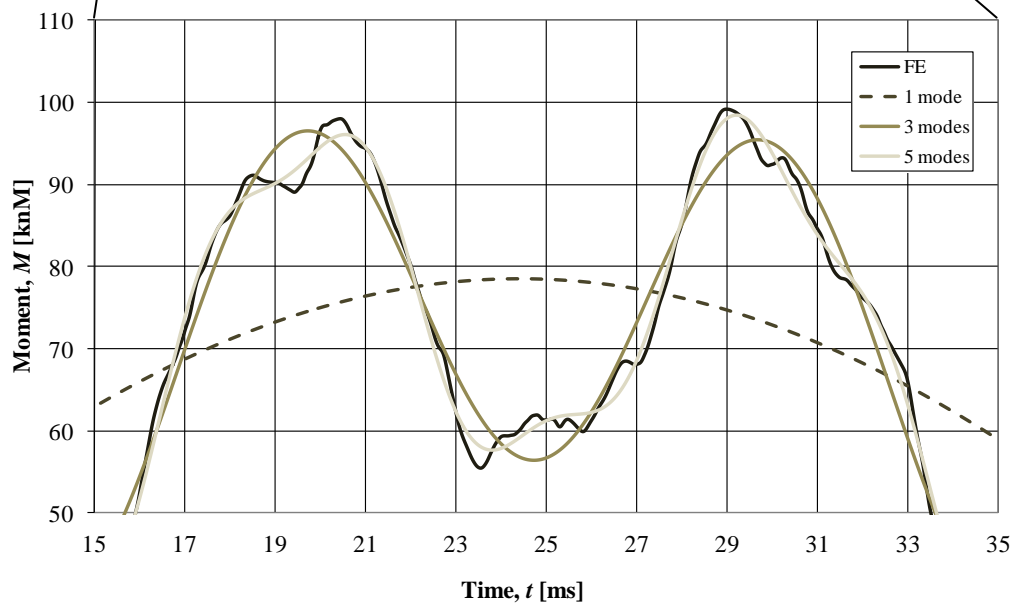
*Figure 5.3.* *(a) Modal-analysis for midpoint moment using one, three and five modes, compared to results from FE-analysis, (b) zoomed in. The maximum moment is about 100 kNm.*

The difference between the modal-analysis and the FE-analysis is also plotted for the midpoint moment, see Figure 5.4. The figure resembles the one for the difference in displacement, Figure 5.2, but when a comparison of the difference is done with the maximum moment one can see that the percentage is of another magnitude. The maximum moment for the FE-analysis is approximately 100 kNm which should be compared to the difference in Figure 5.4.
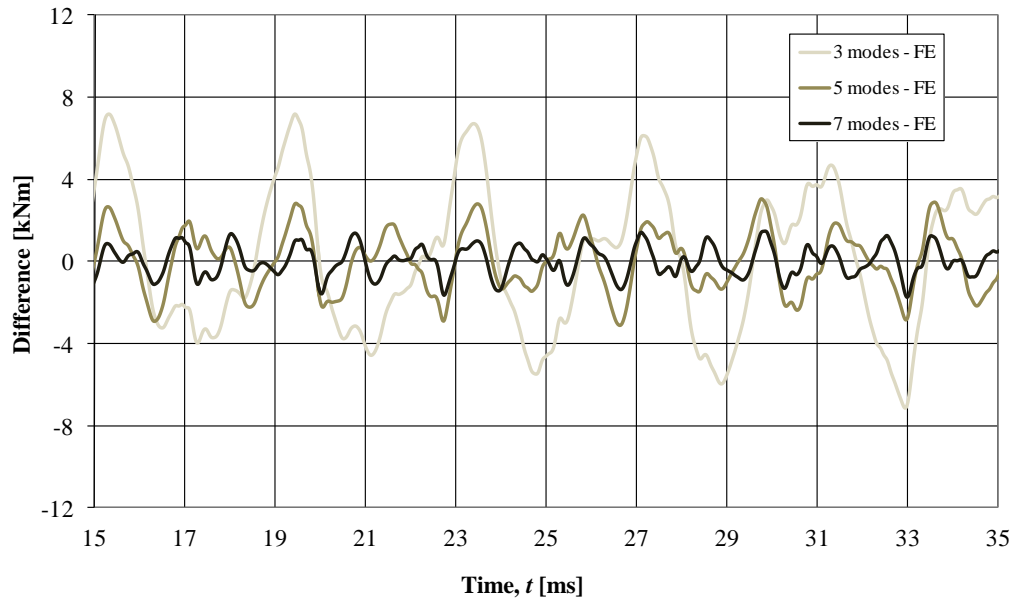
*Figure 5.4.    Difference between midpoint moments for modal-analysis with three, five and seven modes and the FE-analysis. Maximum moment is about 100 kNm, see Figure 5.3.*

Figure 5.4 indicates that the difference between three modes and the FE-analysis can be as large as eight percent if unlucky. When considering the analysis with five modes the difference will most be approximately three percent wrong.

Since the difference in percentage is larger for the moment than for the displacement it is sufficient to include five modes when doing a modal-analysis of this beam. It is shown that the difference will not improve significantly when including a seventh mode. This is true for both the displacement and the moment. However, so far the analyses have only dealt with load case 1, which might be regarded as a fairly gentle impulse. As mentioned in section 2.4.1, a more intense impulse will excite higher frequencies which can lead to a requirement of more modes to be included to get a good agreement between the modal-analysis and the FE-analysis.

In order to draw conclusions an analysis is made with regard to the more intense load case 3, see Figure 3.3 in Section 3.1, and the midpoint displacement can be seen in Figure 5.5.
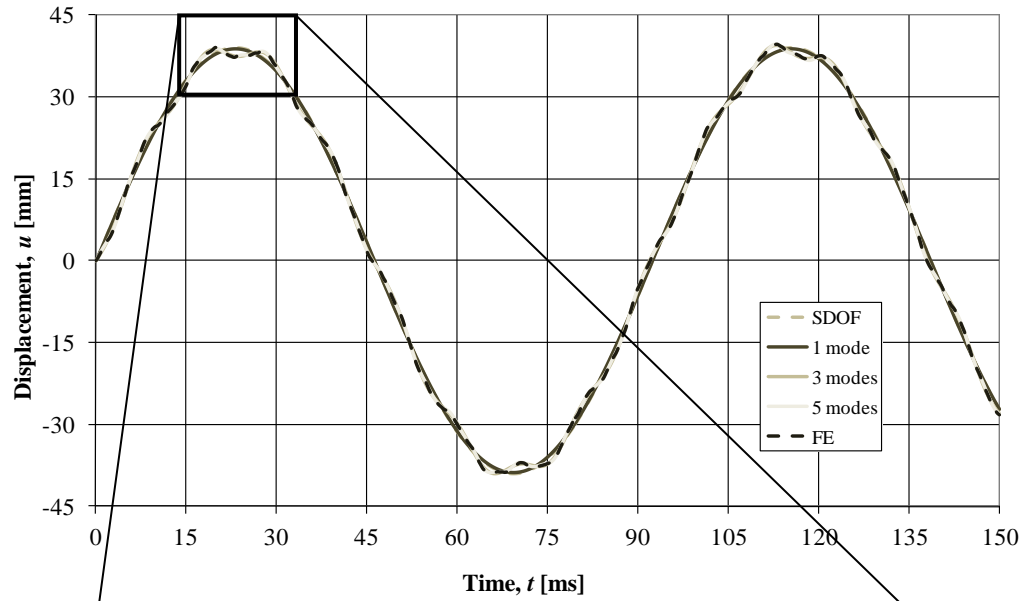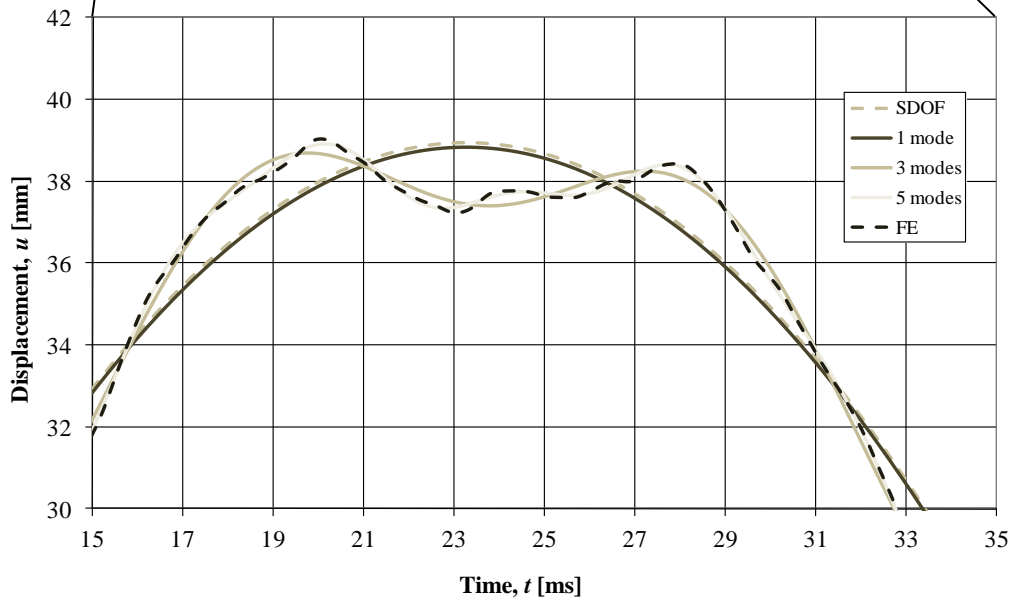
*Figure 5.5. (a) Modal-analysis for midpoint displacement due to LC3 using one, three and five modes, compared to results from SDOF- and FE-analysis, (b) zoomed in. Maximum displacement is about 39 mm.*

The midpoint displacements that arise when subjected to load case 3, seen in Figure 5.5, resemble the displacements for load case 1, seen in Figure 5.1, but there is a significant difference. It can be seen that the curve from the modal-analysis using three modes does not follow the FE-analysis for load case 3 as smoothly as for load case 1, Figure 5.1. To capture a more satisfactory approximation of the FE-analysis for the more impulsive load, it appears as if at least five modes are required. To present a better picture of the accuracy, the difference between the modal-analysis, using three, five and seven modes, and the FE-analysis is shown in Figure 5.6.

83
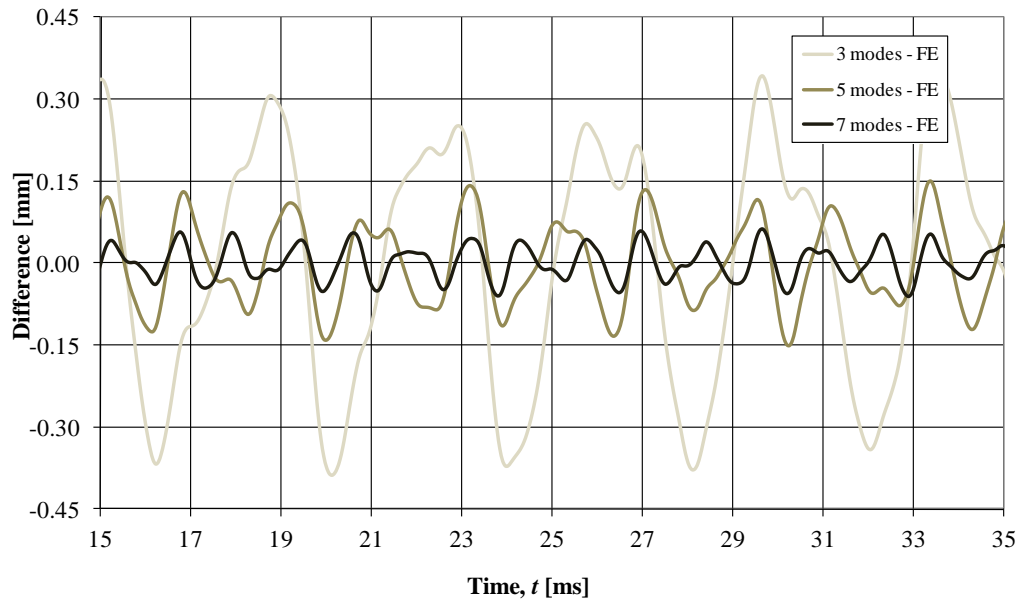
*Figure 5.6. Difference between midpoint displacements due to LC3 for modal-analysis with three, five and seven modes and the FE-analysis.Maximum displacement is about 39 mm, see Figure 5.5.*

With a maximum displacement of about 39 mm, the relative error from only using three modes in the modal-analysis is rather big when it peaks around 0.4-0.45 mm. However, if the error lies within five percent the approximation is acceptable, as mentioned earlier, and when only using three modes it result in an error just over one percent. Tough, the accuracy is greatly improved when using five modes, and although seven modes give a closer approximation to the FE-analysis the difference is still larger than the comparison between the FE-analysis and the modal-analysis using only five modes for load case 1, see Figure 5.2.

Same as for load case 1, an analysis has been made for the midpoint moment for load case 3 and is shown in Figure 5.7. By comparing the midpoint moments in Figure 5.7 and Figure 5.3 it can be seen that the midpoint moment for load case 3 is much more influenced by higher modes than the midpoint moment for load case 1.
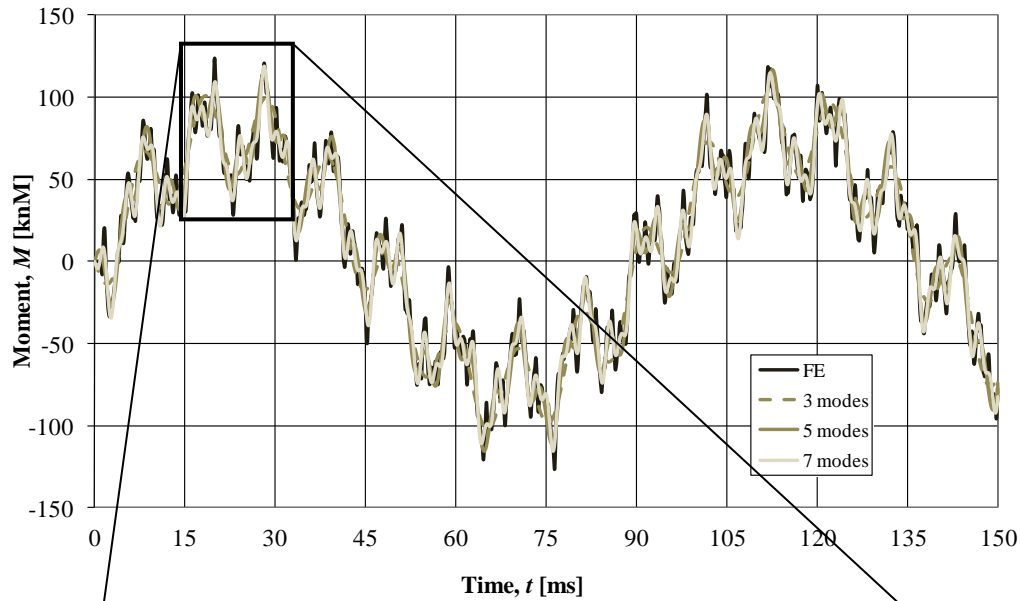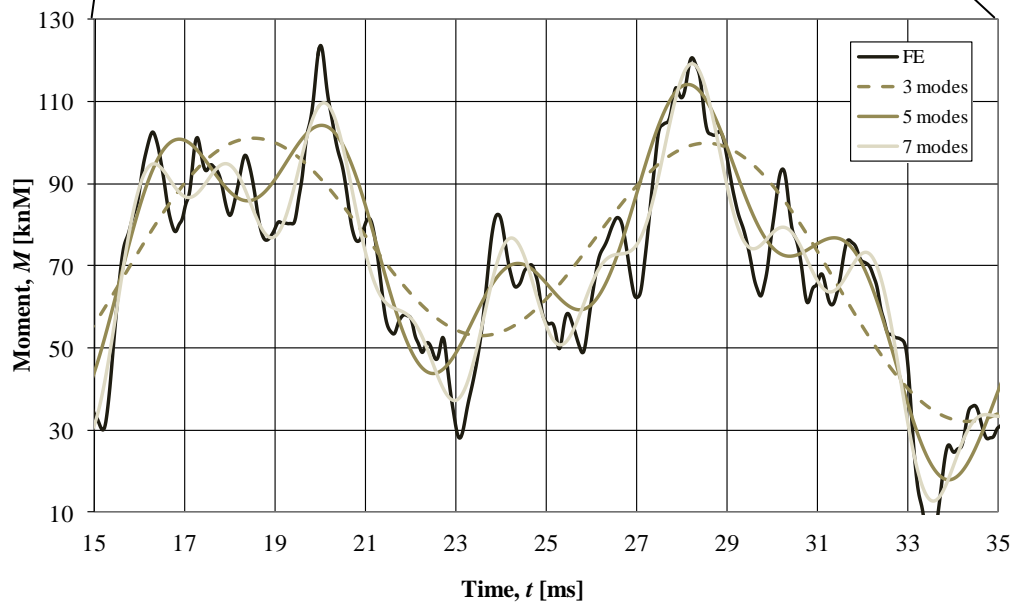
*Figure 5.7.*    *(a) Modal-analysis for midpoint moment due to LC3 using three, five and seven modes, compared to results from FE-analysis, (b) zoomed in. Maximum moment is about 125 kNm.*

As can be seen in Figure 5.7, when the impulse load is more intensive the description of the moment using five modes is still satisfying, even though the moment appears to be worse described than for load case 1. When the impulse is shorter in duration, the peaks in the moment oscillation become larger and more frequent, and compared to the largest peaks at 100 kNm for load case 1, the largest peaks for load case 3 reaches 125 kNm, i.e. 25 percent more. This can be compared to the displacement for the two load cases where the maximum values are more or less the same. The reason for the big increase of midpoint moment, although the displacement stays the same, is that the curvature is more significant for the more impulsive load case. The differences between the FE-analysis and the modal-analysis using three, five and seven modes are

85

shown in Figure 5.8 to once again give the reader a better picture of the magnitude of error attained when not using a sufficient amount of modes.
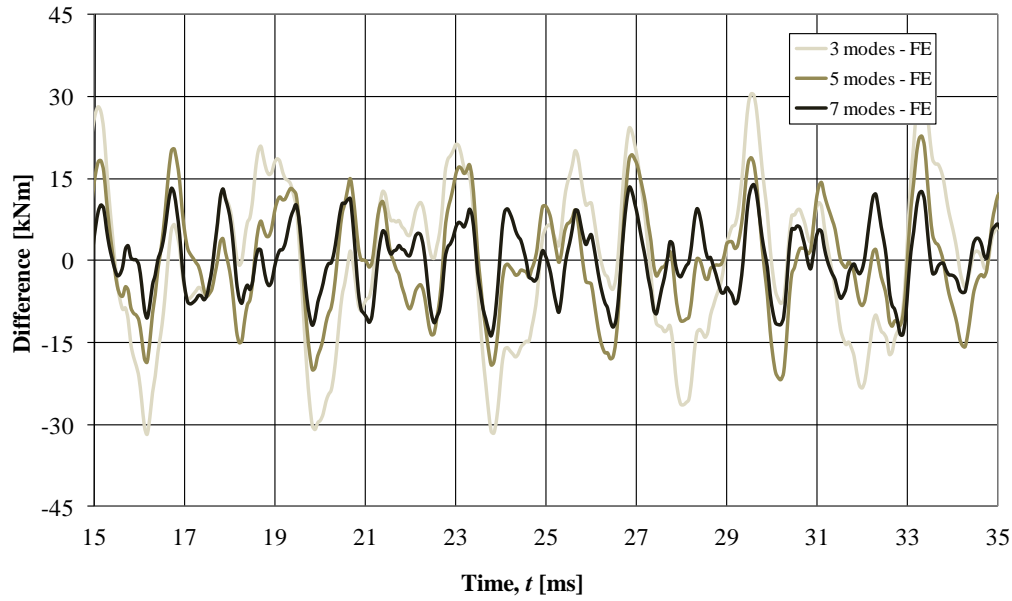


*Figure 5.8.* *Difference between midpoint moments due to LC3 for modal-analysis with three, five and seven modes and the FE-analysis. Maximum moment is about 125 kNm, see Figure 5.7.*

Now that the differences have been shown between modal-analysis and FE-analysis for the whole time interval and in every time step it is of interest to compare only the maximum values for displacement and midpoint moment. This will be an important comparison with respect to the design. The comparison is made with regard to both the displacement and the moment for load case 1 and 3. Table 5.1 is regarding midpoint displacements and

Table 5.2 is regarding midpoint moments. The relative errors, $\xi$, are calculated by comparing the maximum value during the first oscillation, which lies within 35 ms, for the FE-analysis and the different modal-analyses:

$$\xi = \frac{u_{max}^{modal} - u_{max}^{FE}}{u_{max}^{FE}} \cdot 100 \tag{5.1}$$

$$\xi = \frac{M_{max}^{modal} - M_{max}^{FE}}{M_{max}^{FE}} \cdot 100 \tag{5.2}$$

where Equation (5.1) and (5.2) regards displacement and moment respectively. Even though the maximum displacements are about the same for the two load cases, the maximum moments are not. This is partly because a more impulsive load will initiate stronger motions of higher modes than a less impulsive load would. It is also because a more impulsive load will cause a higher magnitude of curvature which is in direct relation to the moment, as shown in Appendix A. It is shown that for a more intense load it is necessary to use more modes in the modal-analysis compared to a less intense load. It is of interest to point out that the error for the midpoint moment for load case 3 using five modes gives a greater error than that for load case 1 by using only three modes. Generally, it is easier to describe the displacement than the moment

with few modes when performing a modal-analysis. It is seen that either different requirements of accuracy can be used for the displacement and the moment, when using a specific number of modes, or the moment analysis can be complemented with more modes to achieve the same relative error as for the displacement analysis. In Section G.1 it is shown that the SDOF-analysis and the modal-analysis with one mode also corresponds very well with regard to the midpoint moment.

*Table 5.1.* *Relative error in maximum midpoint displacement using modal-analysis with one, three, five and seven modes for LC1 and LC3.*

| Type of analysis | Number of modes | LC1 | | LC3 | |
|---|---|---|---|---|---|
| | | $u_{max}$ [mm] | $\xi$ [%] | $u_{max}$ [mm] | $\xi$ [%] |
| FE-analysis | ∞ | 38.3 | - | 39.6 | - |
| SDOF-analysis | 1 mode [1] | 38.8 | 1.3 | 38.9 | -1.8 |
| Modal-analysis | 3 modes | 38.9 | 1.6 | 39.4 | -0.5 |
| Modal-analysis | 5 modes | 39.0 | 1.7 | 39.7 | -0.2 |
| Modal-analysis | 7 modes | 39.0 | 1.8 | 39.6 | 0.0 |

[1] Corresponds well to the modal-analysis with one mode, see Section G.1.

*Table 5.2.* *Relative error in maximal midpoint moment using modal-analysis with one, three, five and seven modes for LC1 and LC3.*

| Type of analysis | Number of modes | LC1 | | LC3 | |
|---|---|---|---|---|---|
| | | $M_{max}$ [kNm] | $\xi$ [%] | $M_{max}$ [kNm] | $\xi$ [%] |
| FE-analysis | ∞ | 102.3 | - | 125.0 | - |
| SDOF-analysis | 1 mode [1] | 76.5 | -25.2 | 76.7 | -38.6 |
| Modal-analysis | 3 modes | 98.5 | -3.7 | 103.1 | -17.6 |
| Modal-analysis | 5 modes | 102.9 | 0.5 | 116.7 | -6.7 |
| Modal-analysis | 7 modes | 101.4 | -0.9 | 124.3 | -0.6 |

[1] Corresponds well to the modal-analysis with one mode, see Section G.1.

## 5.2 Damping analysis

In previous sections the analyses have been made without the effect of damping, which occurs in all real structures. Damping is an effect where energy is lost in the system through movement, and is in direct relation to the velocity. The energy loss arises from when temperature is developed through e.g. mechanical friction, which means that the damping also depends on material and shape. It is believed that the damping for a beam of the kind in this Master thesis will not exceed 10 percent, which is a very strong damping, and is seen as a limit of how high the damping possibly can be. It is more probable that the damping will be of a magnitude of about five percent, as seen in Table 5.3, where recommended damping ratios are shown for different types and conditions of a structure.

*Table 5.3.     Recommended damping values, Chopra (2011).*

| Stress level | Type and condition of structure | Damping ratio |
|---|---|---|
| **Working stress, no more than about 0.5 yield point** | Welded steel, prestressed concrete, well-reinforced concrete (only slight cracking) | 2-3% |
| | **Reinforced concrete with considerable cracking** | **3-5%** |
| | Bolted and/or riveted steel, wood structures with nailed or bolted joints | 5-7% |
| **At or just below yield point** | Welded steel, prestressed concrete (without complete loss in prestress) | 5-7% |
| | **Reinforced concrete**, Prestressed concrete with no prestress left | **7-10%** |
| | Bolted and/or riveted steel, wood structures with bolted joints | 10-15% |
| | Wood structures with nailed joints | 15-20% |

Since the damping of the beam in this case cannot be determined experimentally, possible damping values are compared for a damping ratio of 1, 2, 5 and 10 percent. When using Rayleigh damping the damping matrix is expressed as:

$$\mathbf{C} = \alpha \cdot \mathbf{M} + \beta \cdot \mathbf{K} \tag{5.3}$$

where *C*, *M* and *K* are the damping-, mass- and stiffness matrixes, respectively, and $\alpha$ and $\beta$ are factors determining the mass- and stiffness damping. The $\alpha$- and $\beta$-factors are chosen so that the current damping factor affects the first and fifth mode. This means that the modes between first and fifth, i.e. second, third and fourth, will be affected by lower damping and the higher modes will be more damped, see Figure 5.9.
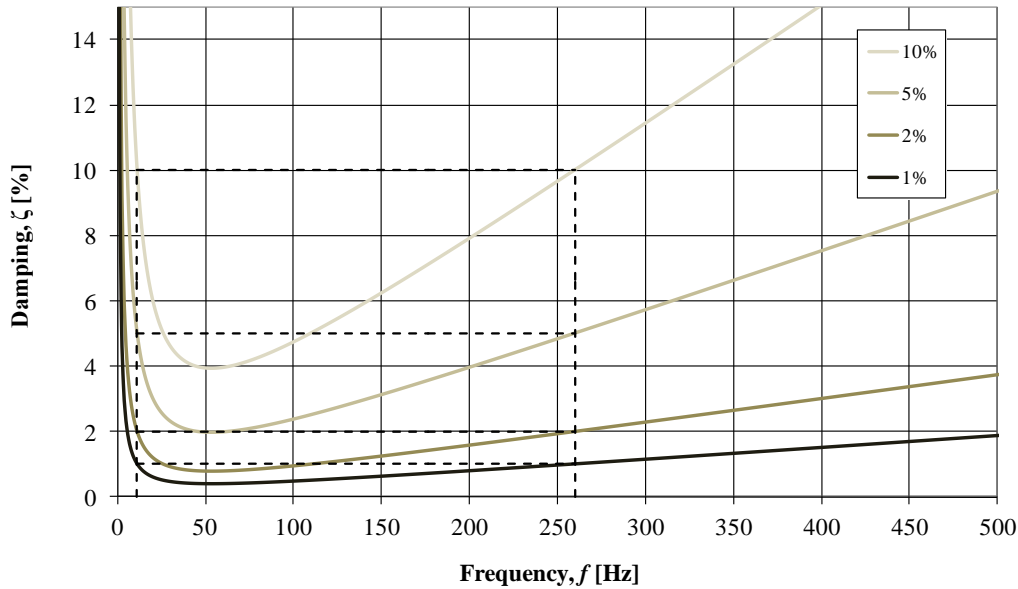
*Figure 5.9.  Rayleigh damping at first and fifth natural frequency for 1, 2, 5 and 10 percent damping.*

From a frequency-analysis in ADINA the frequencies for the first and fifth mode are found. The frequencies are 10.84 Hz and 259.8 Hz, respectively. With these frequencies it is now possible to calculate the corresponding $\alpha$- and $\beta$-factors for the different damping percentages. Below are the factors calculated for one percent Rayleigh damping as an example:

$$\alpha = \zeta \frac{2\omega_i\omega_j}{\omega_i + \omega_j} = 0.01 \cdot \frac{2 \cdot 10.84 \cdot 259.8}{10.84 + 259.8} = 0.208 \tag{5.4}$$

$$\beta = \zeta \frac{2}{\omega_i + \omega_j} = 0.01 \cdot \frac{2}{10.84 + 259.8} = 7.39 \cdot 10^{-5} \tag{5.5}$$

This will then be used to calculate the damping matrix $\boldsymbol{C}$ from equation (5.3) that will be used when considering the Rayleigh-damping, both in the SDOF-model and the FE-model.

The $\alpha$- and $\beta$-factors for the different damping values are shown in Table 5.4, and the eigenfrequencies and the calculated Rayleigh damping for different damping ratios are shown in Table 5.5.

*Table 5.4.*  *Calculated α- and β-factors for different damping values when using Rayleigh damping.*

| Damping | $\alpha$ | $\beta$ |
|---|---|---|
| 1% | 0.208 | $7.39 \cdot 10^{-5}$ |
| 2% | 0.416 | $14.8 \cdot 10^{-5}$ |
| 5% | 1.041 | $36.9 \cdot 10^{-5}$ |
| 10% | 2.081 | $73.9 \cdot 10^{-5}$ |

*Table 5.5.*  *Frequencies and damping values for the considered bending modes when using Rayleigh damping of different magnitudes.*

| Bending mode | Eigenfrequency | Damping value | | | |
|---|---|---|---|---|---|
| | | 1% | 2% | 5% | 10% |
| 1 | 10.84 Hz | 1.00% | 2.00% | 5.00% | 10.0% |
| 3 | 96.14 Hz | 0.46% | 0.93% | 2.32% | 4.63% |
| 5 | 259.8 Hz | 1.00% | 2.00% | 5.00% | 10.0% |
| 7 | 490.0 Hz | 1.83% | 3.66% | 9.16% | 18.3% |

In Figure 5.10 and Figure 5.11 the response is compared for Rayleigh damping and modal damping, respectively. When making an analysis with Rayleigh damping, direct integration have been used and in the modal-analysis seven modes have been included.

It can be seen that it is only 10 percent damping for both cases that is sufficient when the equivalent static load is concerned. However, the five percent damping, which is more reasonable, will also give a satisfactory result. A comparison of the five percent Rayleigh and modal damping is therefore shown in Figure 5.12. It is worth mentioning that, when comparing the Rayleigh damping with the modal damping, it is seen that using Rayleigh damping will damp the minor oscillations more efficiently than when modal damping is used.
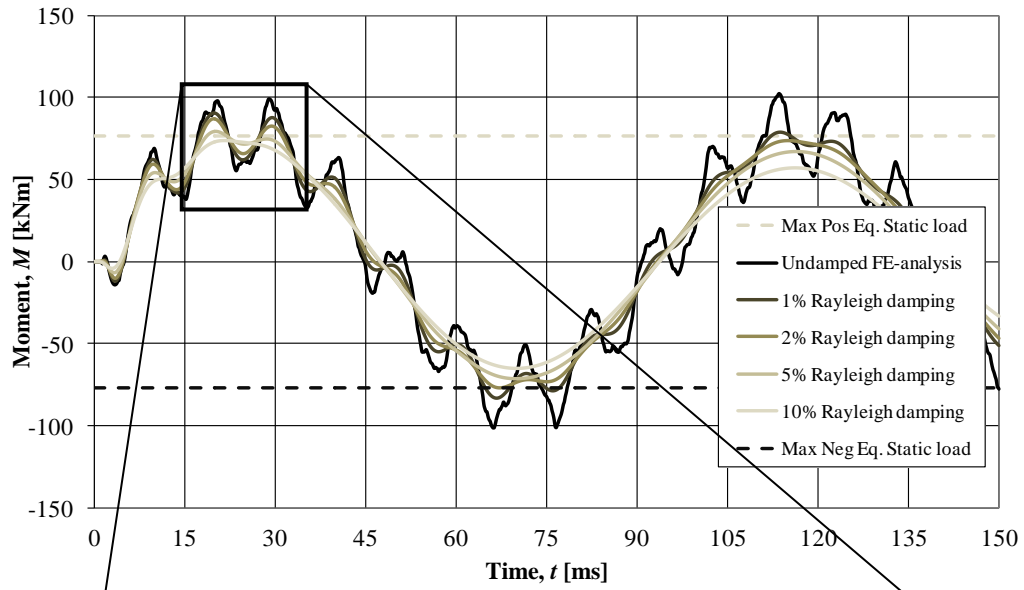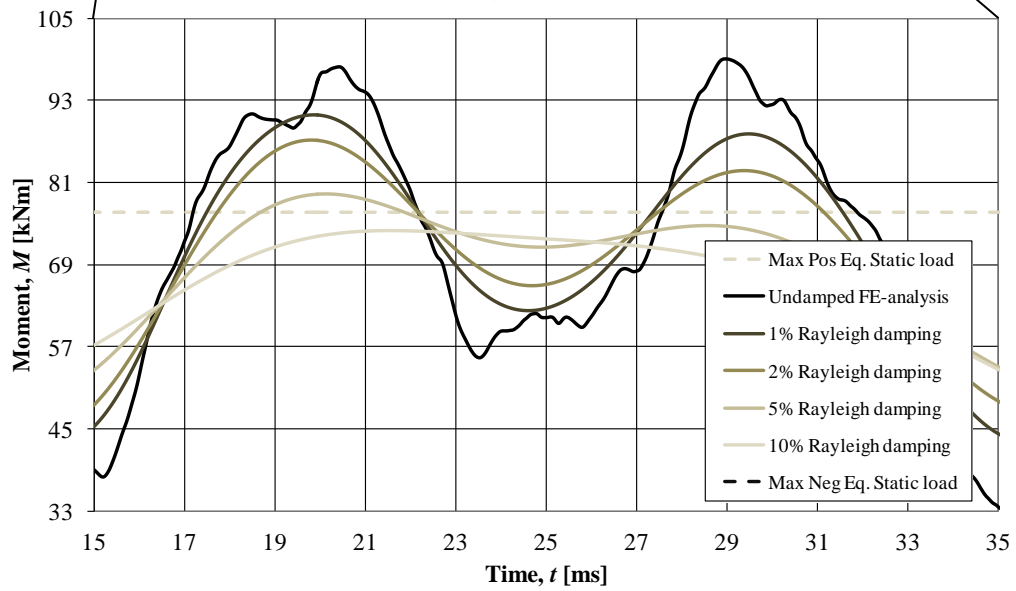
Figure 5.10. *(a) Undamped midpoint moment compared to midpoint moment with 1, 2, 5 and 10 percent Rayleigh damping; (b) zoomed in.*
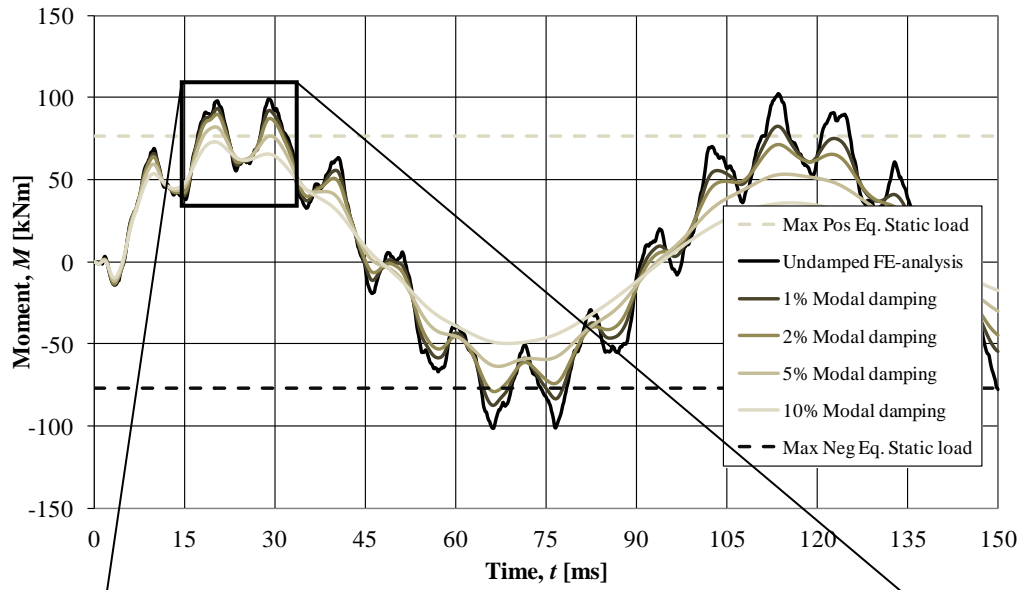
(a)
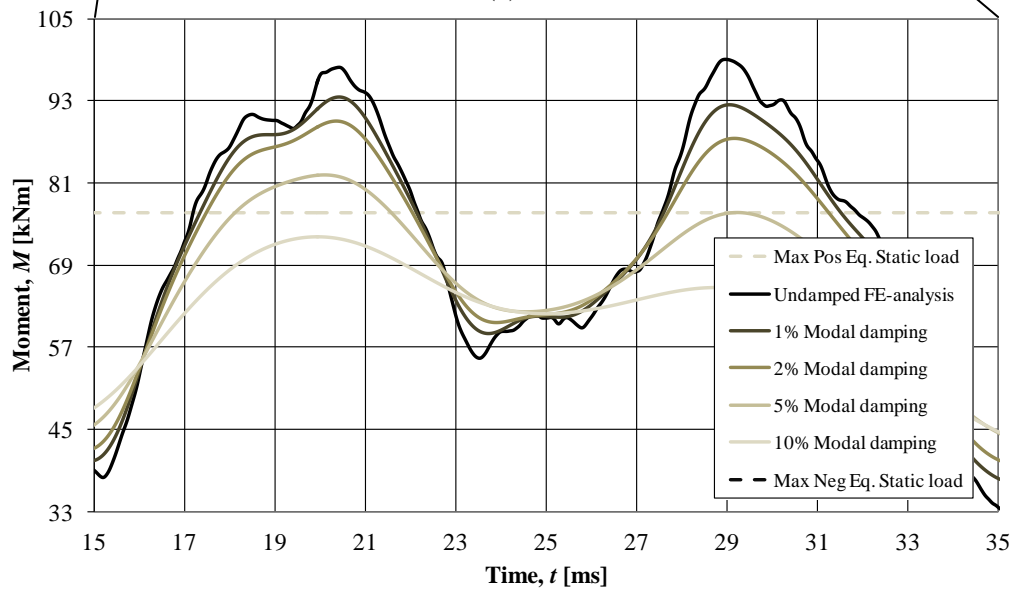


(b)

*Figure 5.11. (a) Undamped midpoint moment compared to midpoint moment with 1, 2, 5 and 10 percent modal damping; (b) zoomed in.*
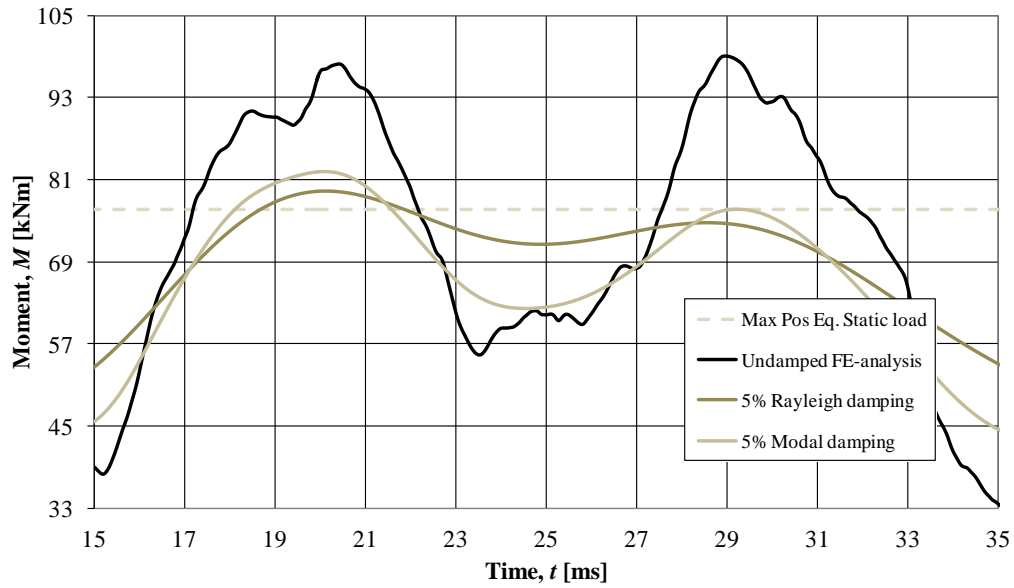
*Figure 5.12. Undamped midpoint moment compared to midpoint moment with 5 percent Rayleigh and modal damping.*

In order to be able to draw conclusions about the damping, an analysis of the moment envelope is also made. In Figure 5.13 and Figure 5.14 the moment envelope is shown with different degree of Rayleigh damping and modal damping, respectively.
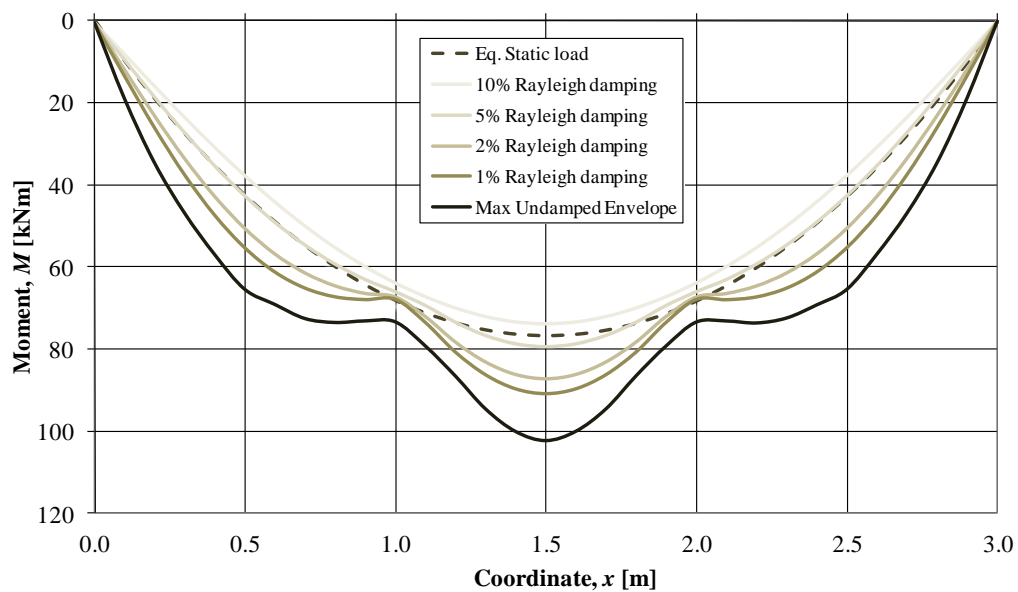


*Figure 5.13. Undamped moment envelope compared to moment envelope with 1, 2, 5 and 10 percent Rayleigh damping.*
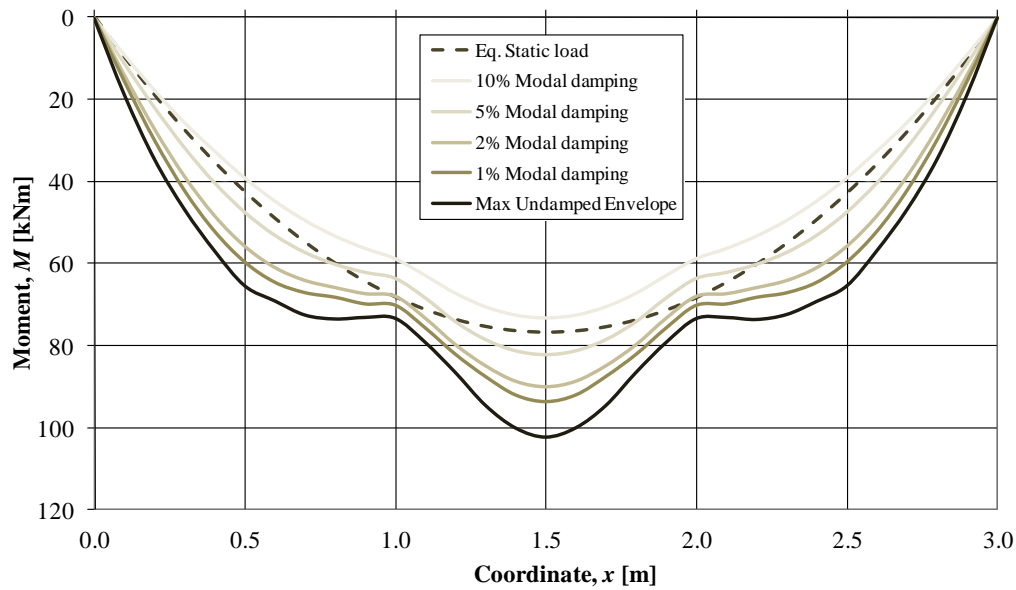
*Figure 5.14. Undamped moment envelope compared to moment envelope with 1, 2, 5 and 10 percent modal damping.*

The conclusion that can be drawn from the damping analysis of this particular scenario is that to be satisfied with the undamped equivalent static load when designing, the actual damping needs to be at least five percent. If that is the case, the equivalent static load will explain the behaviour accurately enough and the design will be acceptable. It has previously also been shown that it is common for concrete structures to have a damping factor of about five percent, see Table 5.3. The reader is reminded that these analyses for the damping have been made with the elastic stadium II material response. Depending on the situation, e.g. a prestressed concrete beam, this might not be the best agreement with a real scenario, with a different material response.

In order to determine how many modes are required to present a good approximation of the displacements and moments for the damped case, an analysis according to the one in Section 5.1 has been made, but this time with five percent modal damping. The displacements over time for load case 1 is shown in Figure 5.15, and it can be seen that one mode is a very close approximation. However, in order to capture the motion of the minor oscillations three modes are needed. The SDOF-analysis is not shown in the figure as it was shown in Figure 5.15 that it is almost identical to the modal-analysis using only one mode.
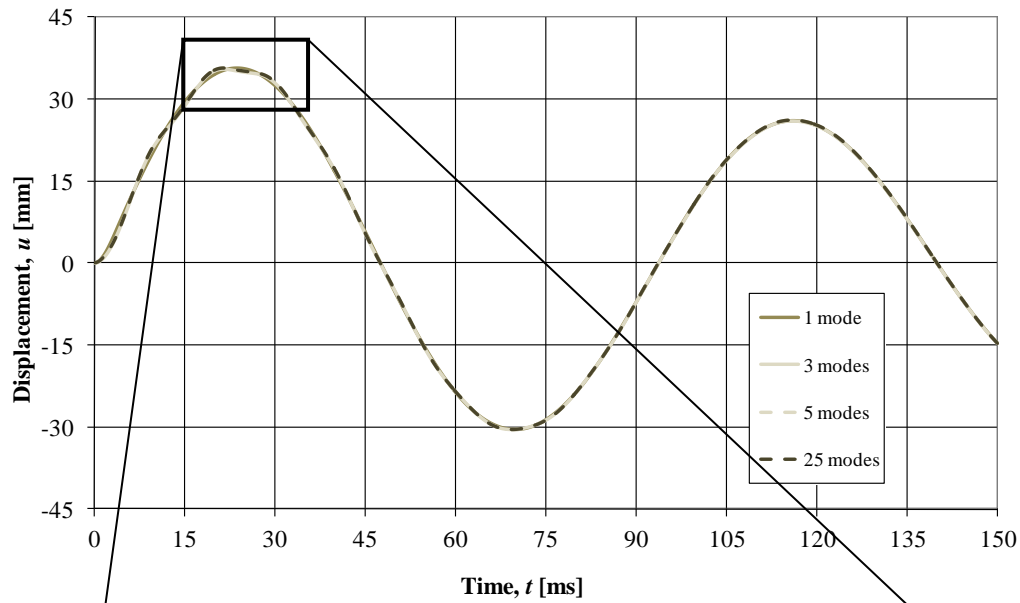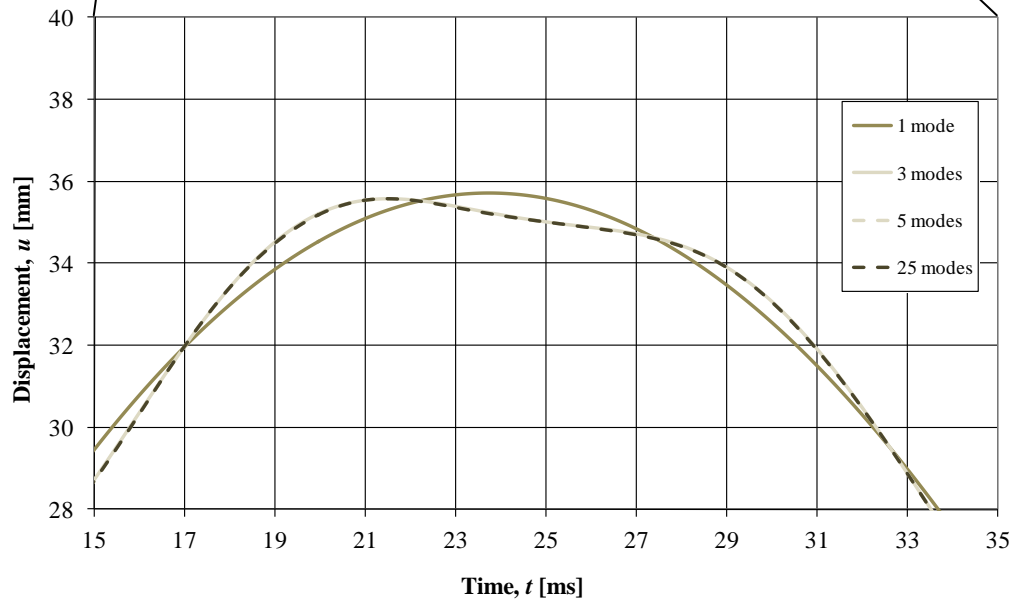
*Figure 5.15. (a) Modal-analysis for midpoint displacement using 1, 3, 5 and 25 modes due to LC1 with 5 percent damping, (b) zoomed in. Maximum displacement is about 36 mm.*

To give a perspective of how good approximation it is to use only one mode, the difference between the modal-analysis for one, three and five modes and the modal-analysis for 25 modes is shown in Figure 5.16. Here, analyses using 25 modes are regarded as an acceptable approximation for the FE-analysis, see Section G.2. The reason to replace the FE-analysis with a modal analysis is to be able to use modal damping, i.e. constant damping for all frequencies. Notice that as the displacement decreases with time, so do the relative errors. By only using one mode the largest errors are about 0.8 mm which is about 2.2 percent of the maximum displacement. When three or five modes are used the relative error is below 0.06 percent.
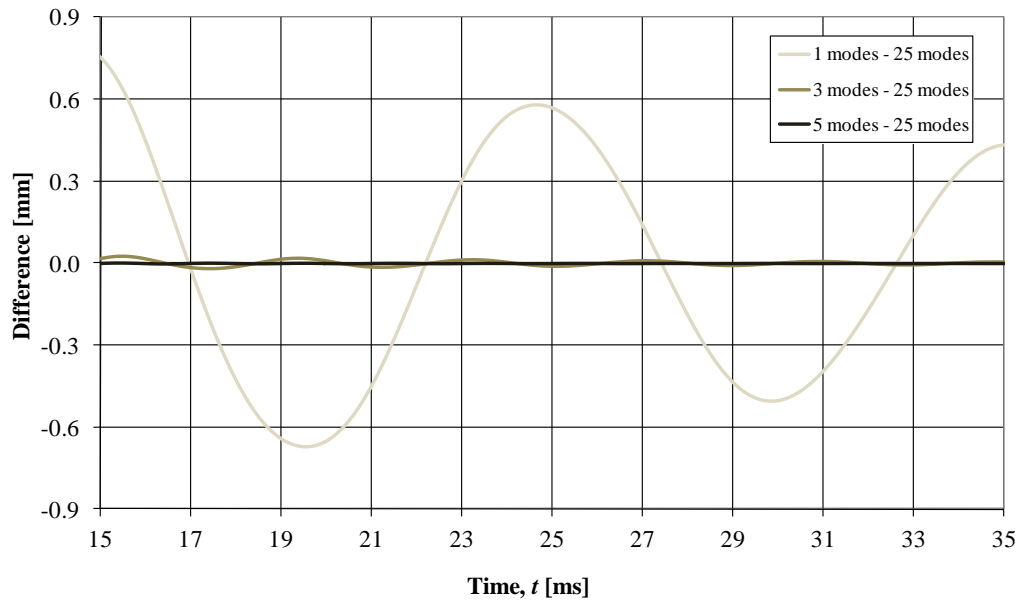
*Figure 5.16. Difference between midpoint displacements due to LC1 for modal-analysis with 1, 3 and 5 modes and the modal-analysis with 25 modes; all with 5 percent damping. Maximum displacement is about 36 mm, see Figure 5.15.*

The midpoint moment is shown in Figure 5.17 for load case 1 with different amount of modes. By only using the first mode it is seen that the result differs significantly from the modal-analysis using more modes. When three modes are used, one can in Figure 5.17 (b) see a slight difference from the modal-analysis using 25 modes, but when five modes are used the difference is negligible.
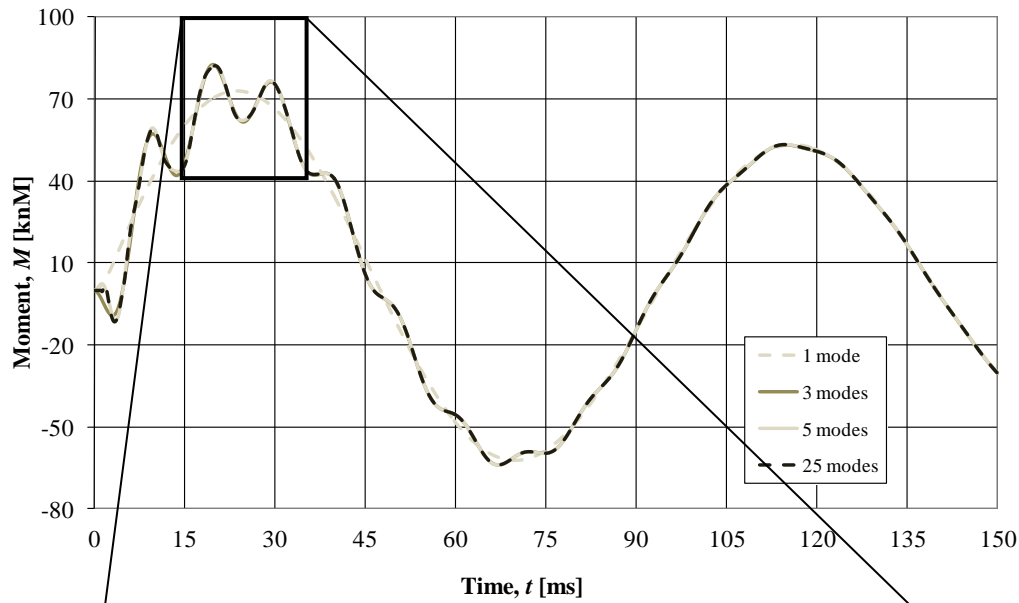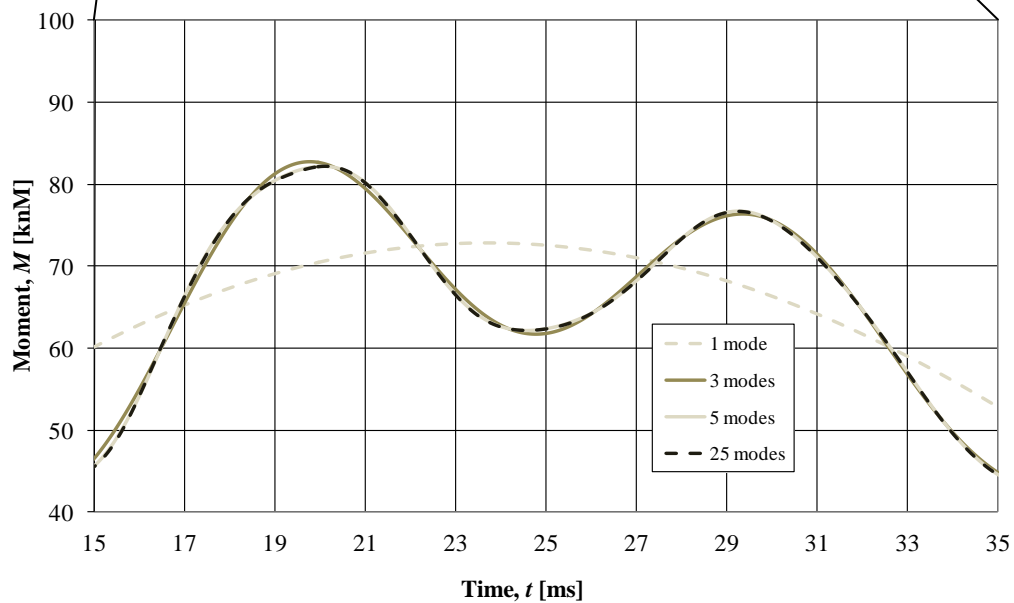
*Figure 5.17. (a) Modal-analysis for midpoint moment using 1, 3, 5 and 25 modes due to LC1 with 5 percent damping, (b) zoomed in. Maximum moment is about 82 kNm.*

The differences between the damped midpoint moments over time for load case 1 using modal-analysis with three, five and seven modes and the modal-analysis using 25 modes are shown in Figure 5.18. As for the displacement, the difference is decreasing with time, but the largest errors are much larger. For the modal-analysis using three modes the largest error is 1.5 kNm and the relative error is about 1.8 percent of the maximum moment for the modal-analysis using 25 modes. When using five modes the error is still about 0.12 percent which is more than double that of the error in displacement using only three modes, but it is still considered as a small error.
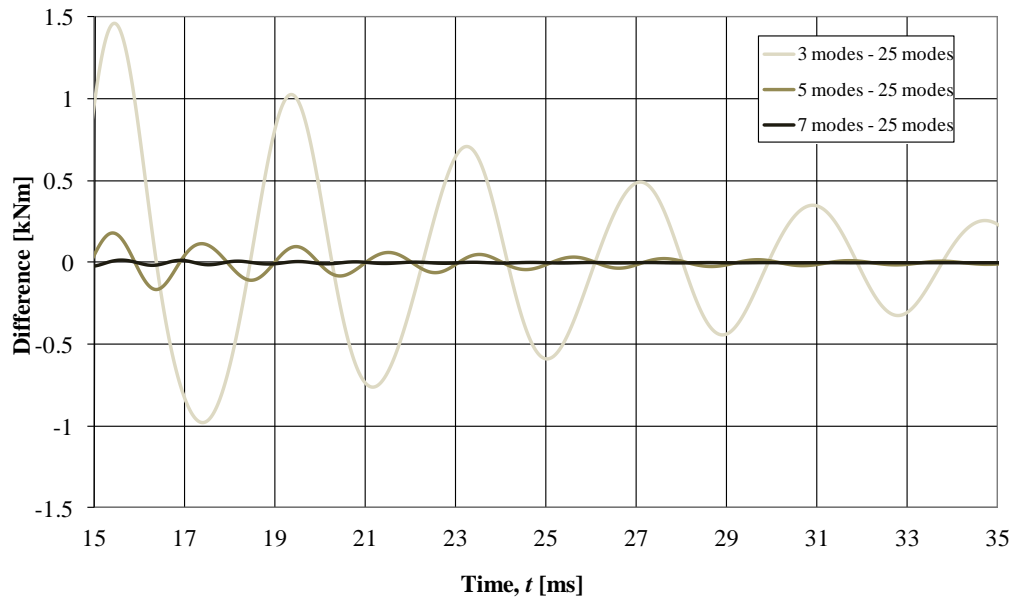
*Figure 5.18. Difference between midpoint moments due to LC1 for modal-analysis with 3, 5 and 7 modes and the modal-analysis with 25 modes; all with 5 percent damping. Maximum moment is about 82 kNm, see Figure 5.17.*

Also for the damping analyses it is interesting to look at the response when the beam is subjected to load case 3. In Figure 5.19 and Figure 5.20 the deformation and the difference in displacement is shown respectively. When comparing these figures to the ones for load case 1, Figure 5.15 and Figure 5.16, the reader can see that the difference is almost not visible.
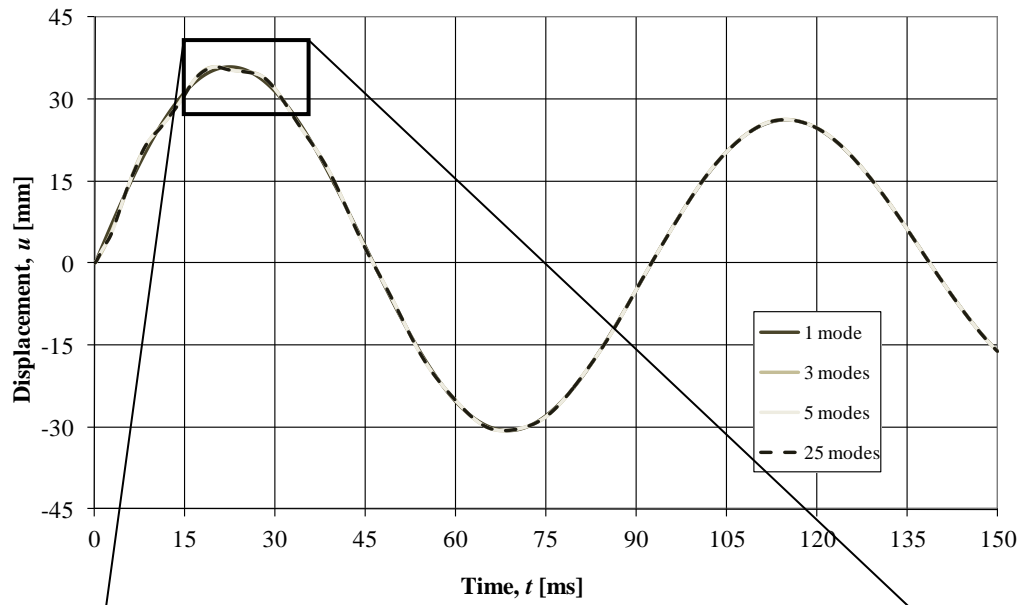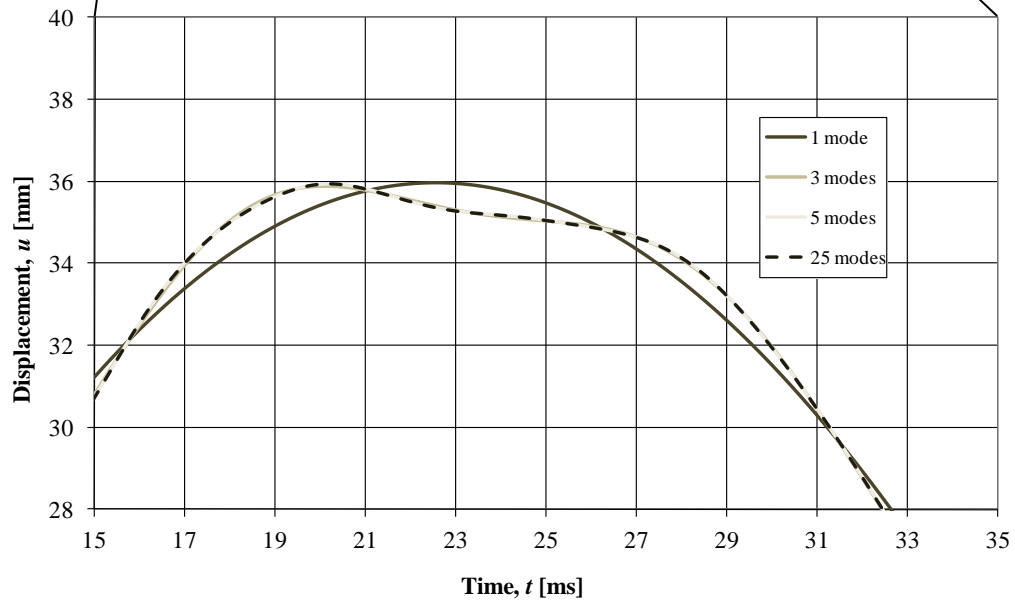
*Figure 5.19. (a) Modal-analysis for midpoint displacement using 1, 3, 5 and 25 modes due to LC3 with 5 percent damping, (b) zoomed in. Maximum displacement is about 36 mm.*
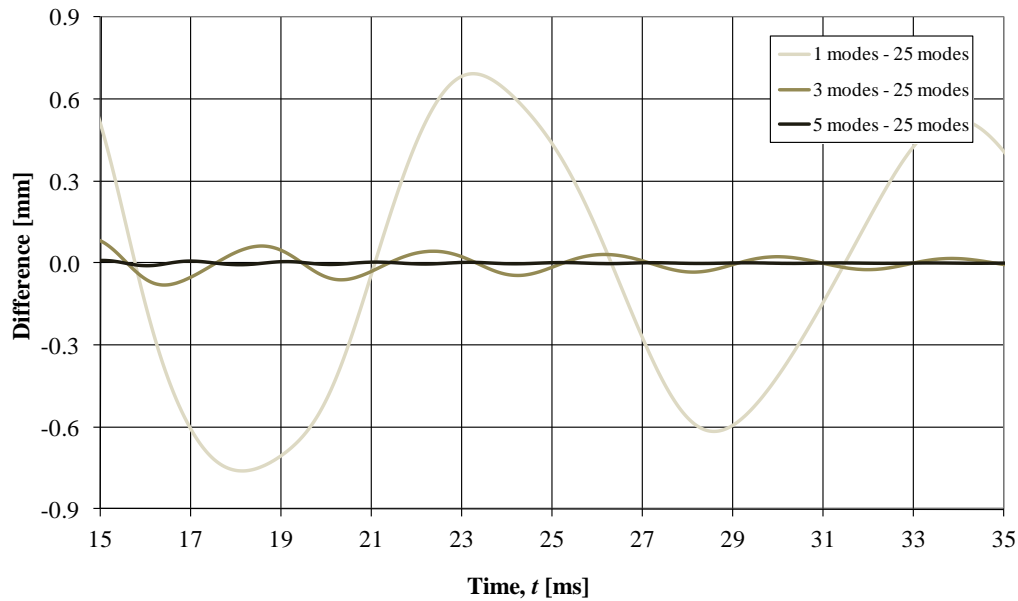
*Figure 5.20.  Difference between midpoint displacements due to LC3 for modal-
analysis with 1, 3 and 5 modes and the modal-analysis with 25 modes;
all with 5 percent damping. Maximum displacement is about 36 mm, see
Figure 5.19.*

In Figure 5.21 and Figure 5.22 the midpoint moments and the differences are shown
respectively. When the damping is regarded it is shown that the responses are very
similar regardless of what type of loading is used. When the beam is subjected to load
case 3 the response will not be very different compared to the response obtained for
load case 1. Even the analyses within the different load cases are very similar. It is
only the SDOF-analysis that differs significantly at the beginning. The curves are
smoothened due to the damping and the differences are decreasing with time and
eventually the analyses will merge with each other irrespective of the amount of
modes in the analyses.
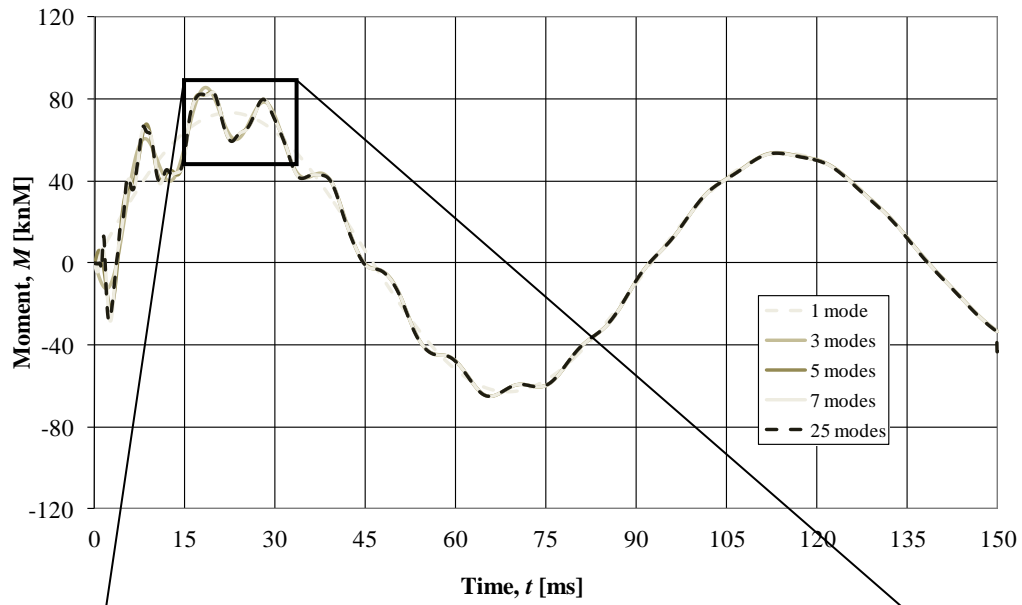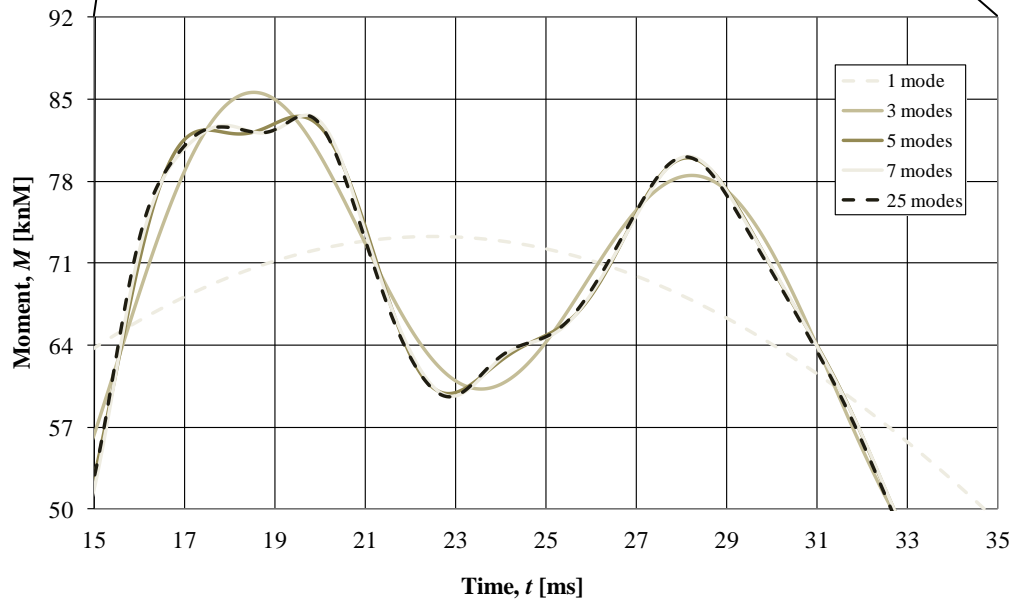
*Figure 5.21. (a) Modal-analysis for midpoint moment using 1, 3, 5, 7 and 25 modes due to LC3 with 5 percent damping, (b) zoomed in. Maximum moment is about 86 kNm.*
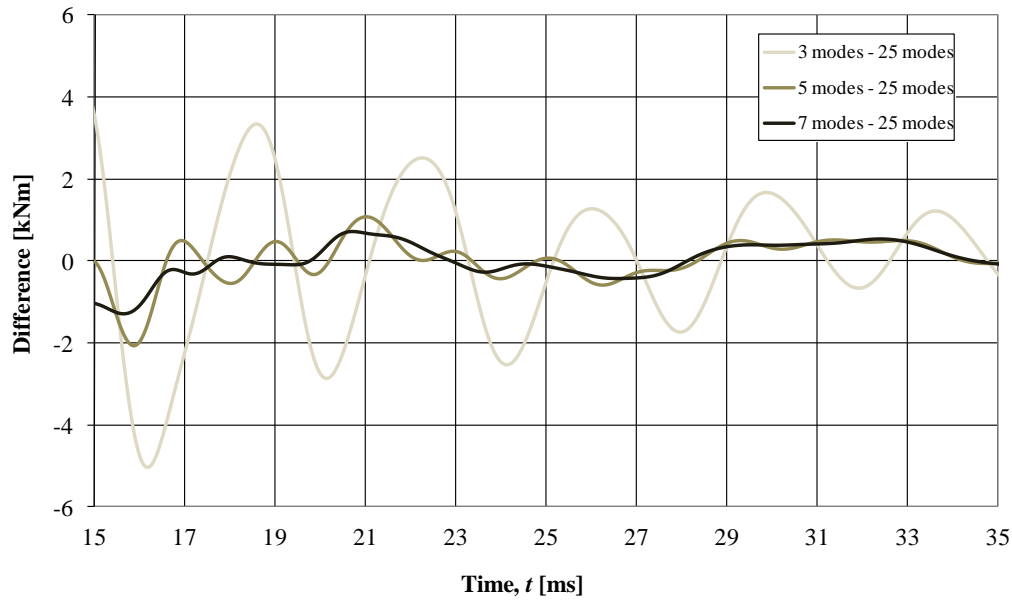
*Figure 5.22. Difference between midpoint moments due to LC3 for modal-analysis with 3, 5 and 7 modes and the modal-analysis with 25 modes; all with 5 percent damping. Maximum moment is about 86 kNm, see Figure 5.21.*

In order to give a more detailed picture of the accuracy of the results when using different amount of modes, analogous to Table 5.1 and

Table 5.2 from Section 5.1, Table 5.6 and Table 5.7 are shown with displacements and moments regarding five percent modal damping. It is seen that for both the displacement- and moment analysis regarding damping, the relative error for load case 1 and 3 is smaller compared to the analyses without damping. The error decreases significantly when more modes are used for the analysis, and it is, when damping is regarded, only the analysis with one mode that differs noticeably.

*Table 5.6.*  *Relative error in maximum midpoint displacement using modal-analysis with one, three, five and seven modes for LC1 and LC3, regarding 5 % damping.*

| Type of analysis | Number of modes | LC1 | | LC3 | |
|---|---|---|---|---|---|
| | | $u_{max}$ [mm] | $\xi$ [%] | $u_{max}$ [mm] | $\xi$ [%] |
| Modal-analysis | Max displacement (25 modes) | 35.6 | - | 35.9 | - |
| SDOF-analysis | 1 mode [1] | 35.9 | 0.8 | 36.1 | 0.6 |
| Modal-analysis | 3 modes | 35.7 | 0.4 | 36.0 | 0.1 |
| Modal-analysis | 5 modes | 35.6 | 0.0 | 35.9 | 0.0 |
| Modal-analysis | 7 modes | 35.6 | 0.0 | 35.9 | 0.0 |

[1] Also corresponds to the modal-analysis with one mode

*Table 5.7.*  *Relative error in maximum midpoint moment using modal-analysis with one, three, five and seven modes for LC1 and LC3, regarding 5 % damping.*

| Type of analysis | Numer of modes | LC1 | | LC3 | |
|---|---|---|---|---|---|
| | | $M_{max}$ [kNm] | $\xi$ [%] | $M_{max}$ [kNm] | $\xi$ [%] |
| Modal-analysis | Max moment (25 modes) | 82.2 | - | 83.7 | - |
| SDOF-analysis | 1 mode [1] | 70.8 | -13.9 | 71.0 | -15.2 |
| Modal-analysis | 3 modes | 82.8 | 0.6 | 85.6 | 2.3 |
| Modal-analysis | 5 modes | 82.2 | 0.0 | 83.5 | -0.2 |
| Modal-analysis | 7 modes | 82.2 | 0.0 | 83.7 | 0.0 |

[1] Also corresponds to the modal-analysis with one mode

The most important fact to point out in these analyses is that the SDOF-analysis, when neglecting the damping, is a good approximation for the modal analysis with 25 modes when the damping is over five percent, especially when looking at the midpoint moment. An example is calculated for load case 1:

$$\xi = \frac{76.5 - 82.2}{82.2} \cdot 100 = -6.9\%$$ (5.6)

This means that one can obtain quite accurate results when designing if neglecting the damping, even though the result is somewhat on the unsafe side. However, since a reinforced concrete beam will yield is seven percent not crucial for the structure. The structure is able to redistribute the tension due to the yielding. In Appendix I other beams have been calculated, as a comparison.

The reader is reminded that this comparison between undamped SDOF and the damped FE-analysis is regarding five percent damping. It should be pointed out that if a prestressed concrete beam is considered the damping may very well be lower than that. According to Table 5.3 is the damping ratio for prestressed concrete between two and three percent.

## 5.3 The transformation factor for damping

Usually when analysing and designing with regard to explosions the damping is neglected and there is no need to have a damping transformation factor. However, when performing a more detailed analysis, the transformation factor could have a significant impact on the result. In Section 2.4.2 it was mentioned that the transformation factor for damping reasonably could be the same as the transformation factor for the stiffness and force. A way to analyse what the transformation factor could be is to use mode superposition with only one mode and compare this with the SDOF-model for a high damping value. This is done for all four load cases with a damping of 20 percent and is here shown for load case 0 and load case 3 in Figure 5.23. It can be seen that the convergence between the FE-analysis and the SDOF-analysis is good with a transformation factor $\kappa_{cF} = 0.8$, which in Figure 5.23 is labelled as SDOF 0.8. When going from a less impulsive load to a more impulsive one the curves are somewhat drawn to the left.
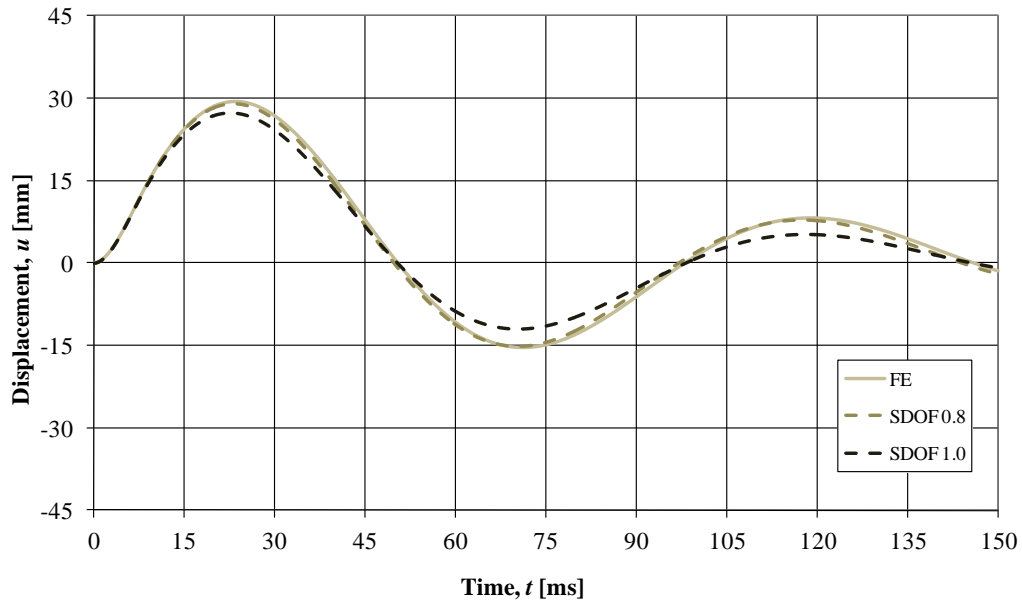
(a)
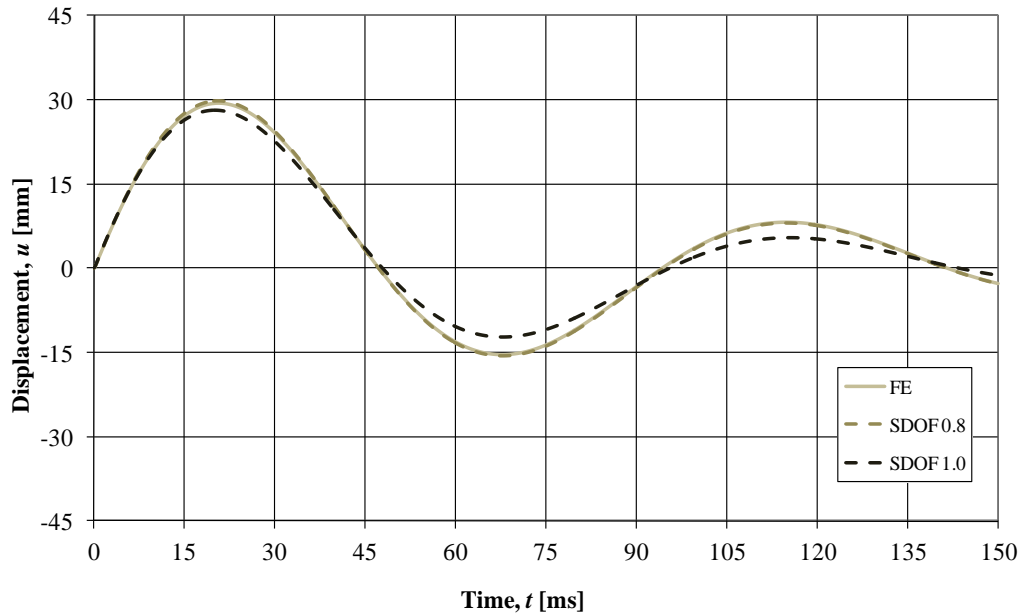


(b)

*Figure 5.23. Difference between midpoint displacements over time for FE-analysis and SDOF-analysis with damping factor 0.8 and 1.0 for beam 1 in (a) LC0 and (b) LC3.*

It is hereby indicated that $\kappa_{cF}$ is not 1.0, but for this case closer to 0.8. The number 0.8 is not proven to be the exact number but it gives a very good approximation. In order to investigate whether this result is just a coincidence for this beam or not, the same analysis has been made for other cross-sections. Instead of varying the geometry of the cross-sections, only the density $\rho$ and Young's modulus for concrete $E_c$ is changed in purpose of keeping the modelling simple. In Figure 5.24 the analysis is made for load case 0 and load case 3 for beam 2 with properties seen in Table 5.8. The beam from Chapter 3, which has been analysed throughout this Master thesis, is hereby referred to as beam 1.

Same as for beam 1 it can be seen that when $\kappa_{cF}$ is set to 0.8 instead of 1.0 a much better convergence is achieved between the SDOF- and the FE-analysis. For detailed info of all five beams and all four load cases the reader is referred to Appendix H. There, it can be seen that if $\kappa_{cF}$ is set to 0.8 the agreement is good for all the beams and all load cases.

The factor 0.8 is not the exact value for $\kappa_{cF}$ but merely a very good approximation. The exact value will not be further investigated in this Master thesis but it could be of interest in future studies.

*Table 5.8.* *Properties of beams 1 to 5.*

| Properties | $E_c$ [GPa] | $\rho$ [kg/m³] |
|---|---|---|
| Beam 1 | 33 | 2400 |
| Beam 2 | 40 | 3000 |
| Beam 3 | 20 | 2000 |
| Beam 4 | 33 | 4800 |
| Beam 5 | 66 | 2400 |
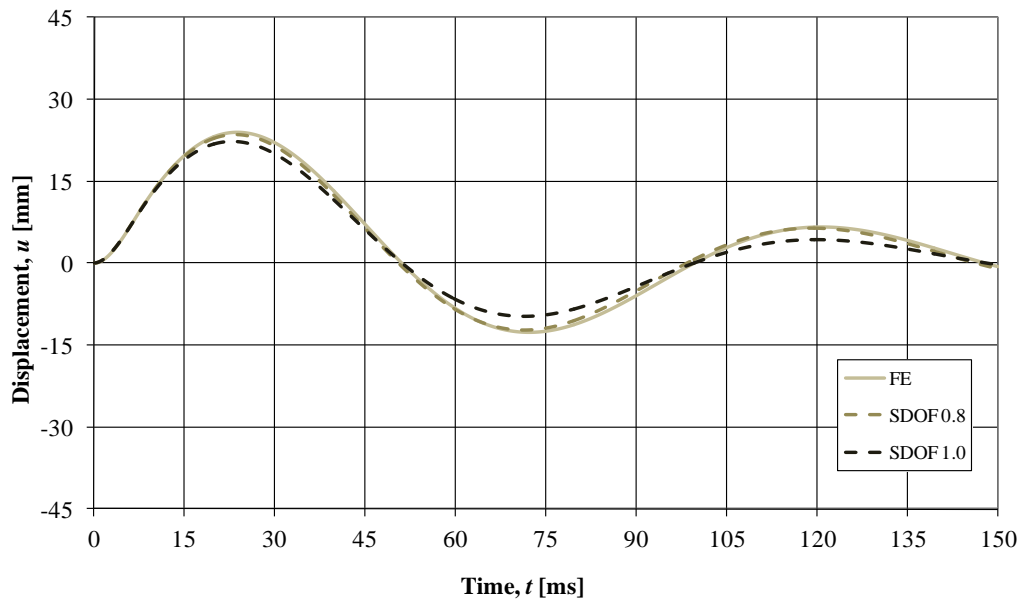
(a)
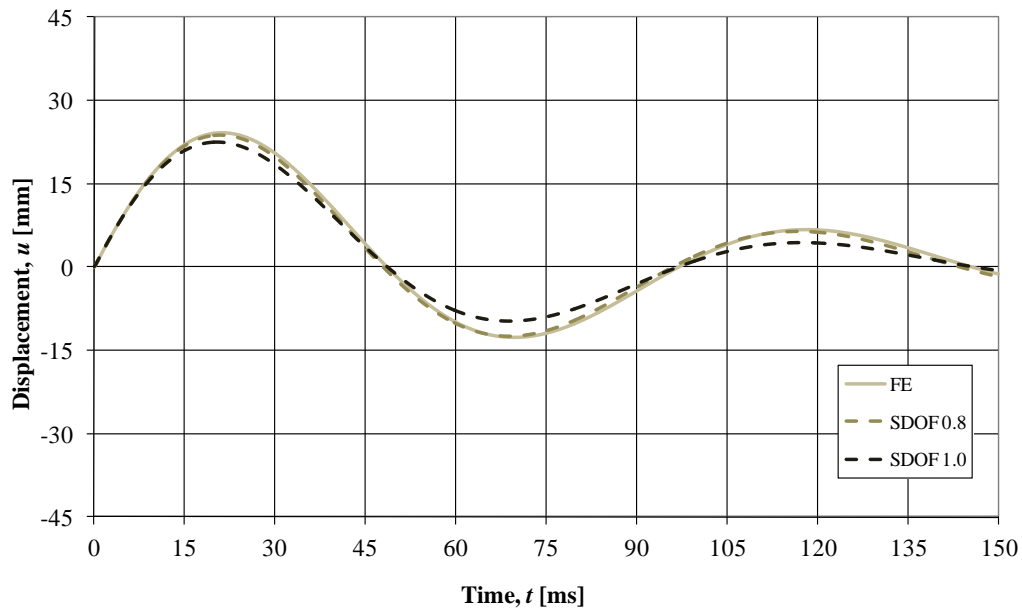


(b)

*Figure 5.24. Difference between midpoint displacements over time for FE-analysis and SDOF-analysis with damping factor 0.8 and 1.0 for beam 2 in (a) LC0 and (b) LC3.*

## 5.4    Discussion

It was seen in Chapter 4 that the demand for the use of several modes to accurately capture the moment of the beam is higher than the demand if the displacement is calculated. In Chapter 5 it was made clear that this is the case. A simply supported beam subjected to a uniformly distributed load will oscillate mainly with its first mode shape and one can accurately capture the displacements by using the SDOF-model. It was shown that the actual deflection shape only significantly differed from the assumed deflection shape within the first few ms, which is before the maximum values have been reached so it is not of any importance. The moment, however, is more visibly influenced by more modes than the displacement and is therefore more difficult to describe with the SDOF-model. The relative errors were also shown to be quite large. For less intense loads, it is not required to use as many modes as for a highly intense load where it was shown that at least five modes should be regarded if the size of the error should not be bigger than for the error for the displacement using the SDOF-model. If one is interested in showing the moments with good accuracy and with a simpler approximation than doing a FE-analysis, one should create an MDOF-model using at least three modes.

Because the beam has a height, it takes time for the wave to propagate through the cross-section which means that there will be an actual delay to the maximum moments. With the height known, and the information speed calculated, it is possible to calculate the time, $t_1$, it takes for the wave to propagate through the beam's cross section, i.e. two times the height. If a moment peak in time is so narrow that time $t_1$ exactly fits between the boundaries of the moment peak, the values above (or below if the moment is negative) this position can be disregarded, so the tip of the peak is cut off. The moment peak in time then only becomes as narrow as the time it takes for the information to travel two heights of the beam. This method could possibly bring down the maximum values from the analysis without damping, but probably not by much. When the damping is applied to the system, the peaks become wider and less prominent so the decrease in moment becomes negligible.

When modelling with damping, the SDOF-analysis generally correlates better to the FE-analysis. In order to be able to be on the safe side for the moment when calculating with the equivalent static load, it was shown that the structure should have a damping of at least 10 percent. This is a very high damping, and in reality it is more likely that a reinforced concrete beam has a damping factor of about five percent. Since the SDOF-analysis give lower maximum moments than the FE-analysis, it can be beneficial to use the maximum moment from the undamped SDOF-analysis as the maximum moment for the actual damped case, as these numbers are closer. Notice that there is still a significant difference in the results, which are on the unsafe side, so an up-scaling factor should be used.

Designing with regard to damping is more advanced and takes more time than when it is neglected, both mathematically and analytically, as the damping factor first needs to be determined before any calculations can be made, and if a too high damping value is chosen the results will no longer be on the safe side. However, if the right damping factor is found, the results will be closer to reality and it can be important to be able to get these more accurate results in analyses where it is difficult to motivate that the capacity of an existing structure is sufficient.

It was successfully shown that when the transformation factor for the damping for the simply supported beam subjected to a uniformly distributed load was set to $\kappa_{cF} = 0.8$

instead of the assumed value of 1.0, a much better convergence was seen between the SDOF- and the modal-analysis using one mode. The damping is a way to describe the energy loss in the system due to heat development, which depends on the velocity and therefore the damping effect should differ for different load cases. In the undamped case the maximum moments are larger for load case 3 than for load case 1, but when damping is applied they are about the same. Hence, this means that the damping effect is higher for a more impulsive load.

Today, the damping factor is not calculated from material properties; it is experimentally determined. It is therefore believed that there is no reason for trying to derive the exact solution for the transformation factor for the damping until there are methods of determining the damping factor analytically. However, it is possible to table values for the transformation factors for different type of loads and boundary conditions. These can be achieved by iterating the SDOF-analysis with different values and comparing to the FE-analysis, both with high damping, until a convergence is met.

# 6    Curtailment

Curtailment, or shortening of reinforcement, is used to decrease the expenses when designing a structure, both for walls and beams. In defence shelters and military structures that are explicitly designed to withstand the load from an explosion, however, curtailment is never used. Hence, analyses with curtailment are not so common when analysing structures with regard to explosions. However, since this Master thesis focuses on civil structures where curtailment is more common, a further detailed analysis is made.

When designing with regard to a static moment it is easy to predict the moment distribution and determine the reinforcement accordingly. In that way less reinforcement is used and money can be saved. However, when looking at the moment distribution when a structure is impulse loaded the moment has been shown not to be similar to the static moment for the first few ms. The moment will be larger closer to the supports than in the middle of the beam. Due to this it is interesting to analyse how a beam with curtailment reacts when loaded with an impulse. Will the beam get large plastic deformations or is the moment capacity exceeded only for a short period of time so that no real harm is done?

As an example, a curtailment analysis of the beam from Chapter 3 is made. By looking at the moment distribution from the equivalent static load, seen in Figure 6.1, two different cases of curtailment are chosen and analysed. It is important to mention that a simplification is made. Usually when designing with curtailment the designing moment is offseted in accordance with the tensile force contribution due to inclined shear cracks. However, when analysing the subjected beam due to curtailment this contribution is disregarded since this effect is not captured in a FE-analysis using beam elements.
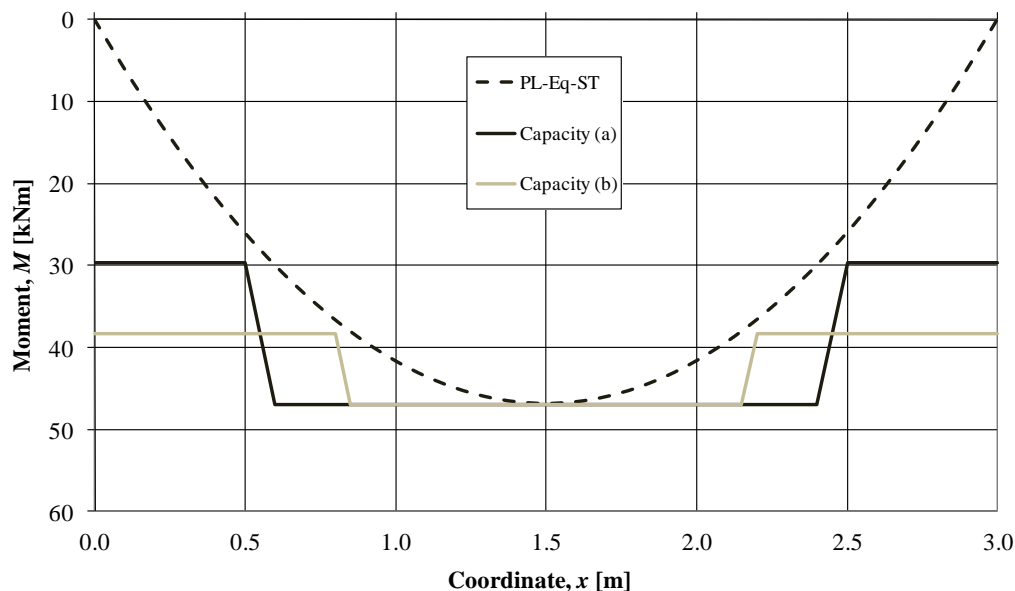


*Figure 6.1.    Moment distribution for plastic material response from equivalent static load, and moment capacity for curtailment at (a) L/6; (b) L/4 from the beam ends.*

The two cases analysed are shown in Figure 6.2. The first case is a curtailment of the bottom reinforcement at L/6 from the ends of the beam. Here, the reinforcement spacing is increased from 150 to 300 mm, decreasing the capacity in this region to 29.6 kNm. In this point the beam is affected by a moment from the equivalent static load of 26.2 kNm. The second case is a curtailment of the bottom reinforcement at L/4 from the ends of the beam. The amount of bottom reinforcement is reduced as the distance between the bars is increased from 150 to 200 mm, decreasing the capacity in this region to 38.3 kNm. In this point the beam is affected by a moment from the equivalent static load of 35.2 kNm.
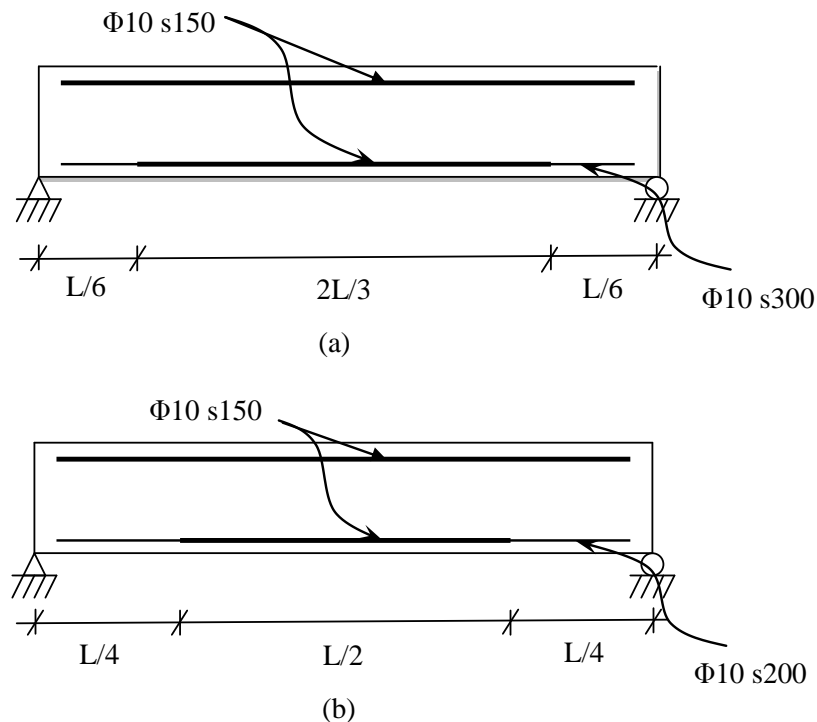


*Figure 6.2. Simply supported beam with curtailment of (a) L/6; (b) L/4 from the ends.*

When analysing the curtailment it is of interest to see how the moment envelope is changed in comparison to the moment capacity. If the moment capacity is not reached then there will be no problem with curtailment. However, if the capacity indeed is reached the beam will start to yield. It is then interesting to see if the capacity is reached for a long or short period of time. If the capacity is reached only for a short period of time the plastic strain will be small and the beam will have no problem to withstand the load, but if it is reached for a longer period of time then large plastic strains can develop and problems may arise. Due to this it is, besides the moment envelope, also interesting to study the development of plastic strain for the beam.

## 6.1 Curtailment analysis

The moment distribution for the two beams has been studied and the progression of the moment envelope is shown in Figure 6.3 for the beam with curtailment at L/6 from the ends. As a comparison, the progression of the moment envelope for the beam without curtailment is shown in Figure 6.4.

112
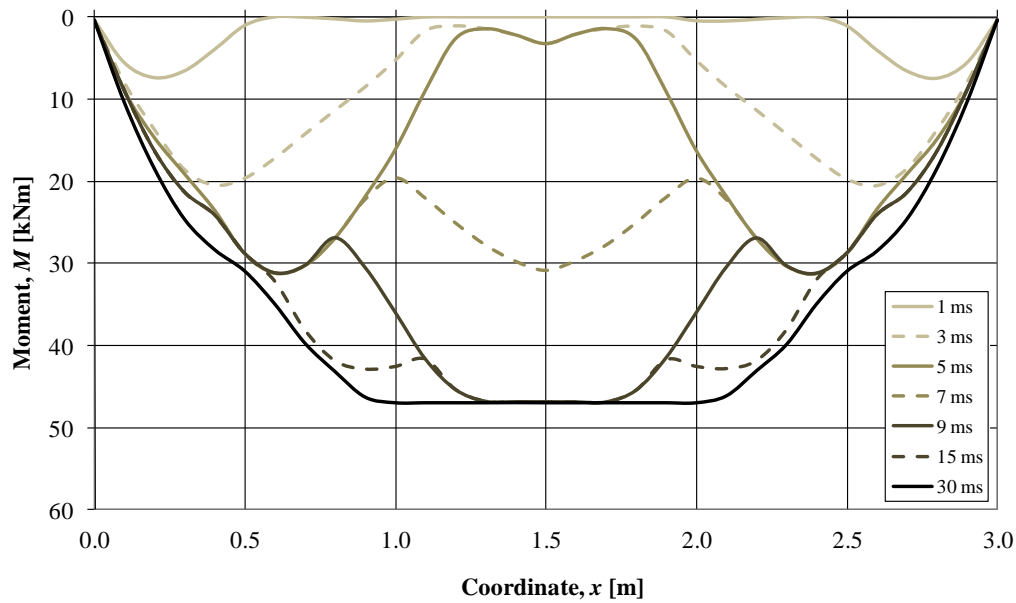
*Figure 6.3.   Moment envelope for beam 1 with curtailment of L/6 from the ends at different times.*
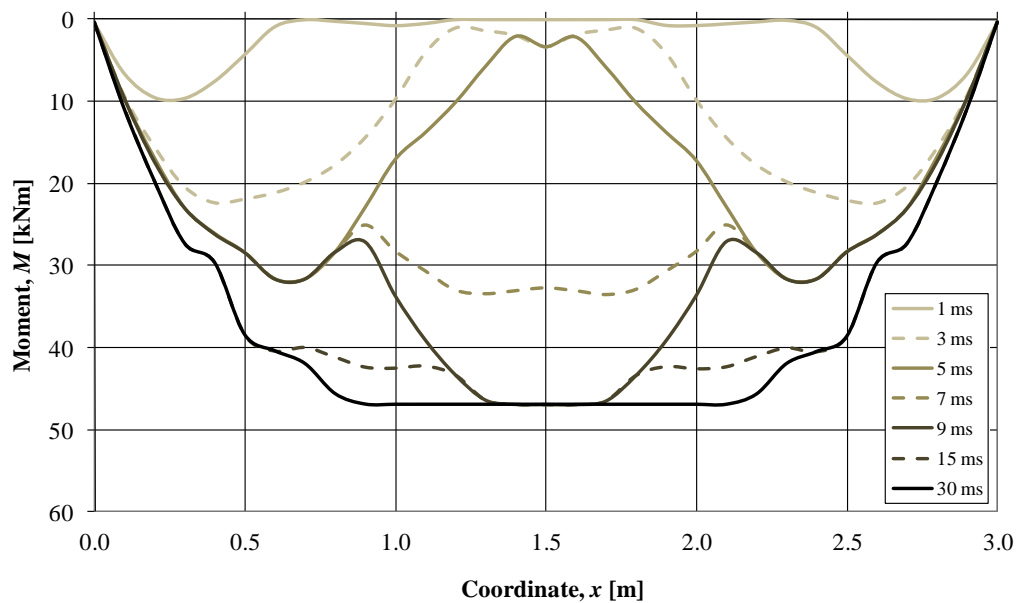


*Figure 6.4.   Moment envelope for beam 1 without curtailment at different times.*

The two moment envelope progressions are very similar for the case with and without curtailment. It can be seen that the moment has progressed further for every time for the case without curtailment, but the most important difference is seen at the final envelope after 30 ms where the moments differ by up to as much as 20 percent in the region within a distance of L/6 from the beam ends. This is not unexpected, though, as the moment capacity differs in these points, and it is possible that the capacity is reached for both cases.

To better show where the moment capacity is reached, for how long and how it differs with different load cases another figure is presented. The final moment envelope is shown in Figure 6.5 for all load cases, together with the moment capacity for the curtailed beam and the moment from the equivalent static load. It can be seen that the

moment capacity is reached at the curtailment where the moment from the equivalent static load would not. As expected, the reduced moment capacity is reached closer to the supports for more impulsive loads, but will this cause the failure of the beam?
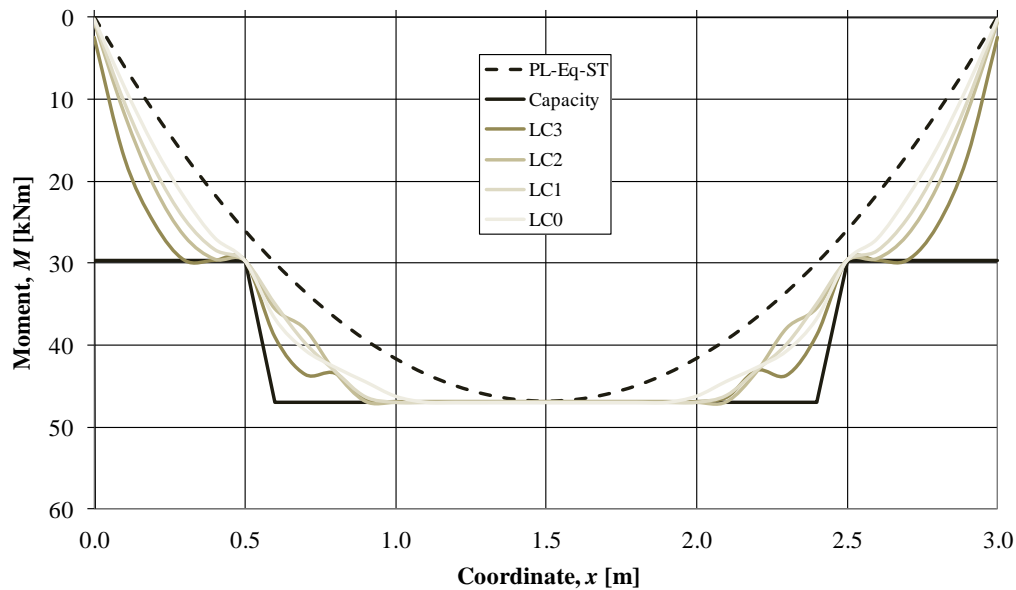


*Figure 6.5. Moment envelope for all load cases and reduced moment capacity due to curtailment at L/6 from edge*

Showing the moment distribution for a beam with ability to deform is not sufficient to determine whether there will be failure or not, and therefore the plastic strains are studied. Because of this, a schematic figure of the moment envelope is shown for one case only, but the strains are studied more thoroughly for both cases presented in Figure 6.2. The beam will be subjected to plastic strain wherever the moment capacity is reached, and the magnitude of the strain is based on how long the moment remains at the limit. It is difficult to determine a certain limit for the strain with regard to failure. However, when the strain in the beam with curtailment at L/6 from the edges exceeds the limit of three to five percent, the probability of failure will be imminent, according to Appendix J. In order to determine where the failure will occur, the plastic strain distributions in the two cases are studied for the different load cases, see Figure 6.6 and Figure 6.7.
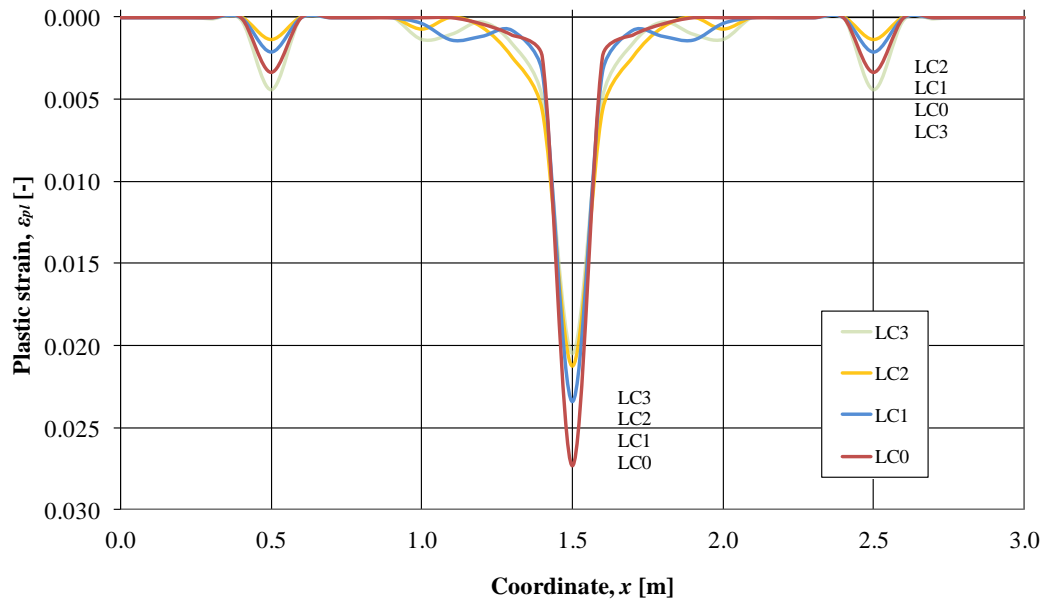
*Figure 6.6.* *Plastic strain for the beam with curtailment of L/6 from the ends.*
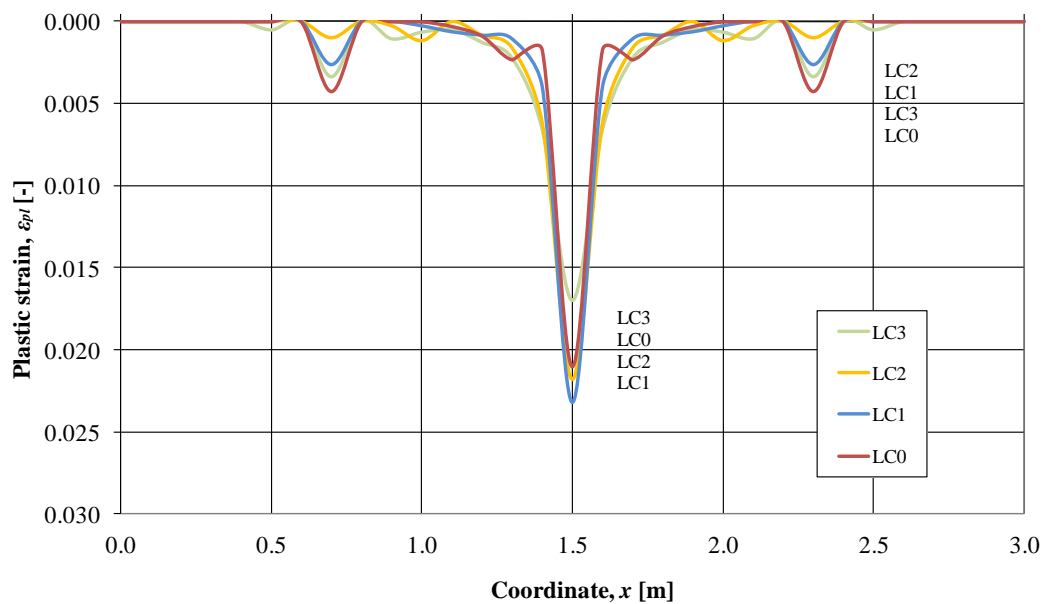


*Figure 6.7.* *Plastic strain for the beam with curtailment of L/4 from the ends.*

As seen from Figure 6.6 and Figure 6.7, one major plastic zone forms in the middle and two minor plastic zones at L/6 and L/4 from the ends for each beam respectively. The reason why the major strain peak in the middle is larger than at the curtailment is because the moment capacity is reached here for a longer duration. It can also be seen that the magnitude of plastic strain differs for the different load cases, but the difference is not consistent with the location in the beam or between the two cases. For instance, for the beam with curtailment at L/6 from the ends, the largest strains at the curtailment will occur for load case 3, but for the beam with curtailment at L/4 from the ends the largest strains at the curtailment will be achieved for load case 0. When looking at the strains in midpoint, the largest plastic strain is achieved for load case 0 for the beam with curtailment at L/6, while the largest plastic strains for the beam with curtailment at L/4 is achieved for load case 1. This means that the

115

magnitude of developed plastic strain is not solely governed by either maximum pressure or load time. This can be shown by looking at the moment over time for the nodes where the strains occur.

The moment over time at the node where the right hand side curtailment starts is shown in Figure 6.8 for the case of curtailment at L/6 from the ends. Even though the moment cannot exceed the yield limit, and is only a product of calculation errors in ADINA, it is shown to easier see how the plastic strains will vary for different load cases. While load case 3 is the most intense of the four load cases and therefore causes the moment capacity to be reached early, the worst case will occur for load case 0 as the capacity is reached for a longer time.
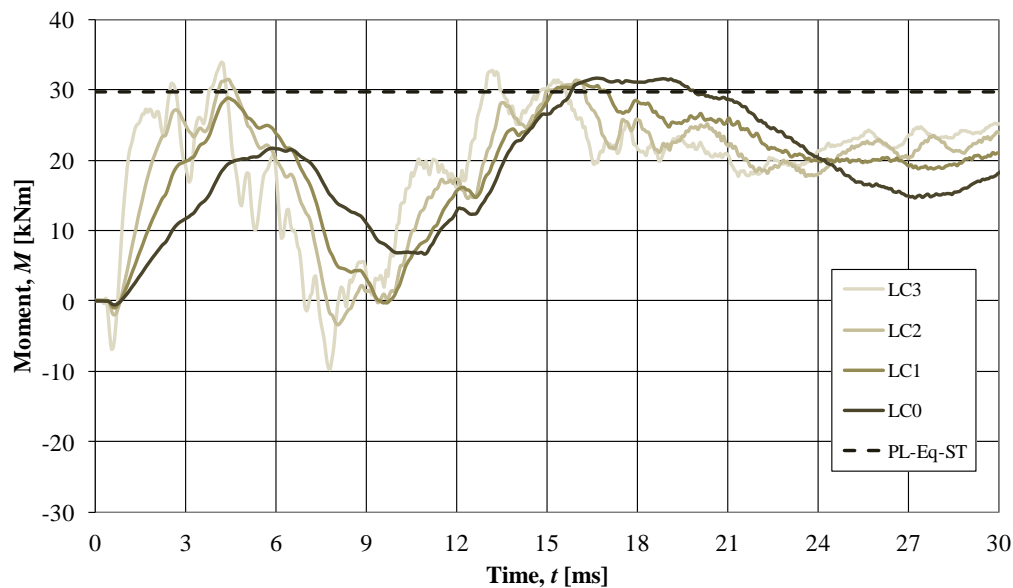


*Figure 6.8.    Moment over time at coordinate x = 5L/6.*

## 6.2    Discussion

It has been shown that for this beam, curtailment will not be a threat of the capacity of the beam, even though the moment envelope seemed dangerous before the curtailment analysis was performed. It is however very clear that the beam will develop plastic hinges at the curtailment points. This will lead to a larger total plastic strain of the beam since it is also indicated that the plastic strain in the middle will be unchanged from the case without curtailment. Hence, the total deformation in the midpoint will increase if the beam is designed with curtailment.

A conclusion is also drawn that it is not possible to say whether the plastic strains will be smaller or larger for more intense loads, which was first assumed. This was actually a surprisingly find. It seems that it is not possible to generally determine which load case is the most dangerous because of the fact that the strain both takes the magnitude of the force and the duration the yield moment is reached into account. It would be interesting to see more studies on this to be sure of the findings.

# 7 Final remarks

## 7.1 Conclusions

It is possible to accurately simplify the displacements of a simply supported beam for different material behaviours with an SDOF-model by using certain transformation factors. Because the beam's initial deflection for a highly impulsive load differs a lot from static deflection shape the simplification is initially poor, but by the time the deflection reaches its maximum value the deflection shapes are very similar and the results converge well.

The modelling of the moments is more complex and requires a multi degree of freedom-model with more modes to get accurate results. It is also possible to describe the maximum moment distribution by using an equivalent static load, but it was shown to underestimate the moment in every node unless a damping of at least 10 percent is used for the FE-analysis. For reinforced concrete beams a reasonable damping would be around five percent.

For design purpose it is of interest to compare the undamped SDOF-model with the FE-analysis using damping. When the moment from the SDOF-model was compared to the FE-analysis using damping, the results were better than for the FE-analysis without damping, but the moment was still underestimated by 6-9 percent in the SDOF-model.

When comparing the displacements from the SDOF-model to the modal-analysis using only one mode, both with high damping, it was seen that a better convergence was obtained when the transformation factor $\kappa_{cF}$ was set to 0.8 instead of the previously assumed value of 1.0.

The analysis of the curtailed beams did not reveal any special problems. Significant plastic strains were noticed at the curtailed area, but the plastic strains in midpoint were at least five times larger for all studied cases. Furthermore, it was not possible to determine a correlation between the intensity of the load and the plastic strain for the beam, as the yielding is a function of both moment and time. These results indicate that the negative effect due to curtailment may be possible to adequately deal with in a reinforced concrete structure; i.e. the possible negative effect due to curtailment is believed to be small.

## 7.2 Further studies

There seems to be a connection between the wave propagation and the moment progression in the beam, and it would be interesting to know more about this. When the beam is modelled in the FE-model for plastic material behaviour a very high initial Young's modulus is used, and it will increase the information speed in the concrete. It is interesting to study this further in order to tell if this modelling method will affect the results significantly.

It is interesting to further study the dynamic response of a structural member with different properties depending on the direction of deflection. If a beam with symmetrical cross-section can withstand the first and largest deflection, there will be no problems with the other deflections. However, if the beam is weaker in the opposite direction a failure might occur because of the recoil. This could be a risk in

for example unsymmetrical reinforced concrete beams or T-cross-sections, and a way of modelling this should be developed.

Both the moment from the SDOF and from the equivalent static load, for the elastic response, will underestimate the maximum moments for an impulsive load, but since they are quick and easy to calculate it is of interest to make them accurately describe the moment on the safe side, and therefore it is of interest to find up-scaling factors for the moment that sufficiently works.

Since the transformation factor for the damping $\kappa_{cF}$ was only handled briefly in this Master thesis there is a need for verifying the accurate value and also list the values for different types of loads and boundary conditions. It should also be investigated whether the transformation factor is dependent of the damping or not. It is of special interest to derive the transformation factor in the future. This might be done with regard to velocity, i.e. the derivative of the displacement.

It is not clear if a beam will obtain more maximum plastic strain when subjected to a highly impulsive load than when subjected to a less impulsive load and this could be of interest to study further in the future.

Also, the analyses made in this Master thesis could be verified by more accurate non-linear FE-models, using solid elements to explicitly model concrete cracking and reinforcement yielding. The modelling should also be extended to cover other materials such as timber and steel.

# 8 References

WRITTEN SOURCES:

Adhikari S., 2000. *Damping Models for Structural Vibrations*. Ph.D. thesis. Engineering department, Cambridge University.

ADINA, 2011. *Theory and Modelling Guide*. Vol 1: ADINA Solids & Structures Report ARD 11-8, ADINA R & D, Inc., Watertown, MA. USA.

Andersson S. and Karlsson H., 2012. *Structural Response of Reinforced Concrete Beams Subjected to Explosions*. Division of Structural Engineering, Concrete Structures, Chalmers University of Technology, Master Thesis 2012:103, Gothenburg, Sweden.

Augustsson R. and Härenstam M., 2010. *Design of reinforced concrete slab with regard to explosions*. Division of Structural Engineering, Concrete Structures, Chalmers University of Technology, Master Thesis 2010:38, Gothenburg, Sweden.

Bathe K-J., 1996. *Finite Element Procedures*. Prentice Hall, New Jersey, USA.

Biggs J.M., 1964. *Introduction to Structural Dynamics*. McGraw-Hill Inc., New York, USA.

CEN 2004. *Eurocode 2: Design of Concrete Structures – Part 1-1: General rules and rules for buildings*. European Comittee for Standardization, Brussels, Belgium.

Chopra A., 2011. *Dynamics of Structures: Theory and Applications to Earthquake Engineering, Third Edition*. Pearson Education, Inc., New Delhi, India.

ConWep 1992: ConWep – Collection of conventional weapons effects calculation based on TM 5-855-1, Fundamentals of Protective Design for Conventional Weapons, U.S. Army Engineer Waterways Experiment Station, Vicksburg, USA.

Ek K-J. and Mattsson P., 2009. *Design with Regard to Blast- and Fragment Loading*. Division of Structural Engineering, Concrete Structures, Chalmers University of Technology, Master Thesis 2009:81, Gothenburg, Sweden.

Isaksson T., Mårtensson A., Thelandersson S., 2010. *Byggkonstruktion*. Studentlitteratur AB, Lund, Sweden.

Johansson M., 1997. *Armeringsseghetens inverkan på deformationsförmågan hos betongkonstruktioner*. Avdelning för Betongbyggnad, Chalmers Tekniska Högskola, Rapport 97:1 Göteborg.

Johansson M., 1999. *Non-linear Finite Element Analyses of Civil Defence Shelter Subjected to Explosion Load or Impact Load*. Avdelning för Betongbyggnad, Chalmers Tekniska Högskola, Rapport 99:8 Göteborg.

Johansson M., 2000. *Structural Behaviour in Concrete Frame Corners of Civil Defence Shelters: Non-Linear Finite Element Analyses and Experiments*. Avdelning för Betongbyggnad, Chalmers Tekniska Högskola, Publikation 00:2 Göteborg.

Johansson M. och Laine L., 2007. *Bebyggelsens motståndsförmåga mot extrem dynamisk belastning, Delrapport 1: Last av luftstötvåg*. Räddningsverket, Rapport B54-232/07, Karlstad.

Johansson M. och Laine L., 2009. *Bebyggelsens motståndsförmåga mot extrem dynamisk belastning, Delrapport 3: Kapacitet hos byggnader*. MSB, Rapport MSB 0142-10, Sweden.

Nyström U., 2006. *Design with regard to explosions.* Division of Structural Engineering, Concrete Structures, Chalmers University of Technology, Master Thesis 2006:14, Gothenburg, Sweden.

Laine L., 2012. *Markstötvåg*. MSB, publication number MSB344, Sweden.


WEB SOURCE:

http://www.engineeringtoolbox.com/sound-speed-solids-d_713.html (2012-03-29)

http://www.bloomberg.com/news/2011-07-27/norway-police-spreads-breivik-terror-probe-europe-wide-after-twin-attacks.html (2011-07-27)

http://www.ndt-ed.org/EducationResources/CommunityCollege/Ultrasonics/Physics/wavepropagation.htm (2009-12-15)

# Appendix A   Beam theory

In structural analysis and design it is important to understand the calculations of the deflection. Large deflections, high tensions and unwanted cracks are all connected, hence, the deflection is a good way to verify the resistance of a beam.

In order to fully comprehend the deflection it is important to understand the symbols for displacement. Displacement in the $x$, $y$ and $z$ directions are connected with the letters $u$, $v$ and $w$ respectively. A vertically loaded ($y$ direction) horizontal beam ($x$ direction) will be deformed into a curve, see Figure A.1. Thus will the deflection $v$ be the displacement in the $y$ direction.
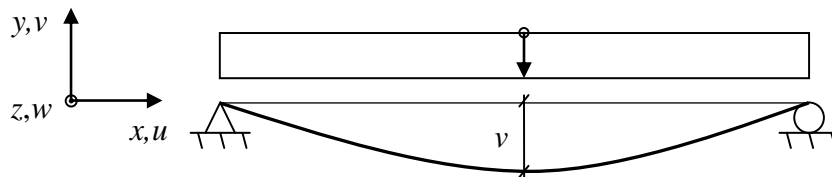


*Figure A.1.   Coordinate system and deflection for vertically loaded beam.*

In order to derive the deflection curve the reader is referred to Figure A.2.
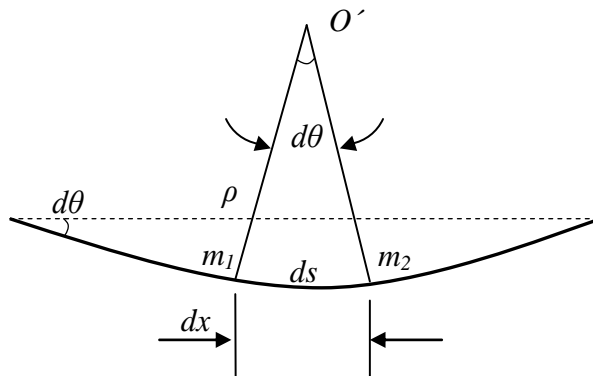


*Figure A.2.   Curvature of a deflected beam.*

With the radius of curvature $\rho$ and the angle between the normal's for $m_1$ and $m_2$ it is possible to derive the curvature:

$$\rho \cdot d\theta = ds \tag{A.1}$$

The curvature can be expressed as the angular change over the curved length.

$$\kappa = \frac{d\theta}{ds} = \frac{1}{\rho} \tag{A.2}$$

According to Figure A.3 the slope of the deflected beam can be expressed as:

$$\tan\theta = \frac{dv}{dx} \tag{A.3}$$

which is the first derivative of the deflection $v$. An expression for $cos\ \theta$ can be found:

$$\cos\theta = \frac{dx}{ds} \tag{A.4}$$
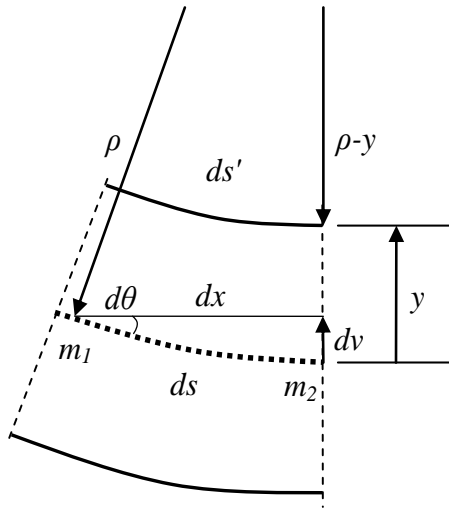


*Figure A.3.    Deformations of a beam in pure bending.*

Assuming small angles and rotations, the following simplifications can be made:

$$\tan\theta \approx \theta \tag{A.5}$$

and

$$\cos\theta \approx 1 \tag{A.6}$$

which leads to

$$\theta \approx \frac{dv}{dx} \tag{A.7}$$

and

$$ds \approx dx \tag{A.8}$$

By inserting Equation (A.7) in Equation (A.2) the following differential equation for the curvature with regard to the deflection $v$ is formed:

$$\kappa = \frac{d}{ds}\left(\frac{dv}{dx}\right) \approx \frac{d^2v}{dx^2} \tag{A.9}$$

From Figure A.3 an expression for the horizontal strain, $\varepsilon_x$, at the distance $y$ from the neutral axis can be derived as

$$\varepsilon_x = \frac{ds'-ds}{ds} = \frac{(\rho - y)d\theta - \rho d\theta}{\rho d\theta} = -\frac{y}{\rho} \tag{A.10}$$

It is known from Hooke's law that

$$\sigma_x = \varepsilon_x E \tag{A.11}$$

which by insertion of Equation (A.10) can be written as

$$\sigma_x = -\frac{y}{\rho} E \tag{A.12}$$

The connection between the curvature and the moment, $M$, can be derived with help of Figure A.4, which shows the linear stress distribution and moment over the cross-section for an arbitrary beam subjected to pure bending. When the moment and curvature are positive the area above the neutral axis is in compression and the stresses $\sigma_x$ are negative; the area below the neutral axis is in tension and the stresses are positive.
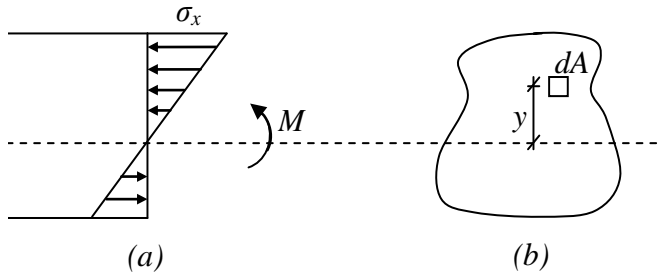


Figure A.4. (a) Side view of normal stress distribution in an arbitrary beam of linear elastic material, and (b) cross section of the same beam.

For an infinitesimal area $dA$ which is subjected to negative stress $\sigma_x$ with the lever $y$ from neutral axis, the positive partial moment is written as

$$dM = -y\sigma_x dA \tag{A.13}$$

By integrating the stresses over the area the moment is given by

$$M = \int_A -y\sigma_x dA = \int_A \frac{Ey^2}{\rho} dA = \frac{E}{\rho} \int_A y^2 dA \tag{A.14}$$

Since the moment of inertia of the cross-sectional area can be written as

$$I_z = \int_A y^2 dA \tag{A.15}$$

Equation (A.14) can be written as

$$M = \frac{EI_z}{\rho} \tag{A.16}$$

which can be rewritten as

$$\frac{M}{EI_z} = \frac{1}{\rho} \tag{A.17}$$

Finally, insertion of Equation (A.17) in (A.2) gives

$$\kappa = \frac{M}{EI_z} \tag{A.18}$$

or

$$\frac{M}{EI_z} = \frac{d^2v}{dx^2} \tag{A.19}$$

which is also called the basic differential equation of the deflection curve of a beam. Hence, the moment is proportional to the curvature.

# Appendix B    Central Difference Method

## B.1 Numerical solution

The central difference method is an explicit method for solving the equation of motion:

$$m\ddot{u} + c\dot{u} + ku = F(t) \tag{B.1}$$

where $m$ is the mass, $c$ is the damping, $k$ is the stiffness, $\ddot{u}$ is the acceleration, $\dot{u}$ is the velocity, $u$ is the displacement and $F(t)$ is the driving force.

By solving an equation explicitly means that in order to calculate $u_{i+1}$ the method uses $u_i$ and $u_{i-1}$. The method also uses a constant time step, $\Delta t$. The index $i$ is stated by the observed time.

By referring to Figure B.1 the velocity and acceleration at time $i$ can be expressed as

$$\dot{u}_i = \frac{u_{i+1} - u_{i-1}}{2\Delta t} \tag{B.2}$$

$$\ddot{u}_i = \frac{\dfrac{(u_{i+1} - u_i)}{\Delta t} - \dfrac{(u_i - u_{i-1})}{\Delta t}}{\Delta t} = \frac{u_{i+1} - 2u_i + u_{i-1}}{(\Delta t)^2} \tag{B.3}$$

respectively in the central difference method. The acceleration in Equation (B.3) is derived as the difference of mid interval velocities (the circles in Figure B.1).
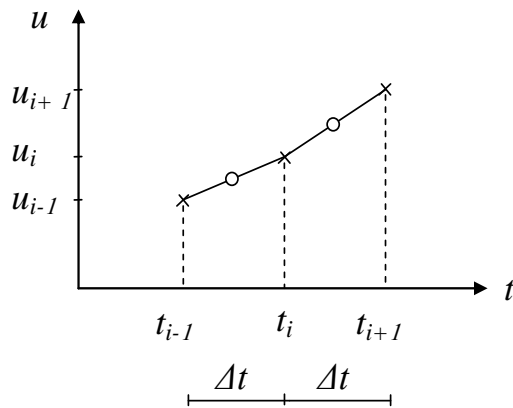


Figure B.1.    The central difference scheme. The method uses $u_{i-1}$ and $u_i$ in order to solve $u_{i+1}$.

By inserting Equations (B.2) and (B.3) in (B.1), an approximation of the equation of motion is given as

$$m\frac{u_{i+1} - 2u_i + u_{i-1}}{(\Delta t)^2} + c\frac{u_{i+1} - u_{i-1}}{2\Delta t} + ku_i = F_i \tag{B.4}$$

where $u_i$ and $u_{i-1}$ are assumed to be known. Rearranging Equation (B.4), by moving the known displacements $u_i$ and $u_{i-1}$ to the right side, gives

$$\left[\frac{m}{(\Delta t)^2} + \frac{c}{2\Delta t}\right]u_{i+1} = F_i - \left[\frac{m}{(\Delta t)^2} - \frac{c}{2\Delta t}\right]u_{i-1} - \left[k - \frac{2m}{(\Delta t)^2}\right]u_i \qquad \text{(B.5)}$$

or

$$\hat{k}u_{i+1} = \hat{F}_i \qquad \text{(B.6)}$$

where

$$\hat{k} = \frac{m}{(\Delta t)^2} + \frac{c}{2\Delta t} \qquad \text{(B.7)}$$

and

$$\hat{F}_i = F_i - \left[\frac{m}{(\Delta t)^2} - \frac{c}{2\Delta t}\right]u_{i-1} - \left[k - \frac{2m}{(\Delta t)^2}\right]u_i \qquad \text{(B.8)}$$

It is now possible to derive the expression for the sought displacement, $u_{i+1}$ as

$$u_{i+1} = \frac{\hat{F}_i}{\hat{k}} \qquad \text{(B.9)}$$

From Equation (B.8) it is seen that $u_i$ and $u_{i-1}$ are used to solve $u_{i+1}$, i.e. in order to determine $u_1$ the displacements $u_0$ and $u_{-1}$ must be known. The initial displacement $u_0$ is assumed to be known, it is zero in this Master thesis. The displacement $u_{-1}$ can be determined by setting $i=0$ in Equation (B.2) and (B.3), then solving for $u_1$ in Equation (B.2) and substituting in (B.3).

The starting step of solving the central difference method is then given as

$$u_{-1} = u_0 - \Delta t \dot{u}_0 + \frac{(\Delta t)^2}{t}\ddot{u}_0 \qquad \text{(B.10)}$$

## B.2 Stability

A solution is said to be stabile if errors in the initial conditions do not grow during the iterations, which can easily happen if the chosen time step is not short enough. According to Chopra, (2011), the requirement of stability for the central difference method is specified as

$$\frac{\Delta t}{T_n} < \frac{1}{\pi} \qquad \text{(B.11)}$$

If this requirement is not met, the central difference method will "blow up" and quickly become useless. For explosions this is seldom a problem since much smaller time steps usually are used anyway to obtain accurate enough results.

# B.3 Non-linear material response

The central difference method is also an excellent method when dealing with a non-linear material response. The method derived in Appendix B.1 is for a linear stiffness but can easily be altered to be able to calculate the displacement for a structure with a non-linear material response. Similar to the displacement, the stiffness $k$ can be calculated at different times as a response of the displacement:

$$k_i = k_i(u_i) \tag{B.12}$$

In a system with a non-linear material response the stiffness will change with time

$$k_i \neq k_{i+1} \neq k_{i+2} \tag{B.13}$$

while it for a linear material response will stay the same:

$$k_i = k_{i+1} = k \tag{B.14}$$

When analysing the structural response it is however more of interest to derive the inner resistance for a certain time than focusing on the stiffness, thus, the stiffness $k_i$ will be inserted in the equation for the inner resistance as follows:

$$R_i = k_i \cdot u_i \tag{B.15}$$

In Figure B.2 it is shown how the response changes for different displacements.
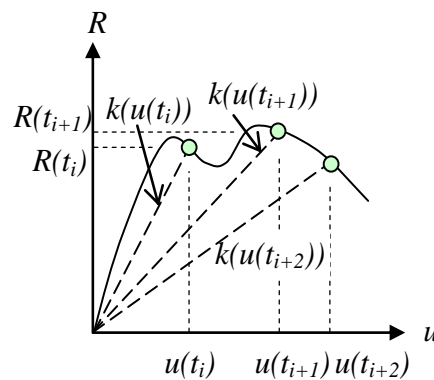


*Figure B.2.    The stiffness at time $t_i$ for a non-linear material response.*

# Appendix C  Deformation shape and moment over time

In order to help the reader the deformation shape and the moment distribution have been plotted over time. Then one can see how the beam will deflect when subjected to an explosion. It is also very interesting to see how the moment develops over time. The figures are showing an elastic stadium II, plastic and elasto-plastic material response for the beam described in Chapter 3, beam 1.

## C.1 Linear elastic



t = 0.1 ms



t = 0.2 ms



t = 0.3 ms

t = 0.4 ms



t = 0.5 ms



t = 0.6 ms



t = 0.7 ms

130
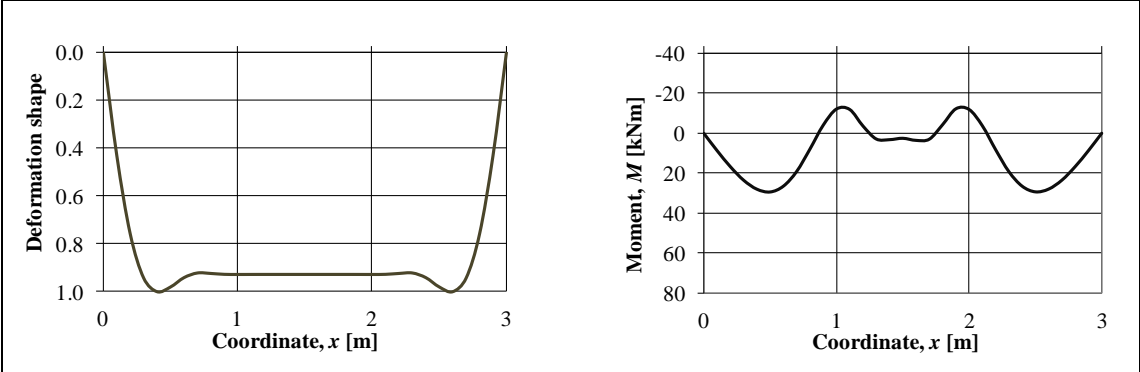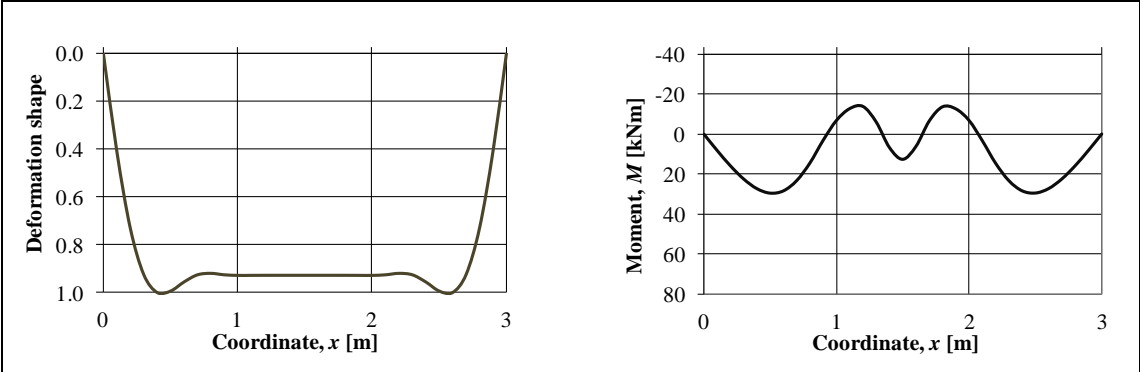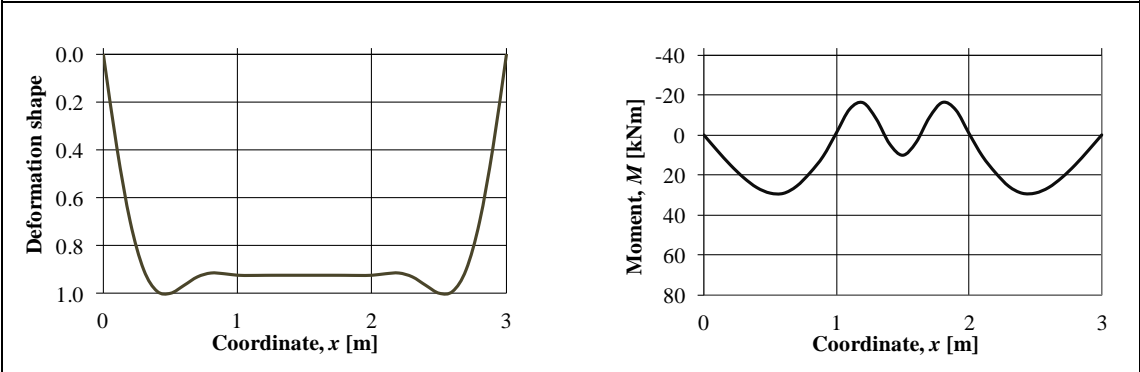
t = 0.8 ms



t = 0.9 ms



t = 1.0 ms
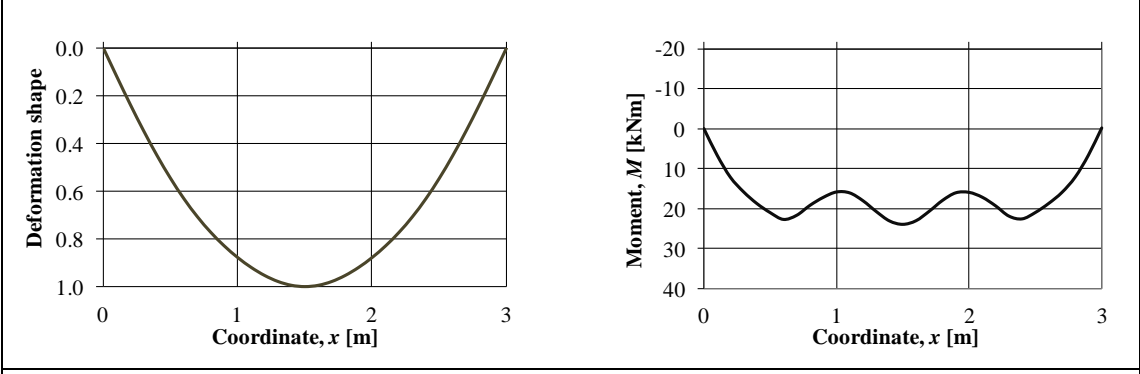


t = 1.5 ms

t = 2.0 ms



t = 2.5 ms



t = 3.0 ms



t = 3.5 ms

132

t = 4.0 ms



t = 4.5 ms
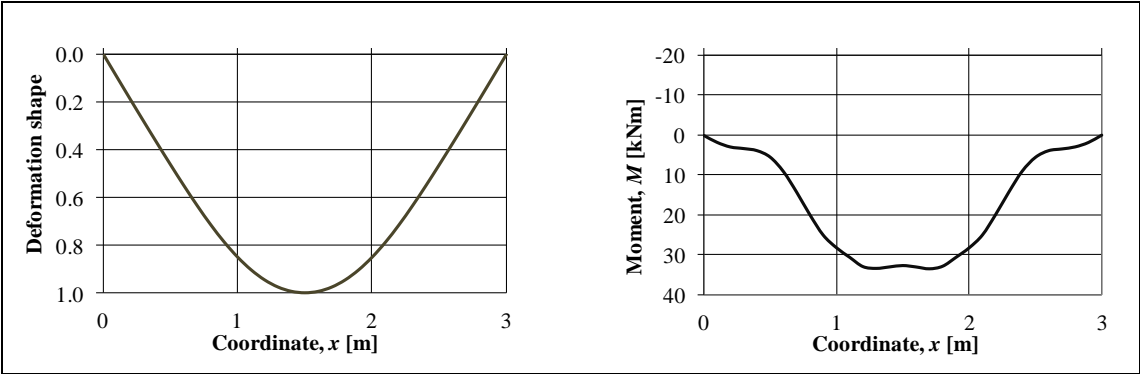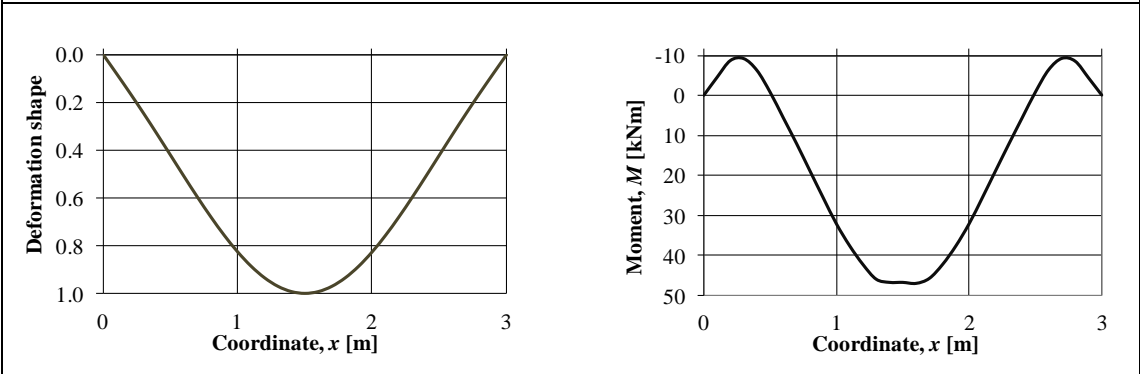


t = 5.0 ms



t = 6.0 ms

133

t = 7.0 ms



t = 8.0 ms



t = 9.0 ms



t = 10.0 ms

134

t = 11.0 ms



t = 12.0 ms



t = 13.0 ms



t = 14.0 ms

t = 15.0 ms

t = 20.0 ms

t = 25.0 ms

t = 30.0 ms

136

# C.2 Ideal plastic



t = 0.1 ms



t = 0.2 ms



t = 0.3 ms

| t = 0.4 ms |
| --- |



| t = 0.5 ms |
| --- |



| t = 0.6 ms |
| --- |



| t = 0.7 ms |
| --- |



| t = 0.8 ms |
| --- |

139

t = 0.9 ms



t = 1.0 ms



t = 1.5 ms



t = 2.0 ms

140
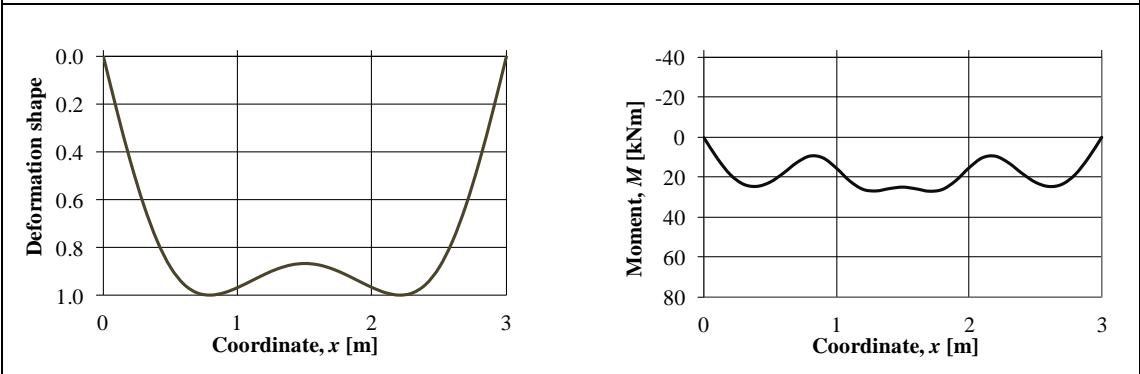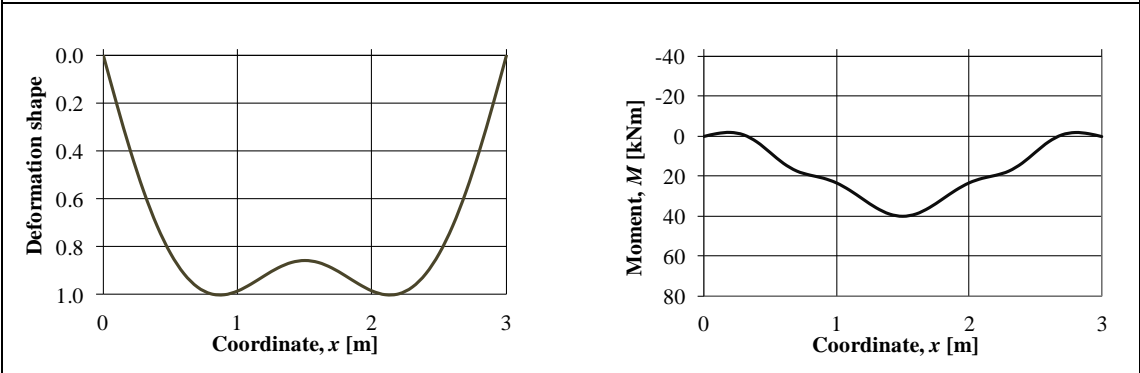
t = 2.5 ms



t = 3.0 ms



t = 3.5 ms



t = 4.0 ms

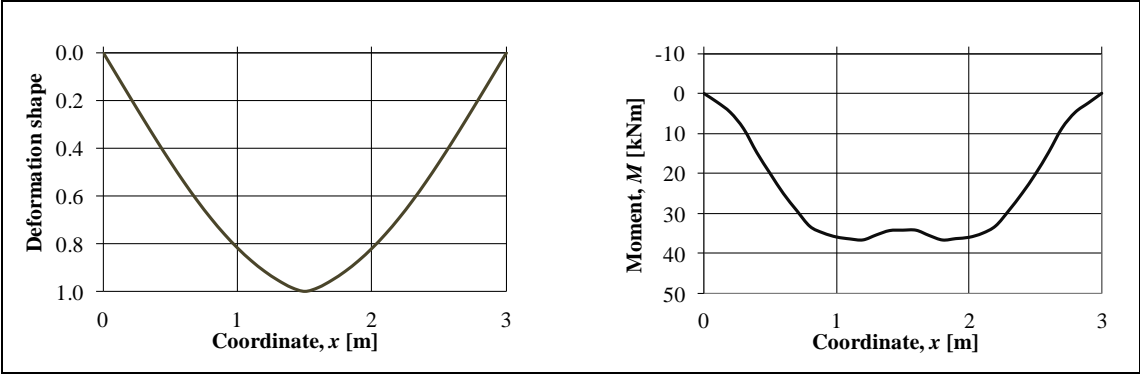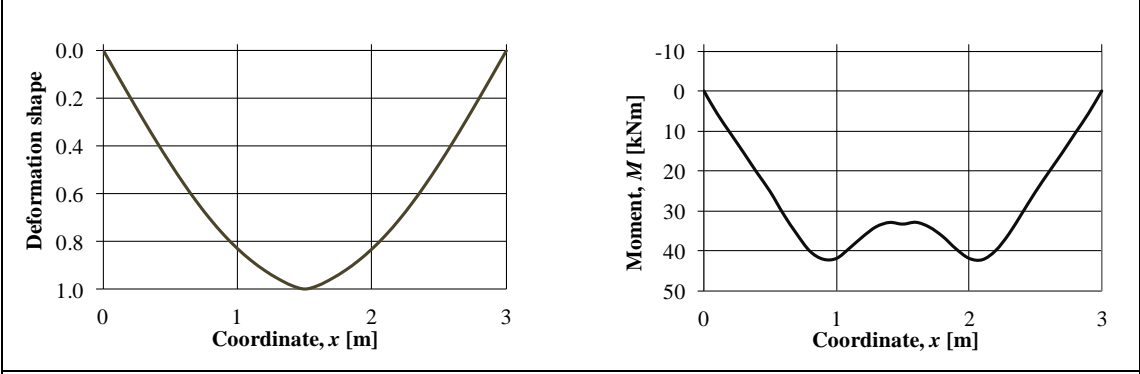t = 4.5 ms



t = 5.0 ms



t = 6.0 ms



t = 7.0 ms

142

t = 8.0 ms



t = 9.0 ms



t = 10.0 ms



t = 11.0 ms
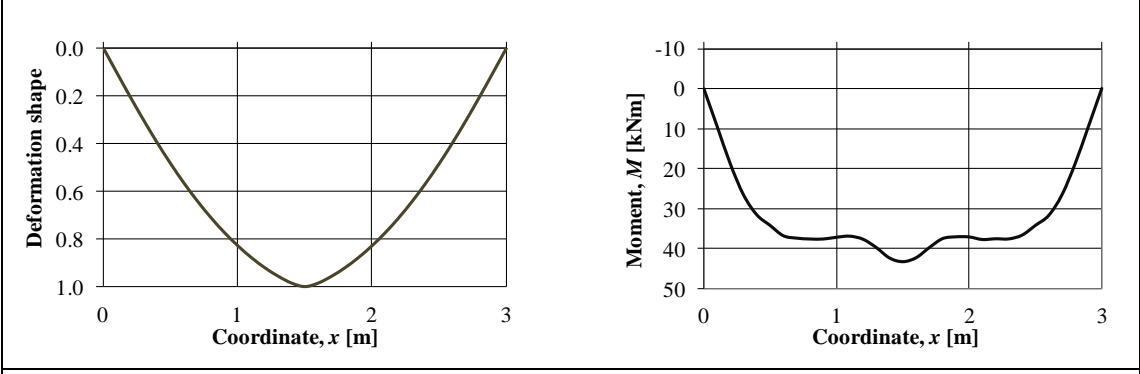
t = 12.0 ms
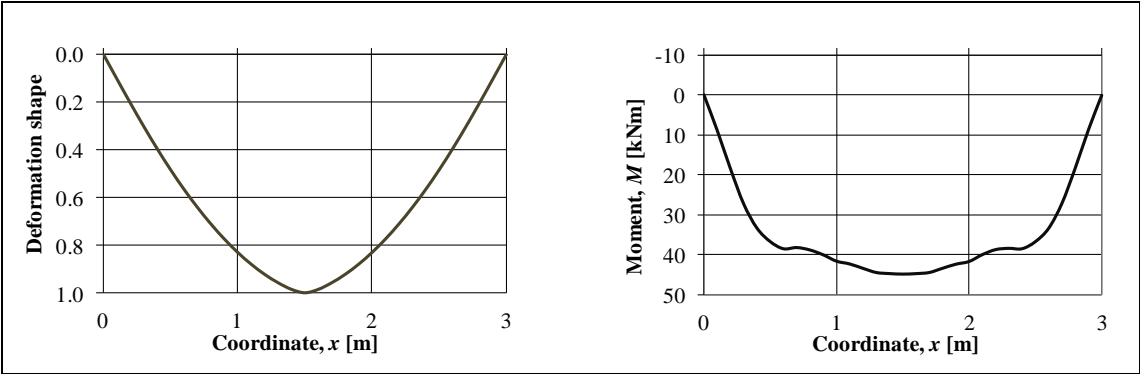


t = 13.0 ms



t = 14.0 ms



t = 15.0 ms

144

t = 20.0 ms



t = 25.0 ms



t = 30.0 ms



145
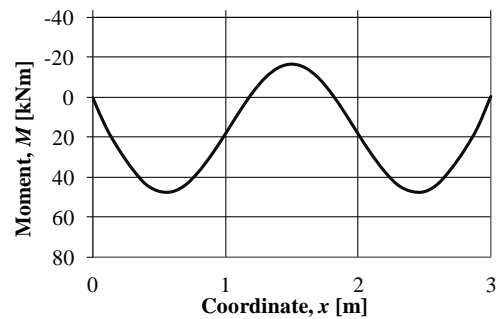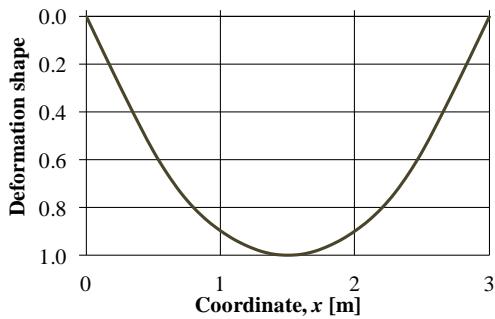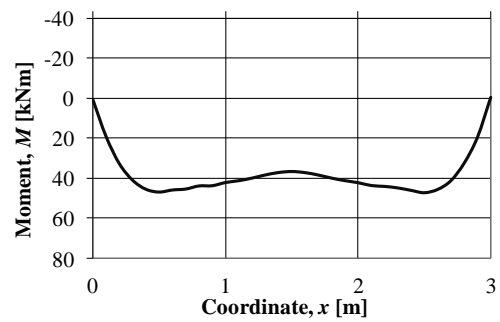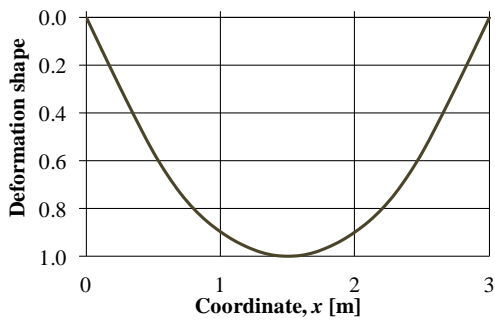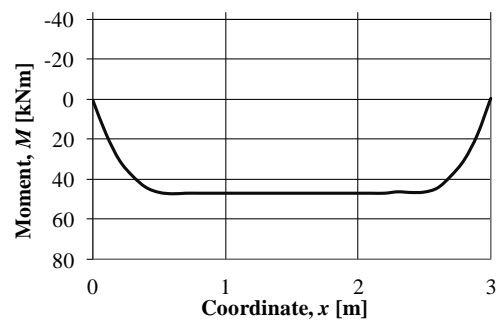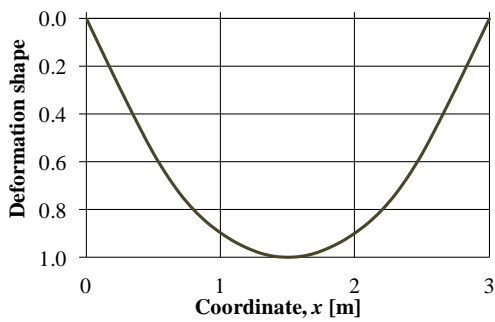
## C.3 Elasto-plastic
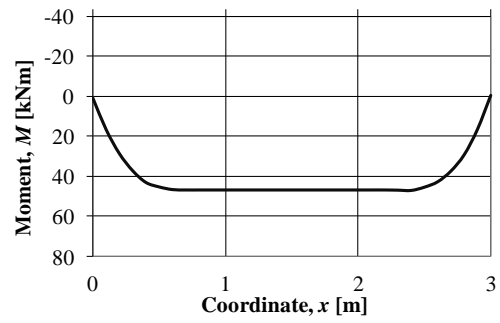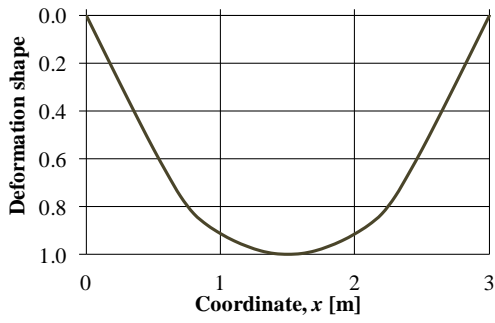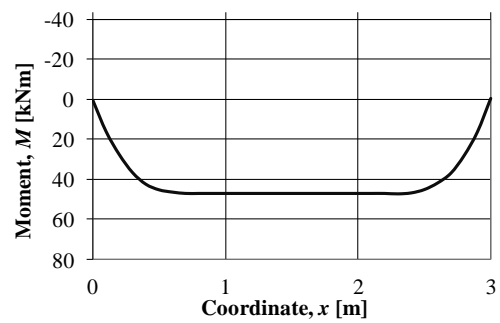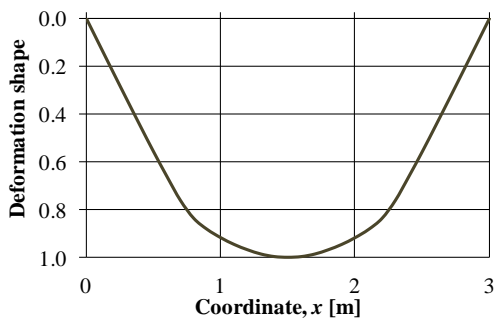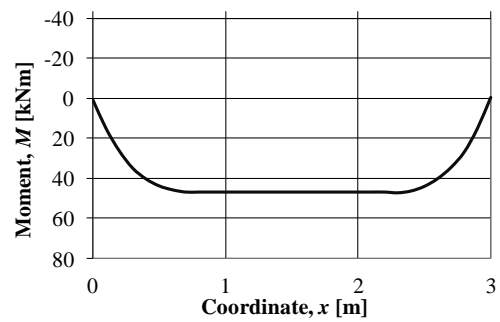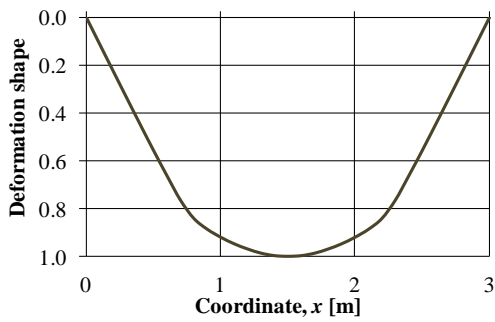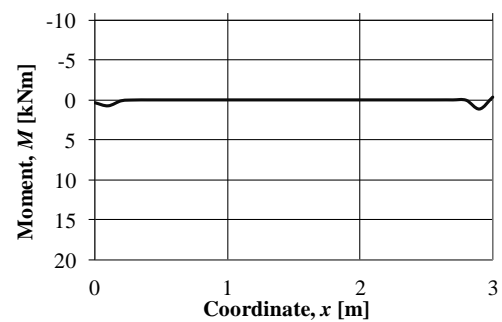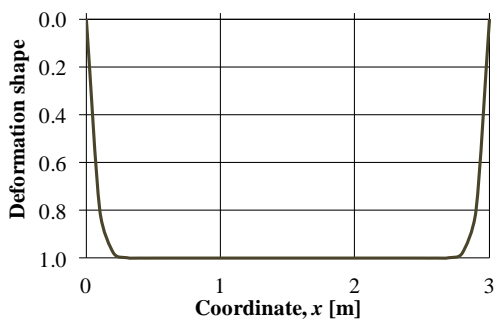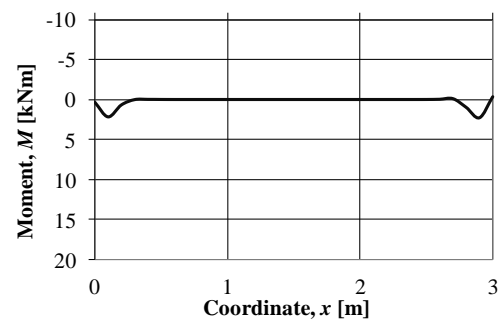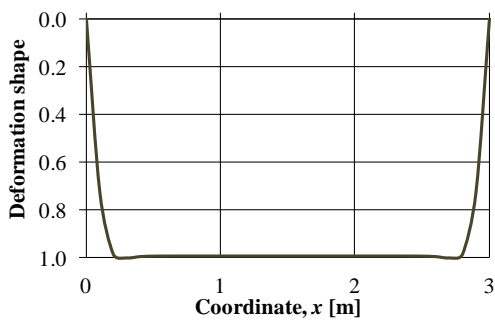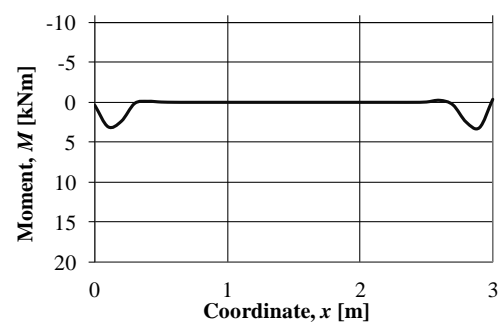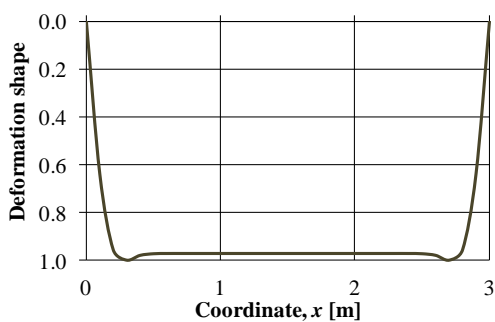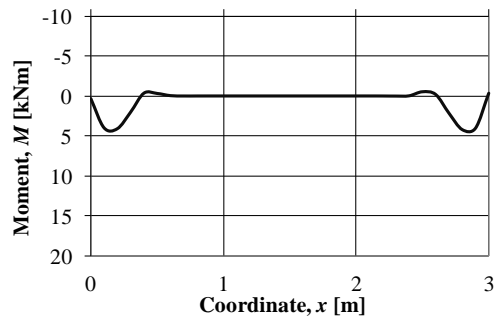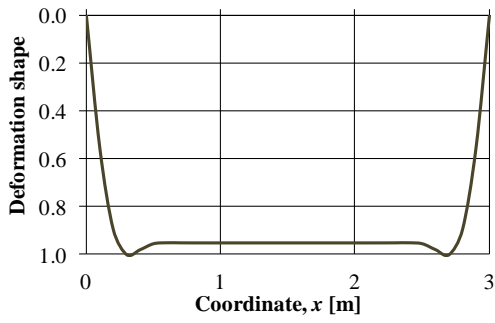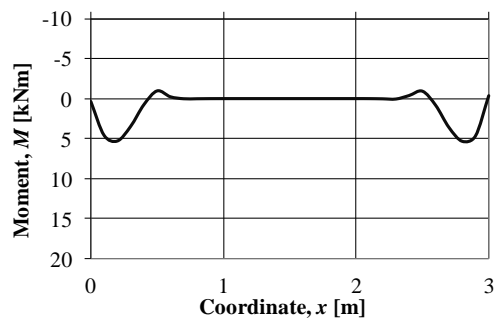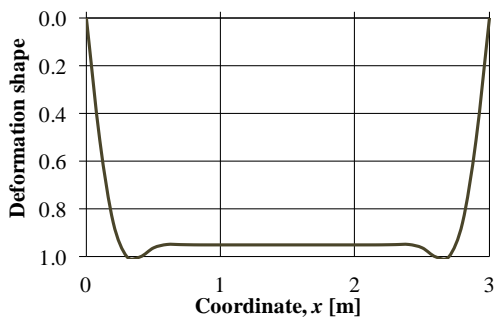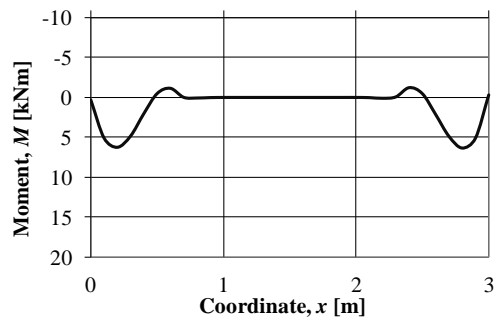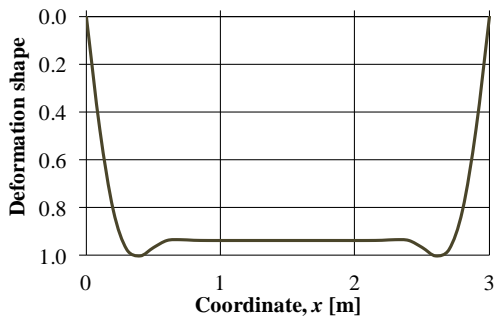
| t = 0.4 ms |
| --- |



| t = 0.5 ms |
| --- |



| t = 0.6 ms |
| --- |



| t = 0.7 ms |
| --- |



| t = 0.8 ms |
| --- |

t = 0.9 ms



t = 1.0 ms



t = 1.5 ms



t = 2.0 ms

148

t = 2.5 ms



t = 3.0 ms



t = 3.5 ms



t = 4.0 ms

149

t = 4.5 ms
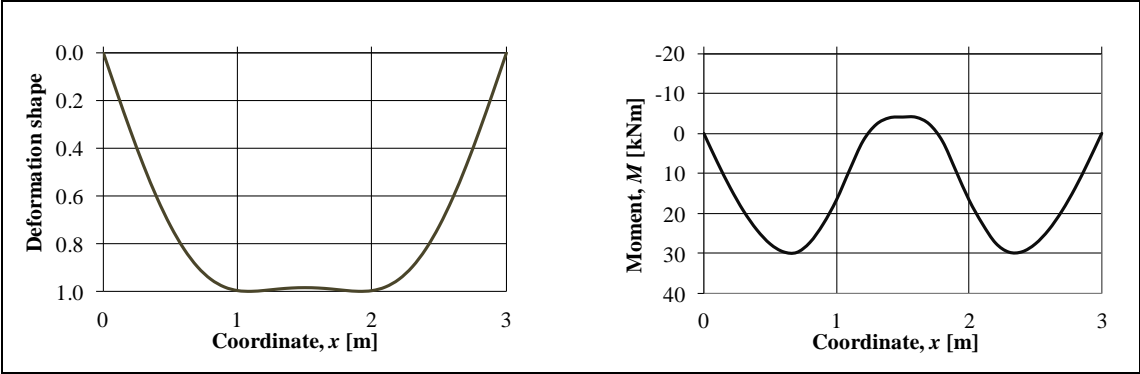


t = 5.0 ms
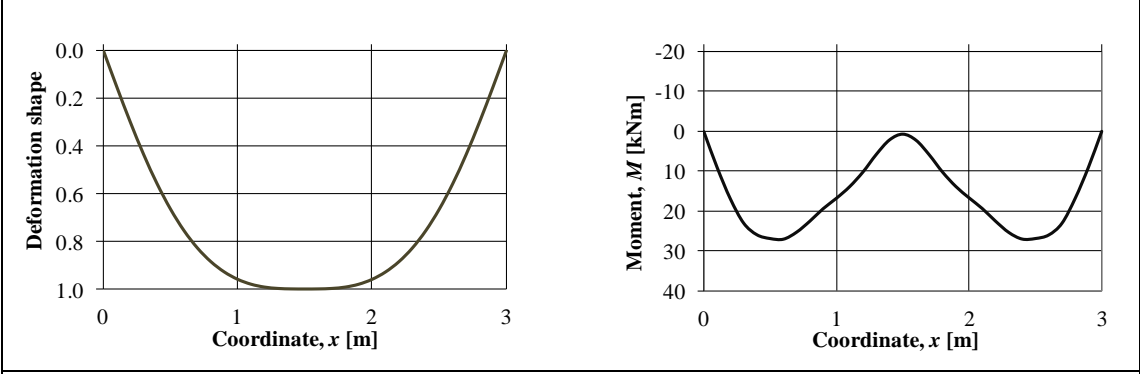


t = 6.0 ms



t = 7.0 ms

t = 8.0 ms



t = 9.0 ms



t = 10.0 ms



t = 11.0 ms

t = 12.0 ms



t = 13.0 ms
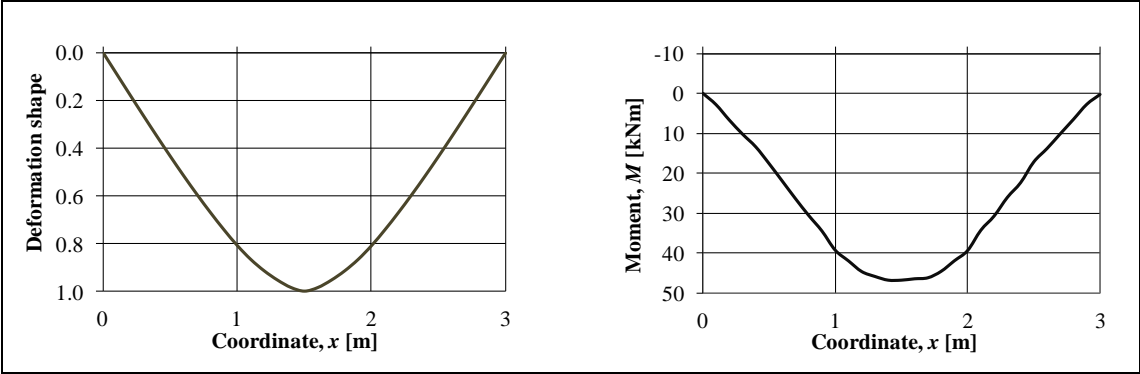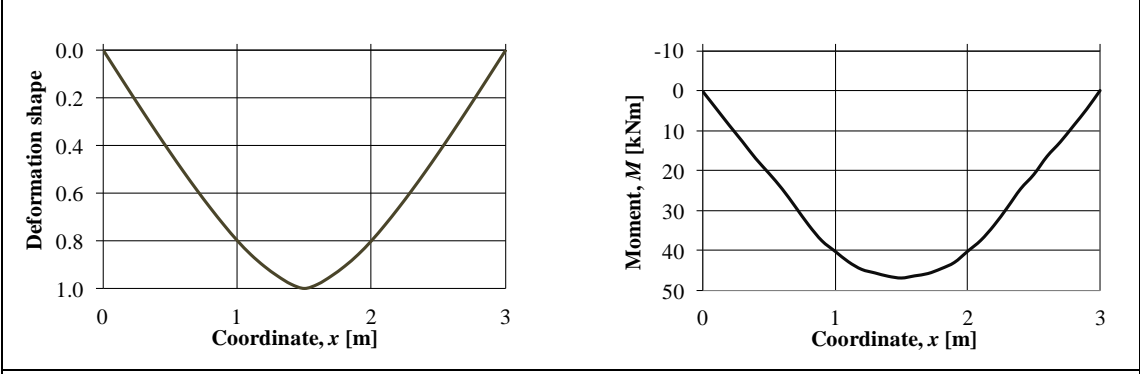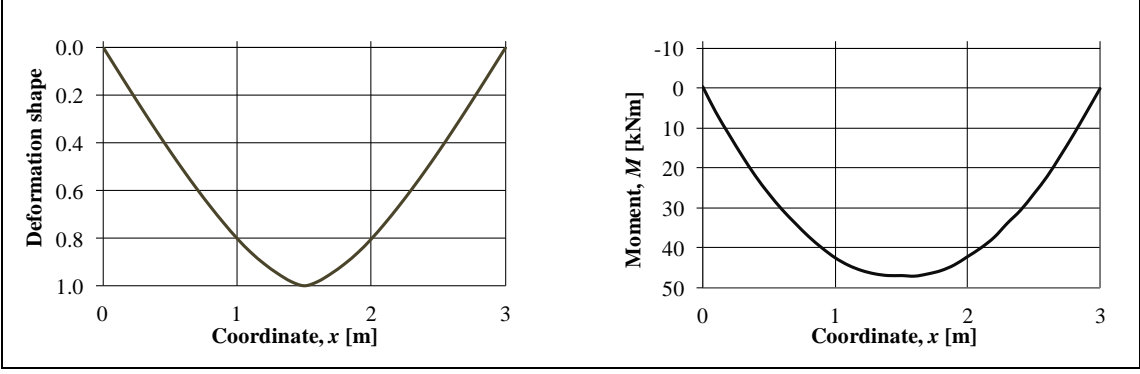


t = 14.0 ms



t = 15.0 ms

t = 20.0 ms



t = 25.0 ms



t = 30.0 ms



153
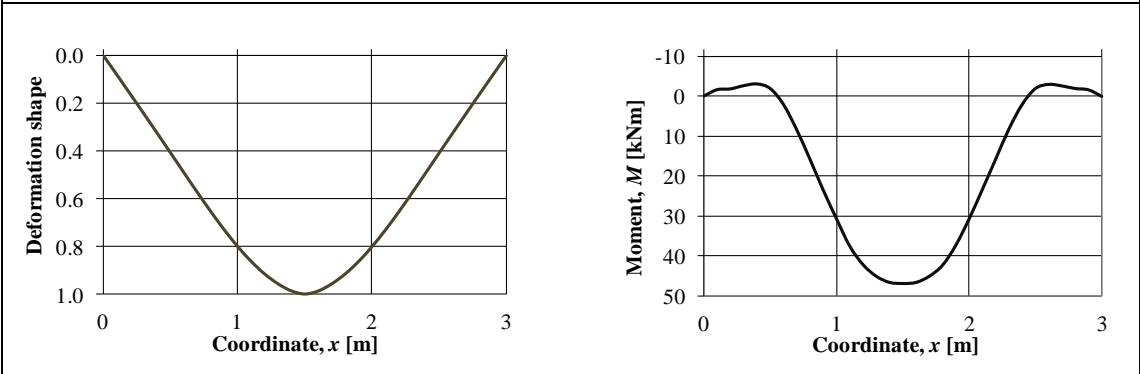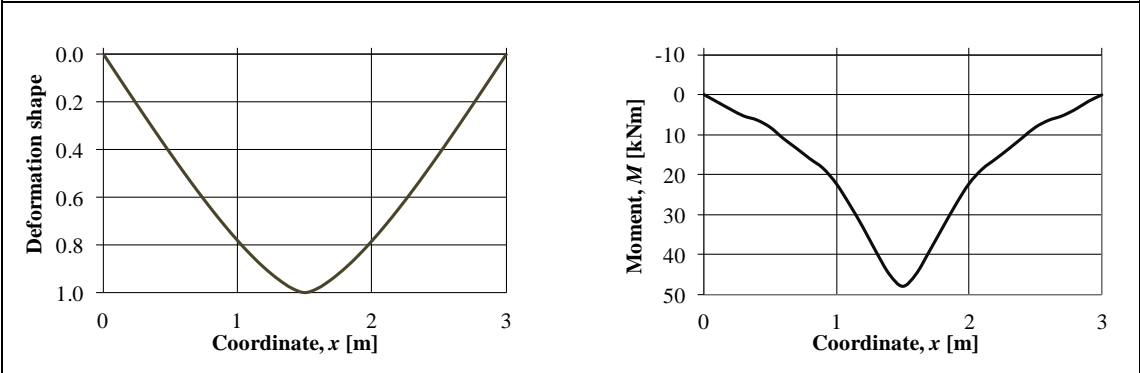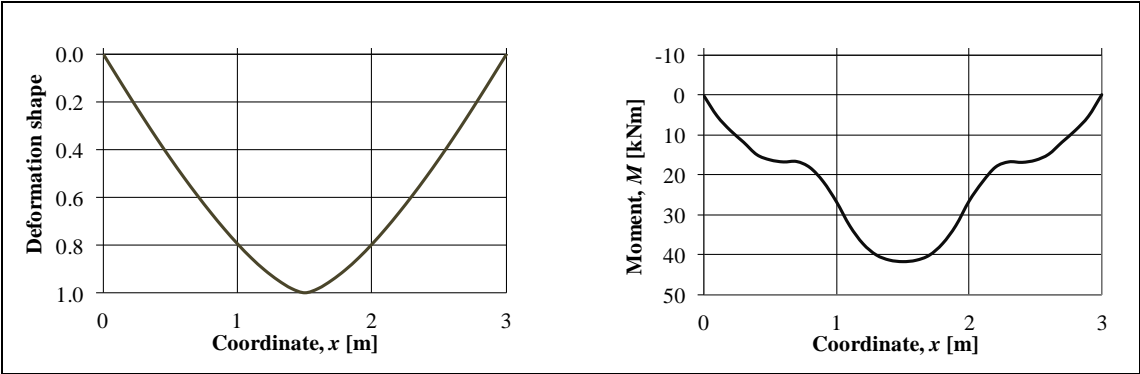
# Appendix D    Mode superposition

To solve the equation of motion for an MDOF-system, for an elastic response, matrix calculations are used. These calculations often become heavy and cumbersome for complex systems. If the damping is neglected it is possible, by using the free vibration mode shapes, to uncouple the equations and solve them separately. This is done by insertion of so called modal coordinates. The exact solution to the original equation is given when all equations are added together, but if a faster solution is wanted it is possible to create an approximation of the solution by only using some modes. For many systems it is often sufficient to include only the first few modes, and still attain a good approximation. Each equation can be solved as an SDOF-system of its own and thereby an $n$-DOF-system will have $n$ natural frequencies and $n$ corresponding mode shapes.

The undamped free vibration of motion is written as

$$\mathbf{m}\ddot{\mathbf{u}}(t) + \mathbf{k}\mathbf{u}(t) = \mathbf{p}(t) \tag{D.1}$$

To solve this equation we insert modal coordinates, $q$, such as

$$u(t) = \phi_1 q_1(t) + \phi_2 q_2(t) + \dots + \phi_n q_n(t) \tag{D.2}$$

where $\phi_i$ are modal vectors describing the shape of mode $i$ and Equation (D.2) is called a modal expansion of $u$. For all modes, the vector $\boldsymbol{u}$ can then be written as

$$\mathbf{u} = \mathbf{\Phi}\mathbf{q} \tag{D.3}$$

where

$$\mathbf{\Phi} = (\phi_1 \ \phi_2 \ \dots \ \phi_n) \tag{D.4}$$

$$\mathbf{q} = (q_1 \ q_2 \ \dots q_n) \tag{D.5}$$

Since $\ddot{u}$ is the second derivative of $u$, the vector $\ddot{\boldsymbol{u}}$ can be written as

$$\ddot{u}(t) = \phi_1 \ddot{q}_1(t) + \phi_2 \ddot{q}_2(t) + \dots + \phi_n \ddot{q}_n(t) \tag{D.6}$$

or in matrix form

$$\ddot{\mathbf{u}} = \mathbf{\Phi}\ddot{\mathbf{q}} \tag{D.7}$$

Insertion of Equation (D.3) and Equation (D.7) in (D.1) gives

$$\mathbf{m}\mathbf{\Phi}\ddot{\mathbf{q}}(t) + \mathbf{k}\mathbf{\Phi}q(t) = \mathbf{p}(t) \tag{D.8}$$

Premultiply with the mode shapes $\Phi^T$ gives

$$\mathbf{\Phi}^T\mathbf{m}\mathbf{\Phi}\ddot{\mathbf{q}}(t) + \mathbf{\Phi}^T\mathbf{k}\mathbf{\Phi}q(t) = \mathbf{\Phi}^T\mathbf{p}(t) \tag{D.9}$$

Using orthogonality:

$$\phi_i^T m \phi_i = M_i \tag{D.10}$$

$$\phi_i^T k \phi_i = K_i \tag{D.11}$$

$$\phi_i^T p_i(t) = P_i(t) \tag{D.12}$$

$$\mathbf{\Phi}^T \mathbf{m} \mathbf{\Phi} = \begin{bmatrix} \phi_1^T m \phi_1 & \phi_1^T m \phi_2 & \dots & \phi_1^T m \phi_n \\ \phi_2^T m \phi_1 & \phi_2^T m \phi_2 & \dots & \phi_2^T m \phi_n \\ \vdots & \vdots & \ddots & \vdots \\ \phi_n^T m \phi_1 & \phi_n^T m \phi_2 & \cdots & \phi_n^T m \phi_n \end{bmatrix} \tag{D.13}$$

where

$$\phi_i^T m \phi_j = 0; i \neq j \tag{D.14}$$

$$\phi_i^T k \phi_j = 0; i \neq j \tag{D.15}$$

which leads to

$$\mathbf{\Phi}^T \mathbf{m} \mathbf{\Phi} = \begin{bmatrix} \phi_1^T m \phi_1 & 0 & \dots & 0 \\ 0 & \phi_2^T m \phi_2 & \dots & 0 \\ \vdots & \vdots & \ddots & \vdots \\ 0 & 0 & \cdots & \phi_n^T m \phi_n \end{bmatrix} = \begin{bmatrix} M_1 & 0 & \dots & 0 \\ 0 & M_2 & \dots & 0 \\ \vdots & \vdots & \ddots & \vdots \\ 0 & 0 & \dots & M_n \end{bmatrix} \tag{D.16}$$

and so

$$\mathbf{\Phi}^T \mathbf{k} \mathbf{\Phi} = \begin{bmatrix} \phi_1^T k \phi_1 & 0 & \dots & 0 \\ 0 & \phi_2^T k \phi_2 & \dots & 0 \\ \vdots & \vdots & \ddots & \vdots \\ 0 & 0 & \cdots & \phi_n^T k \phi_n \end{bmatrix} = \begin{bmatrix} K_1 & 0 & \dots & 0 \\ 0 & K_2 & \dots & 0 \\ \vdots & \vdots & \ddots & \vdots \\ 0 & 0 & \dots & K_n \end{bmatrix} \tag{D.17}$$

The equation of motion is now uncoupled and known as the modal equations

$$\begin{bmatrix} M_1 & 0 & \dots & 0 \\ 0 & M_2 & \dots & 0 \\ \vdots & \vdots & \ddots & \vdots \\ 0 & 0 & \dots & M_n \end{bmatrix} \begin{bmatrix} \ddot{q}_1(t) \\ \ddot{q}_2(t) \\ \vdots \\ \ddot{q}_n(t) \end{bmatrix} + \begin{bmatrix} K_1 & 0 & \dots & 0 \\ 0 & K_2 & \dots & 0 \\ \vdots & \vdots & \ddots & \vdots \\ 0 & 0 & \dots & K_n \end{bmatrix} \begin{bmatrix} q_1(t) \\ q_2(t) \\ \vdots \\ q_n(t) \end{bmatrix} = \begin{bmatrix} P_1(t) \\ P_2(t) \\ \vdots \\ P_n(t) \end{bmatrix} \tag{D.18}$$

or

$$M_i \ddot{q}_i(t) + K_i q_i(t) = P_i(t) \tag{D.19}$$

156

With the natural frequency $\omega_i$ for mode $i$ is defined as

$$\omega_i = \sqrt{\frac{K_i}{M_i}} \tag{D.20}$$

the uncoupled Equations (D.19) can be written as

$$\ddot{q}_i(t) + \omega_i^2 q_i(t) = \frac{P_i(t)}{M_i} \tag{D.21}$$

where each equation is an SDOF-system of its own, and the exact solution is given from

$$q_i = A_i \cos \omega_i t + B_i \sin \omega_i t \tag{D.22}$$

where the coefficients $A$ and $B$ are determined from the initial conditions:

$$\begin{cases} u(0) = \sum_1^n \phi_i A_i \\ \dot{u}(0) = \sum_1^n \phi_i \omega_i B_i \end{cases} \tag{D.23}$$

Generally, when damping is included in the equation of motion, it can no longer be uncoupled and instead the damping matrix can be described as a linear combination of mass and stiffness. This is called Rayleigh damping.

# Appendix E    Rayleigh damping

When designing structures for impulse loads one does not need to regard the damping, since the worst case will always be when there is no damping, but for analysis it is important to regard it in order to obtain an accurate representation of the response.

According to Chopra (2011), if the structure is assumed to consist of similar parts with similar damping properties, a so called classical damping can be adapted. Classical damping is a special case of viscous damping where a proportional damping is assumed for the system, and it is possible to apply this on the uncoupled equations of motion that allow MDOF systems to be treated as a collection of SDOF oscillators, Adhikari (2000).

If the structure is either non-linear or has non-classical damping, a damping matrix is needed. In this Master thesis, however, the damping has been regarded as classical damping, and Rayleigh and modal damping is used.

Rayleigh damping consists of both mass-proportional damping and stiffness-proportional damping and the relationship is written as

$$\mathbf{C} = \alpha \cdot \mathbf{M} + \beta \cdot \mathbf{K} \tag{E.1}$$

where $C$ is the diagonal damping matrix, $M$ is the mass matrix, $K$ is the stiffness matrix and $\alpha$ and $\beta$ are coefficients to the mass- and stiffness term, respectively. The coefficients are obtained by choosing a specific mode frequency, $\omega$, and its damping ratio, $\zeta$, which for mode $n$ is written as

$$\zeta_n = \frac{\alpha}{2}\frac{1}{\omega_n} + \frac{\beta}{2}\omega_n \tag{E.2}$$

Since Equation (E.2) has two unknowns it can only be uniquely solved by using the two damping ratios $\zeta_i$ and $\zeta_j$ for the $i$th and $j$th mode, respectively. In matrix form this is expressed as

$$\begin{bmatrix} \zeta_i \\ \zeta_j \end{bmatrix} = \frac{1}{2}\begin{bmatrix} 1/\omega_i & \omega_i \\ 1/\omega_j & \omega_j \end{bmatrix}\begin{bmatrix} \alpha \\ \beta \end{bmatrix} \tag{E.3}$$

which, if the damping ratios are assumed to be the same, leads to the two algebraic equations for solving $\alpha$ and $\beta$:

$$\alpha = \zeta\frac{2\omega_i\omega_j}{\omega_i + \omega_j} \tag{E.4}$$

$$\beta = \zeta\frac{2}{\omega_i + \omega_j} \tag{E.5}$$

As can be seen from the typical Rayleigh damping curve shown in Figure E.1, the mass term affects the damping more for lower frequencies while the stiffness term dominates the damping for higher frequencies. This results in the damping being

lower in the interval between the two chosen frequencies, and higher outside the aforementioned interval.
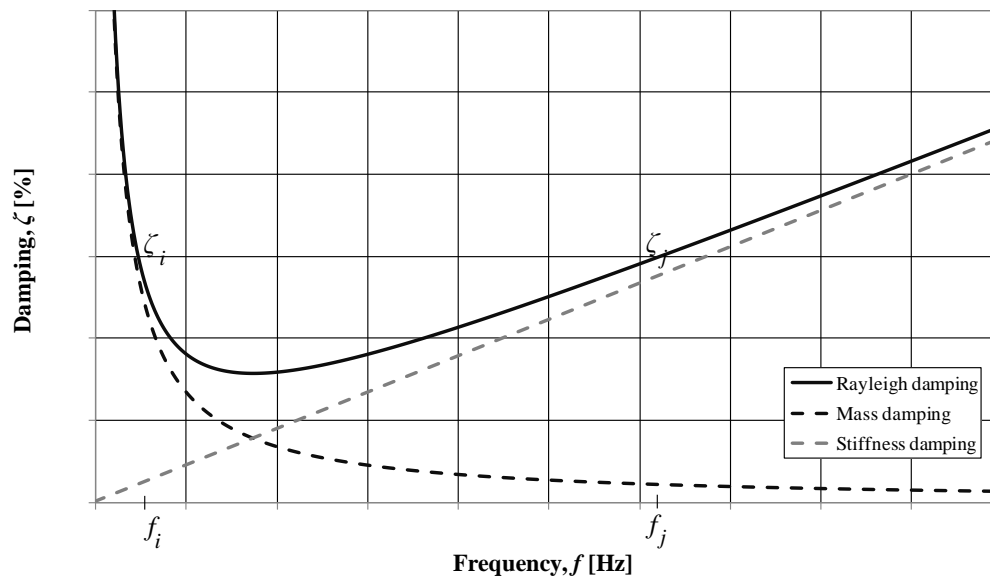


*Figure E.1.   Rayleigh damping and its contribution from mass- and stiffness-proportional damping.*

To attain the frequencies, *f*, in hertz, the angular velocity is divided by $2\pi$, as seen in Equation (E.1).

$$f = \frac{\omega}{2\pi}$$
(E.6)

# Appendix F    Mode shapes and eigenfrequencies, Beam 1

In ADINA the mode shapes seen in Figure F.1 represent the first 10 mode shapes for the simply supported beam 1 as three other modes are seen on third, seventh and ninth place. These three modes are longitudinal stretching modes that appear because one of the supports does not have a restriction in the x-direction, and they have been disregarded in this Master thesis.

| Bending modes | Eigenfrequencies |
|---|---|
| 1st mode | 10.84 Hz |
| 2nd mode | 43.11 Hz |
| 3rd mode | 96.14 Hz |
| 4th mode | 168.8 Hz |
| 5th mode | 259.8 Hz |
| 6th mode | 367.4 Hz |
| 7th mode | 490.0 Hz |
| Longitudinal stretching mode (in ADINA) | 89.79 Hz, 269.6, Hz, 450.2 Hz |
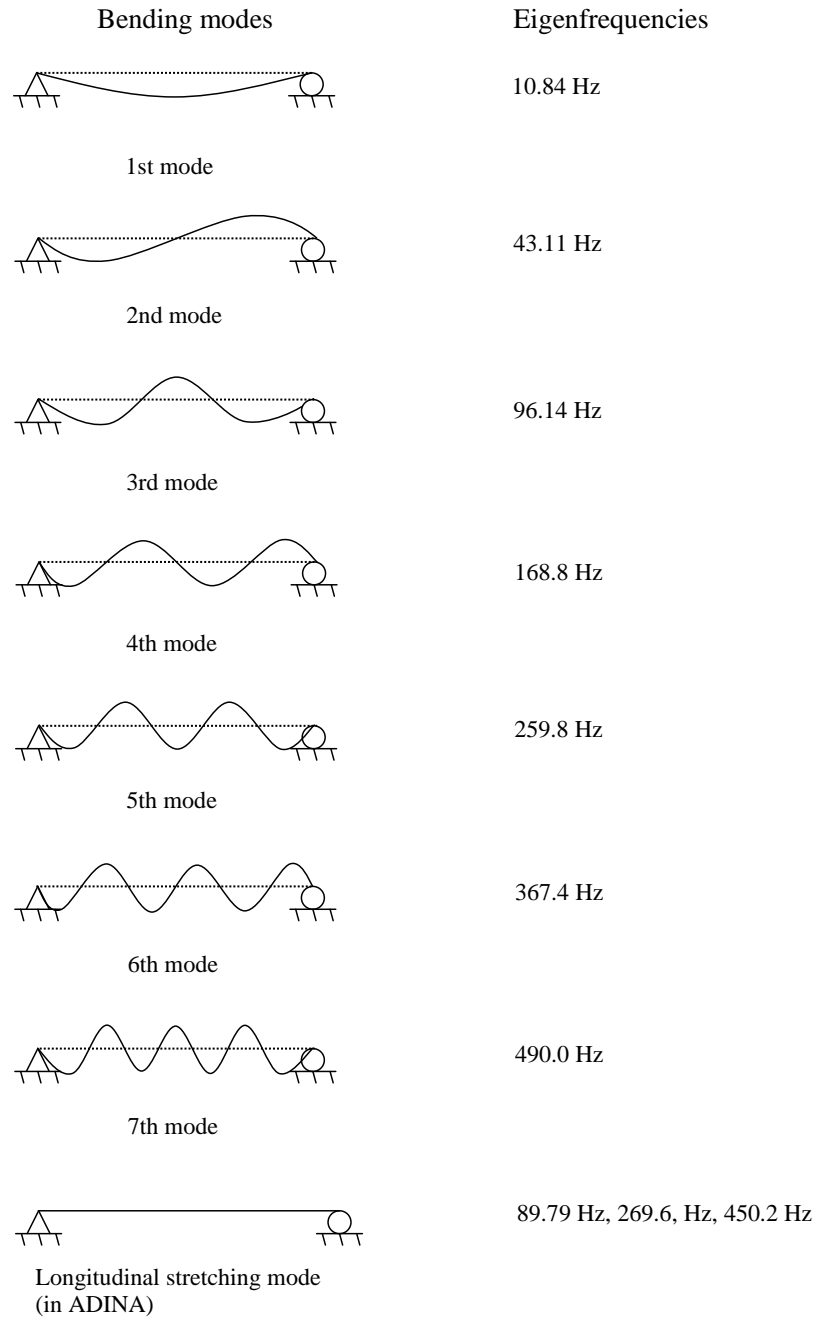
*Figure F.1.    First seven mode shapes and a longitudinal stretching mode and their eigenfrequencies for the simply supported beam, Beam 1, from Chapter 3.*

# Appendix G    Verification of different analyses

## G.1 SDOF-analysis versus modal-analysis with one mode

An analysis is made in order to study the similarity of the SDOF-analysis and the modal-analysis when only including one mode. This analysis has already been made for the displacement in Section 5.1 and here it is made for the moment. In theory these two analyses should give the same result. In Figure G.1 it is shown that they are very similar and they are assumed to give the same result. Because of this, where modal-analysis with one mode is shown, the same applies to the SDOF-analysis and vice versa.
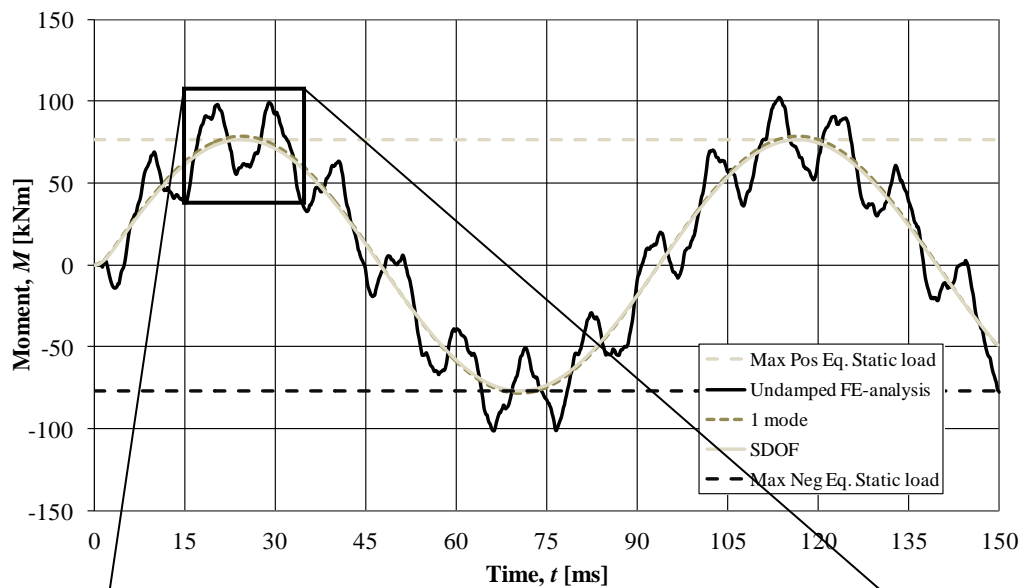


(a)
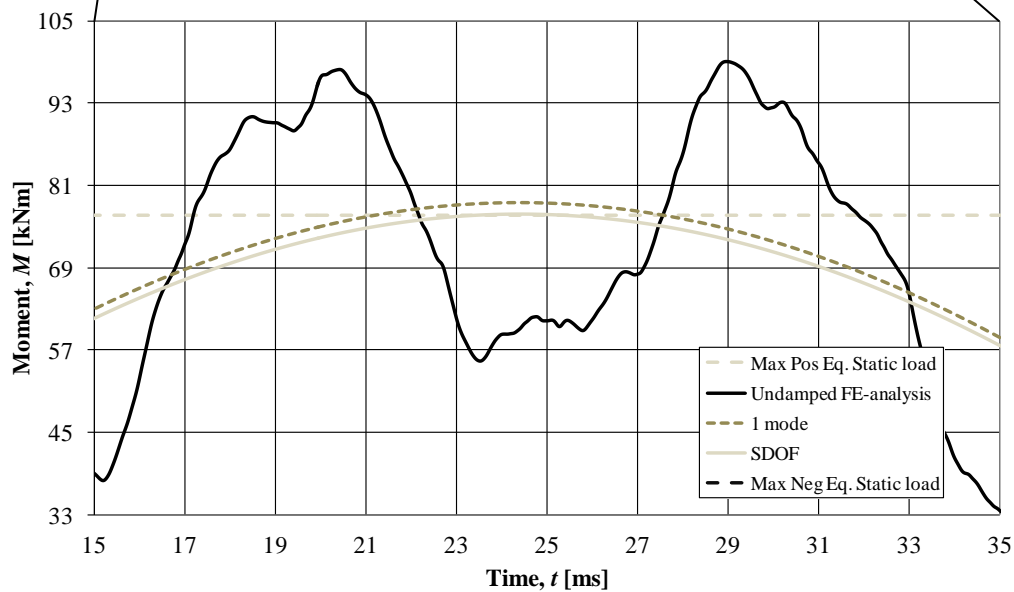
(b)

*Figure G.1.    (a) The similarity of the SDOF-analysis and the modal-analysis with one mode, when subjected to LC1, (b) zoomed in.*

## G.2 Modal-analysis with 25 modes versus FE-analysis (direct integration)

To be able to compare the number of modes required when analysing with regard to 5% modal damping a modal-analysis with 25 modes is made. This is because when analysing with modal damping the ordinary FE-analysis (direct integration) can not be used. The difference between the modal-analysis consisting of 25 modes and the FE-analysis is shown in Figure G.2, with comparison with the seven-mode-difference. When including 25 modes the results are almost identical to the FE-analysis. Hence, in this case when regarding modal damping the number of modes required is compared to a modal-analysis using 25 modes.
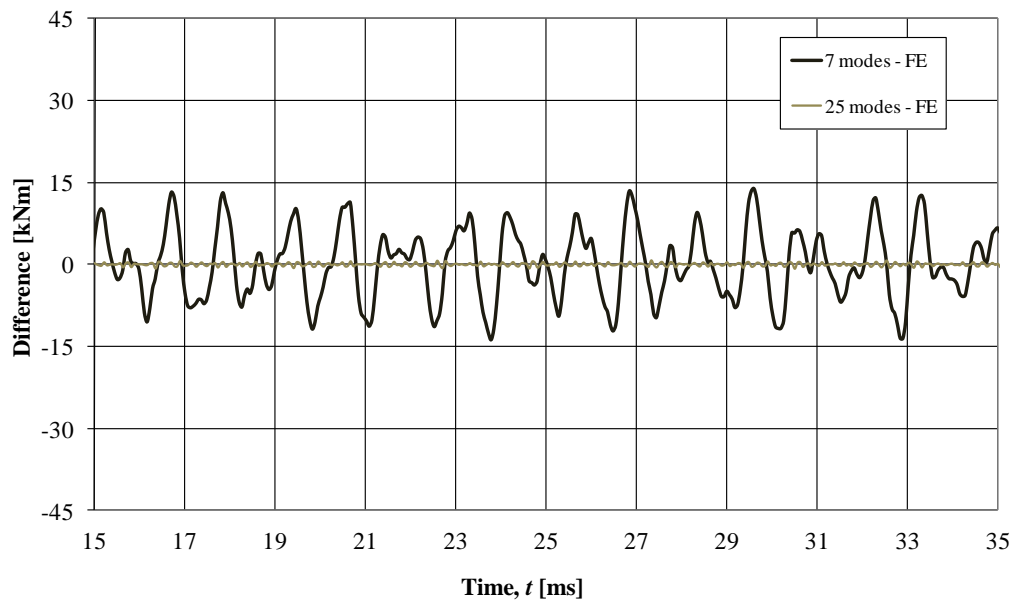


*Figure G.2. Difference between midpoint moments for modal-analysis with 7 and 25 modes and the FE-analysis when subjected to LC3.*

# Appendix H Verification of the transformation factor for damping, $\kappa_c$

In this appendix the figures are showing the response of the five different beams, simply supported, when struck by the four different load cases, uniformly distributed, in an elastic material response, hence elastic transformation factors. The damping ratio is set to 20 percent in order to make it easier to capture the damping effect. Since the plastic response is badly described by the SDOF without damping it is difficult to determine the plastic transformation factor and is not analysed. However, the elastic material response includes the FE-analysis and the SDOF-analysis when the damping term is multiplied with $\kappa_{cF}$ equals 1.0 and 0.8:

$$\kappa_{mF} m\ddot{u} + \kappa_{cF} c\dot{u} + ku = F(t) \tag{H.1}$$

where

$$\kappa_{cF} = \frac{\kappa_c}{\kappa_F} \tag{H.2}$$

When $\kappa_{cF}$ equals 0.800 the transformation factor for the damping, $\kappa_c$, equals 0.512. As mentioned earlier, Section5.3, will the exact value for the transformation factor not be determined. Further studies on the subject can be done including different boundary conditions and the plastic material response. It is also necessary to do analyses with different damping values than the high damping of 20 percent used here. It will also be interesting to compare the moment when performing those analyses.

*Table H.1.    Properties of beams 1 to 5.*

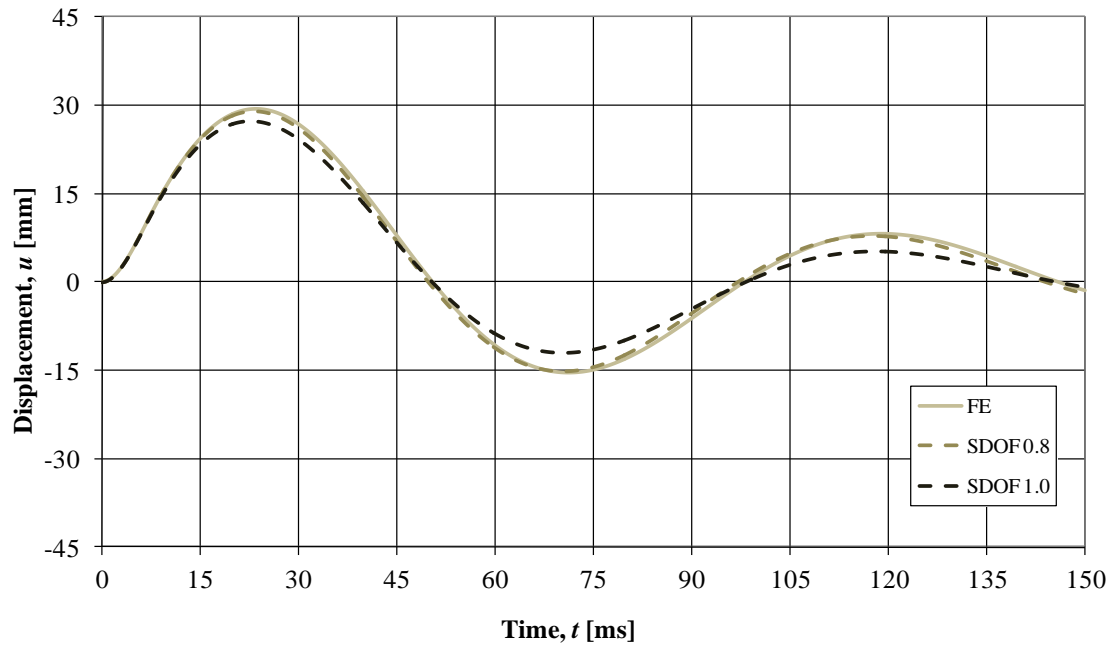| Properties | First eigenfrequency [Hz] | $E_c$ [GPa] | $\rho$ [kg/m³] |
|------------|---------------------------|-------------|----------------|
| Beam 1 | 10.8 | 33 | 2400 |
| Beam 2 | 10.7 | 40 | 3000 |
| Beam 3 | 9.2 | 20 | 2000 |
| Beam 4 | 7.7 | 33 | 4800 |
| Beam 5 | 15.3 | 66 | 2400 |

# H.1 Beam 1



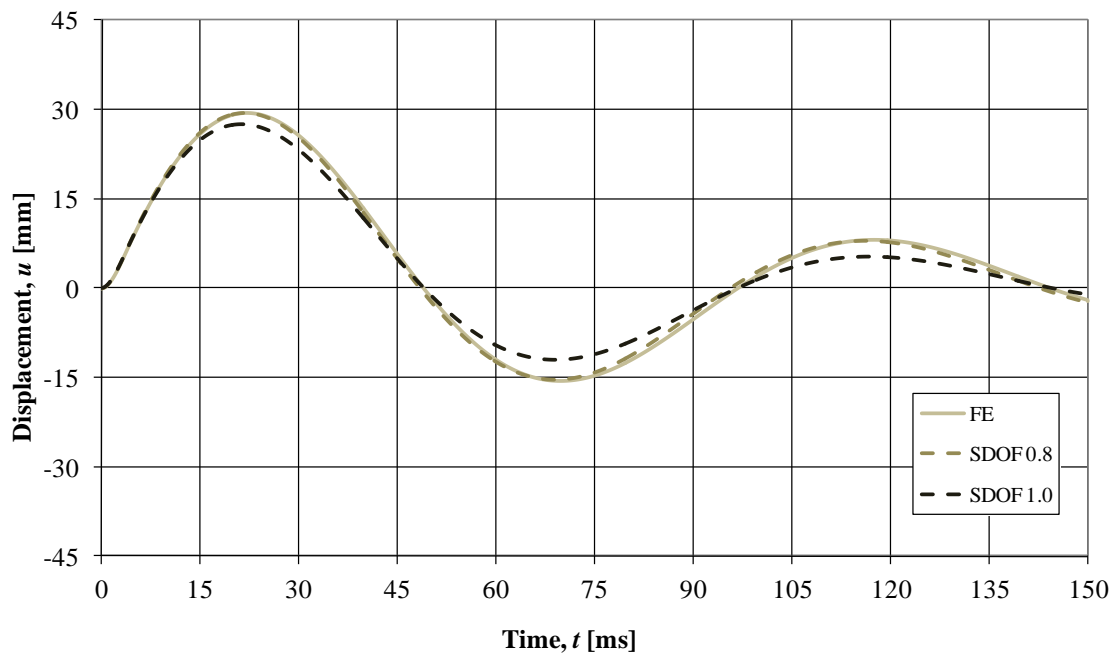*Figure H.1.  Beam 1, LC0*



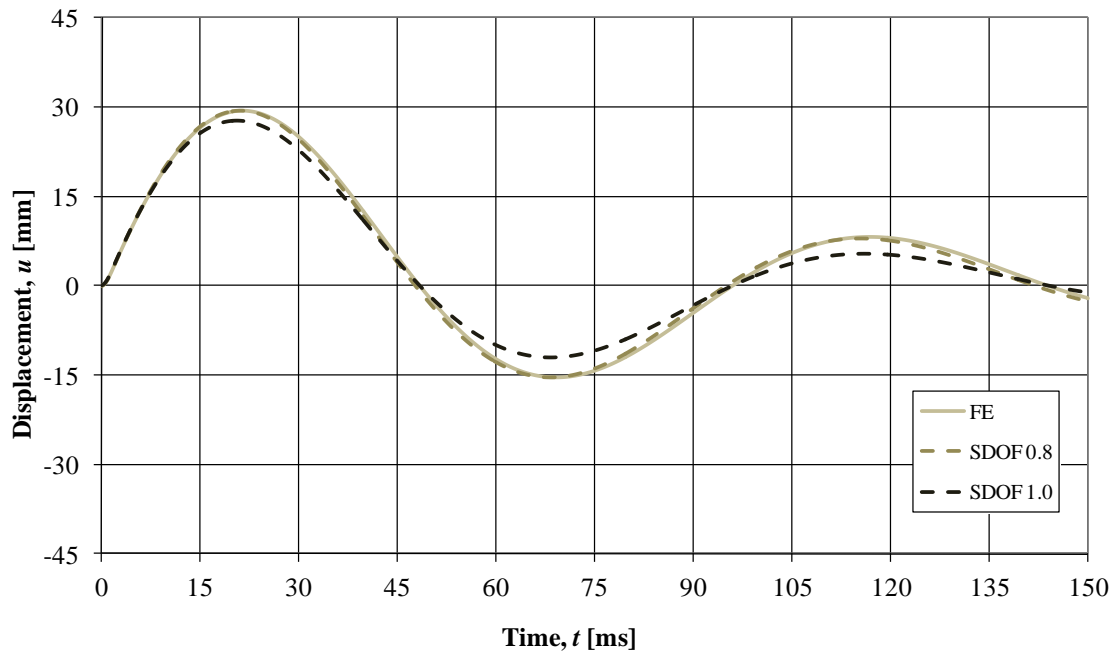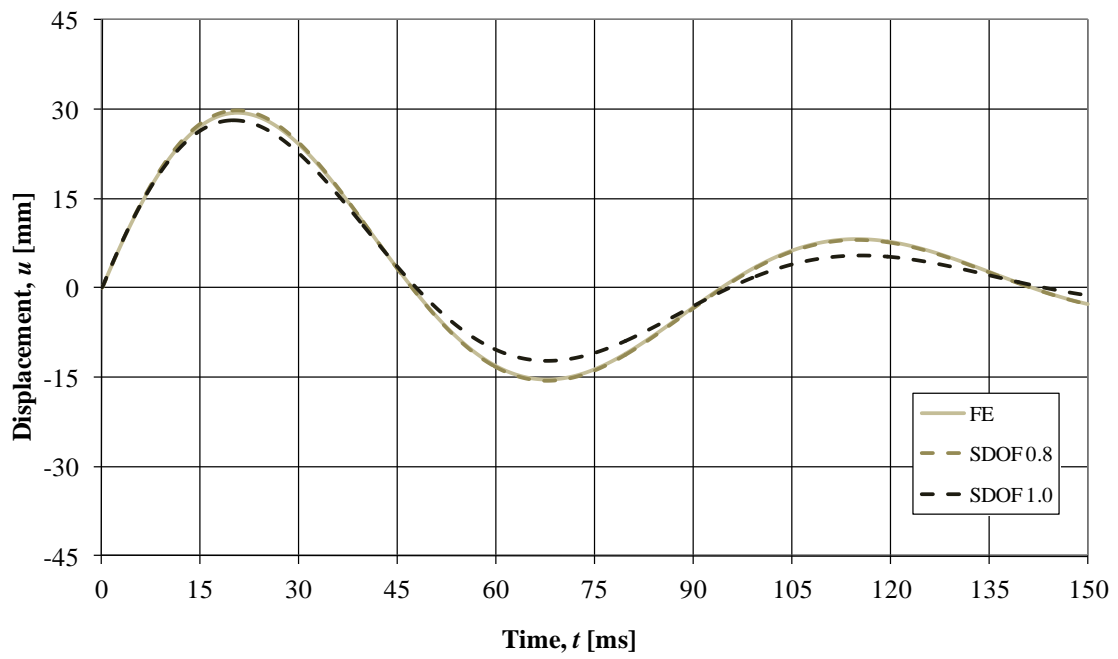*Figure H.2.  Beam 1, LC1*

*Figure H.3.   Beam 1, LC2*



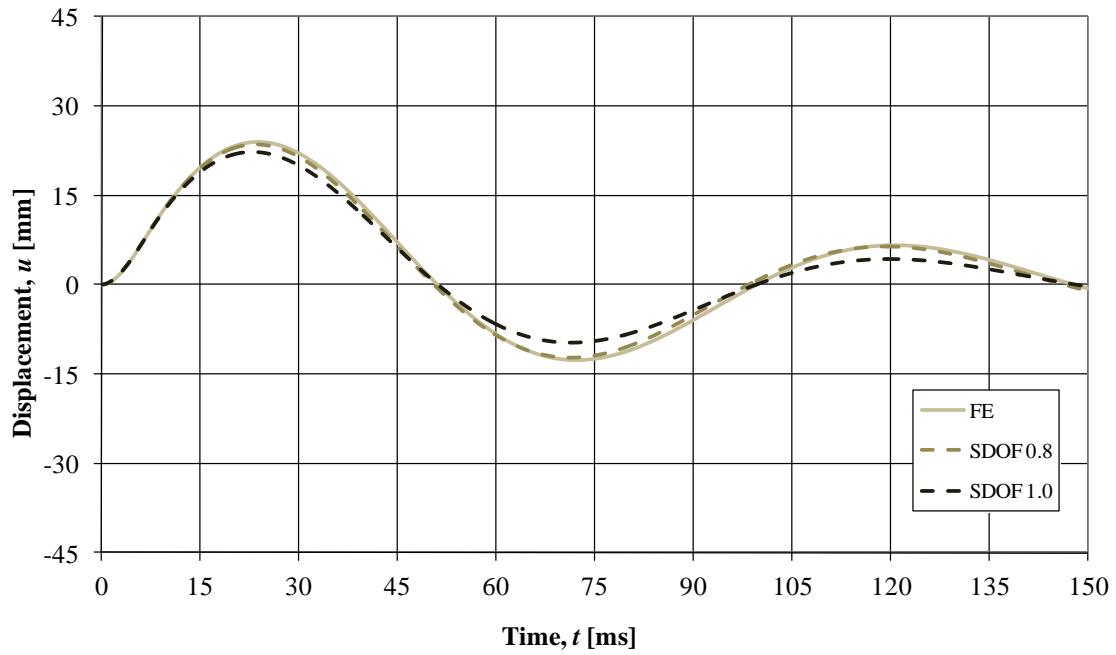*Figure H.4.   Beam 1, LC3*

167

## H.2 Beam 2
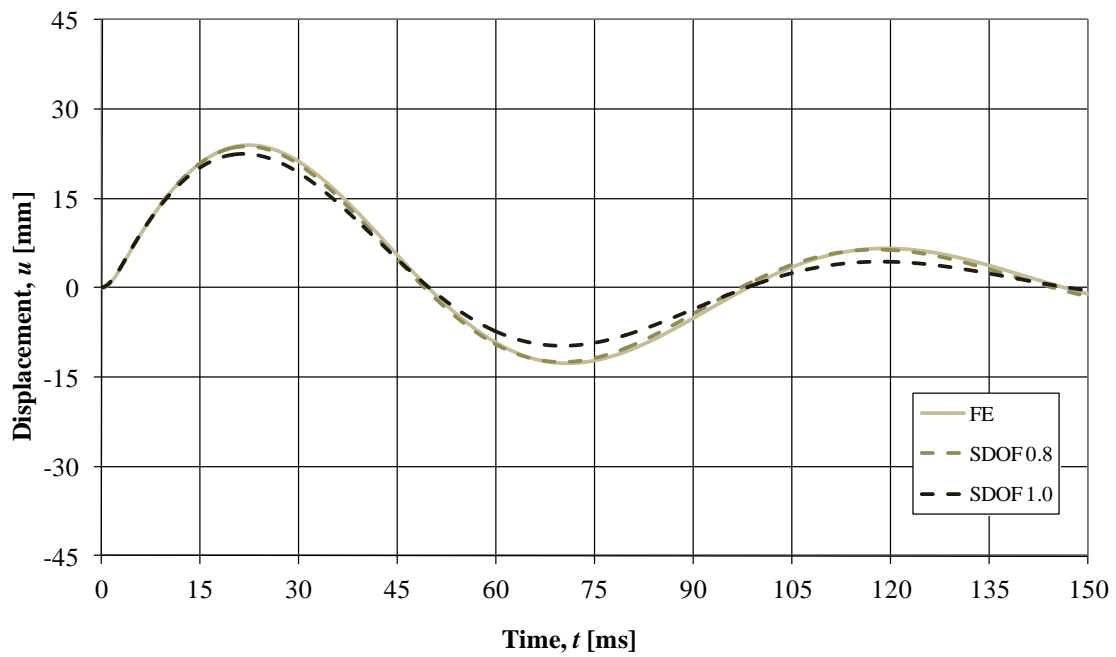


*Figure H.5.   Beam 2, LC0*
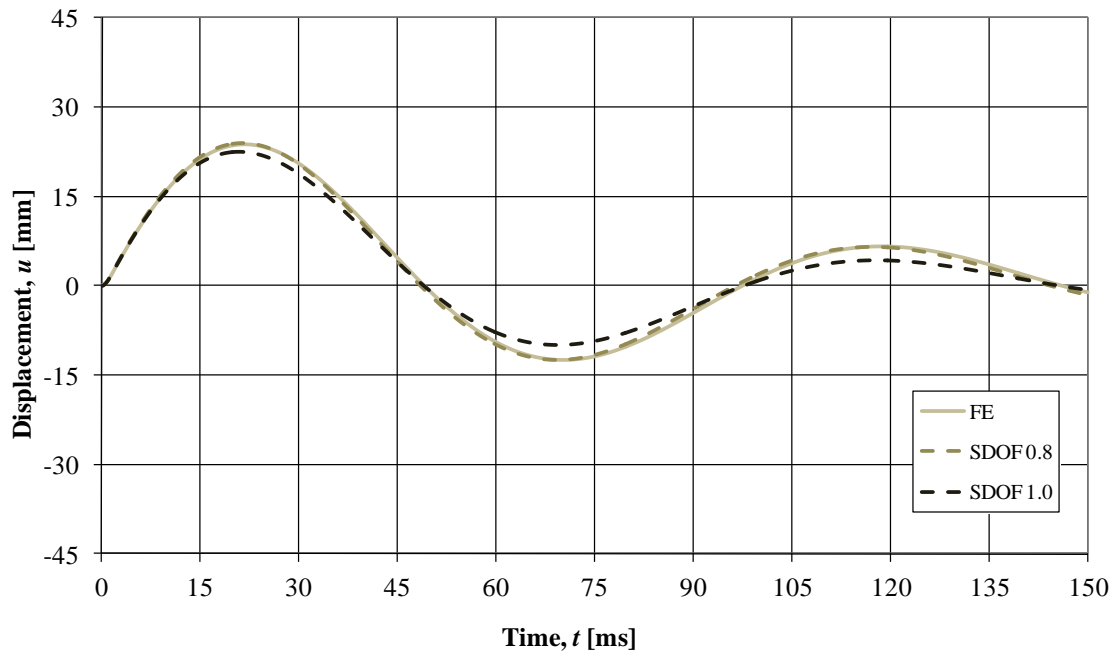


*Figure H.6.   Beam 2, LC1*
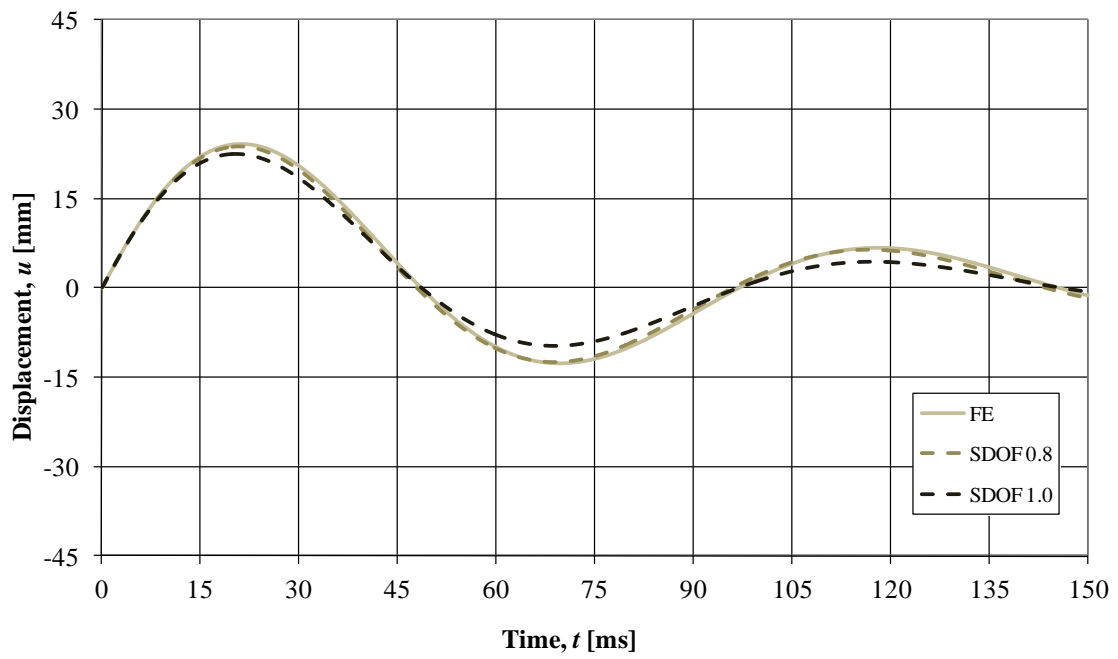
*Figure H.7.    Beam 2, LC2*



*Figure H.8.    Beam 2, LC3*

## H.3 Beam 3
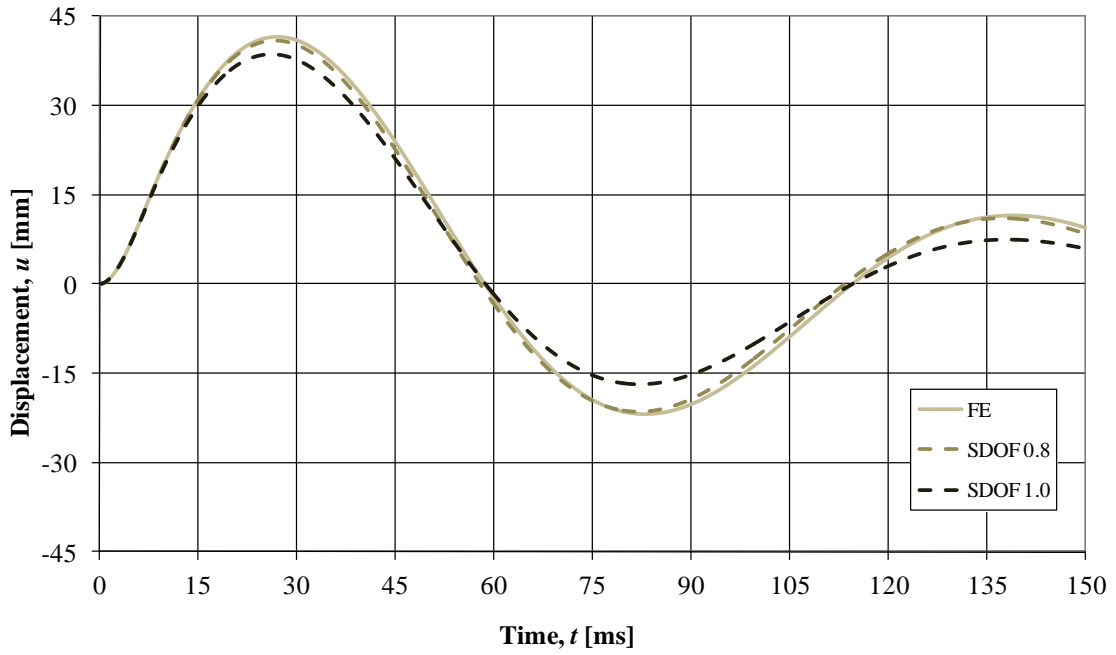


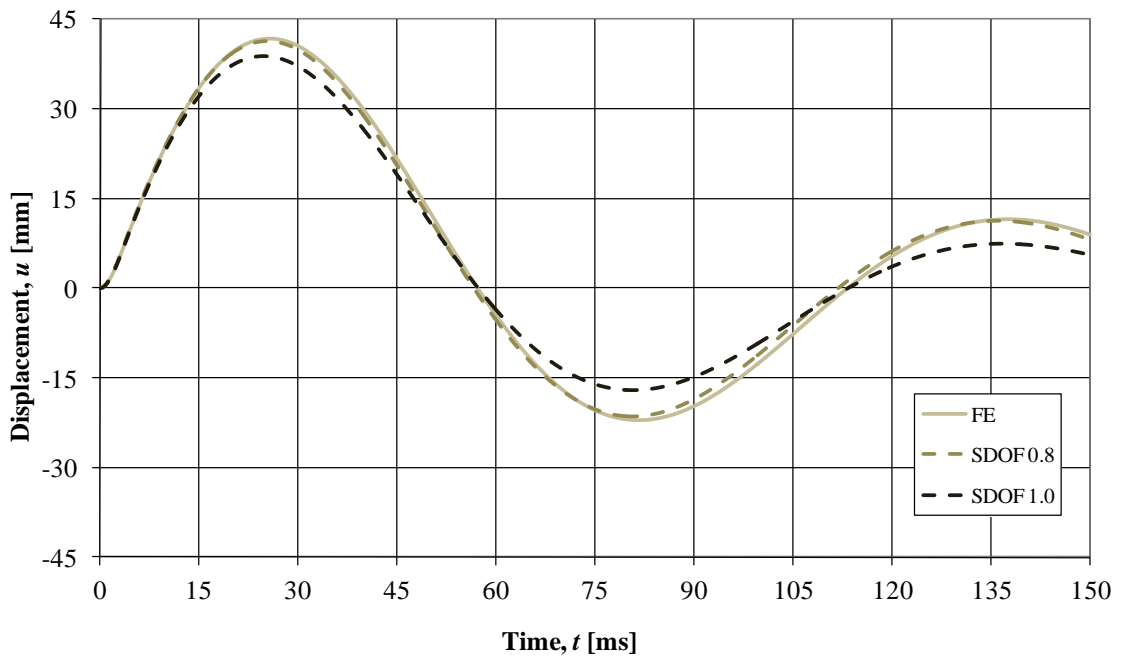Figure H.9.     Beam 3, LC0



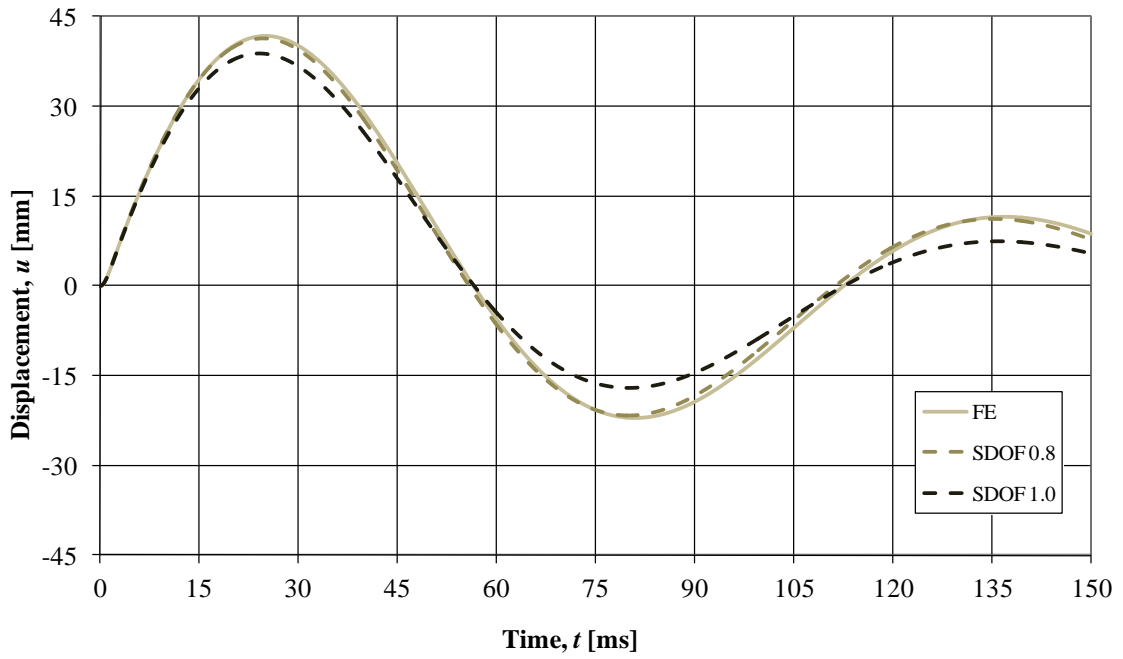Figure H.10.   Beam 3, LC1
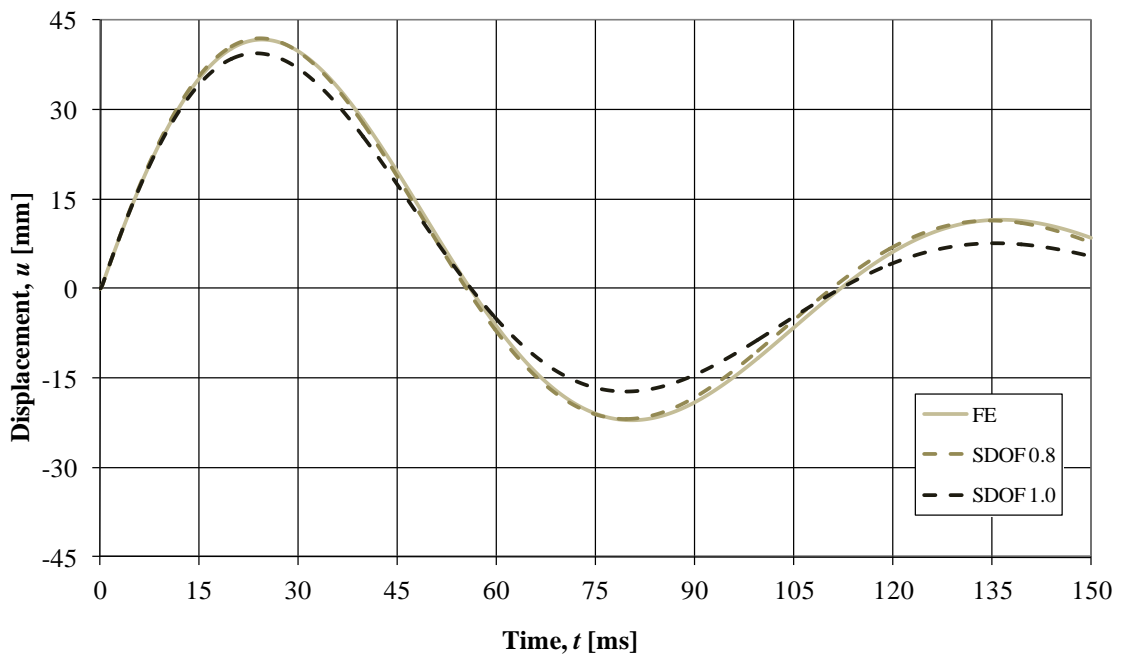
Figure H.11.    Beam 3, LC2



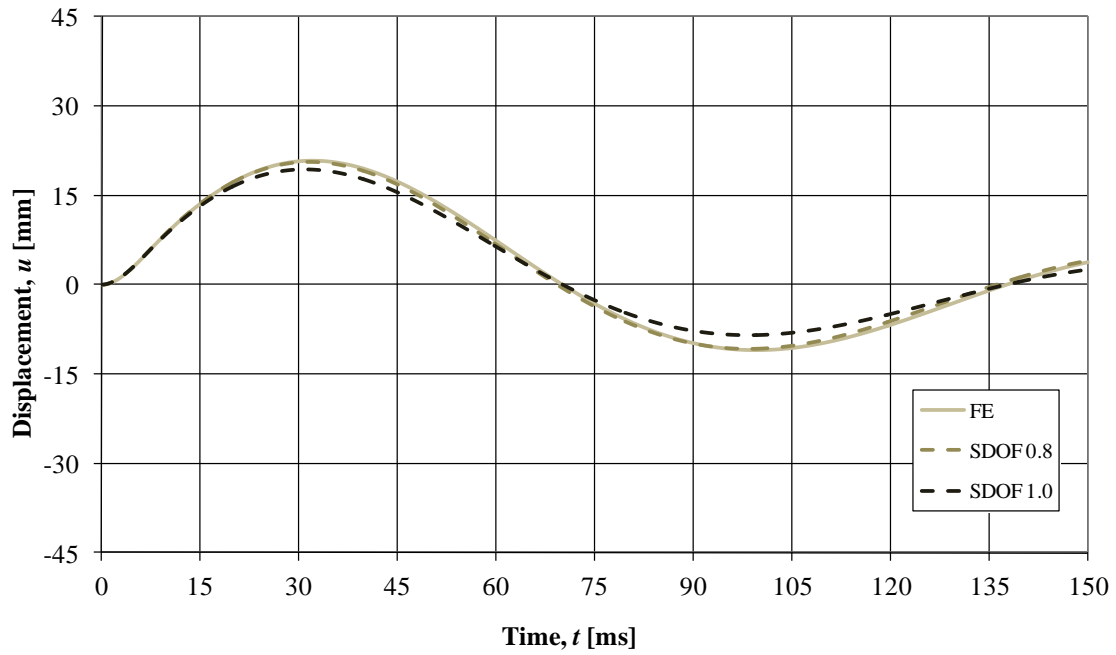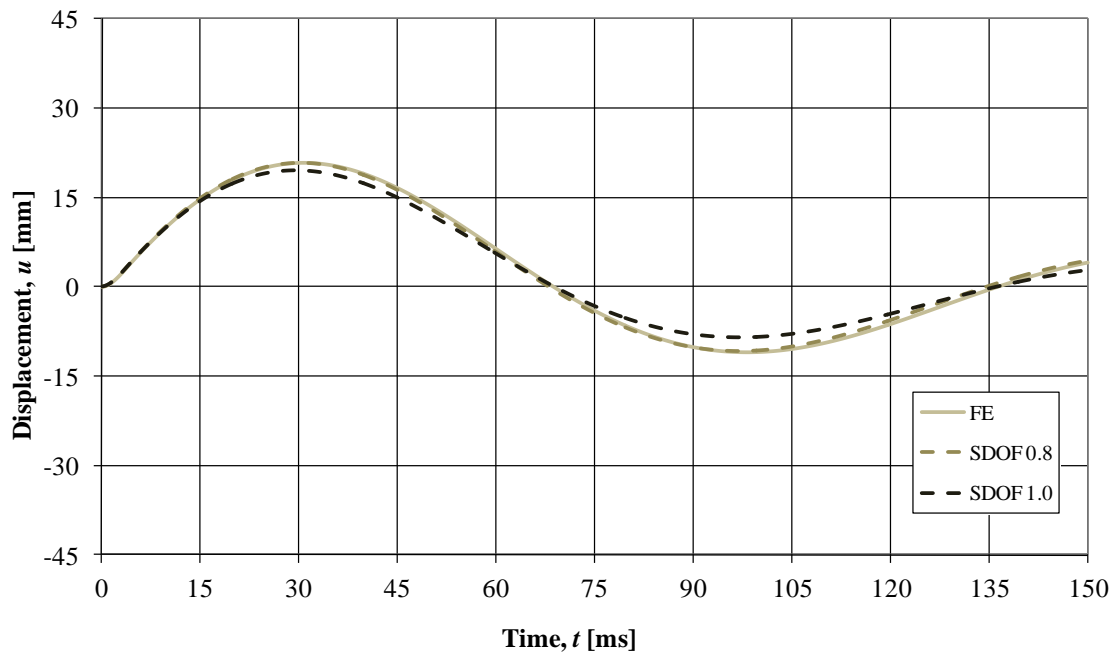Figure H.12.    Beam 3, LC3

## H.4 Beam 4



Figure H.13.   Beam 4, LC0



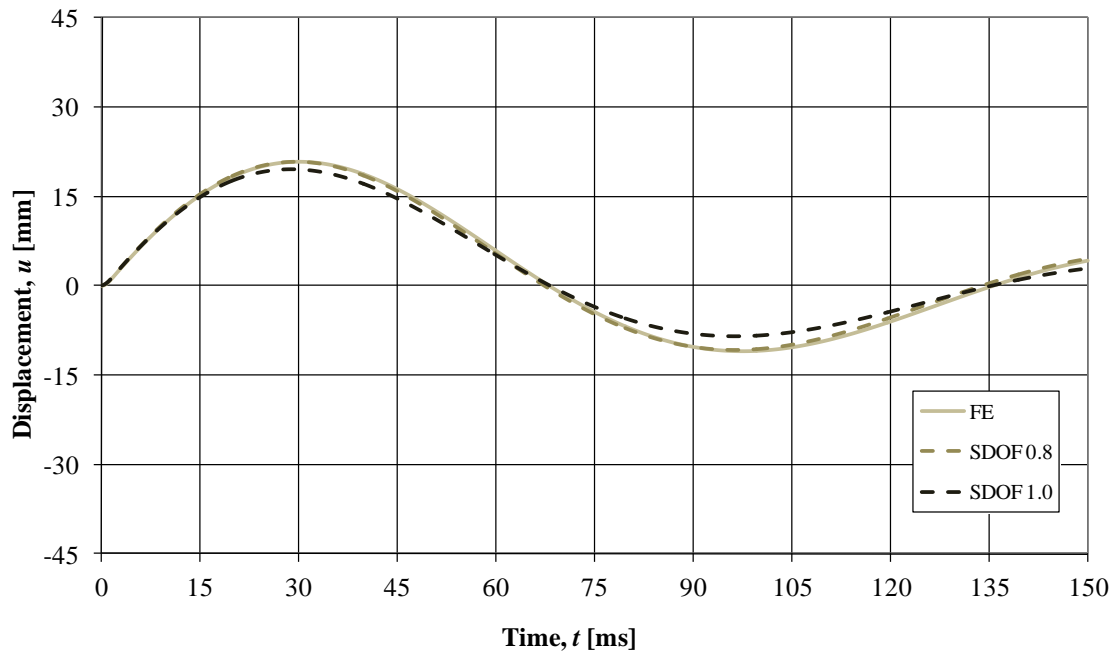Figure H.14.   Beam 4, LC1

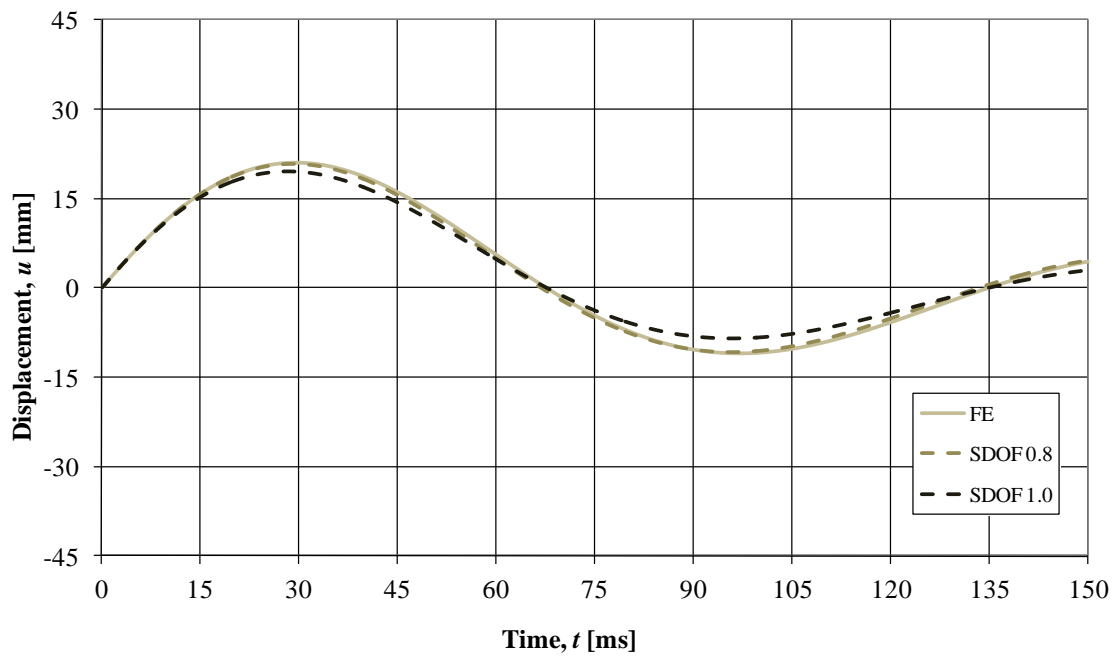*Figure H.15. Beam 4, LC2*



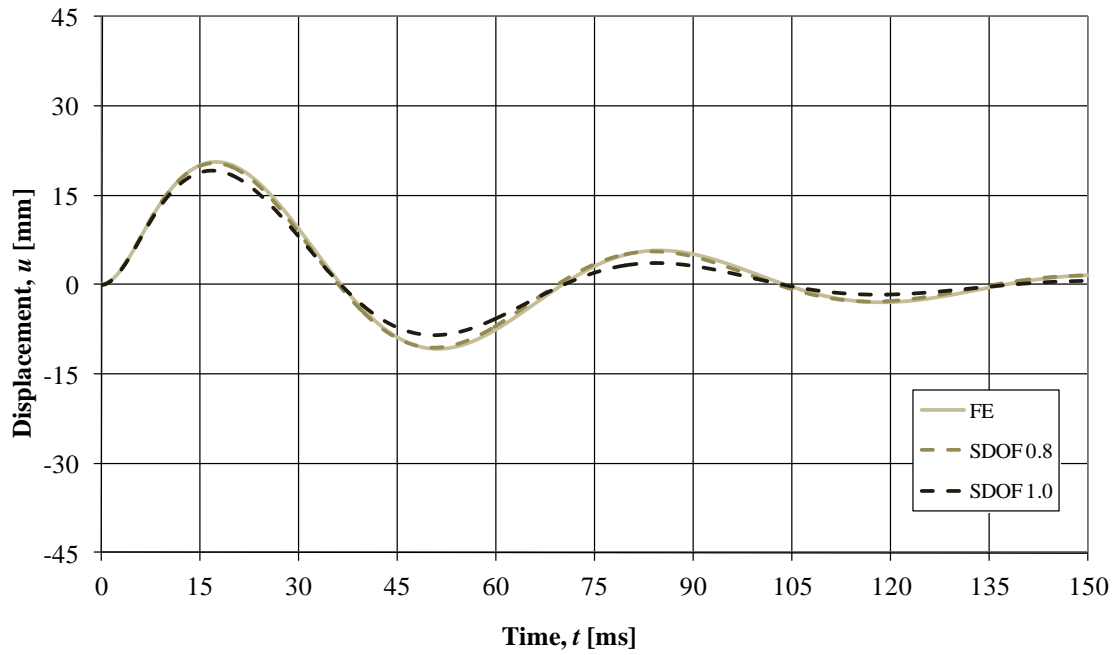*Figure H.16. Beam 4, LC3*

173

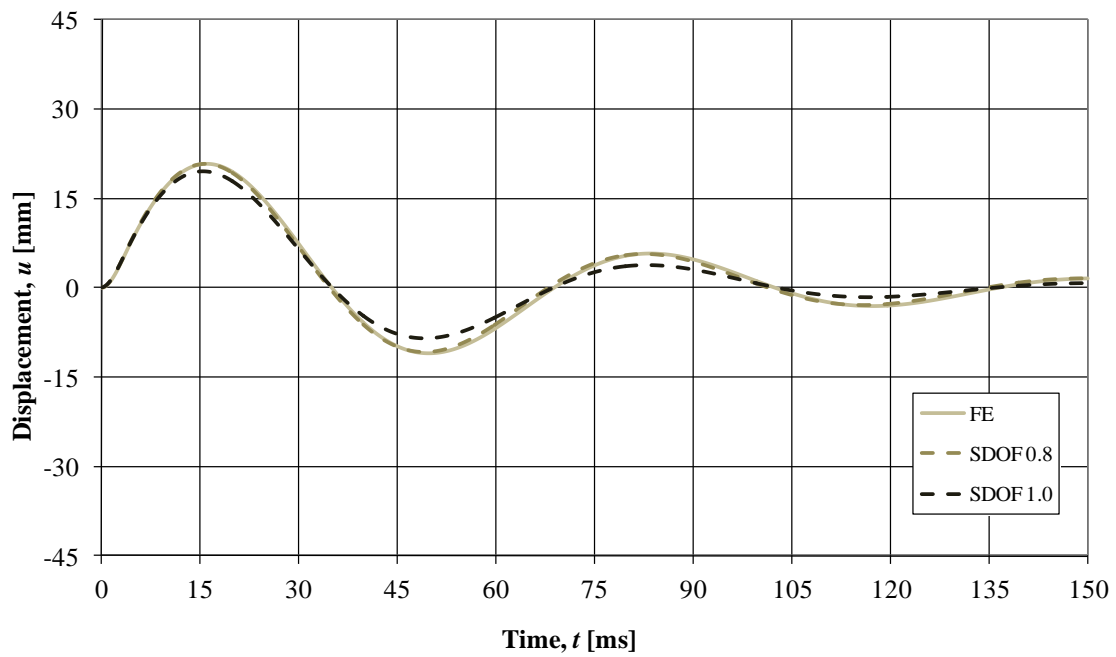## H.5 Beam 5



*Figure H.17. Beam 5, LC0*
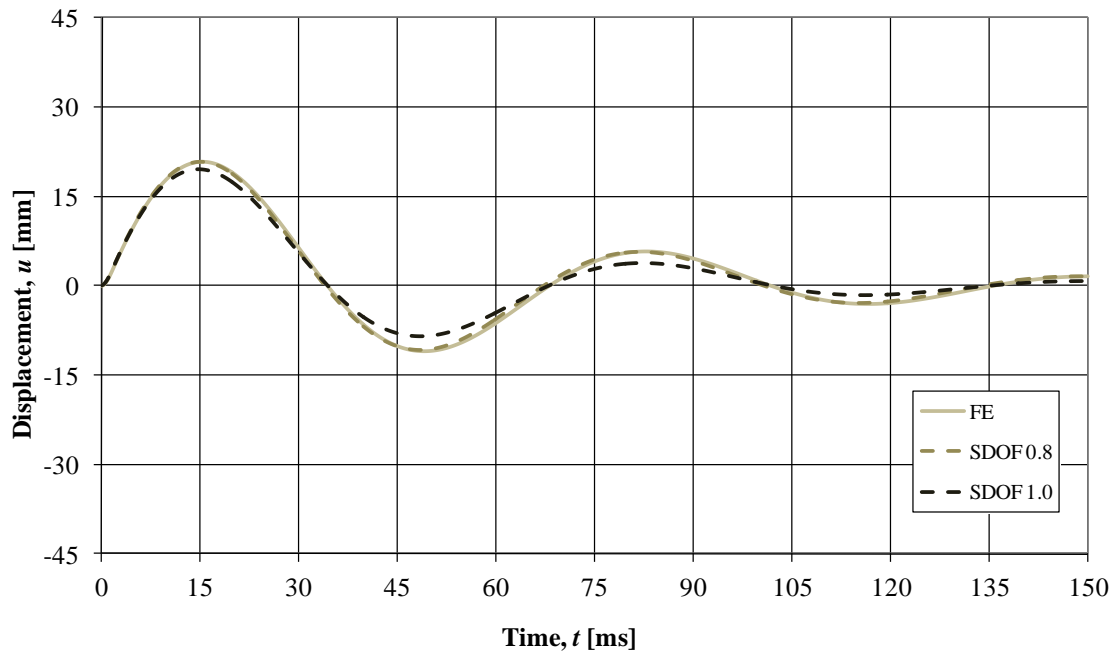


*Figure H.18. Beam 5, LC1*
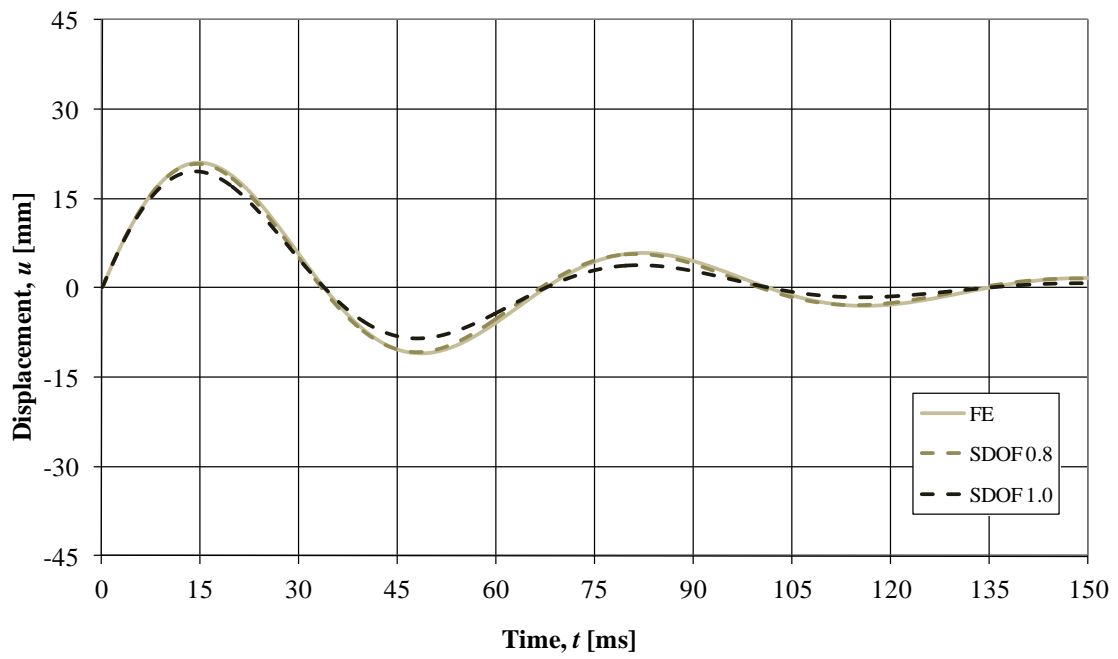
*Figure H.19. Beam 5, LC2*



*Figure H.20. Beam 5, LC3*

# Appendix I    Comparison between the SDOF-model without damping and the FE-model with damping

For design purpose is it interesting to compare the SDOF-analysis without damping with the FE-analysis, which is the modal analysis with 25 included modes, with modal damping. Then one can see how accurate the results are from a simple approximation such as the SDOF-model. In Table I.1 the comparison have been made with regard to the displacement and in Table I.2 the comparison is made with regard to moment. The different beams used can be found in Appendix H.

*Table I.1.    Comparison between the SDOF-analysis without damping and the FE-analysis when regarding 5 % damping for all beams and for LC1 and LC3 for the displacement.*

| | | SDOF [mm] | FE [mm] | Difference [%] |
|---|---|---|---|---|
| LC1 | Beam 1 | 38.8 | 35.6 | 9.1 |
| | Beam 2 | 31.5 | 29.3 | 7.7 |
| | Beam 3 | 54.6 | 50.8 | 7.6 |
| | Beam 4 | 27.5 | 25.5 | 7.6 |
| | Beam 5 | 27.4 | 25.4 | 7.9 |
| LC3 | Beam 1 | 38.9 | 35.9 | 8.4 |
| | Beam 2 | 31.6 | 29.6 | 7.0 |
| | Beam 3 | 54.8 | 51.2 | 7.0 |
| | Beam 4 | 27.5 | 25.7 | 7.0 |
| | Beam 5 | 27.5 | 25.7 | 7.0 |

*Table I.2.* *Comparison between the SDOF-analysis without damping and the FE-analysis when regarding 5 % damping for all beams and for LC1 and LC3 for the moment.*

|  |  | SDOF [kNm] | FE [kNm] | Difference [%] |
|---|---|---|---|---|
| LC1 | Beam 1 | 76.5 | 82.2 | -7.0 |
|  | Beam 2 | 75.3 | 80.0 | -5.9 |
|  | Beam 3 | 65.2 | 69.4 | -6.0 |
|  | Beam 4 | 54.1 | 57.6 | -6.1 |
|  | Beam 5 | 107.9 | 113.8 | -4.7 |
| LC3 | Beam 1 | 76.7 | 83.7 | -8.3 |
|  | Beam 2 | 75.6 | 81.4 | -7.2 |
|  | Beam 3 | 65.4 | 70.5 | -7.2 |
|  | Beam 4 | 54.3 | 58.5 | -7.2 |
|  | Beam 5 | 108.5 | 116.8 | -7.1 |

It is interesting to see that for the displacement is the SDOF-model giving values on the safe side, approximately from seven to nine percent, while for the moment the model is giving values on the unsafe side, approximately from six to eight percent lower.

# Appendix J Evaluation of the capacity of beam 1

## J.1 Beam 1 without curtailment

In order to evaluate the beam, the rotation capacity from Section 2.2.5 and Figure 2.15 is used. If the rotation capacity for the beam is known, it can be converted to a maximum midpoint displacement. This is an easy and fast way to check the capacity of the beam.
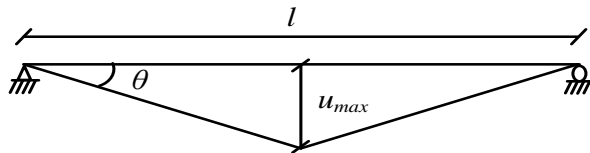


*Figure J.1.    Maximum deformation*

The following calculations are made in ultimate limit state. The upper reinforcement is taken into account as in Section 3.2.2. A new distance $d$ is used since the distance $d'$ is not taken into account in the equation. Since the upper reinforcement also is in tension the distance $d$ will equal 100 mm:

$$x/d = 26/100 = 0.26 \tag{J.1}$$

With this value the allowed plastic rotation can be determined when regarding the reinforcement, B500B which is Class B, and the concrete, C 30/37 is approximated to C 50/60.

$$\theta_{pl} = 11.0 \cdot 10^{-3} \text{ rad} \tag{J.2}$$

Now the shear slenderness, $\lambda$, needs to be determined and if it has another value than 3.0 the allowed plastic rotation will have to be multiplied with a factor. The shear slenderness is calculated as:

$$\lambda = \frac{l_0}{d} = \frac{1500}{100} = 15 \tag{J.3}$$

where $l_0$ is the length between the point of zero moment and the plastic hinge, and $d$ is the effective depth to the reinforcement.

$$k_\lambda = \sqrt{\frac{\lambda}{3}} = 2.24 \tag{J.4}$$

$$\theta_{rd} = k_\lambda \cdot \theta_{pl} = 2.24 \cdot 11.0 \cdot 10^{-3} = 24.6 \cdot 10^{-3} \text{ rad} \tag{J.5}$$

The maximum deformation can now easily be calculated:

$$u_{max} = \frac{\theta_{pl} \cdot l}{2} = \frac{24.6 \cdot 10^{-3} \cdot 3000}{2} = 37.0 \text{ mm} \tag{J.6}$$

So, the deformation capacity in the midpoint of the beam is calculated to be 37 mm. This will be compared to the displacement from the SDOF-analyses and the FE-

analysis with the elasto-plastic material response. Three SDOF-analyses were made in Section 4.1: one with elastic-, one with plastic and one with both transformation factors. The results from these were approximately 45 mm, 49 mm and 41 mm, respectively, while the FE-analysis also showed a displacement of 49 mm for the midpoint. This means that the allowed plastic rotation is exceeded by all of the analyses. Hence, the beam would probably fail if loaded with load case 1.

# J.2 Beam 1 with curtailment at L/6

When the beam is fully reinforced without curtailment the method for evaluating the capacity is pretty straight forward. However, when curtailment of the beam is a fact the method for evaluating the capacity is more difficult, and above all, uncertain.
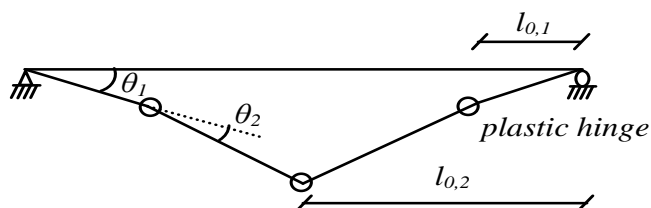


*Figure J.2.    Deformation when plastic hinges have developed.*

One way of determining if the plastic strain in the curtailment point is of concern is to compare it with the strain in the midpoint with regard to the rotation capacity.
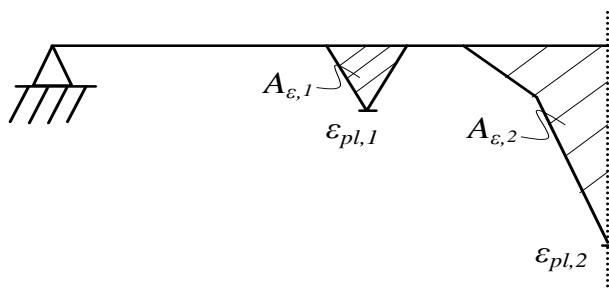


*Figure J.3.    Schematic figure of the plastic strains for half the beam.*

If the smaller plastic strain is of no concern the following statement should apply:

$$\frac{A_{\varepsilon,1}}{A_{\varepsilon,2}} \leq \frac{\theta_{rd,1}}{\theta_{rd,2}}$$

(J.7)

In order to determine this, the allowed plastic rotation capacity for $\theta_{rd,1}$ needs to be calculated. First, the compression zone is calculated. This is done in line with Section 3.2.2, but now only with the curtailment taken into account:

$$x = \frac{A_s'\sigma_s' + A_s\sigma_s}{0.8 \cdot f_{ccd}} = \frac{25 \cdot \dfrac{\pi}{0.15} \cdot 500 + 25 \cdot \dfrac{\pi}{0.30} \cdot 500}{0.8 \cdot \dfrac{30}{1.2} \cdot 10^6} = 19.6 \, \text{mm}$$

(J.8)

Now, the allowed plastic rotation can be determined with use of Figure 2.15. The distance $d$ is set to 100 mm:

$$x/d = 19.6/100 = 0.196 \tag{J.9}$$

which leads to:

$$\theta_{pl,1} = 12.5 \cdot 10^{-3} \text{ rad} \tag{J.10}$$

Same as for the beam without curtailment, the shear slenderness $\lambda$, scaling factor $k_\lambda$ and ultimately the new allowed rotation capacity $\theta_{rd,1}$ are calculated:

$$\lambda = \frac{l_{0,1}}{d} = \frac{500}{100} = 5 \tag{J.11}$$

where $l_{0,1}$ is the length between the point of zero moment and the plastic hinge.

$$k_\lambda = \sqrt{\frac{\lambda}{3}} = 1.29 \tag{J.12}$$

$$\theta_{rd,1} = k_\lambda \cdot \theta_{pl,1} = 1.29 \cdot 12.5 \cdot 10^{-3} = 16.1 \cdot 10^{-3} \text{ rad} \tag{J.13}$$

The allowed plastic rotation for $\theta_{rd,2}$ is already calculated for the beam without curtailment in Section J.1:

$$\theta_{rd,2} = 24.6 \cdot 10^{-3} \text{ rad} \tag{J.14}$$

The following step is to determine the areas of the plastic strains with regard to load case 1 from Figure J.4.
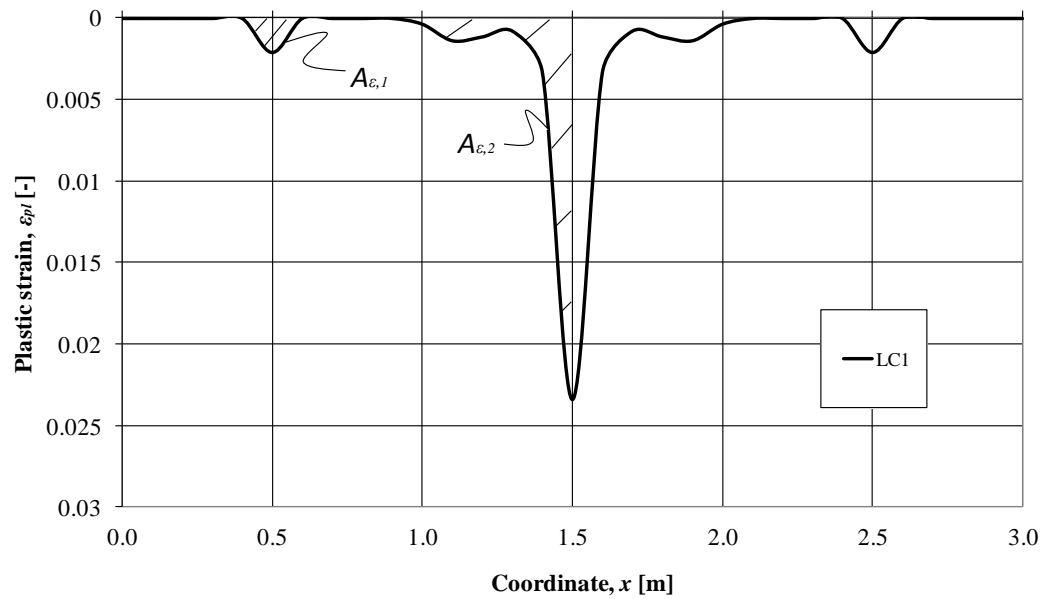


*Figure J.4.    Plastic strain for the beam with curtailment of L/6 from the ends.*

$$A_{\varepsilon,1} = \frac{0.0020 \cdot 0.2}{2} = 2.0 \cdot 10^{-4} \tag{J.15}$$

$$A_{\varepsilon,2} = \frac{0.023 \cdot 0.1}{2} + \frac{0.002 \cdot 0.4}{2} = 15.5 \cdot 10^{-4} \tag{J.16}$$

Now Equation (J.7) can be checked:

$$\frac{2.0 \cdot 10^{-4}}{15.5 \cdot 10^{-4}} = 0.129 \leq \frac{16.1 \cdot 10^{-3}}{24.6 \cdot 10^{-3}} = 0.654 \tag{J.17}$$

Consequently, it is approximately a factor 5 between, which indicates that the strain at the curtailment point is not critical.

Another way to evaluate the capacity is to convert the allowed rotation capacity into an allowed plastic strain. This can be done when assuming different forms and distribution of the plastic strain. If one assumption is on the safe side and the other on the unsafe side, the allowed plastic strain can be narrowed down to an interval. With use of Figure J.5 and Equations (J.18) to (J.20) the interval is calculated.
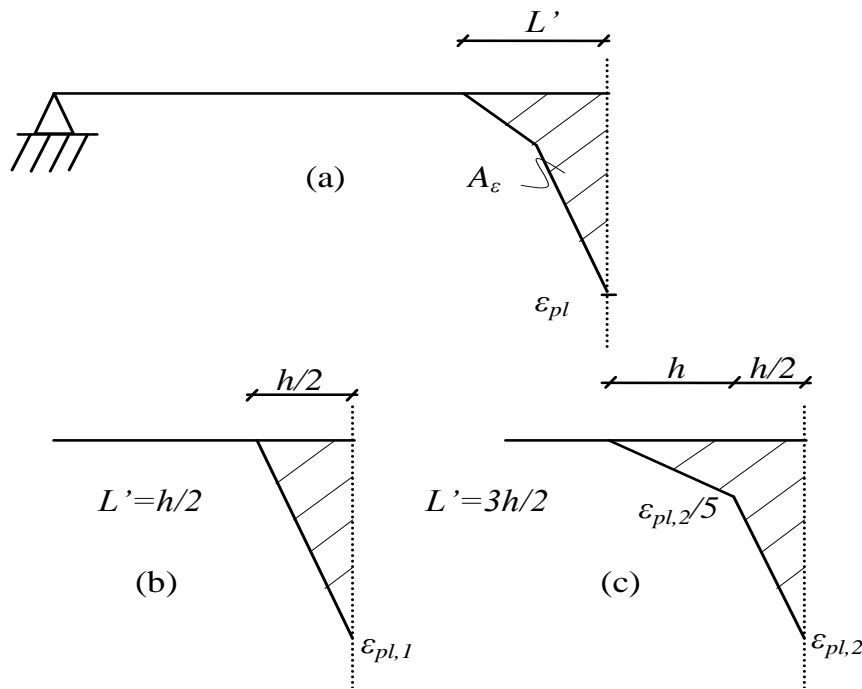


*Figure J.5.* *Schematic figure of the plastic strains for half the beam where (a) is the real strain, (b) strain limit for failure on the unsafe side and (c) strain limit for failure on the safe side.*

$$A_{\varepsilon} = \alpha \cdot L' \cdot \varepsilon_{pl} \tag{J.18}$$

where $\alpha$ is a factor depending on the form and distribution.

$$\theta = \frac{2}{h} A_{\varepsilon} \tag{J.19}$$

$$\varepsilon_{pl,1} = \frac{\theta \cdot h}{2 \cdot \alpha \cdot L'} \tag{J.20}$$

For the simple case of Figure J.5 (b) the $\alpha$-factor is 0.5 and the equation for the limit of plastic strain before failure for a calculation on the unsafe side is:

$$\varepsilon_{pl,1} = \frac{\theta_{rd} \cdot h}{2 \cdot 0.5 \cdot \dfrac{h}{2}} = 2 \cdot \theta_{rd} = 2 \cdot 24.6 \cdot 10^{-3} = 4.9\% \tag{J.21}$$

For the case on the safe side the $\alpha$-factor is more difficult to determine so the area is calculated with use of Figure J.5 (c):

$$A_{\varepsilon 2} = \frac{\left( h \cdot \dfrac{\varepsilon_{pl,2}}{5} \right)}{2} + \left( \frac{h}{2} \cdot \frac{\varepsilon_{pl,2}}{5} \right) + \frac{\left( \dfrac{h}{2} \cdot \left( \varepsilon_{pl,2} - \dfrac{\varepsilon_{pl,2}}{5} \right) \right)}{2} \tag{J.22}$$

$$A_{\varepsilon 2} = \frac{2 \cdot h \cdot \varepsilon_{pl,2}}{5} \tag{J.23}$$

With use of Equation (J.19) the limit of plastic strain before failure, for a calculation on the safe side, is determined:

$$\varepsilon_{pl,2} = \frac{\theta_{rd} \cdot h}{2} \cdot \frac{5}{2 \cdot h} = \frac{5}{4} \cdot \theta_{rd} = \frac{5}{4} \cdot 24.6 \cdot 10^{-3} = 3.1\% \tag{J.24}$$

The limit for plastic strain before failure has now been set to an interval between approximately 3 and 5 percent. This should be compared to Figure J.4 where the plastic strain is 2.4 percent, which indicates that the beam will not break due to load case 1. This result was not anticipated since the beam in Section J.1 without curtailment was subjected to the same load and did actually break. This indicates that the beam actually can increase its resistance if curtailment is used. This could be derived to the increased plastic zone which will help with regard to deformation.

It is difficult to determine if this way to analyse the beam is satisfying. One must be very careful when drawing conclusions from this result since it is uncertain if it is in line with EC2. One should keep in mind that the model used in this analysis is based on a elasto-plastic model while the suggestions in EC2 are based on experimental tests on reinforced concrete beams. Hence, there may be some discrepancies in between them.